ANALYSIS OF SUBSTRATE INTEGRATED WAVEGUIDES

by

Robin Nag

A thesis submitted to the University of Kent for the degree of Master of Philosophy in the subject of Electronic Engineering

by

Robin Nag

2017

ABSTRACT

By using a transverse resonance technique, the frequency characteristics of slotted substrate integrated waveguides (SSIWs), slotted half mode substrate integrated waveguides (slotted HMSIWs) and slotted parallel plate SIWs loaded with capacitances and inductances are analyzed theoretically and related to those of conventional waveguides. In practice, the slotted SIWs and HMSIWs are distributed structures, so that they are loaded with ladders of capacitances and inductances across their slots. The cut-off frequencies of the slotted SIWs and HMSIWs loaded with specific capacitances and inductances are then calculated from our analytic technique. These numerical predictions are both compared with and also in some cases used to clarify the corresponding values of cut-off frequencies estimated by HFSS and also by CST Microwave Studio by means of using S-parameters. Field plots for some of these practical examples are used to provided further insights regarding the design and operation of these structures. A tuneable resonator and tuneable single port narrow band antenna are designed. A rudimentary design of a bandpass filter (in the form of a SIW loaded with both inductances and capacitances in series across the slot) is also outlined.

Finally, a modal analysis technique for a general composite waveguide structure, essentially consisting of three sections of SIW, is developed from first principles. This method is used to establish matrices which are used to calculate the S-parameters of the full structure. Though the technique itself is not entirely original, its application is a novel one which can be applied to a whole range of hybrid waveguide structures. Some specific examples of the general case which have practical importance, namely rectangular SIW sections at either end of a slotted SIW region via means of a step with E-planes and H-planes respectively, are considered. The operational characteristics of these waveguide structures are analyzed by means of examining their S-parameters over a suitable range of frequencies. These predicitions are then compared with, and also in some cases, used to interpret the S-parameter estimates from HFSS. The calculated predictions from the modal analysis for these examples are useful for the determination of frequency characteristics of SSIWs, which are instrumental in the novel design of a plethora of microwave devices. In fact, the mode matching method is compared with CST Microwave Studio to estimate the cutoff frequency of a slot SIW antenna.

Acknowledgements

I am most indebted to my supervisor Dr. P.R. Young for his expert guidance and deep insight, and also for his patience and encouragement.

I would also like to thank all the staff in the School of Engineering and Digital Arts at the University of Kent.

TABLE OF CONTENTS

1. Introduction

1.1. Applications of the microwave spectrum

Attenuation of outdoor radio propagation plays a major role in wireless technology. The amount of attenuation is dependent on several factors such as temperature, pressure and humidity. Oxygen and water molecules absorb the energy from electromagnetic waves, and the level of this attenuation rises for larger frequencies. This is illustrated in the following figure from [1].

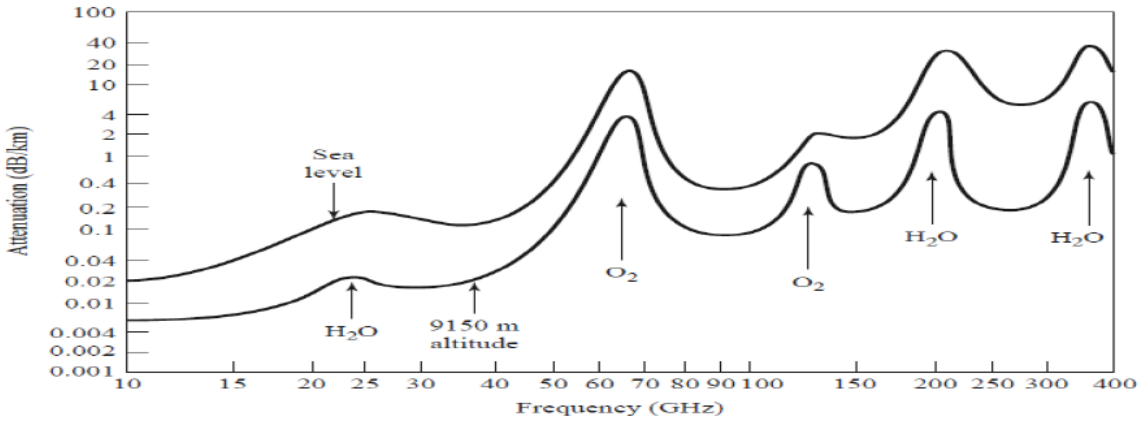

Figure 1.1: Average atmospheric attenuation vs frequency

1.2. Historical milestones

The study of electromagnetic theory began with the work of James Clerk Maxwell [1] in 1873. Maxwell's efforts were concisely recast by Oliver Heaviside [2] into a more modern format. Heinrich Hertz subsequently devised a series of experiments from 1887 to 1891 which vindicated Maxwell's theory of electromagnetism. This led to pioneering work in the 1890s by Ferdinand Braun, Oliver Lodge and Jagadish Chandra Bose in wireless telegraphy and radio microwave optics. Guglielmo Marconi was able to turn this groundbreaking research into a commercial application by bringing long-distance radio transmission to the masses. In December 1902, Marconi and his colleagues successfully managed to send the first ever transatlantic message. It was not until the Second World War and the introduction of radar that microwave technology began to thrive. Hollow tube waveguides were first proposed by Lord Rayleigh [3] in 1897. They were

independently rediscovered in the 1930s by George C. Southworth [4] of Bell Labs and William L. Barrow [5] of MIT. Waveguides were essential for the development of radar by the British in 1937. In the United States, radar theory and its practical applications were intensively investigated during the 1940s by a number of key figures such as Hans Bethe, Julian Schwinger, Isidor Rabi, Carol Montgomery, Edward Purcell, Robert Dicke and Nathan Marcuvitz. Their work on microwave engineering is summarized in the classic 28 volume Radiation Laboratory Series.

1.3. Substrate integrated waveguides

Transmission lines and waveguides are fundamental components of both microwave and millimetre-wave circuits. A waveguide, being a single conductor, does not support TEM waves. Instead, a waveguide supports a higher order of modes, namely TE waves and TM waves (for which there is no electric and no magnetic field in the direction of propagation, respectively) during its operation. Each TE and TM mode has a limited bandwidth in which it will propagate, so that there exists a cutoff frequency below which these modes do not work.

The standard transmission lines used in microwave integrated circuits are usually either microstrip or coplanar waveguide because, being planar, both their accurate construction and integration with other components are achieved easily. However, both microstrip and coplanar waveguide lines are far less efficient than rectangular waveguides. On the other hand, rectangular waveguides are relatively bulky three-dimensional structures. This means that rectangular waveguides are not only difficult to manufacture with sufficient precision, but they also are not easily integrated with active circuits at millimetre-wave frequencies. Consequently, rectangular waveguides are only used for high performance communication systems.

However, the current state of play is set to change with the advent of multilayer fabrication techniques and low temperature co-fired ceramics (LTCC) which allow circuits to be built on multiple layers. This could potentially pave the way for integrated three-dimensional circuits such as embedded waveguides.

Rectangular waveguides of smaller dimensions can be used if they are filled with dielectric materials. They can then be integrated with planar devices on the same substrate. These types of RWG are known as substrate integrated waveguides (SIWs). In practice, two periodic rows of metallic vias are used to connect the top and bottom ground planes, instead of conducting sidewalls. The diameter and spacing of the vias are much smaller than the operating wavelength, and so their presence is equivalent to that of a conducting wall.

Metallized via holes have been used in PCBs for decades in order to reduce coupling between electronic elements. The idea of using via holes in a waveguide was conceived by Shigeki [6] in 1994. Bandpass waveguide filters had been designed by inserting metal posts for decades. Marcuvitz [7] has provided a survey of these techniques by taking various practical cases into account. One such design is that of the inductive post, in which multiple metal posts with adjustable insertion depths are aligned parallel to the incident E-field of a specific fundamental or higher order mode. The incident wave then induces a current on the surface of a post. This results in a scattering field around the post which may be analyzed by using an equivalent circuit model. In the 1970s, Bradshaw [8] calculated the scattering field of a partially inserted thin post in a waveguide filter. In the early 1980s, Leviatan [9] used the Method of Moments to analyze the instance of a waveguide with a single large post. Prior to that time, a post was represented by just a single a surface current parameter. However, Leviatan's innovative step was to model the large post with multiple thin surface currents in terms of Fourier series. Leviatan subsequently extended this work when he collaborated with Li [10] by using an array of multiple posts. In 1998, Ando and Hirokawa managed to build a waveguide antenna from a PCB structure with a metallized post array [11]. In this particular design, the parallel plate antenna and the feed structure shared the same grounded planar dielectric substrate, and the waveguide was fabricated by drilling an array of copper-plated via holes directly into the dielectric material. In 2000, Tzuang [12] improved Hirokawa's design by integrating a microstrip feedline with a via-post waveguide. Tzuang used a photolithography procedure on a PCB to do this. Hiroshi [13] introduced the concept of a laminated waveguide in 1998. By incorporating ideas from Hirokawa, Tzuang and Hiroshi on post-wall and laminated waveguides, Wu [14] introduced the design of the SIW in 2001

that is widely adopted today. In this thesis, the cross-sectional width and height of the SIW is denoted, with the standard notation, as a and b (as shown in the following figure overleaf), respectively.

SIWs can be fabricated using photo-imageable thick film [15] and Multilayer LTCC [16]. Moreover, a substrate integrated waveguide does not support TM modes because its thickness is so small. SIW technology has been incorporated in the design of several microwave and millimetre components.

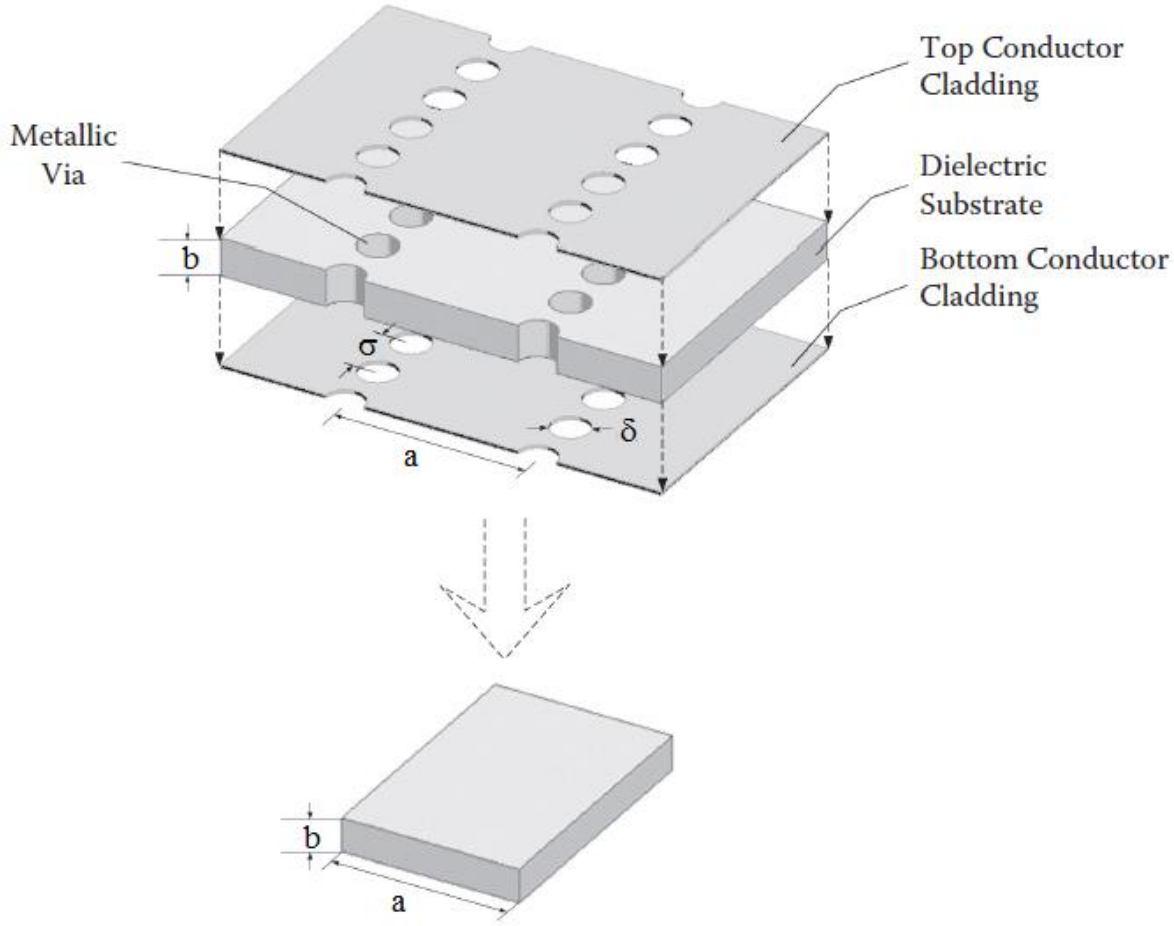

Figure 1.1: Standard schematic configuration of an SIW [17]

1.4. Folded substrate integrated waveguides

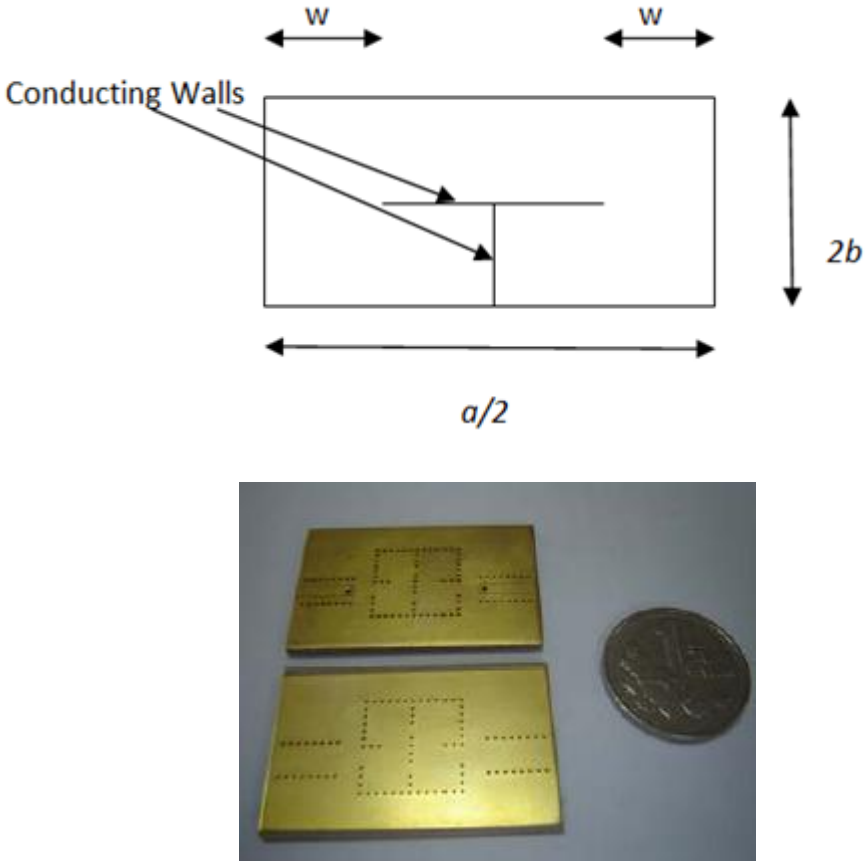

Figure 1.2: Basic schematic diagram and photograph of FSIW

SIWs can still be significantly wider than their planar counterparts, especially at low microwave frequencies. This has led to the introduction of the folded substrate integrated waveguide (FSIW), as described in [18]. The folded waveguide is a rectangular SIW whose sides have been folded underneath its centre. This is illustrated in Figure 1.2. Consider folding a dielectric-filled rectangular waveguide with cross-sectional width *a* and cross-sectional height *b*. Then the resulting folded waveguide has cross-sectional width and height *a/2* and *2b* respectively, as shown above.

Since *a* is much larger than *b*, it follows that FSIWs are viable small-sized waveguides which are easily integrated with planar devices, even at low microwave frequencies.

It has been demonstrated in [18] that an FSIW offers the same performance as a standard air filled waveguide with width 6 times as large when using a substrate with a relative permittivity of 9.

The cut-off frequency f_c of a FSIW is approximately equal to that of a conventional waveguide, which, from [19] or [20], is given by

$$f_c = \frac{c}{2a\sqrt{\varepsilon_r}} \quad , \qquad (1.1)$$

where a is the width of the substrate, ε_r is its relative permittivity and c is the speed of light in a vacuum. The exact value of the gap width w (see Fig. 1) also affects the cut-off frequency . It then becomes necessary to choose w so that both the cut-off frequency and propagation constant are sufficiently close to that of the equivalent full width waveguide. The horizontal propagation constant β is given by

$$\beta = \sqrt{\varepsilon_r k_0^2 - \left(\frac{m\pi}{a}\right)^2}, \qquad (1.2)$$

where $k_0 \left(= \frac{\omega}{c}\right)$ is the wave number in free space and m is the number of variations in the horizontal direction.

1.5. Half mode substrate integrated waveguides

Another improvement on the standard SIW is the half mode substrate integrated waveguide (HMSIW) which was introduced in [21]. The HMSIW can be regarded as half of an SIW. One side wall of the HMSIW is composed of a linear array of metallic vias which synthesize a conducting wall, and the other side is open, as shown in Figure 1.2. Since the ratio of waveguide width to height is relatively large, the open side can be considered as a magnetic wall. It follows that only the TE modes can propagate in the HMSIW. Substrate integrated circular cavities (SICCs) and half mode integrated circular cavities (HSICCs) have also been investigated in [22] and [23] respectively. HMSICs are much easier to manufacture with precision than SICs because they consist of fewer layers in the substrate.

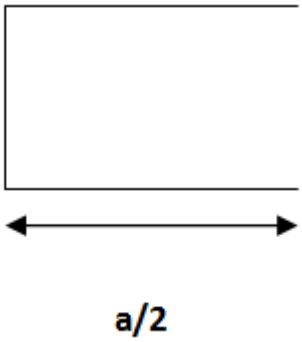

Figure 1.3: Diagram showing the dimensions of a HMSIW

1.6. Components designed with SIWs and SICCs

SIWs and SICCs have recently been implemented in the design of several different kinds of microwave devices. For example, the HSICC structure is used to construct a power divider in [23]. In [24] a 3dB coupler is designed by using a HMSIW structure. SIWs are used to build filters in [25] and [26]. In [27], a SIW is used as a diplexer and an HMSIW is used in the development of a bandpass filter in [28]. A HMSIW is used to feed transverse slot arrays in [29].

The full-mode SIW integrated with periodic components is proposed in [30]. There has been a great deal of investigation in this field. Examples include antennas [31]-[34], filters [35]-[37], transverse electromagnetic (TEM) waveguides [38] and miniaturized waveguides and antennas in [39] and [40]. However, the characteristics of the guided modes has not received as much attention, and so we introduce our own mathematical model to describe periodic loaded components.

It cannot be understated that one of the most important applications of the SIW is the substrate integrated waveguide phase shifter.

The phase shifter occupies a fundamental role in signal transmission systems, especially in radar systems [41]. A phase shift of the signal allows for beam steering in antenna arrays [42].

Conventional phase shifters are either digital or analogue. Digital phase shifters depend on switching devices such as pin diodes or transistors (see [43] and [44]). Unfortunately,

however, several switches produce significant insertion loss. As a result, a large phase shift range is compromised by this insertion loss. This means that there is greater demand for analogue phase shifters which are constructed by adding embedded devices like varactor diodes [45]. A substrate integrated waveguide variable phase shifter is formed by capacitively loading a slotted waveguide with varactor diodes. These structures have now been developed so that they are tuneable and very simple to fabricate, as in [46] and [47].

1.7. Slotted substrate integrated waveguides

This thesis explores aspects of design and analysis of a certain type of SIW. Possible applications for the slotted SIW (SSIW) include bandpass filters, phase shifters and leaky wave antennas. The SIW is a rectangular box filled with a dielectric of relative permittivity 2.2 and with metal walls of thickness 0.5 mm. A slotted line of the dielectric material is then placed on the top surface of the SIW. This slot runs from one end of the guide to the other, as shown in the figures below. The modelling involves propagating electromagnetic waves through this SIW via an input port at one end and an output port at the other. Electromagnetic radiation is then leaked out of the structure via the slot.

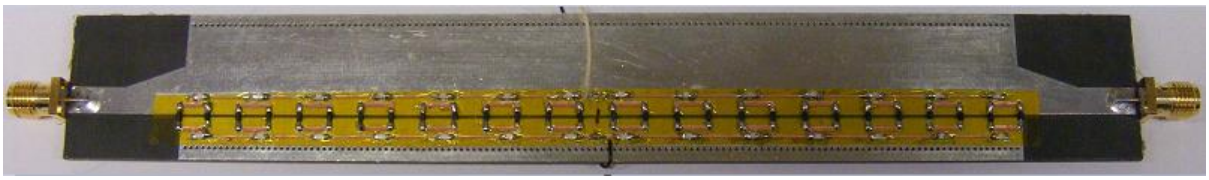

Figure 1.4: A loaded slotted SIW attenuator

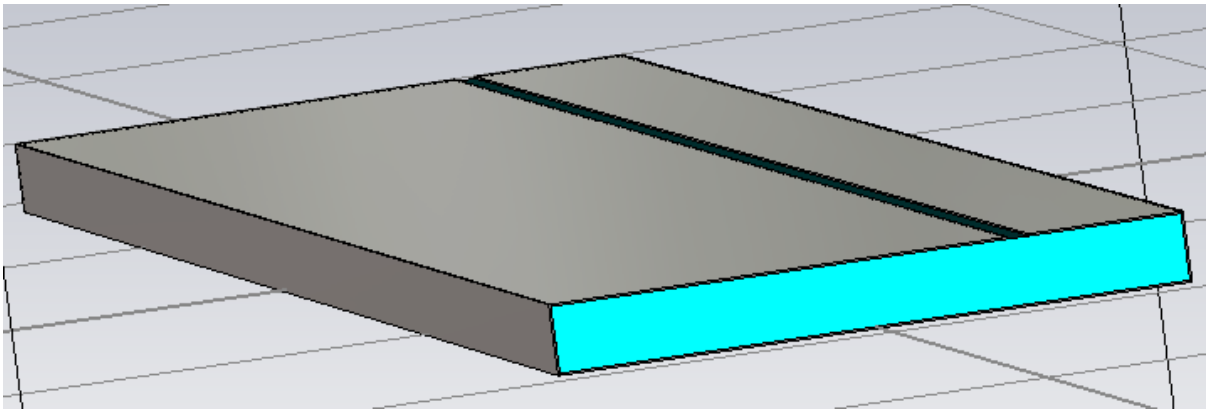

Figure 1.5: A schematic from CST Microwave Studio of a slotted SIW

Slotted waveguides have several important applications. One such microwave device is a SIW switch. If the switch is open, then the propagating mode is the $TE_{\frac{1}{2}0}$ mode. If the switch is closed then the structure becomes a conventional waveguide in which the TE_{10} mode propagates. In practice, the function of the switch is performed by pin diodes connected across the slot, as shown in the following figures.

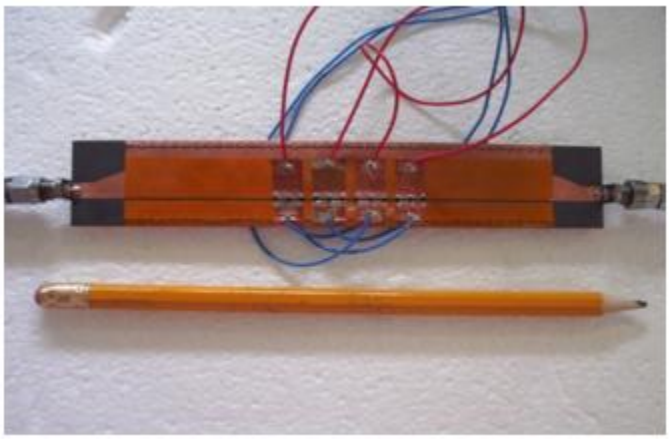

Figure 1.6: Switchable substrate integrated waveguide

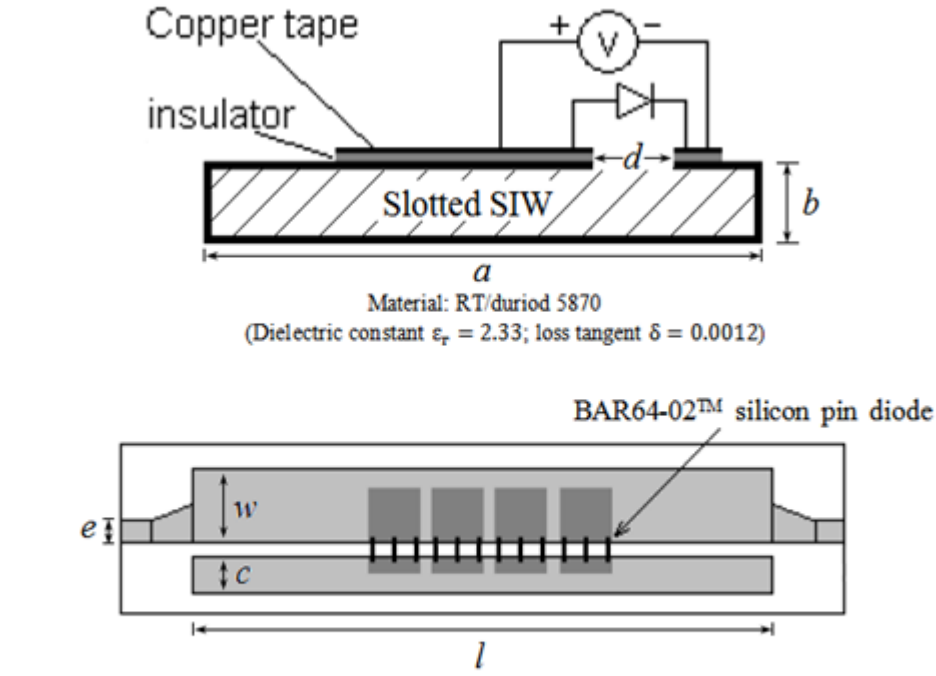

a	b	c	d	e	w	l
21	1.575	5.5	0.5	4.6	15	120

Figure 1.7: Specifications for a switchable substrate integrated waveguide [48]

As the voltage bias to the pin diodes is adjusted, the resistance represented by them can also be changed. Each diode needs to be capacitively coupled to the waveguide by using a very thin insulating material capped with two pads of copper tape, so that a voltage can be applied across it without any risk of a short circuit occurring.

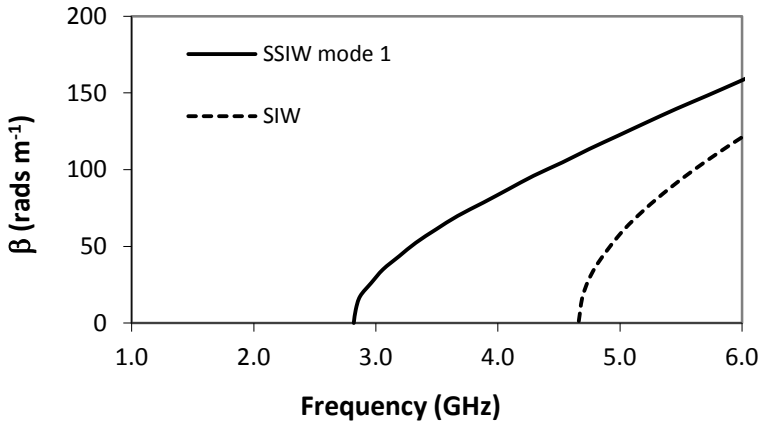

Figure 1.8: Dispersion characteristics for SIW switch [48]

It is therefore possible to switch (i.e. bias) the pin diodes so that cutoff frequency can be raised from just under 3GHz to almost 5GHz, as shown in the corresponding dispersion curves.

In [49], a slotted SIW is used to design a travelling wave attenuator, in which pin diodes are placed across the slot.

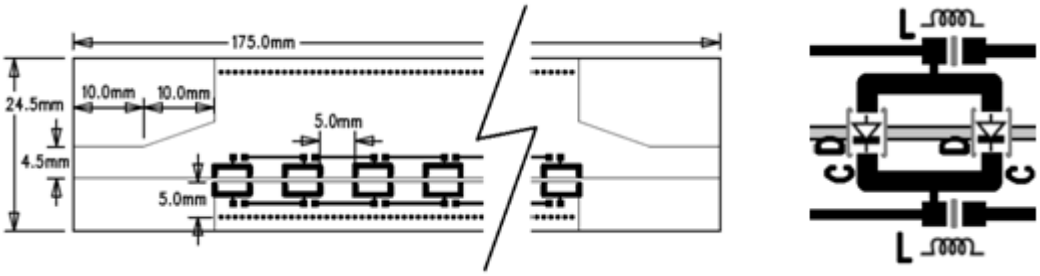

Figure 1.9: Specifications for a travelling wave attenuator [49]

Since each pin diode can act as an electronically controlled resistor by adjusting the voltage bias, it follows that the resulting structure is equivalent to having a variable resistor across the slot. The attenuation constant of the waveguide can therefore be adjusted by changing the load resistance across the slot. This structure is capacitively coupled in the same way as the switchable SIW device. The following figure shows the attenuation for various loading resistances. As the resistance is decreased, the propagating mode eventually turns into the TE_{10} mode, at which point the structure becomes a conventional SIW.

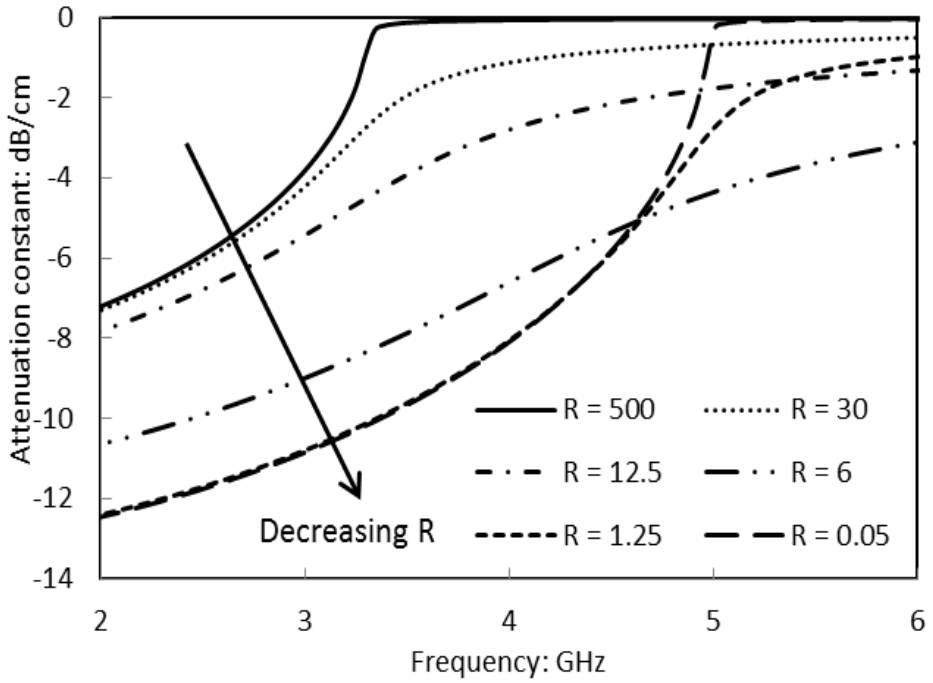

Figure 1.10: Effect of resistive loading for a travelling wave attenuator [49]

1.8. Brief outline of thesis

Transverse resonance analysis is used to determine cut-off frequencies for various slotted SIW structures in the subsequent content of this thesis. In the second chapter, the cutoff frequencies of the fundamental mode for slotted SIWs, where the slots are loaded with a range of inductances and capacitances and are placed in different positions, are calculated and compared with results from simulations in both CST Microwave Studio and HFSS. These comparisons are also carried out for slotted HMSIWs in the third chapter. The non-trivial methods by which cutoff frequencies are determined from the simulations are also described in significant detail in the next chapter.

The second, third and fourth chapters each begin with using the analytic transverse resonance technique to analyze the characteristics of the cutoff frequencies for the first five modes over the full range of normalized loaded capacitances and inductances for SIW, HMSIW and parallel plate SIW structures respectively.

In the latter parts of the second chapter, various SIW devices with loaded capacitances and inductances are designed in CST Microwave Studio by considering their respective resonant frequencies. The work on establishing cutoff frequencies in the earlier parts of the second chapter is used to design a rudimentary bandpass waveguide filter. The remainder of the second chapter includes novel designs for a two-port tuneable waveguide resonator and a single port tuneable narrow band antenna which both function over extremely large operational bandwidths. The work on the antenna is intended to be the subject of a forthcoming paper.

In the fifth chapter, a mode matching technique which determines S-parameters for novel hybrid structures consisting of slotted SIWs. Though this method is neither new nor completely original, it has novel applications regarding SIW technology which are considered in the fifth chapter and are intended for a forthcoming publication. This technique is also presented in a more general form than elsewhere. A survey on the extensive literature on mode matching is also discussed. S-parameters of hybrid structures containing E-plane and H-plane steps are analyzed and compared with HFSS simulations.

Finally, this mode matching technique is used to estimate the cutoff frequencies of some slot SIW antenna structures, and these solutions are compared with corresponding results from CST Microwave Studio.

Conclusions and potential future work are provided in the sixth chapter.

1.9. References

1. J.C. Maxwell, "A treatise on electricity and magnetism," Macmillan and Co., London, 1873.
2. O. Heaviside, "Electromagnetic theory," Benn, London, 1893.
3. Lord Rayleigh, "On the passage of electric waves through tubes, or the vibrations of dielectric cylinders," Phil. Mag., vol. XLIII, pp. 125-132, 1897.
4. G.C. Southworth, "Hyper-frequency waveguides – General considerations and experimental results," The Bell System Technical Journal, vol. 15, No.2, pp. 284-309, 1936.
5. W.L. Barrow, "Transmission of electromagnetic waves in hollow tubes of metal," Proc. I.R.E., vol. 24, No.10, pp. 1298, 1936.
6. F. Shigeki, "Waveguide Line," Japan Patent, 06-53 711, Feb. 25, 1994.
7. N. Marcuvitz, "Waveguide Handbook," vol.10, MIT Radiation Laboratory Series, McGraw-Hill, New York, pp.257-262, 271-272, 285-286, 1951.
8. J.A Bradshaw, "Scattering from a round metal post or gap," IEEE Trans. on Microwave Theory and Tech., vol.21, no.5 pp.313-322, May 1973.
9. Y. Leviatan, P.G. Li, A.T. Adams and J. Perini, "Single-post inductive obstacle in rectangular waveguide," IEEE Trans. on Microwave Theory and Tech., vol. MTT-31, pp. 806-812, Oct. 1983.
10. P.G. Li, A.T. Adams, Y. Leviatan and J. Perini, "Multiple-post inductive obstacles in rectangular waveguide," IEEE Trans. on Microwave Theory and Tech., vol. MTT-32, no.5, pp.365-373, Apr. 1984.
11. J. Hirokawa and M. Ando, "Single-layer feed waveguide consisting of posts for plane TEM wave excitation in parallel plates," IEEE. Trans. Antennas Propagate, vol.46, no.5, pp.625-630, May 1998.
12. C.K.C Tzuang, K.C. Chen, C.J. Lee, C.C Ho and H.S Wu , "H-plane mode conversion and application in printed microwave integrated circuit" Proc. 30th Europ. Microw. Conf., pp.1-4, Oct. 2000.
13. U. Hiroshi, T. Takeshi and M. Fujii, "Development of a laminated waveguide," IEEE Trans. on Microwave Theory and Techniques Electron.Lett., vol.46, No.12, pp.2438-2443. 1998.
14. D. Deslandes and K.Wu, "Integrated microstrip and rectangular waveguide in planar form," IEEE Microw. Wireless Compon. Lett., vol. 11, no. 2, pp. 68–70, Feb. 2001.
15. A.J. Farrall and P.R. Young, "Integrated waveguide slot antennas," Electron.Lett., vol.40, No.16, August 2004, pp.974-975.
16. C.Y. Chang and W.C.Hsu, "Photonic bandgap dielectric waveguide filter," IEEE Microwave wireless Compon.Lett., Vol.12, no.4, pp.137-139, April 2002.
17. Y.J. Cheng, "Substrate integrated antennas and arrays," CRC Press, Taylor and Francis Group, 2016.
18. N. Grigoropoulos and P.R. Young, "Compact folded waveguides," 34th European Microwave Conference, Amsterdam 2004.
19. D.M. Pozar, "Microwave engineering," 2nd edition, Wiley, New York, 1998.
20. R.E. Collin, "Foundations for microwave engineering," McGraw-Hill, New York, 1992.

21. W. Hong, B. Liu, Y.Q. Wang, Q.H. Lai and K.Wu, "Half mode substrate integrated waveguide: a new guided wave structure for microwave and millimetre wave application," (Keynote Talk), Joint 31st Int. Conf. on infrared and millimetre waves and 14th Int. Conf. on terahertz electronics, Shanghai, September 2006.
22. H.J. Tang, W. Hong, J.-X. Chen, G.Q. Luo, and K. Wu, "Development of millimetre-wave diplexers based on complementary characters of dual-mode substrate integrated waveguide filters with circular and elliptic cavities," IEEE Progress in Electromagnetics Research Letters, Vol. 10, 2009.
23. J. Gu, Y. Fan, Y. Zhang and D. Wu, "A novel 3-D transition and power divider based on half mode SICC structure," Progress in Electromagnetics Research Letters, Vol.10, 125-133, 2009.
24. B. Liu, W. Hong, Y.-Q. Wang, Q,-H . Lai and K. Wu, "Half mode substrate integrated waveguide (HMSIW) 3-db coupler," IEEE Microwave and Wireless Components Letters, Vol.17, No. 1, 22, 2007.
25. R. Wang, L.S. Wu and X.-L. Zhou, "Compact folded substrate integrated waveguide cavities and bandpass filters" Progress in Electromagnetics Research, PIER 84, 135-147, 2008.
26. A. Ismail, M.S. Razalli, "X-band and trisection substrate integrated waveguide quasi-elliptic filter," Progress in Electromagnetics Research, PIER 85, 133-145, 2008.
27. S. Han, X-L Wang, Y. Fan, Z. Yang and Z. He, "The generalized Chebyshev substrate integrated waveguide diplexer," Progress in Electromagnetics Research PIER 73, 29-38, 2007.
28. Y.Q. Wang, W. Hong, Y.D. Dong, B. Liu, H.J. Tang, J.X. Chen, X.X Yin and K. Wu, "Half mode substrate integrated waveguide (HMSIW) bandpass filter," IEEE Microw. Wireless Compon. Lett, Vol. 17, no.4, pp.265-267, 2007.
29. Q.H. Lai, W. Hong, Z.Q. Kuai, Y.S. Zhang and K. Wu, "Half-mode substrate Integrated waveguide transverse slot array antennas," IEEE Transactions on Antennas and Propagation, Vol. 57, No. 4, 2009.
30. H.-S. Wu and C.-K. C. Tzuang, "Artificially integrated synthetic rectangular waveguide," IEEE Trans. Microw. Theory Tech., vol. 53, no. 9, pp. 2872–2881, Sep. 2005.
31. R. Coccioli, F.-R. Yang, K.-P.Ma, and T. Roh, "Aperature-coupled patch antenna on UC-PBG substrate," IEEE Trans. Microwave Theory Tech., vol. 47, no. 11, pp. 2123–2130, Nov. 1999.
32. S. Maci, R. Magliacani, and A. Cucini, "Leaky-wave antennas realized by using artificial surfaces," in Proc. IEEE Antennas Propag. Int. Symp., pp. 1099–1102, 2003.
33. K.C. Chen, Y. Qian, C.K.C. Tzuang, and T. Itoh, "A periodic microstrip radial antenna array with a conical beam," IEEE Trans. Antennas Propag., vol. 51, no. 4, pp. 756–765, Apr. 2003.
34. C.K. Wu, Y.C. Chen, and C.K.C. Tzuang, "Compressed-width leaky EH mode PBG antenna," IEEE Microwave Wireless Comp. Lett., vol. 13, no. 8, pp. 343–344, Aug. 2003.
35. D. Deslandes and K. Wu, "Single-substrate integration technique of planar circuits and waveguide filters," IEEE Trans. Microwave Theory Tech., vol. 51, no. 2, pp. 593–596, Feb. 2003.

36. H. Xin, A. Higgins, J. Hacker,M. Kim, and M. Rosker, "Electromagnetic crystal (EMXT) waveguide band-stop filter," IEEE Microwave Wireless Comp. Lett., vol. 13, no. 3, pp. 108–110, Mar. 2003.
37. H. Xin, A. Higgis, and M. Kim, "Tunable millimeter-wave band-stop filter using electromagnetic crystal (EMXT) surfaces," in *2003 IEEE AP-S Int. Microwave Symp. Dig.*, pp. 1107–1110, 2003.
38. M. N. M. Kehn and P.S. Kildal, "The N-guide: a novel miniaturized hard quasi-TEM waveguide," in Proc. IEEE Antennas Propag. Int. Symp., pp. 1111–1114, 2003. 159
39. S. Pioch and J.-M. Laheurte, "Size reduction of microstrip antennas by means of periodic metallic patterns," Electron. Lett., vol. 39, no. 13, pp. 959–961, Jun. 2003.
40. H.-S. Wu and C.-K. C. Tzuang, "Miniaturized synthetic rectangular waveguide," in 2003 IEEE MTT-S Int. Microwave Symp. Dig., Philadelphia, PA, Jun. 8–13, pp. 1099–1102, 2003.
41. Rober V. Garver, "Microwave Diode control Devices," Artech House, Inc, 1976.
42. Sellal k., Talbi L., Denidni, T.A., and Lebel J., "Design and implementation of a substrate integrated waveguide phase shifter," IET Microw. Antennas Propag., vol. 2, no. 2, pp. 194-199, 2008.
43. Z. Jin, S. Ortiz, and A. Mortazawi, " Design and performance of a new digital phase shifter at X-band," IEEE Microwave Wireless Comp. Lett., vol.14, no.9, pp.428-430, 2004.
44. S. Cheng, E. Öjefors, P. Hallbjörner, and A. Rydberg, "Compact reflective microstrip phase shifter for traveling wave antenna applications," IEEE Microwave Wireless Comp. Lett., vol.16, no.7, pp.413 433, 2006.
45. Elisa Sbarra, Luca Marcaccioli, Roberto Vincenti Gatti and Roberto Sorrentino, "Ku-band analogue phase shifter in SIW technology," in 39th European Microwave Conference, pp. 264-267, 2009.
46. Cheng Y. J., Hong W. and Wu K., Broadband Self-Compensating Phase Shifter Combining Delay Line and Equal-Length Unequal-Width Phaser," IEEE Trans. Microwave Theory and Tech., Vol 58 , Issue 1, pp. 203 – 210, 2010. 161
47. Sellal K., Talbi L., Denidni, T.A. and Lebel J., "Design and implementation of a substrate integrated waveguide phase shifter," IET Microw. Antennas Propag., vol. 2, no. 2, pp. 194-199, 2008.
48. R.F. Xu, B. Sanz Izquierdo and P.R. Young 2011, "Switchable Substrate Integrated Waveguide," IEEE Microwave Wireless Compon. Lett., vol. 21, no.4, pp. 194-196, 2011.
49. R.F. Xu, A.J. Farrall and P.R. Young 2014, "Analysis of loaded substrate integrated waveguides and attenuators," IEEE Microwave Wireless Compon. Lett., vol. 24, no. 1, pp. 62-65, 2014.

2. Transverse Resonance Technique for the Slotted SIW

2.1. Introduction

This chapter begins with using a transverse resonance technique to analyze the characteristics of the cutoff frequencies for the first five modes over the full range of normalized loaded capacitances and inductances for SIW structures.

Then the transverse resonance technique is used to calculate specific cutoff frequencies of the fundamental mode for slotted SIWs loaded with a range of actual capacitances and inductances. These estimates of cutoff frequencies are compared with those from simulations in both CST Microwave Studio and HFSS, which depend upon defining the cutoff frequency by using the group delay and setting the phase to zero, respectively.

This work on establishing cutoff frequency is subsequently used to attempt to design a rudimentary bandpass waveguide filter, which is matched by increasing the thickness of the SIW. This confirms earlier S-parameter plots from CST Microwave Studio that loaded SIWs are better suited for the construction of narrow band devices. This leads to the novel design of a two-port tuneable waveguide resonator which functions over a large operational bandwidth of several hundred MHz. After showing that a two port tuneable antenna cannot be designed with the afore-mentioned types of loaded SIWs, a single port tuneable narrow band antenna is designed. This work on the antenna is intended to be the subject of a forthcoming paper. Both devices can be finely tuned by using loaded capacitances. The single-port antenna can be tuned over a huge range of almost 1GHz.

2.2. Background theory

The approach described here will be slightly different from the classical theory of electromagnetic waveguides, as presented in [1]-[5]. Any rectangular waveguide can be analyzed in Cartesian coordinates by considering its width a and height b.

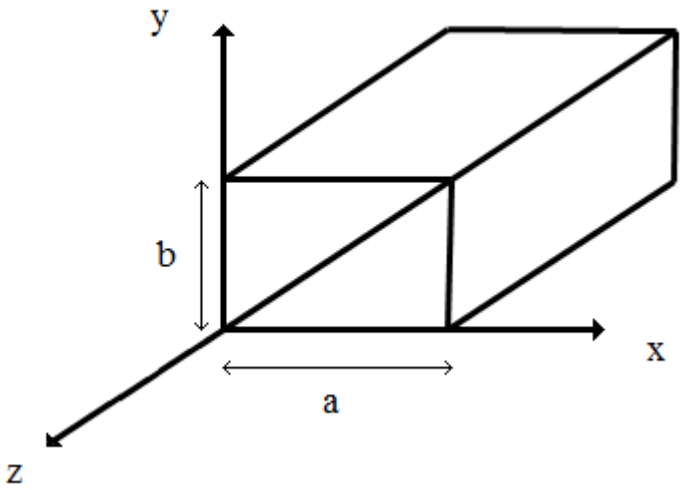

Figure 2.1: Schematic diagram for a standard rectangular waveguide.

The topic interest of this chapter is concerned with periodically loaded slotted SIWs. The identical load elements are connected along the slot of the top layer of the SIW, as shown in the subsequent figure. Two cases are subsequently considered, namely when every load element is either a purely capacitive or purely inductive component. A transverse resonance technique for the slotted waveguide is used to determine frequency characteristics. This technique is described in further detail here. The width of the slot is denoted by *w*, the longitudinal distance between the centre of each load element is represented by d, and the horizontal distance from each sidewall to the boundary of the slot is given by L_1 and L_2 respectively, such that $L_1 \geq L_2$ and $a = L_1 + L_2 + w$.

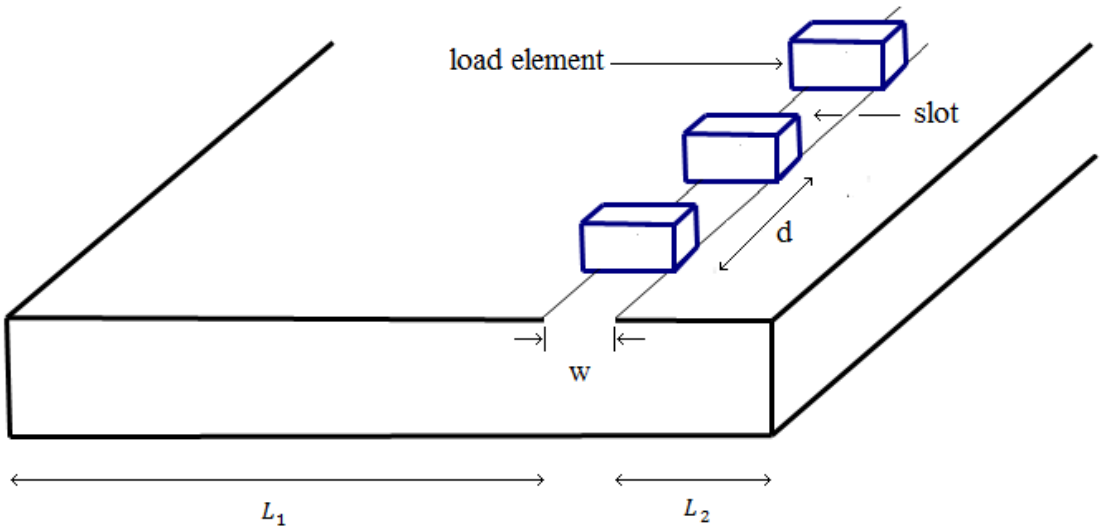

Figure 2.2: Schematic of a periodically loaded slotted SIW.

This is based on the fact that in a rectangular waveguide the wave travels with wave vector

$$\boldsymbol{k} = k_x \boldsymbol{i} + \beta \boldsymbol{j}\,, \qquad (2.1)$$

where $\boldsymbol{i}$ and $\boldsymbol{j}$ are the components in the directions along the length and width of the rectangular waveguide respectively. This is illustrated in the following figure.

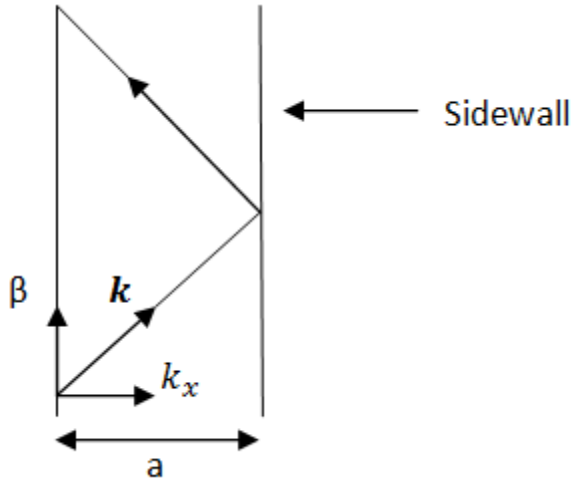

Figure 2.3: Wave propagating through a rectangular waveguide

The horizontal component k_x of the wave vector $\boldsymbol{k}$ is known as the wave number, and is given by

$$k_x = \omega\sqrt{\mu\varepsilon}\,. \qquad (2.2)$$

Note that the waveguide width and height are given by *a* and *b* respectively.

Firstly, consider the special c ase at cut-off in a rectangular waveguide without a slot when β=0, so that the wave bounces back and forth between the two sidewalls in such a way that its direction of propagation is perpendicular to them both. In this particular instance, it is possible to model the waveguide as a parallel plate transmission line terminated by short circuits. This can be used to determine the characteristic impedance Z_0 (over a distance *d*) of the transmission line, which is given by

$$Z_0 = \frac{b}{d}\sqrt{\frac{\mu}{\varepsilon}}\,, \qquad (2.3)$$

where μ and ε are the permeability and permittivity of the substrate.

The next step is to determine the cut-off frequency of the SIW without a slot. This cut-off frequency is equivalent to the resonant frequency on the terminated transmission line. Take a point on the transmission line. Then the resonant frequency of the terminated transmission line, which is when the input and output impedances are equal in magnitude but opposite in sign, is therefore given by

$$Z_{in\,1} = -Z_{in\,2}\,. \qquad (2.4)$$

This is equivalent to matching the voltage and current. These impedances are opposite in sign due to to the different current directions.

It is well known (see [6] or [7]) that the input impedance of a lossless terminated line of length L_0 is given by

$$Z_{in} = Z_0 \cdot \frac{Z_{Load} + jZ_0 \tan k_x L_0}{Z_0 + jZ_{Load} \tan k_x L_0}\,. \qquad (2.5)$$

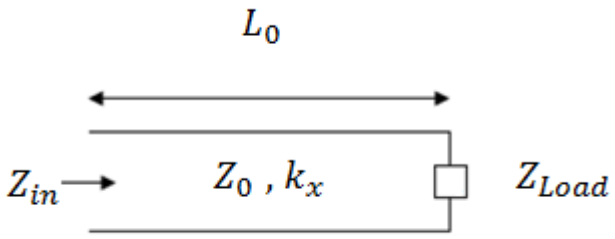

Figure 2.4: Terminated loaded transmission line.

Since the waveguide is being modelled as as a parallel plate transmission line terminated by short circuits, it is evident that $Z_{Load} = 0$.

Then at $L_0 = a$ we have

$$Z_{in\,1} = jZ_0 \ tan\,(k_x a)\,, \quad (2.6)$$

$$Z_{in\,2} = 0\,. \quad (2.7)$$

It follows that

$$jZ_0 \ tan\, k_x a = 0\,. \quad (2.8)$$

Hence

$$k_x a = n\pi \ \Rightarrow \ k_x = \frac{n\pi}{a}\,, \quad \text{where } n = 1,2,3,\ldots\ . \quad (2.9)$$

At the point of cutoff, the angular frequency ω of a propagating electromagnetic wave may be denoted as ω_c , so that (2.2) may be rewritten as

$$k_x = \omega_c\sqrt{\mu\varepsilon}\,. \quad (2.10)$$

It is evident from (2.10) that the cutoff frequency of a TE_{n0} rectangular waveguide is given by

$$f_c = \frac{n}{2a\sqrt{\mu\varepsilon}}\,, \quad \text{where } n = 1,2,3,\ldots\ . \quad (2.11)$$

The value of the cutoff frequency allows us to choose a suitable value for a, which we can take to be about 20 mm.

Now it is possible to model a slotted SIW as a lumped element transmission line circuit. The load elements across the slot can be modelled by a single impedance, as shown in the equivalent circuit diagram below.

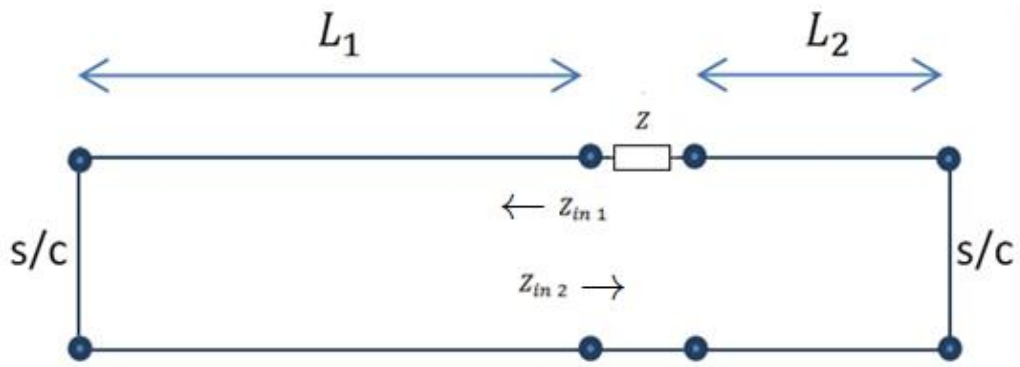

Figure 2.5: Equivalent circuit model of slotted SIW

Then

$$Z_{in\,1} = jZ_0 \tan k_x L_1 , \qquad (2.12)$$

$$Z_{in\,2} = Z + jZ_0 \tan k_x L_2 . \qquad (2.13)$$

Since

$$Z_{in\,1} = -Z_{in\,2} , \qquad (2.14)$$

it may be deduced that

$$jZ_0 \tan k_x L_1 = -Z - jZ_0 \tan k_x L_2 . \qquad (2.15)$$

If $Z = jX$, then

$$\tan k_x L_1 = -\frac{X}{Z_0} - \tan k_x L_2 . \qquad (2.16)$$

Note that if the total load across slot is being modelled by a capacitance C , then set

$$X = -\frac{1}{\omega C} . \qquad (2.17)$$

Alternatively, if the slot is loaded with an inductance L , then set

$$X = \omega L \ . \qquad (2.18)$$

By substituting (2.10) and (2.17) into (2.16), it is evident that

the cutoff equation is

$$\tan \omega L_1 \sqrt{\mu\varepsilon} = \frac{1}{\omega C Z_0} - \tan \omega L_2 \sqrt{\mu\varepsilon} \ , \qquad (2.19)$$

for a capacitive impedance,

and, by replacing (2.17) by (2.18) in the above procedure, it follows that the cutoff equation is

$$\tan \omega L_1 \sqrt{\mu\varepsilon} = -\frac{\omega L}{Z_0} - \tan \omega L_2 \sqrt{\mu\varepsilon} \ , \qquad (2.20)$$

for an inductive impedance.

2.3. Cutoff frequency equations

If the SSIW is capacitively loaded, then define *C'* to be the capacitance per unit length along the slot which could be taken to be in the range of anything from 0.1 pF/m to 100 pF/m. If the SSIW is inductively loaded, then define *L'* to be the inductance per unit length. Then for a distance *d* along the length of the slot, the total capacitance and inductance along the slot is given by

$$C = C' d \ , \qquad (2.21)$$

and

$$L = L' d \ , \qquad (2.22)$$

for the capacitively and inductively loaded SSIWs respectively. By setting $d = 1$ in (2.3), it follows that

$$Z_0 C = C' b \sqrt{\frac{\mu}{\varepsilon}} \ , \qquad (2.23)$$

and that

$$\frac{\omega L}{Z_0} = \frac{\omega L'}{b\sqrt{\frac{\mu}{\varepsilon}}} \ . \qquad (2.24)$$

Then the cutoff frequency equations for capacitive and inductive impedances can be rewritten by substituting (2.23) into (2.19) and (2.24) into (2.20), and are given by

$$tan\ \omega L_1\sqrt{\mu\varepsilon} = \frac{1}{\omega C' b\sqrt{\frac{\mu}{\varepsilon}}} - tan\ \omega L_2\sqrt{\mu\varepsilon}\ , \qquad (2.25)$$

and

$$tan\ \omega L_1\sqrt{\mu\varepsilon} = -\frac{\omega L'}{b\sqrt{\frac{\mu}{\varepsilon}}} - tan\ \omega L_2\sqrt{\mu\varepsilon}\ , \qquad (2.26)$$

respectively. Note that the angular cutoff frequency is given by ω and f_c represents the actual cutoff frequency, where

$$\omega = 2\pi\ f_c \ . \qquad (2.27)$$

Now set

$$\theta = \omega L_1\sqrt{\mu\varepsilon}\ , \qquad (2.28)$$

$$\hat{C} = \frac{C' b}{\varepsilon}\ , \qquad (2.29)$$

$$\hat{L} = \frac{L'}{b\mu}\ , \qquad (2.30)$$

so that θ, $\hat{C}$, $\hat{L}$ represent normalized parameters of frequency, capacitance and inductance, respectively. Then the respective cutoff equations for capacitive and inductive impedances given by (2.25) and (2.26) may be rewritten as

$$tan\ \theta + tan\ \frac{\theta}{\Gamma} = \frac{1}{\hat{C}\theta}\ , \qquad (2.31)$$

and

$$tan\ \theta + tan\ \frac{\theta}{\Gamma} = -\hat{L}\theta\ , \qquad (2.32)$$

where $\Gamma = \frac{L_1}{L_2}$.

Since the cutoff equations are transcendental, θ can only be determined numerically over a suitable range of values for $\hat{C}$ and $\hat{L}$ respectively. In order to find the solutions of θ in these equations, we determine successive intervals of θ inside which possible solutions may exist over a full range of normalized parameters denoted by $\hat{C}$ and $\hat{L}$ respectively. Note that, for $r > 1$, the r^{th} such interval is used to determine larger values of θ than the $(r-1)^{th}$ interval over the same range of $\hat{C}$ or $\hat{L}$ for capacitively or inductively loaded slots, respectively. Hence, the n^{th} order mode corresponds to the solutions in the n^{th} such interval, where n is any positive integer.

2.4. Normalized solutions of cutoff equations

The software package Maple has been used to calculate the solutions of θ for the first five modes (for values of $\Gamma = 3,4,5,6$) over a suitable range of $\hat{C}$ and $\hat{L}$, respectively. These results are presented below as theoretical design curves. In order to see the results over a suitably large range of $\hat{C}$ and $\hat{L}$ respectively, we have used a logarithmic scale. By considering the cut-off frequency equations, the vertical axis of each design curve, being represented by $\frac{\theta}{\pi}$, is proportional to the angular cut-off frequency ω. The horizontal axis of each design curve is given by the reciprocal of either $\hat{C}$ or $\hat{L}$, which is regarded as normalized elastance or reluctance, respectively. The reason for using these reciprocal quantities is so that the full range and continuity of the cut-off frequencies can be easily illustrated over all effective capacitances and inductances. Therefore, these design curves show how the normalized cut-off frequency varies with the normalized capacitance or inductance across the slot, respectively. Some explanations for these design curves are offered in the subsequent section.

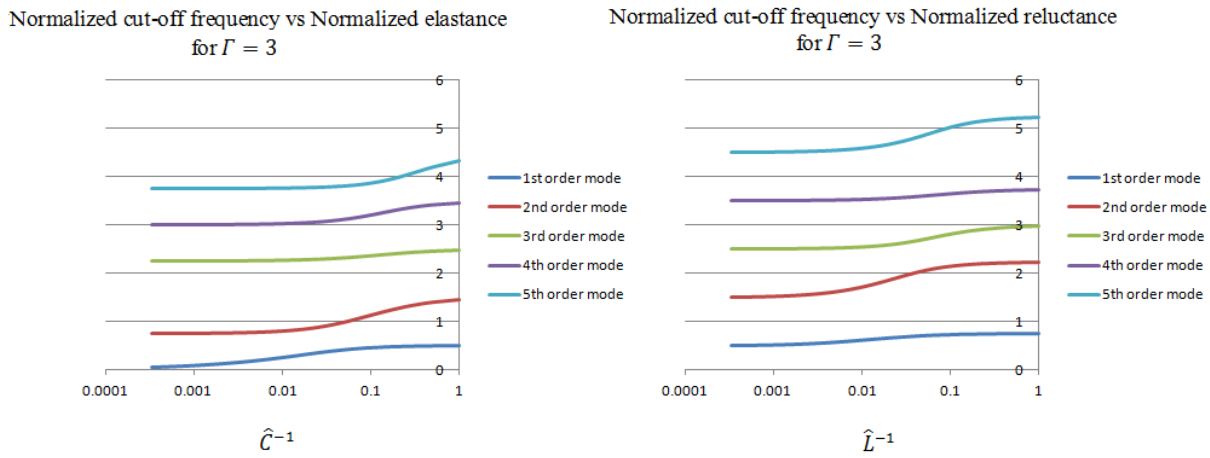

Figure 2.6: Design curves for loaded capacitances and inductances for Γ=3

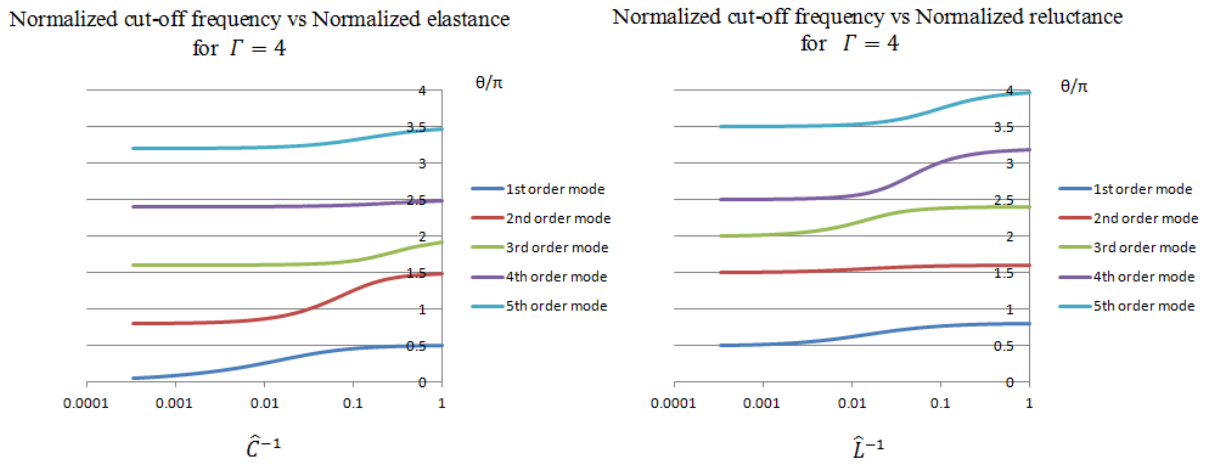

Figure 2.7: Design curves for loaded capacitances and inductances for Γ=4

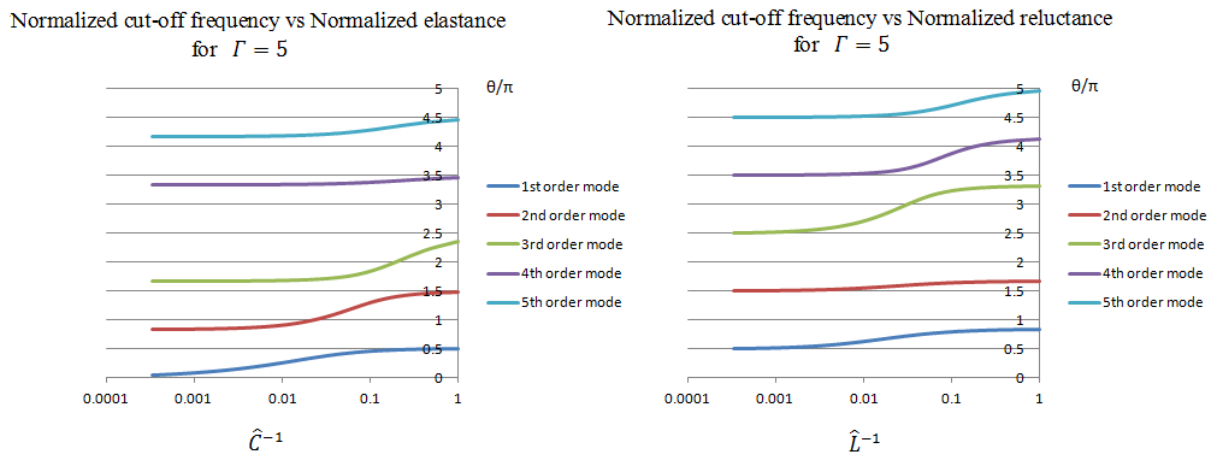

Figure 2.8: Design curves for loaded capacitances and inductances for Γ=5

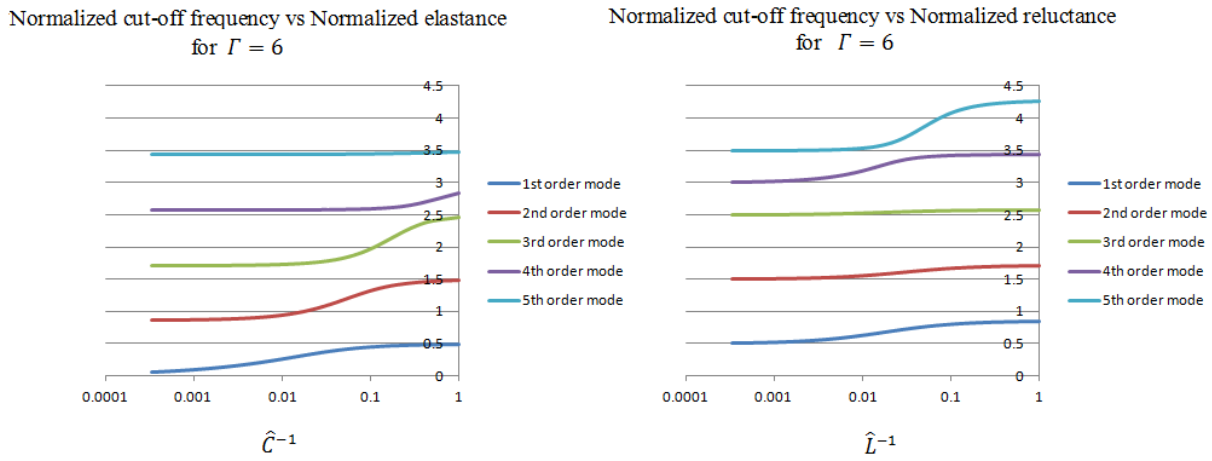

Figure 2.9: Design curves for loaded capacitances and inductances for Γ=6

2.5. SSIW with small capacitive loads

A very small capacitance is equivalent to an open circuit. Therefore, the SIW slotted with a very small capacitance is equivalent to a half mode rectangular waveguide. Consider the quarter cosine waveform which envelopes the electric field pattern of the 1st order mode in the half mode rectangular waveguide (illustrated in the following figure). It now follows that an n^{th} order mode in this capacitively slotted waveguide has the cut-off frequency of an n^{th} order mode in a half mode waveguide, where $n = 1,2, \ldots$. This is in agreement

with the graphs above where $\theta \to \frac{\pi}{2}$, $\theta \to \frac{3\pi}{2}$ and $\theta \to \frac{5\pi}{2}$ as the capacitance $\hat{C} \to 0$ for the 1st , 2nd and 3rd order modes respectively, regardless of the choice for Γ.

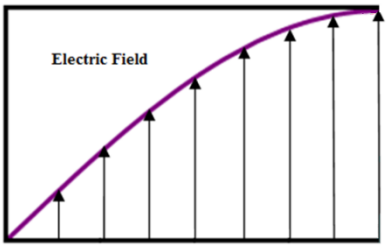

Figure 2.10: Transverse Section of Electric Field pattern of the 1st order mode in a half mode waveguide

2.6. SSIW with large inductive loads

A sufficiently large inductance is equivalent to an open circuit. Therefore, the SIW slotted with a sufficiently large inductance is equivalent to a half mode rectangular waveguide.

Consider once again the quarter cosine waveform (see Figure 2.10) which envelopes the electric field pattern of the 1st order mode in the half mode rectangular waveguide. By observing that this 1st order mode corresponds to all values of $\theta \in \left(0, \frac{\pi}{2}\right)$, and by noting that there are no solutions in this interval in any of the design curves for normalized reluctance given earlier, this particular mode cannot also be a mode of a waveguide slotted with a large inductance.

It follows that an $(n-1)^{th}$ order mode in this waveguide slotted with a very large inductance has the cut-off frequency of an n^{th} order mode in a half mode waveguide, where $n = 2,3, \ldots$. This is in agreement with the design curves where $\theta \to \frac{\pi}{2}$ as the inductance $\hat{L} \to \infty$ for the 1st order modes, irrespective of the choice of Γ. Likewise, $\theta \to \frac{3\pi}{2}$ and $\theta \to \frac{5\pi}{2}$ as the inductance $\hat{L} \to \infty$ for the 2nd and 3rd order modes respectively, and this is also independent of Γ.

2.7. SSIW with large capacitive loads

If the load across the slot is either an adequately large capacitance or relatively small inductance, it behaves more like a short circuit. As this capacitance is increased, the cut-off frequency decreases (as demonstrated in the design curves given earlier) until eventually the electric field concentrates itself around the slot, at which point the mathematics of our transverse resonance technique breaks down. In particular, the cut-off frequency of the 1st order mode in the SIW slotted with a sufficiently large capacitance decreases to almost zero.

It follows that the cut-off frequency of the n^{th} order mode in the SIW slotted with a sufficiently large capacitance is equivalent to the cut-off frequency of the $(n-1)^{th}$ order mode in a rectangular waveguide, where $n = 2,3, \ldots$.

Consider the half cosine waveform which envelopes the electric field pattern of the 1st order mode in the standard rectangular waveguide (illustrated in the following figure).

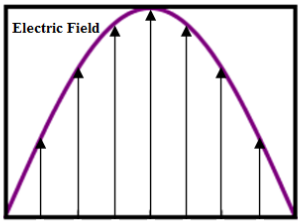

Figure 2.11: Transverse Section of Electric field pattern of the 1st order mode in a rectangular waveguide

Defining x to be the transverse axis of the rectangular waveguide with width a, the standard condition at cut-off of the $(n-1)^{th}$ order mode in the rectangular waveguide is then given by $\theta = k_x L_1 a = (n-1)\pi$, where $n = 2,3, \ldots$, and where θ is obtained from (2.28) and the wave number k_x is defined in (2.2). It follows from the earlier part of the argument that the condition at cut-off of the n^{th} order mode of the SIW slotted with a sufficiently large capacitance is the same as for the $(n-1)^{th}$ order mode of the rectangular waveguide at cut-off, namely that $\theta = (n-1)\pi$, where $n = 2,3, \ldots$. Note that x and a can

therefore also be taken to be the transverse axis and width of this particular slotted SIW respectively.

Note that k_x is given by (2.2) and that $a = L_1 + L_2$, since the width of the slot w is negligibly small with respect to a.

Then the condition at cut-off for the n^{th} order mode of the SIW slotted with a sufficiently large capacitance, where $n = 1,2, \ldots$, is given by

$$\theta = \frac{(n-1)\pi L_1}{L_1 + L_2} = \frac{(n-1)\pi}{\left(1 + \frac{1}{\Gamma}\right)} \quad . \qquad (2.33)$$

For example, if $n = 2$ (i.e. considering the 2nd order mode of the slotted SIW), then it follows from the last equation that for $\Gamma = 3$, $\theta \to \frac{3}{4}\pi$ for very large capacitances. Also, if $n = 2$, then for $\Gamma = 4$, $\theta \to \frac{4}{5}\pi$ for very large capacitances. This is in agreement with the 2nd order mode solution (when $\Gamma = 3,4$ respectively) design curve value for normalized frequency for very large capacitances. By the above equation, we can see, for the 2^{nd} order mode, that as Γ becomes sufficiently large, then, theoretically, $\theta \to \pi$ for very large capacitances.

2.8. SSIW with small inductive loads

If the inductance is very small it behaves more like a short circuit. Therefore, the SIW slotted with a sufficiently small inductance is equivalent to a standard rectangular waveguide. Consider the half cosine waveform which envelopes the electric field pattern of the 1^{st} order mode in the standard rectangular waveguide in the last figure. This particular 1^{st} order mode corresponds to all values of $\theta \in \left(0, \frac{\pi}{2}\right)$, and so, by the same argument in the section before last, it cannot also be a mode of a waveguide slotted with a large inductance.

It follows that if the cutoff frequency of the $(n-1)^{th}$ order mode in the SIW slotted with a sufficiently small inductance is equivalent to the n^{th} order mode in a rectangular waveguide, then it is necessary that $n \in \{2,3, \ldots\}$.

Recall that the right hand side of the inductive cutoff equation, given by (2.32), is negative. Define x to be the transverse axis of the inductively slotted waveguide. On the grounds of the preceding argument, suppose that the cut-off frequency of the $(n-1)^{th}$ order mode in the SIW slotted with a sufficiently small inductance is equivalent to the n^{th} order mode in a rectangular waveguide, where $n \epsilon \{2,3, ...\}$. If this assumption is shown to be not strictly correct for all designated values n, then it will be modified accordingly. It follows from this assumption that the condition at cut-off for this slotted waveguide is then given by $\theta = k_x L_1 a = (n-1)\pi$, where $n \epsilon \{2,3, ...\}$.

Then the condition at cut-off for the $(n-1)^{th}$ order mode of the SIW slotted with a sufficiently small inductance, where $n \epsilon \{2,3, ...\}$, is given by (2.33).

For example, for $\Gamma = 3$, if $n = 2$ (i.e. considering the 1st order mode of this slotted SIW which is equivalent to 2nd order mode of the corresponding rectangular waveguide), then it follows from the last equation that $\theta \to \frac{3}{4}\pi$ for very small inductances. This is validated by the fact that $tan\,\theta + tan\,\frac{\theta}{3} = 0$ (by setting the right hand side of (2.32) to zero) at $\theta = \frac{3}{4}\pi$ is shown as the first zero in the positive θ-axis of the function $y = tan\,\theta + tan\,\frac{\theta}{3} = 0$ in the Cartesian plot below. This result that $\theta \to \frac{3}{4}\pi$ is in agreement with the design curve (showing normalized frequency versus normalized inductance) for very small inductances in the 1st order mode when $\Gamma = 3$.

For $\Gamma = 3$, if $n = 3$, then it follows from (2.33) that $\theta \to \frac{3}{2}\pi$ for very small inductances.

However, for the case with $\Gamma = 3$, setting $n = 3$ does not correspond to the 2nd order mode of the SIW slotted with a small inductance in the corresponding design curve (showing normalized frequency versus normalized inductance) above. An explanation for this is given as follows.

A Cartesian plot of the terms in the corresponding inductive cut-off equation for $\Gamma = 3$ (as shown below) demonstrates that $\theta = \frac{3}{2}\pi$ is in fact an asymptote. Let $h' = -\hat{L}$. By considering (2.32), it follows that the condition that $tan\,\theta + tan\,\frac{\theta}{3} \to h'\theta$ as $\theta \to \frac{3}{2}\pi$ is satisfied only as $h' \to \infty$, and not when h' is very small (as $h' \to 0$, $y = h'\theta$ coincides with

the θ-axis in the Cartesian plot below). Therefore, for the case where $\Gamma = 3$, there exists no mode of an SIW slotted with a sufficiently small inductance for which $\theta = \frac{3}{2}\pi$.

Figure 2.12: Cartesian plot of left and right hand side terms of the inductive cut-off equation for Γ=3 and h'= -1.

Therefore, for $\Gamma = 3$, the instance where $n = 3$ for the SIW slotted with a very small inductance must be neglected. It follows by considering periodicity that the standard rectangular waveguide has certain modes which do not appear in the SIW loaded with a very small inductance.

For $\Gamma = 3$, if $n = 4$ (i.e. considering the 2nd order mode of this slotted SIW which is equivalent to the 4th order mode of the corresponding rectangular waveguide), then it follows from (2.33) that $\theta \to \frac{9}{4}\pi$ for very small inductances. This is validated by the fact that $\tan\theta + \tan\frac{\theta}{3} = 0$ at $\theta = \frac{9}{4}\pi$ is shown as the second zero in the positive θ-axis of the function $y = \tan\theta + \tan\frac{\theta}{3} = 0$ in the last Cartesian plot. This result that $\theta \to \frac{9}{4}\pi$ is in agreement with the design curve (showing normalized frequency versus normalized inductance) for very small inductances in the 2nd order mode when $\Gamma = 3$.

For $\Gamma = 3$, if $n = 5$ (i.e. considering the 3rd order mode of this slotted SIW which is equivalent to the 5th order mode of the corresponding rectangular waveguide), then it follows from (2.33) that $\theta \to 3\pi$ for very small inductances. This is validated by the fact that $tan\,\theta + tan\,\frac{\theta}{3} = 0$ at $\theta = 3\pi$ is shown as the third zero in the positive θ-axis of the function $y = tan\,\theta + tan\,\frac{\theta}{3} = 0$ in the last Cartesian plot. This result that $\theta \to 3\pi$ is in agreement with the design curve (showing normalized frequency versus normalized inductance) for very small inductances in the 3rd order mode when $\Gamma = 3$.

Now consider the cases where $\Gamma = 4$.

For $\Gamma = 4$ and $n = 2$ (i.e. considering the 1st order mode of this slotted SIW which is equivalent to 2nd order mode of the corresponding rectangular waveguide), then it follows from (2.33) that $\theta \to \frac{4}{5}\pi$ for very small inductances. This is validated by the fact that $tan\,\theta + tan\,\frac{\theta}{4} = 0$ (by setting $h' = 0$ in (2.32)) at $\theta = \frac{4}{5}\pi$ is shown as the first zero in the positive θ-axis of the function $y = tan\,\theta + tan\,\frac{\theta}{4} = 0$ in the Cartesian plot below. This result that $\theta \to \frac{4}{5}\pi$ is in agreement with the design curve (showing normalized frequency versus normalized inductance) for very small inductances in the 1st order mode when $\Gamma = 4$.

For $\Gamma = 4$ and $n = 3$ (i.e. considering the 2nd order mode of this slotted SIW which is equivalent to 3rd order mode of the corresponding rectangular waveguide), then it follows from (2.33) that $\theta \to \frac{8}{5}\pi$ for very small inductances. This is validated by the fact that $tan\,\theta + tan\,\frac{\theta}{4} = 0$ (setting $h' = 0$ in the inductive cut-off equation) at $\theta = \frac{8}{5}\pi$ is shown as the second zero in the positive θ-axis of the function $y = tan\,\theta + tan\,\frac{\theta}{4} = 0$ in the Cartesian plot below. This result that $\theta \to \frac{8}{5}\pi$ is in agreement with the design curve (showing normalized frequency versus normalized inductance) for very small inductances in the 2nd order mode when $\Gamma = 4$.

For $\Gamma = 4$ and $n = 4$ (i.e. considering the 3rd order mode of this slotted SIW which is equivalent to 4th order mode of the corresponding rectangular waveguide), then it follows

from (2.33) that $\theta \to \frac{12}{5}\pi$ for very small inductances. This is validated by the fact that $tan\,\theta + tan\,\frac{\theta}{4} = 0$ (setting $h' = 0$ in the inductive cut-off equation) at $\theta = \frac{12}{5}\pi$ is shown as the third zero in the positive θ-axis of the function $y = tan\,\theta + tan\,\frac{\theta}{4} = 0$ in the Cartesian plot below. This result that $\theta \to \frac{12}{5}\pi$ is in agreement with the design curve (showing normalized frequency versus normalized inductance) for very small inductances in the 3rd order mode when $\Gamma = 4$.

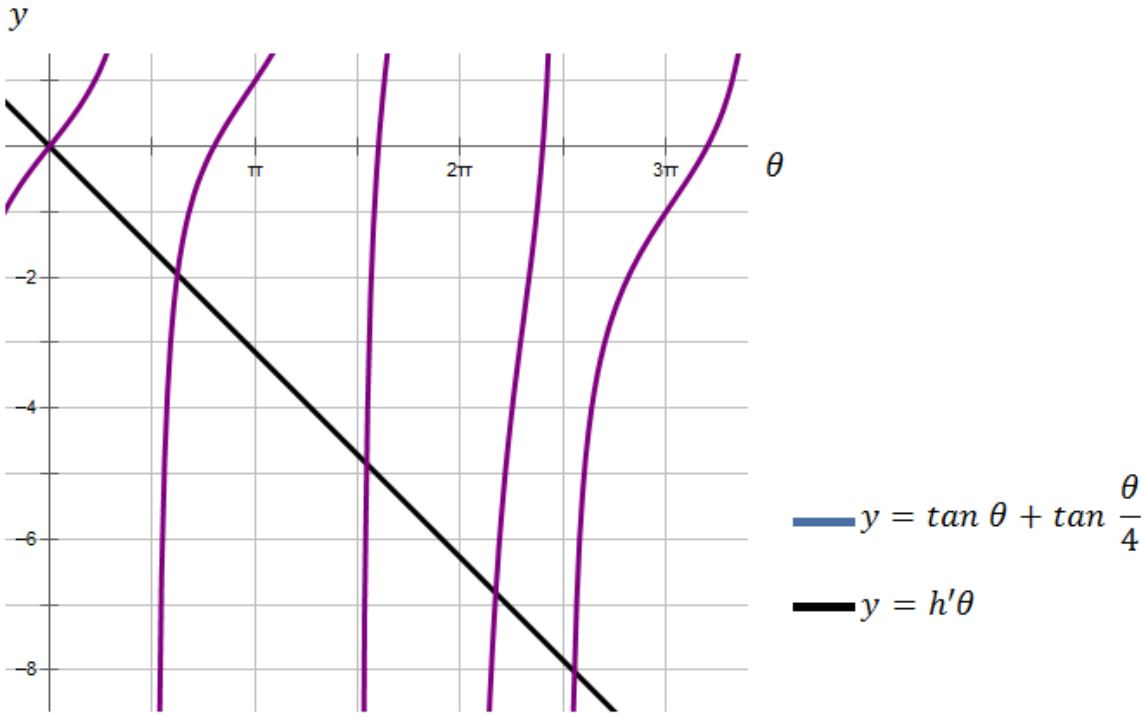

Figure 2.13: Cartesian plot of left and right hand side terms of the inductive cut-off equation for Γ=4 and h'= -1.

2.9. Calculation of load-element capacitances across a slot

Recall that the cutoff equation for a purely capacitive slot with capacitance C' per unit length is given by (2.31). By substituting (2.2) into (2.31), it is easily seen that

$$tan\ k_x L_1 = \frac{1}{\omega C' b\sqrt{\frac{\mu}{\varepsilon}}} - tan\ k_x L_2 . \qquad (2.34)$$

Since $\Gamma = \frac{L_1}{L_2}$, it follows that

$$tan\,\theta + tan\,\frac{\theta}{\Gamma} = \frac{1}{\omega C' b\sqrt{\frac{\mu}{\varepsilon}}} , \qquad (2.35)$$

where, by applying (2.2) with (2.28),

$$\theta = k_x L_1 . \qquad (2.36)$$

By noticing that

$$\frac{1}{\omega C' b\sqrt{\frac{\mu}{\varepsilon}}} = \frac{\varepsilon}{k_x C' b} = \frac{\varepsilon L_1}{\theta C' b} = \frac{\varepsilon L_1}{\theta C' b} = \frac{L_1}{\hat{C}\theta} , \qquad (2.37)$$

for which (2.29) is used to establish the last equality, it now follows easily that

$$tan\,\theta + tan\,\frac{\theta}{\Gamma} = \frac{L_1}{\hat{C}\theta} , \qquad (2.38)$$

from which θ can be determined for suitable values of C'.

At the point of cutoff, we have from (2.2) and (2.36) that

$$\theta = \omega\sqrt{\mu\varepsilon}L_1 = 2\pi f_c\sqrt{\mu\varepsilon}L_1 , \qquad (2.39)$$

where the cutoff frequency is denoted as f_c. It follows that

$$f_c = \frac{\theta}{2\pi\sqrt{\mu\varepsilon}L_1} = \frac{\theta}{\pi}\bullet\frac{v_p}{2L_1} = \frac{\theta}{\pi}\bullet\frac{c}{2\sqrt{\varepsilon_r}L_1} , \qquad (2.40)$$

where we make use of the fact that the phase velocity v_p is given by

$$v_p = \frac{1}{\sqrt{\mu\varepsilon}} = \frac{1}{\sqrt{\mu_0\varepsilon_0\varepsilon_r}} = \frac{c}{\sqrt{\varepsilon_r}} , \qquad (2.41)$$

for which c is the speed of light in a vacuum.

These last equations may therefore be used to obtain calculated predictions for the cutoff frequency f_c over an appropriate range of values of C'. Comparisons of these predictions will now be made with those from CST Microwave Studio and HFSS.

It is mentioned in [6] that in practice the inherent capacitance per unit length of the slot (which is referred to as C_{slot}) can be taken to be 0.1 pF over a distance of 5 mm, i.e. $C_{slot} = 20$ pF/m. The slot is loaded with additional capacitance. This total loaded capacitance is the sum of a ladder of identical elemental capacitances, each of which are connected across the slot at an interval spacing of $d = 5$ mm apart (along the full length of the waveguide) in parallel to one another. Each load-element capacitance is defined to be C_{load}. The total loaded capacitance per unit metre across the slot is therefore given by $\frac{C_{load}}{d}$, and it can also regarded as being in parallel with C_{slot} , so that the total capacitance per unit metre of the slot is given by

$$C' = C_{slot} + \frac{C_{load}}{d} . \qquad (2.42)$$

It follows immediately that

$$C_{load} = (C' - C_{slot}) \bullet d \ , \qquad (2.43)$$

from which, because the total slot capacitance per unit length C' is at least 20 pF/m in practice, it is evident that

$$C_{load} = (C' - 20) \bullet 5 \times 10^{-3} \ , \qquad (2.44)$$

in pF. It follows from the last formula that it is possible to calculate corresponding values of C_{load} for C' (as shown in the table below) which are then used to model specific slotted waveguide structures in CST Microwave Studio and HFSS.

C' (pF/m)	C_{load} (pF)
20	0
100	0.4
200	0.9
350	1.65
500	2.4
750	3.65
1000	4.9

Figure 2.14: Table for loaded capacitances

It will be demonstrated how CST Microwave Studio and HFSS can be used to predict the cut-off frequencies from the subsequent definitions for the values for C' in the table above. The slotted SIW structures which are considered have width $a = 20$ mm, height $b = 1.575$ mm and relative permittivity $\varepsilon_r = 2.2$. Three such waveguide structures are considered, namely those with $\Gamma = \frac{3}{2}, 3, 6$.

2.10. Two standard definitions for the cutoff frequency

The cutoff frequency of microwave devices can be defined in several different ways. Two such cutoff conditions are described in this section, namely the 3dB cutoff frequency and the point at which the phase constant β in (2.45) is zero. These concepts are subsequently explained in greater detail.

i). 3dB cutoff frequency

In the case of a filter, the cutoff frequency is usually defined by a 3dB point. This is typically a frequency corresponding to a boundary point where a passband and transition band meet for which S_{21} is -3dB of the optimum passband value.

ii). Zero phase constant definition of cutoff frequency

The complex propagation constant of a plane electromagnetic wave is defined to be given by

$$\gamma = \alpha + j\beta \,, \qquad (2.45)$$

where $Re\{\gamma\} = \alpha$ is the attenuation constant (Np/m) and $Im\{\gamma\} = \beta$ is the phase constant (rad/m). The cutoff frequency can be defined by setting $\beta = 0$. This is equivalent to the condition described in (2.47), and is explained as follows.

By considering (1.2) , whilst noting that the waveguide is modelled by a lossless structure , it is evident that the propagation constant of a travelling electromagnetic wave is given by

$$\gamma = j\beta = j\sqrt{\varepsilon_r k_0^2 - {k_x}^2}\,, \qquad (2.46)$$

where k_x is given by (2.9), so that cutoff condition of $\beta = 0$ whilst noting (2.11) (from which the cutoff frequency f_c can be determined) also corresponds to the case when

$$\varepsilon_r k_0^2 = \left(\frac{m\pi}{a}\right)^2 . \qquad (2.47)$$

This method of evaluating the cutoff frequency at $\beta = 0$ is employed by HFSS, and it will be presented in further detail later.

2.11. Elimination of the 3dB cutoff frequency definition

The well-known Helmholtz equation for the electric phasor field (see [1] or [2]) is given by

$$\nabla^2 \boldsymbol{E} = -\gamma^2 \boldsymbol{E}\,, \qquad (2.48)$$

which may be derived directly from Maxwell's equations (as in [1]) .

Suppose, as in standard notation from [1] or [2], that left hand rectangular x, y, z-coordinates (on axes parallel to the width, height and length of the SIW, respectively) are applied. By considering that the TE_{10} mode in a rectangular waveguide, the last equation may be reduced to

$$\frac{\partial^2 E_y}{\partial z^2} - \gamma^2 E_y = 0\,, \qquad (2.49)$$

from which it is evident (and indeed well-known from [1] and [2]) that the solution of a forward-travelling electromagnetic wave for the time harmonic case at angular frequency ω is given by

$$E_x(z) = E^+ e^{-j\gamma z}\,, \qquad (2.50)$$

where E^+ represents the amplitude coefficient of the electromagnetic wave. Suppose that z_l represents the length of the waveguide. By noting that if either α or β are vanishly small, then the corresponding frequency f at $z = z_l$ is either larger or smaller than the cutoff frequency f_c, respectively. Hence the S-parameter S_{21} is given by

$$S_{21} = \begin{cases} e^{-j\beta z_l}, & f > f_c . \\ e^{-\alpha z_l}, & f < f_c . \end{cases} \quad (2.51)$$

Hence S_{21} depends upon the length z_l of the waveguide. Therefore, by taking into consideration that the frequency is in fact a continuous parameter, it follows that if the cutoff frequency f_c is defined to be the 3dB point of S_{21}, then it would also be determined exclusively by the length of the waveguide. This cannot possibly be correct because the length of the loaded SSIW is not being varied. The fact the cutoff frequency $f_c$is not related to the length z_l of the waveguide can be confirmed by the following simple example. Consider two TE_{01} rectangular waveguides which have the same width $a = 20$ mm and height $b = 1.575$ mm , but which differ in length z_l so that one is 25 mm long and the other is 50 mm. By taking the standard dielectric constant $\varepsilon_r = 2.2$, the exact value for the cutoff frequency of each of these waveguides c an be evaluated from (2.11) to be 5.05GHz. The following two figures are HFSS simulations which illustrate how S_{21} varies with frequency in the shorter and longer waveguides, respectively. Both these S-parameter graphs support the fact that both waveguides share the same cutoff frequency.

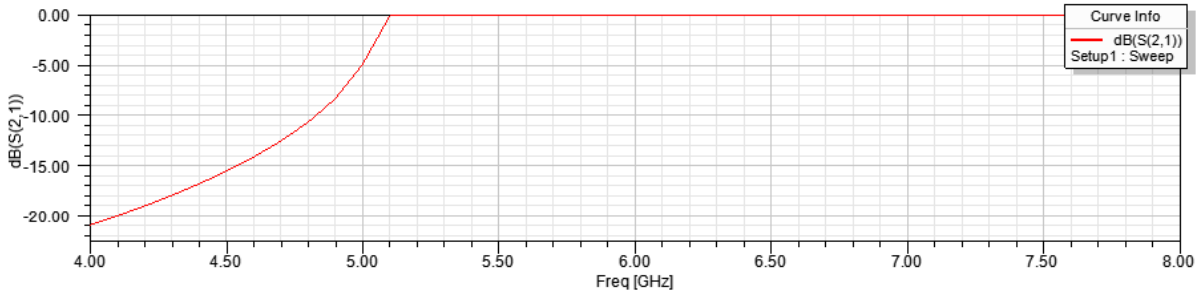

Figure 2.15: S-parameter plot for SIW of length 25 mm, with a=20mm and b=1.575mm.

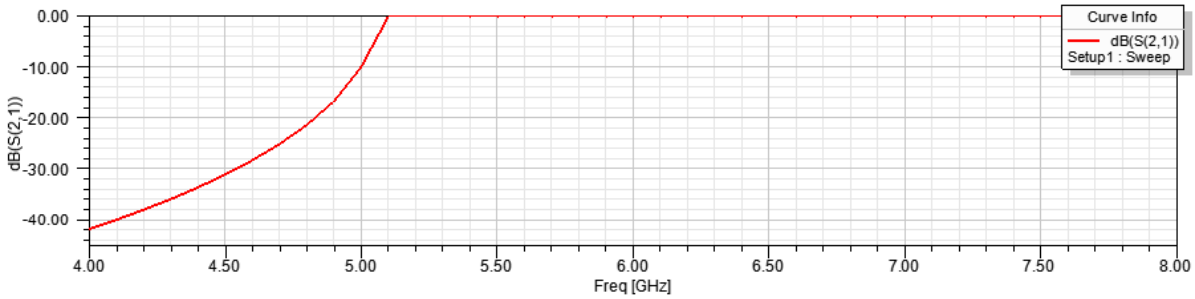

Figure 2.16: S-parameter plot for SIW of length 50 mm, with a=20mm and b=1.575mm.

Hence, the cutoff frequency of a waveguide is not related to its length, and so it cannot be defined by the 3dB point of any S-parameter. Other means of determining the cutoff frequency must therefore be sought.

2.12. Group delay definition for cutoff frequency

The phase of a propagating electromagnetic wave is given by

$$\varphi = -\beta L\,, \qquad (2.52)$$

over a distance L along the length of the waveguide. By considering the classical dispersion curve of β against frequency f (which can easily be determined either from (1.2) from the introductory chapter or from the Appendix at the end), the cut-off frequency corresponds to the point for which $\frac{d\beta}{df}$ is at its maximum value. It follows that this instance is also one for which the group delay, given by $\frac{d\varphi}{df}$, is at an infinitely negative value. In other words, the frequency gradient of the phase of the parameter S_{21} is at its most negative value at the point of cut-off. The fundamental cutoff frequency is not just identified by the group delay. It also occurs in a region for which the magnitude of S_{21} has just risen from zero for the first time (and, likewise, the magnitude of S_{11} has just started to reduce from its maximum value of 1), since electromagnetic fields are radiated from the slot at cutoff. An application of radiative fields from the slot are important in the construction of slot antennas which are investigated in [7]-[11].

2.13. Modelling specific capacitances across a slot

The group delay and S-parameter criteria in the preceding section are used to determine the cutoff frequency from CST Microwave Studio. Consider the case where $\Gamma = 3$ and $C' = 20$ pF/m, for which the following two figures are plots from CST Microwave Studio of how the magnitude and phase of the S-parameters (namely S_{11} and S_{21}) varies with frequency respectively. It is clear that the magnitude of S_{21} is rising from zero for the first time when the frequency is between 3GHz and 3.5 GHz. It remains to find exactly where in this frequency interval that gradient of the phase of S_{21} (i.e. group delay) is at an infinitely negative value. This is the point at which the frequency is approximately 3.09 GHz. Hence the cut-off frequency is approximately 3.09 GHz. It will also be illustrated later on that all such estimates of the cutoff frequency from CST are in close agreement with those from HFSS. It is also apparent from the phase plot, that the slotted waveguide can behave like a phase shifter. This is treated in more detail in [12]-[18].

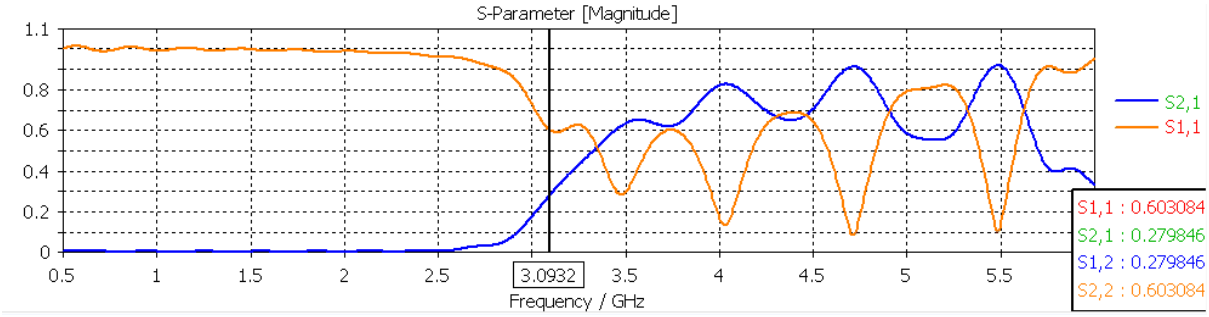

Figure 2.17: Magnitudes of S-parameters for Γ=3, C' = 20 pF/m

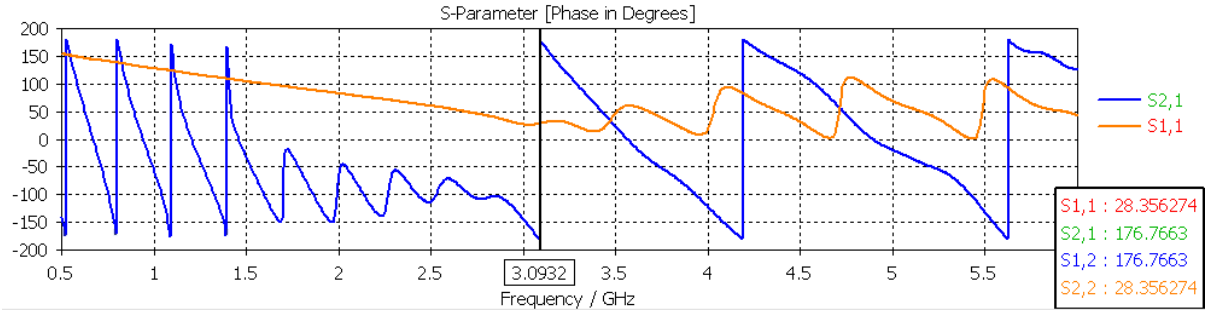

Figure 2.18: Phase plots of S-parameters for Γ=3, C' = 20 pF/m

In this way, the cut-off frequencies from CST Microwave Studio for the other values of C' are obtained for $\Gamma = 3,6,\frac{3}{2}$. These cut-off frequencies are shown with the subsequent plots of the magnitudes of the S-parameters. These simulation plots exhibit some degree of

ripple because of mismatch effects both below and above cut-off. However, this does not present ant difficulties, since only the cutoff frequencies are of interest. All the S-parameter plots that follow should not be regarded as representing the frequency characteristics of a working device. Instead, they signify different regions of operation which can be used to provide better understanding the behaviour of the slotted waveguides. It should be noted that these loaded waveguides are extremely complicated structures which are not easy to analyze. For instance, by considering the above phase plot of the S_{21} parameter, it is evident that in there is a fast mode region (after the point of capacitive cutoff) from 3GHz to 5.5GHz, since the phase varies less rapidly as compared with before. Selected S-parameter plots from CST Microwave Studio are shown in the subsequent figures along with their respective cutoff frequencies for the waveguide specifications given earlier.

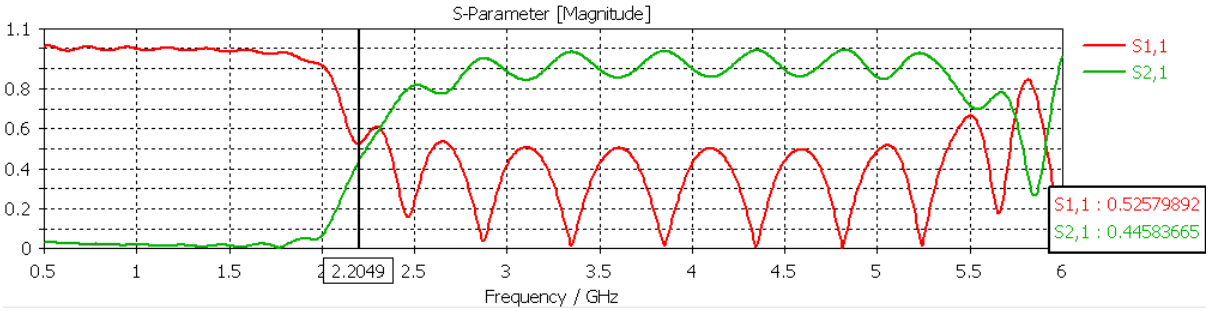

Figure 2.19: Magnitudes of S-parameters for Γ=3, C' = 100 pF/m

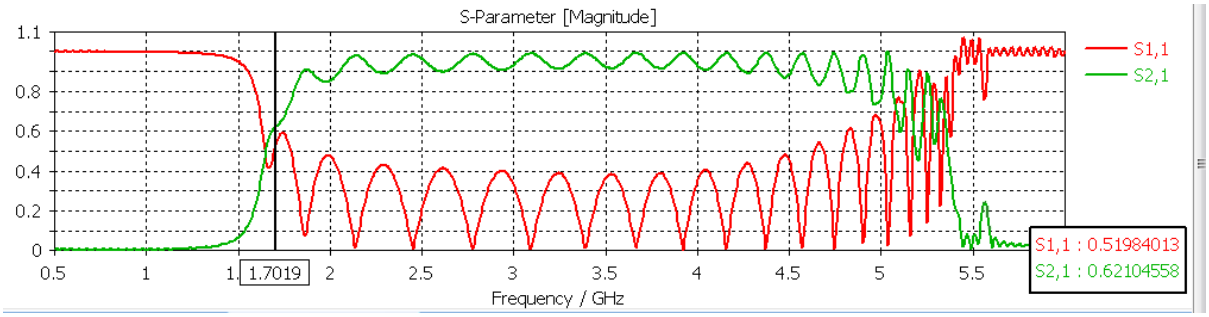

Figure 2.20: Magnitudes of S-parameters for Γ=3, C' = 200 pF/m

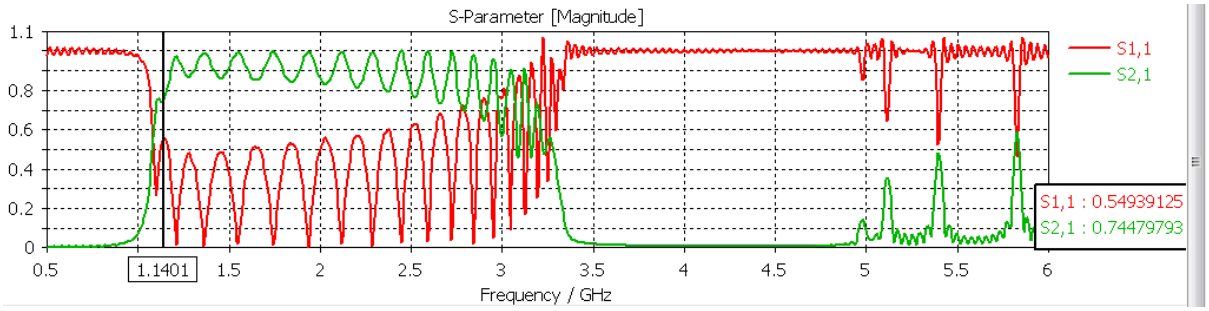

Figure 2.21: Magnitudes of S-parameters for Γ=3, C' = 500 pF/m

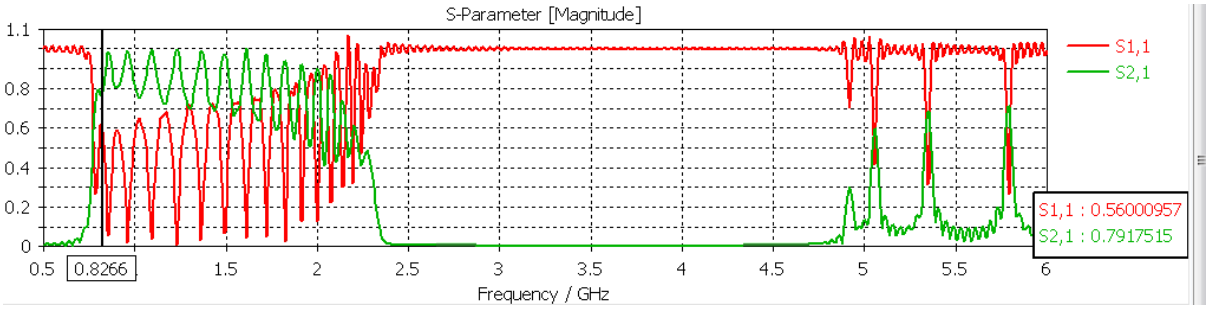

Figure 2.22: Magnitudes of S-parameters for Γ=3, C' = 1000 pF/m

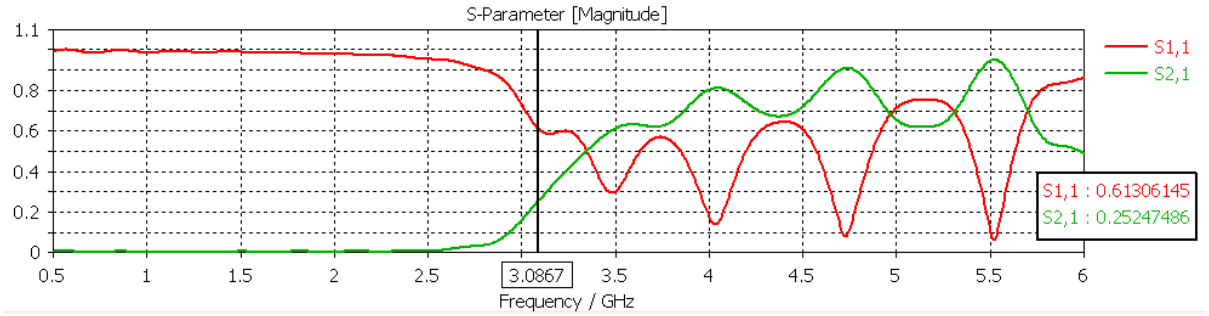

Figure 2.23: Magnitudes of S-parameters for Γ=6, C' = 20 pF/m

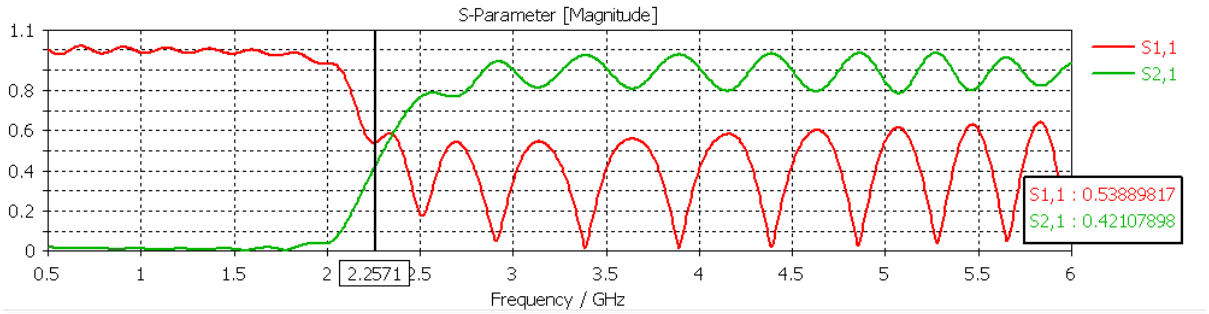

Figure 2.24: Magnitudes of S-parameters for Γ=6, C' = 100 pF/m

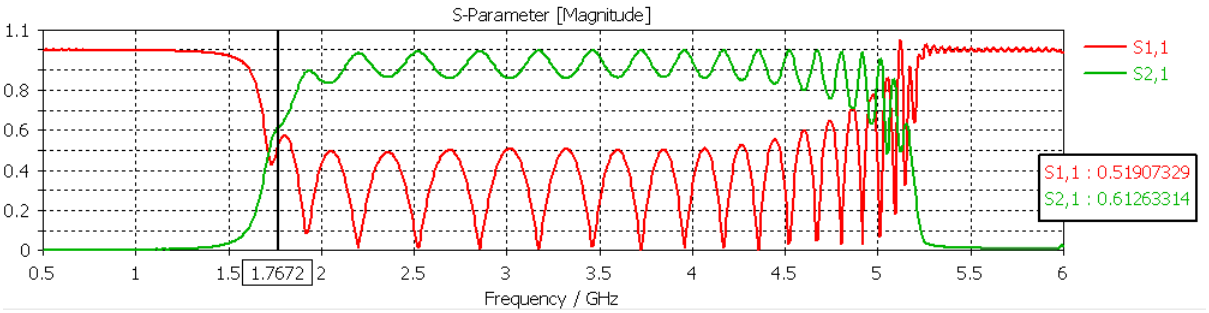

Figure 2.25: Magnitudes of S-parameters for Γ=6, C' = 200 pF/m

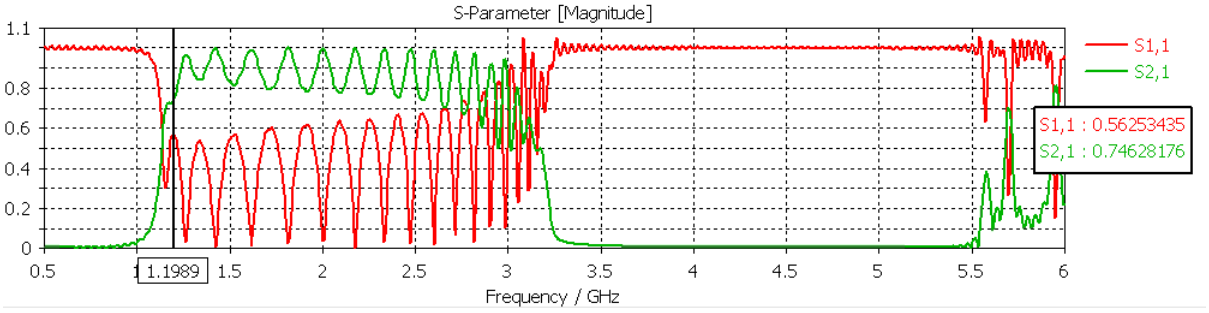

Figure 2.26: Magnitudes of S-parameters for Γ=6, C' = 500 pF/m

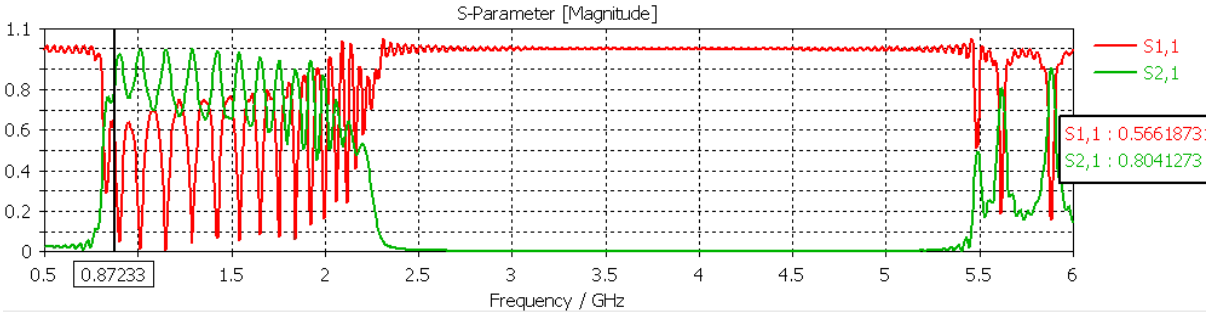

Figure 2.27: Magnitudes of S-parameters for Γ=6, C' = 1000 pF/m

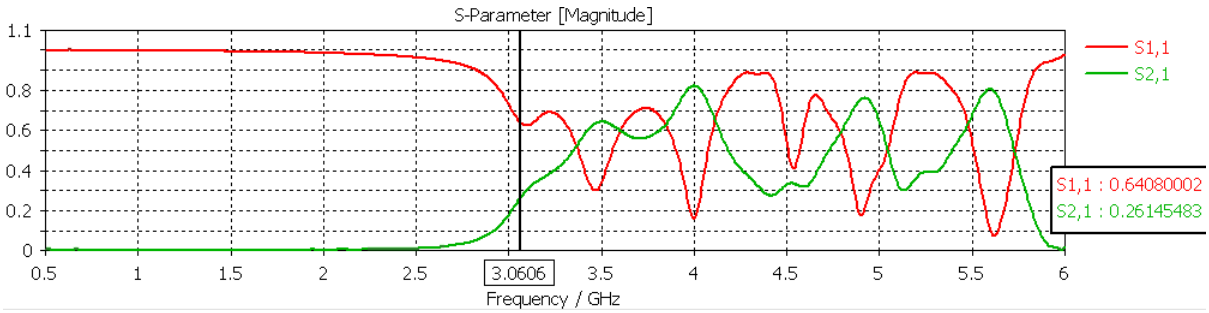

Figure 2.28: Magnitudes of S-parameters for Γ=1.5, C' = 20 pF/m

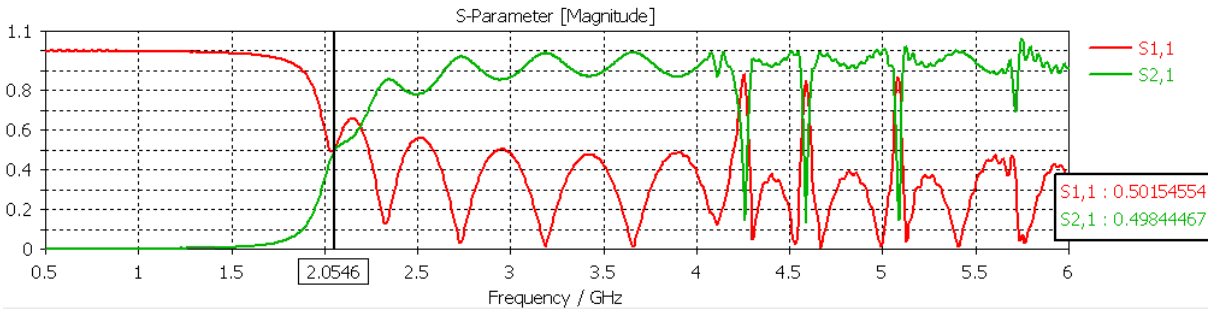

Figure 2.29: Magnitudes of S-parameters for Γ=1.5, C' = 100 pF/m

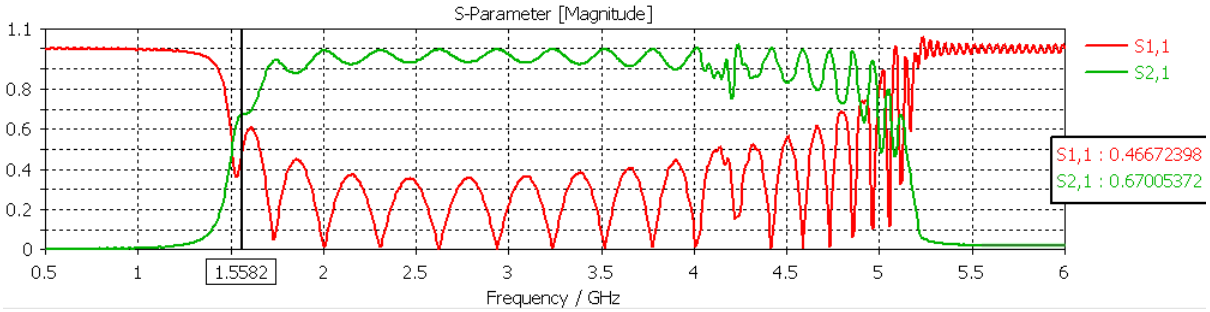

Figure 2.30: Magnitudes of S-parameters for Γ=1.5, C' = 200 pF/m

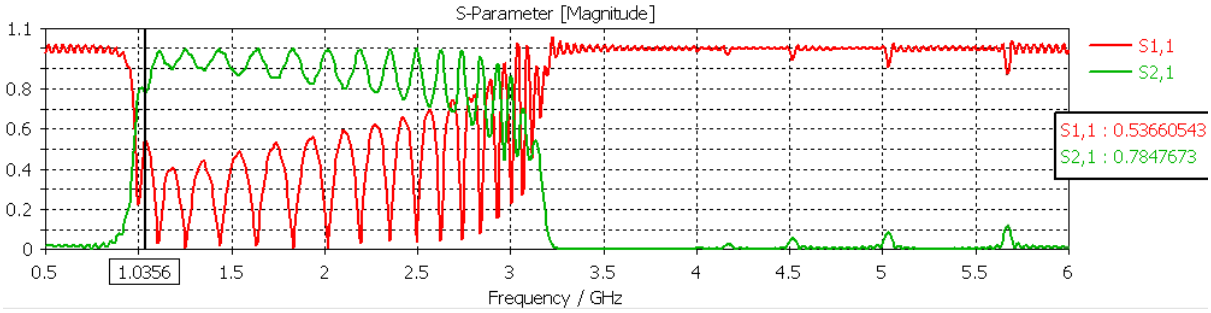

Figure 2.31: Magnitudes of S-parameters for Γ=1.5, C' = 500 pF/m

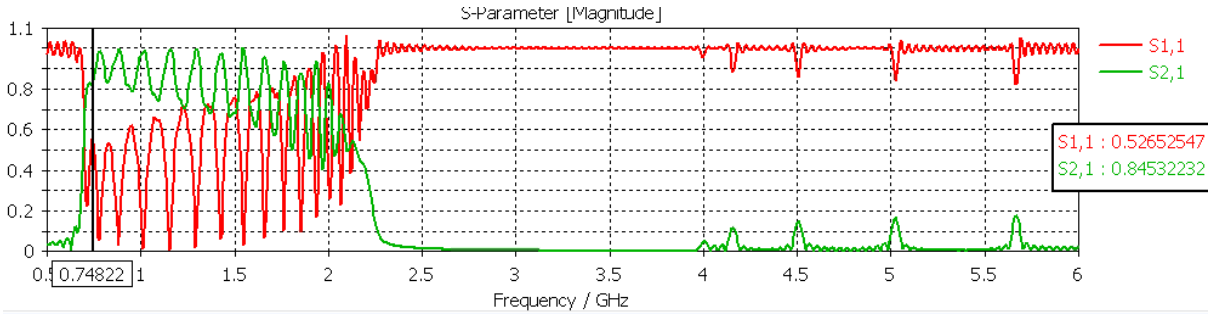

Figure 2.32: Magnitudes of S-parameters for Γ=1.5, C' = 1000 pF/m

The method of evaluating the cutoff frequency by using the zero phase constant definition is employed by using an eigenmode solver in HFSS. This eigenmode solver considers a single cell of the periodic structure (sketched in Figure 2.2) and calculates a resonance frequency associated with specific phase change on either side of this cell. The resonant frequency for zero phase (for which $\beta = 0$) corresponds to the HFSS estimate of the cutoff

frequency of the structure. Dispersion curves (for the same range of capacitances and waveguide structures) from HFSS are given as follows.

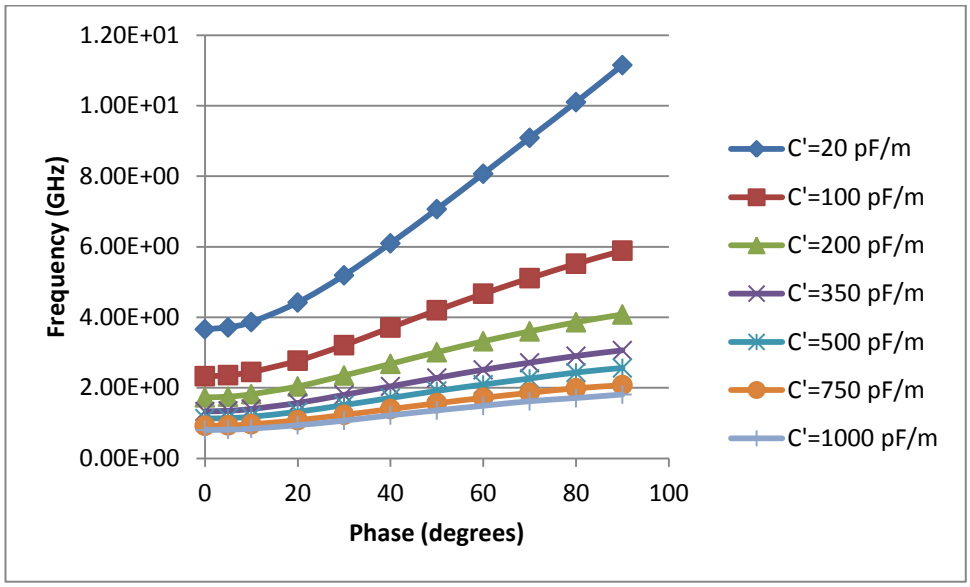

Figure 2.33: Dispersion curve from HFSS for SIW with Γ=1.5

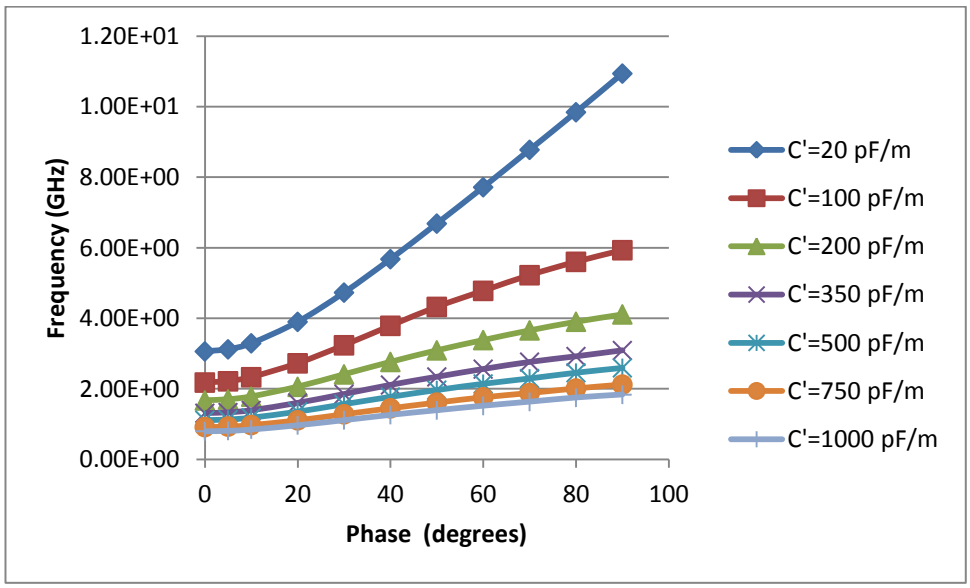

Figure 2.34: Dispersion curve from HFSS for SIW with Γ=3

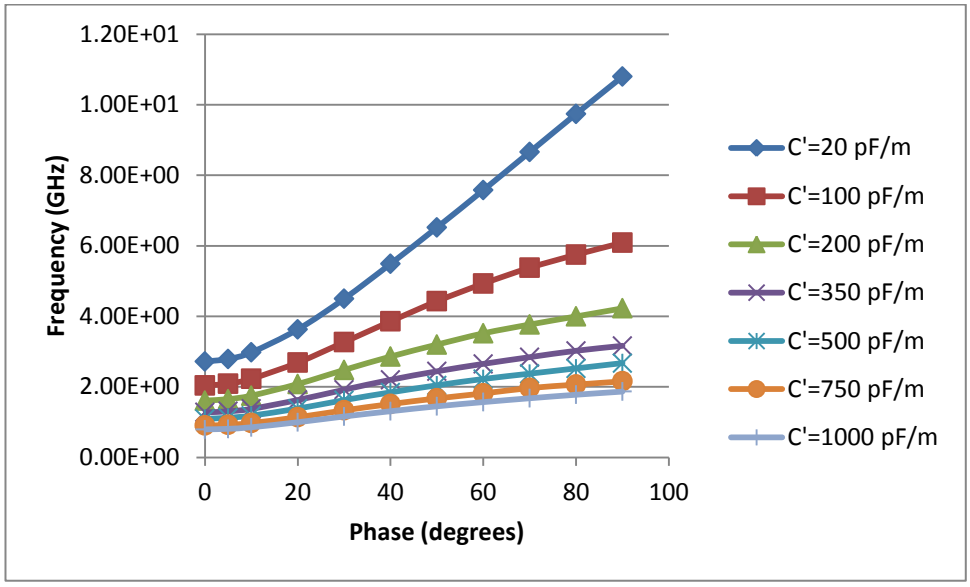

Figure 2.35: Dispersion curve from HFSS for SIW with Γ=6

The predictions for the cut-off frequencies of the fundamental mode by both CST Microwave Studio and HFSS are in close agreement with those made by the transverse resonance technique, as shown in the following three figures.

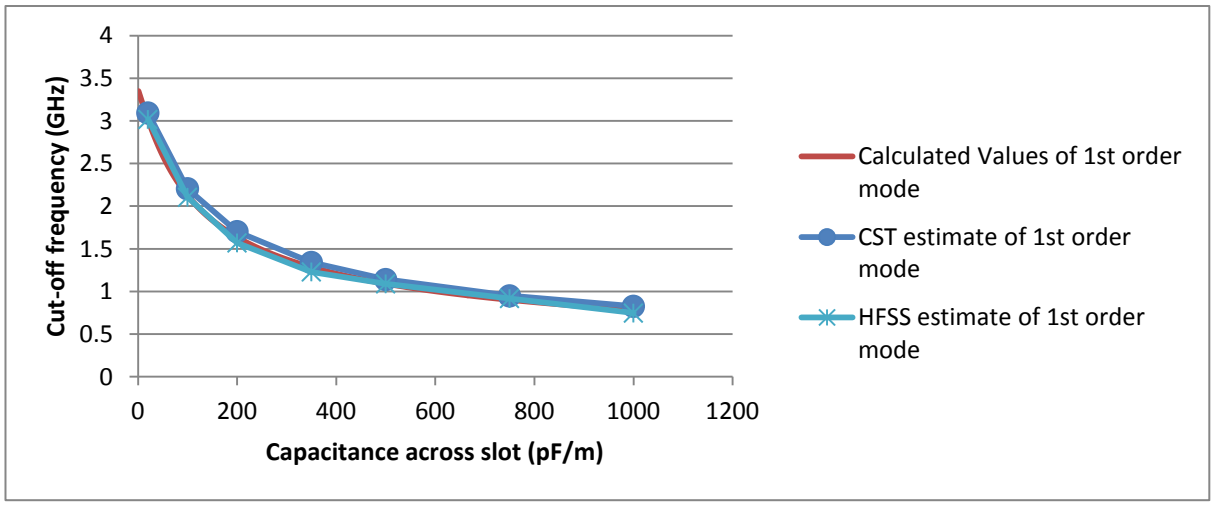

Figure 2.36: Predictions for cut-off frequency for Γ=3

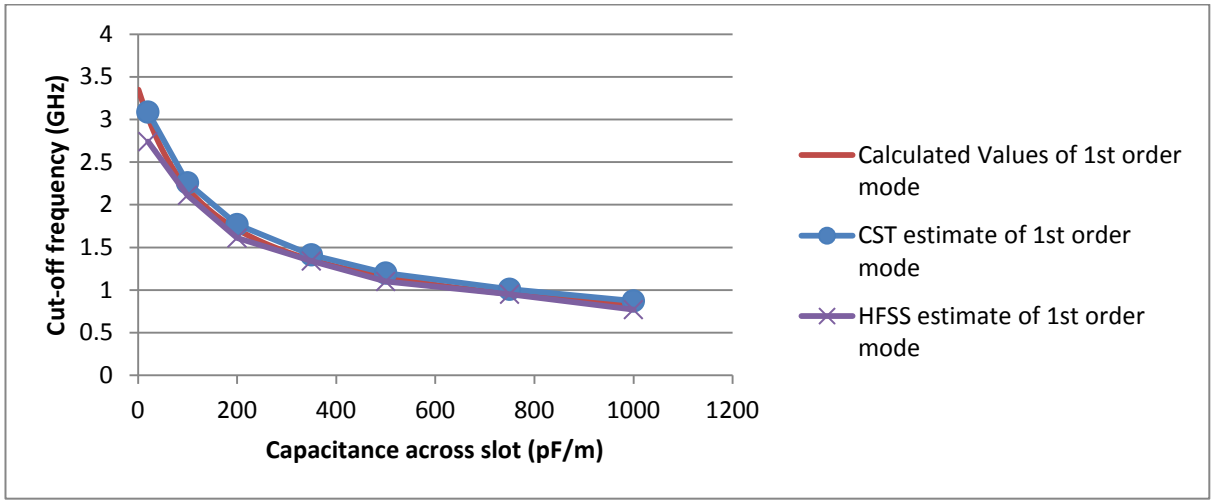

Figure 2.37: Predictions for cut-off frequency for Γ=6

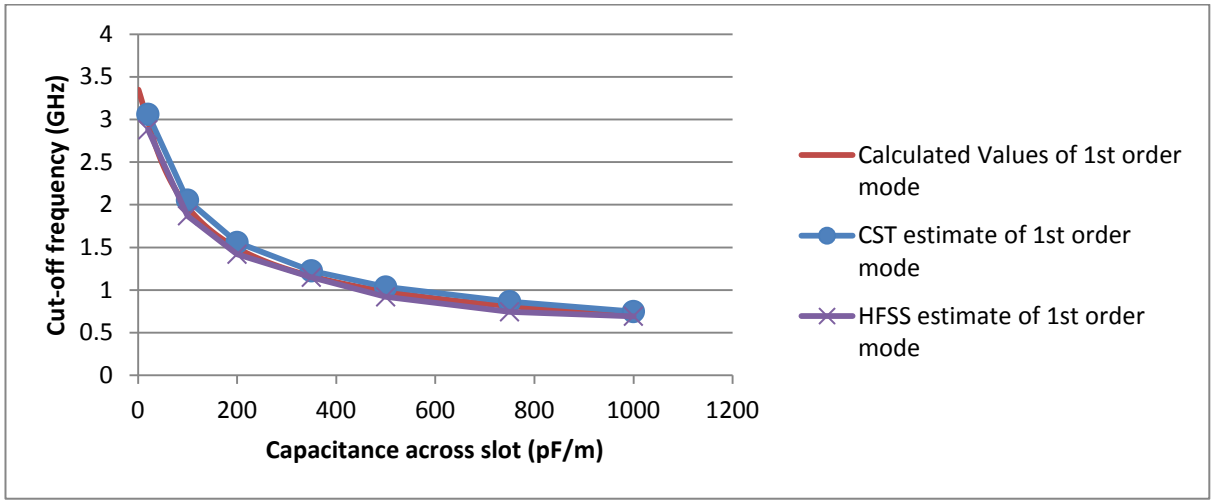

Figure 2.38: Predictions for cut-off frequency for Γ=1.5

The following figure shows that the design curves cut-off frequencies for the specified values of Γ are relatively close to one another.

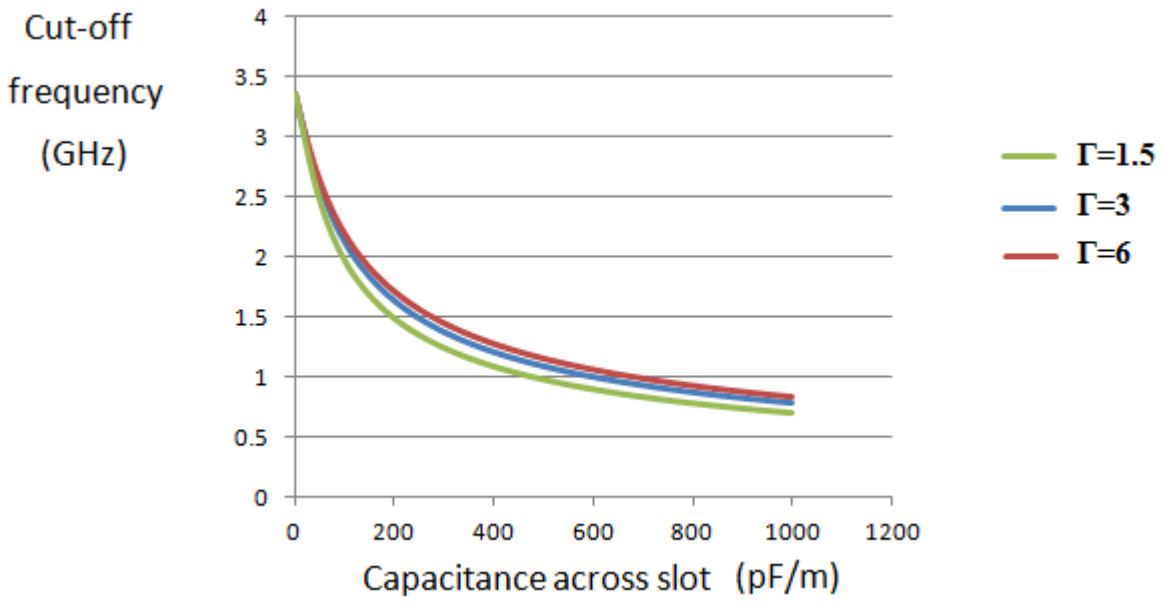

Figure 2.39: Predictions for cut-off frequency from transverse resonance technique

Some field plots in a certain interesting case considered above, namely for $\Gamma = 3$ and C'=500pF/m at 1.5GHz (which is just above the cut-off frequency), are presented here. The next figure shows the pattern of the component of electric field which travels from the top of the guide to its base. It is evident from this that the alternating electric field oscillates throughout the length of the guide.

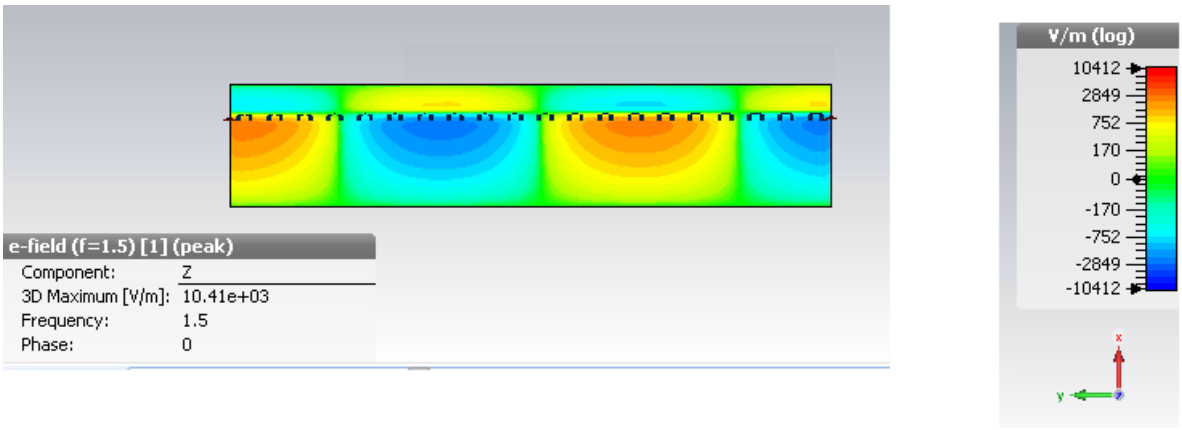

Figure 2.40: An aerial view field plot of E_z 0.4mm from the base of the guide for Γ=3 and a slot loaded with C' = 500 pF/m at 1.5GHz

The following figure shows that the cross-sectional electric field vector pattern on the incident port of the waveguide is largest when closest to the slot.

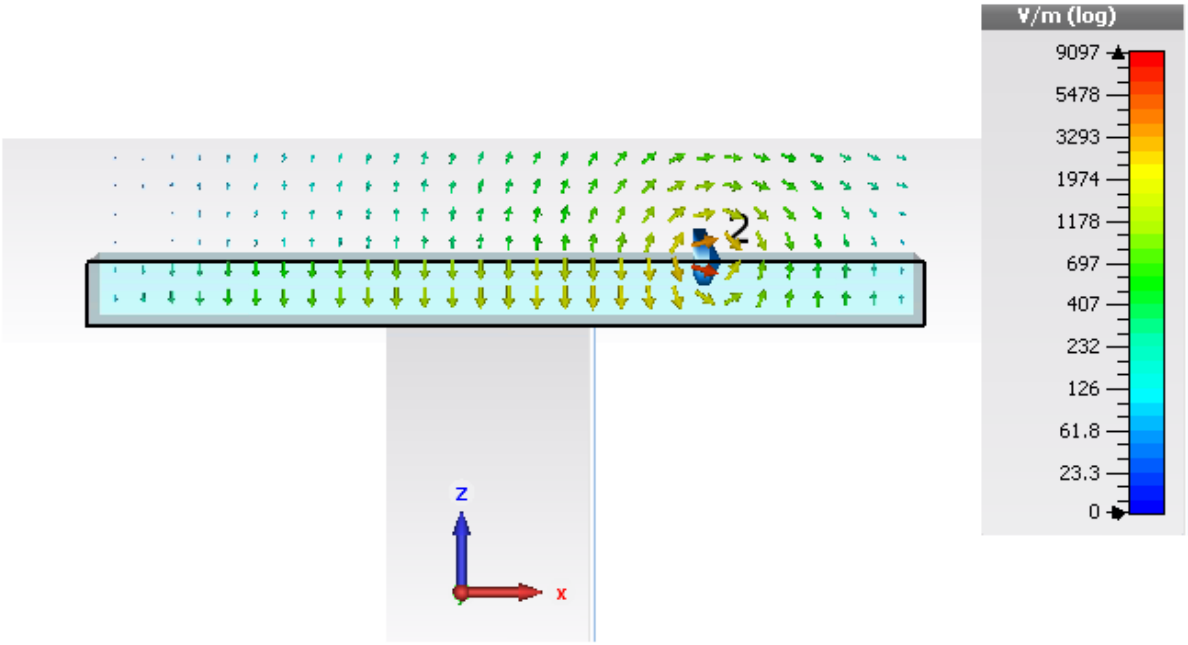

Figure 2.41: A cross-sectional E-field plot 5mm inside the incident port of the guide for Γ=3 and a slot loaded with C' = 500 pF/m at 1.5GHz

It turns out that the field patterns do not significantly change so much at higher frequencies which are close to the next higher order mode.

2.14. Modelling specific inductances across a slot

The cut-off equation for a purely inductive slot with inductance L' per unit length is given by (2.20), which, by using the expression for k_x given by (2.2), may be rewritten as

$$tan\ k_x L_1 = -\frac{\omega L'}{b\sqrt{\frac{\mu}{\varepsilon}}} - tan\ k_x L_2\ . \qquad (2.53)$$

Since $\Gamma = \frac{L_1}{L_2}$, it follows that

$$tan\ \theta + tan\ \frac{\theta}{\Gamma} = -\frac{\omega L'}{b\sqrt{\frac{\mu}{\varepsilon}}}\ , \qquad (2.54)$$

where $\theta = k_x L_1$ by (2.28) and (2.2).

By noticing that

$$\frac{\omega L'}{b\sqrt{\frac{\mu}{\varepsilon}}} = \frac{\omega\sqrt{\mu\varepsilon}L'}{b\mu} = \frac{k_x L_1 L'}{b\mu L_1} = \frac{\theta L'}{L_1 b\mu} = \frac{\hat{L}\theta}{L_1}, \qquad (2.55)$$

where $\hat{L} = \frac{L'}{b\mu}$ by using (2.30), it now follows easily that

$$tan\,\theta + tan\,\frac{\theta}{\Gamma} = -\frac{\hat{L}\theta}{L_1}, \qquad (2.56)$$

from which θ may be determined from suitable values of L'.

By applying (2.39), (2.40) and (2.41) and (2.56) it is possible to obtain the cut-off frequency f_c over an appropriate range of values of L'.

In this way, calculated predictions for the cut-off frequency f_c are made over an appropriate range of values of L' from 0.3 pH/m to 300pH/m. These predictions are compared with those from CST Microwave Studio.

The slot is loaded with an inductance as follows. This total loaded inductance is the sum of a ladder of identical elemental inductances, each of which are connected across the slot at an interval spacing of $d = 5 \times 10^{-3}$ m apart (along the full length of the waveguide) in parallel to one another. The total number of of these identical elemental inductances over a length l, where l is a positive integer multiple of d, is therefore given by

$$N = \frac{l}{d}. \qquad (2.57)$$

Each load-element inductance is defined to be L_{load}. The total loaded inductance per unit length l across the slot can be denoted as equivalent to N identical elemental inductances in parallel to one another, and so it is given by

$$L' = \frac{L_{load}}{(Nl)}. \qquad (2.58)$$

The last two equations then imply that

$$L' = \frac{L_{load} \bullet d}{l^2} \ , \qquad (2.59)$$

where the length l is set to 1m, so that L' represents inductance per unit metre and $N = 200$. It follows from the last formula that we can calculate corresponding values of L_{load} for L' (as shown in the table below) which are then used to model specific inductively slotted waveguide structures in CST Microwave Studio and HFSS as before.

L' (pH/m)	L_{load} (nH)
0.3	0.06
3	0.6
30	6
100	20
200	40
300	60

Figure 2.42: Table for loaded inductances

Now both CST Microwave Studio and HFSS is used in the same manner as before to predict the cut-off frequencies from the values for L' in the table above. Once again, slotted SIW structures with width $L_1 = 15$ mm, height $b = 1.575$ mm and relative permittivity $\varepsilon_r = 2.2$, are investigated. The same three waveguide structures are considered, namely those with $\Gamma = 3,6,\frac{3}{2}$. Selected S-parameter plots from CST Microwave Studio are shown along with their respective cutoff frequencies as follows.

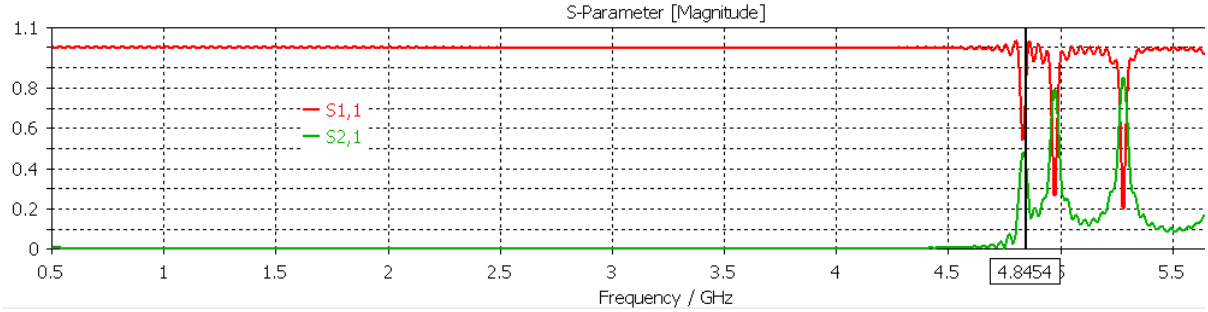

Figure 2.43: Magnitudes of S-parameters for Γ=3, L' = 0.3 pH/m

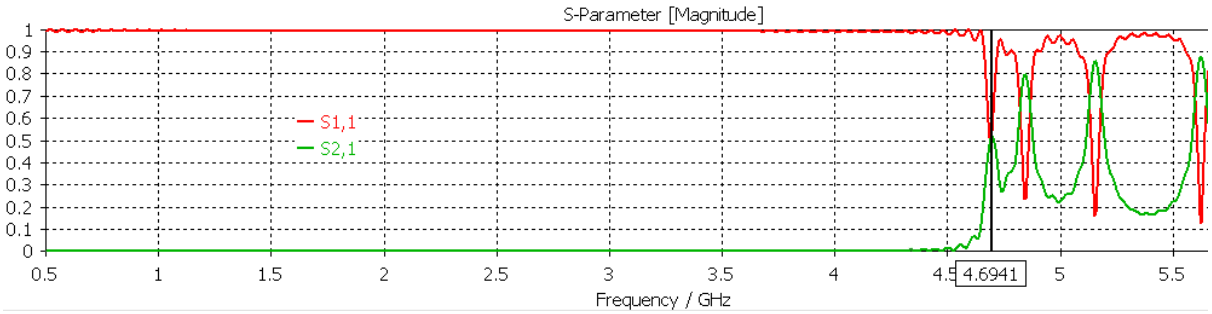

Figure 2.44: Magnitudes of S-parameters for Γ=3, L' = 3 pH/m

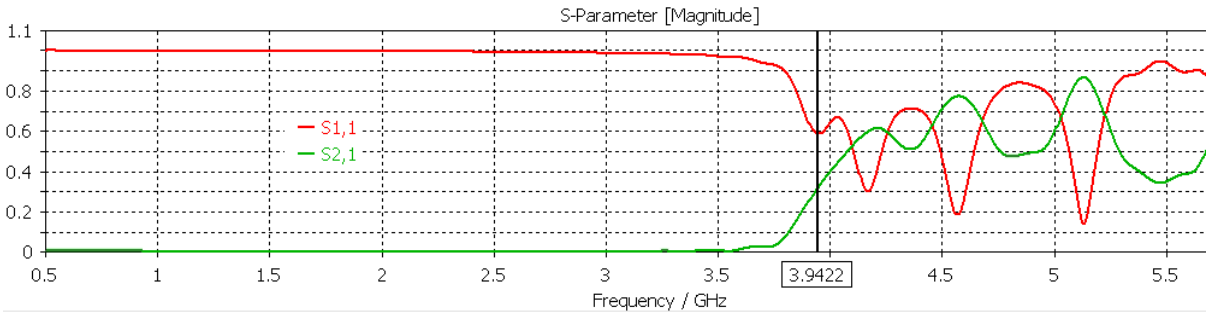

Figure 2.45: Magnitudes of S-parameters for Γ=3, L' = 30 pH/m

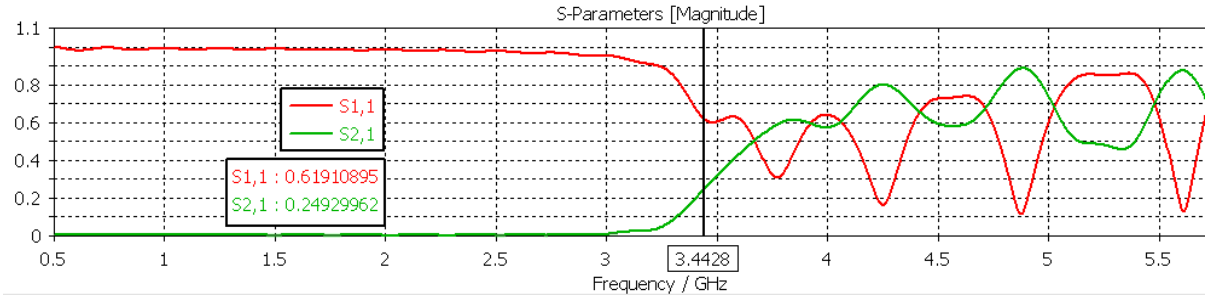

Figure 2.46: Magnitudes of S-parameters for Γ=3, L' = 100 pH/m

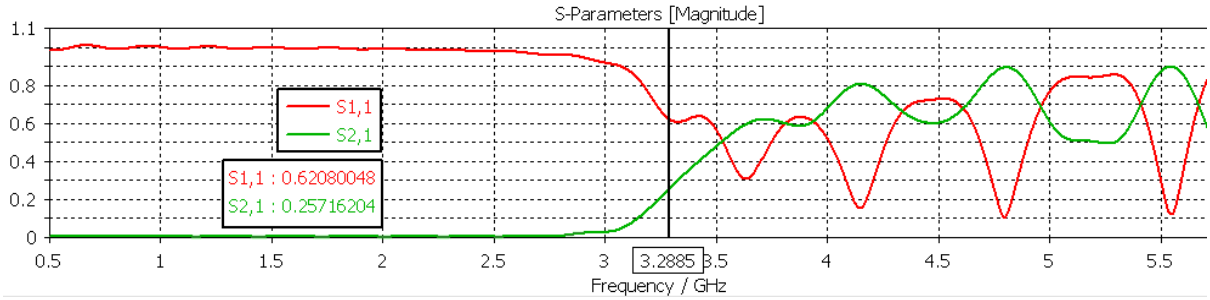

Figure 2.47: Magnitudes of S-parameters for Γ=3, L' = 200 pH/m

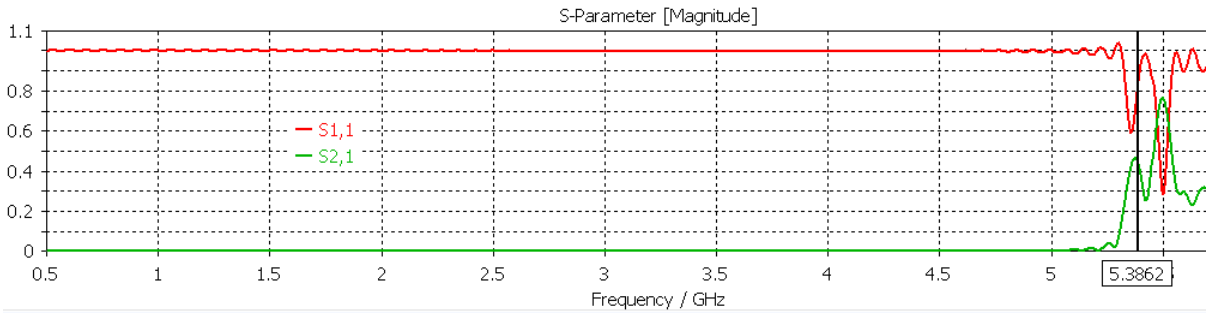

Figure 2.48: Magnitudes of S-parameters for Γ=6, L' = 0.3 pH/m

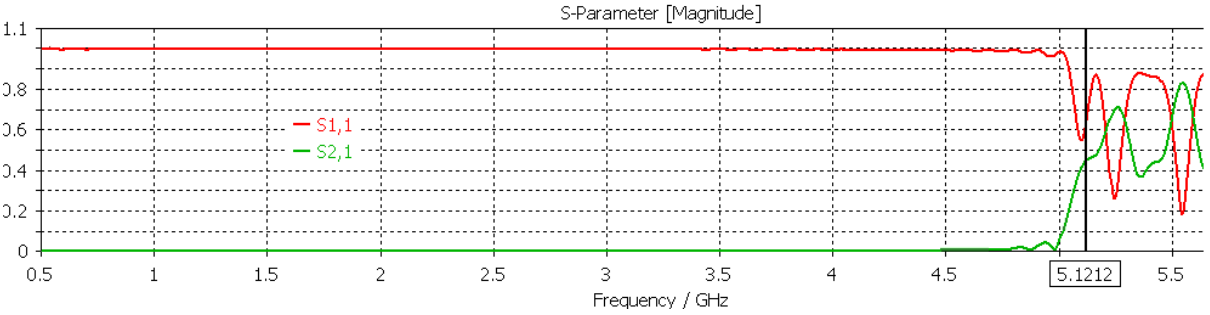

Figure 2.49: Magnitudes of S-parameters for Γ=6, L' = 3 pH/m

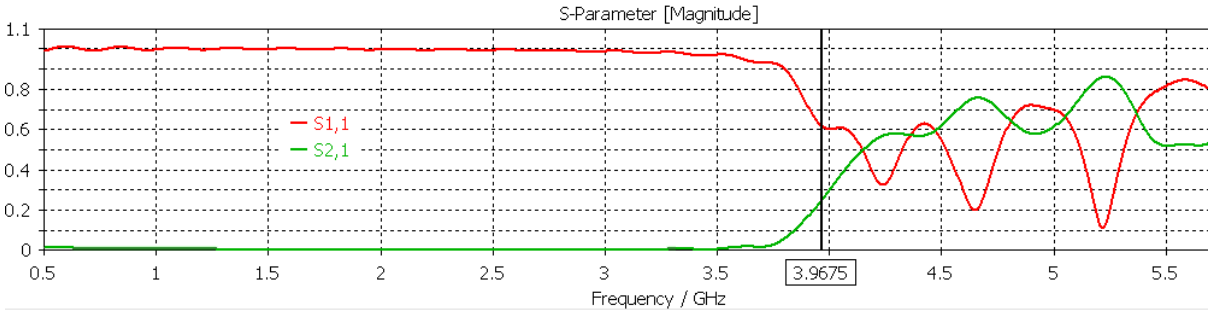

Figure 2.50: Magnitudes of S-parameters for Γ=6, L' = 30 pH/m

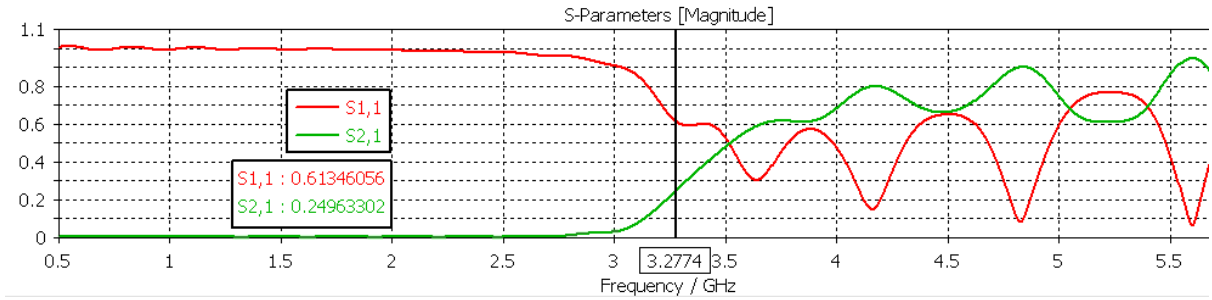

Figure 2.51: Magnitudes of S-parameters for Γ=6, L' = 200 pH/m

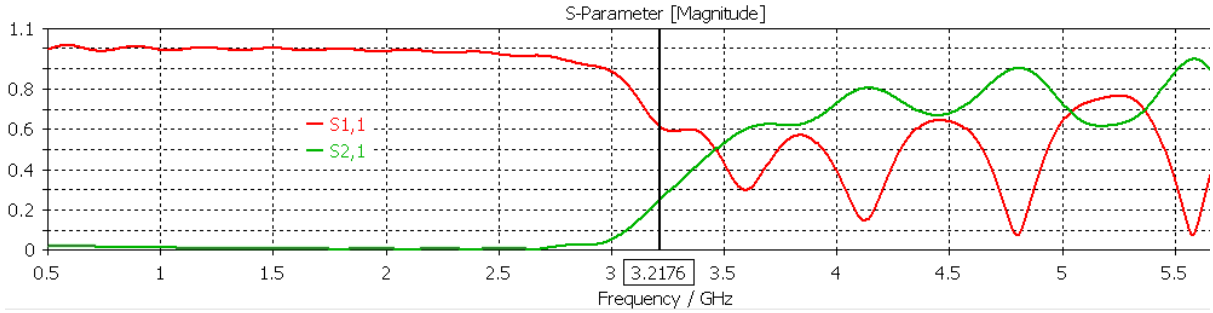

Figure 2.52: Magnitudes of S-parameters for Γ=6, L' = 300 pH/m

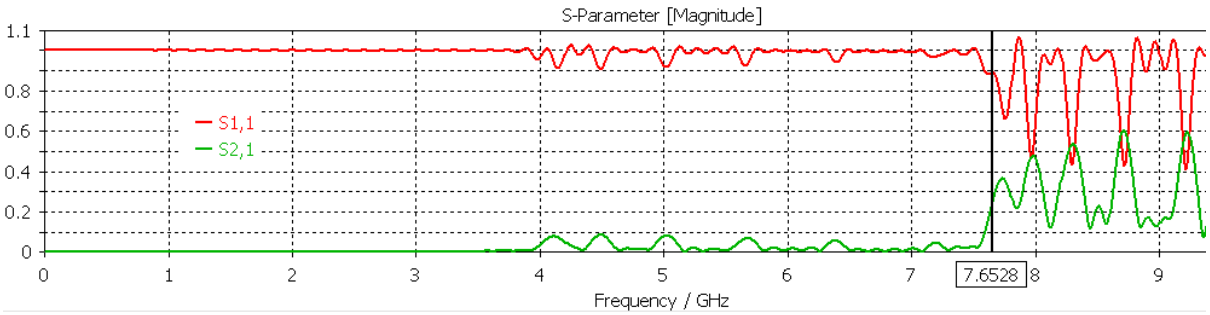

Figure 2.53: Magnitudes of S-parameters for Γ=1.5, L' = 0.3 pH/m

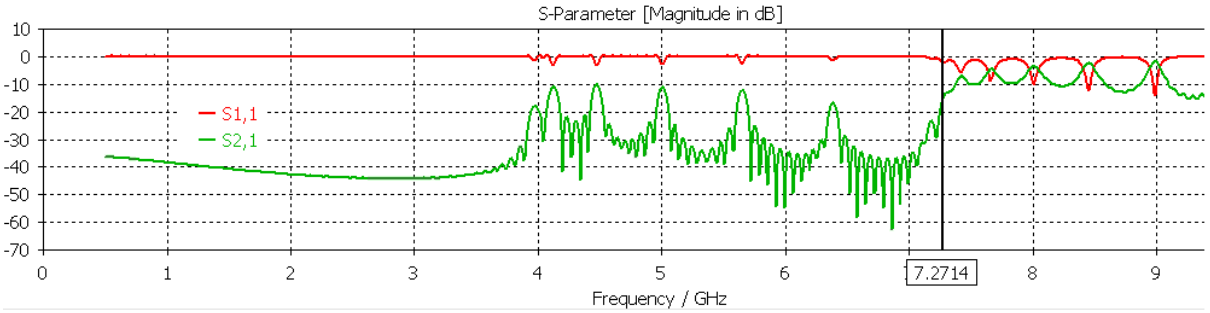

Figure 2.54: Magnitudes of S-parameters for Γ=1.5, L' = 3 pH/m

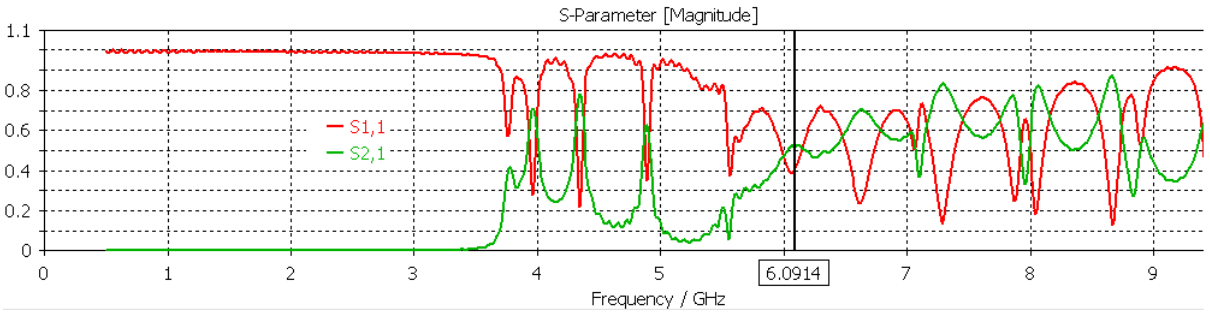

Figure 2.55: Magnitudes of S-parameters for Γ=1.5, L' = 30 pH/m

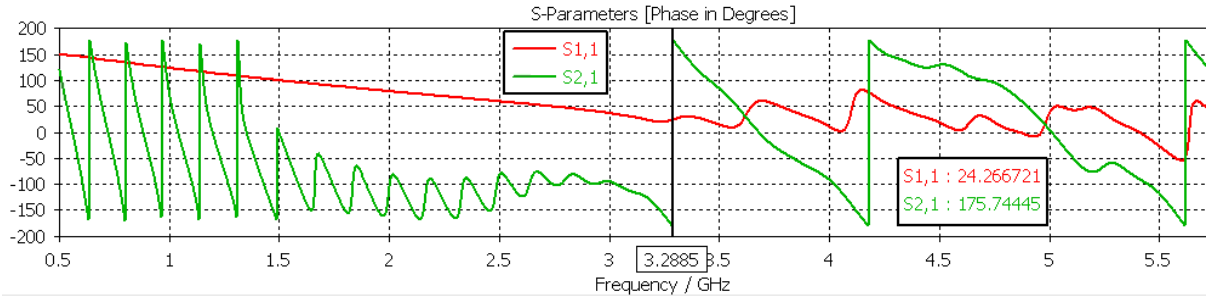

Figure 2.56: Magnitudes of S-parameters for Γ=1.5, L' = 200 pH/m

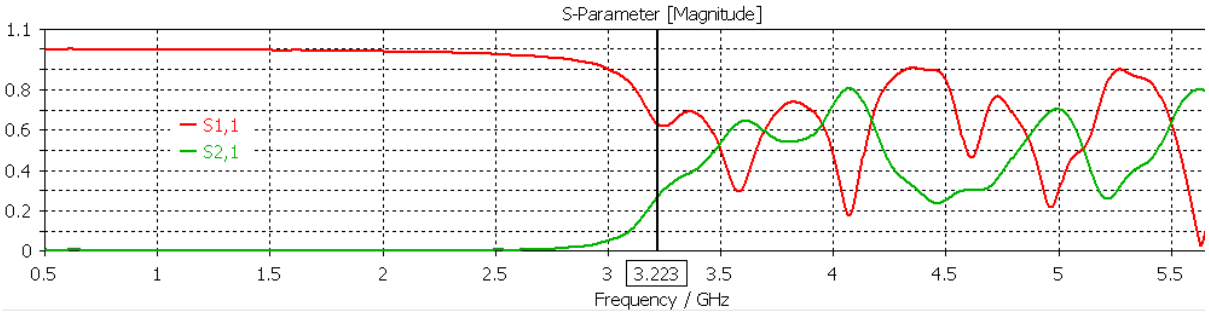

Figure 2.57: Magnitudes of S-parameters for Γ=1.5, L' = 300 pH/m

The corresponding dispersion curves from HFSS, which are obtained in the same manner as before, are provided in the following figures. Recall that the cutoff frequency estimate from HFSS is obtained by considering $\beta = 0$.

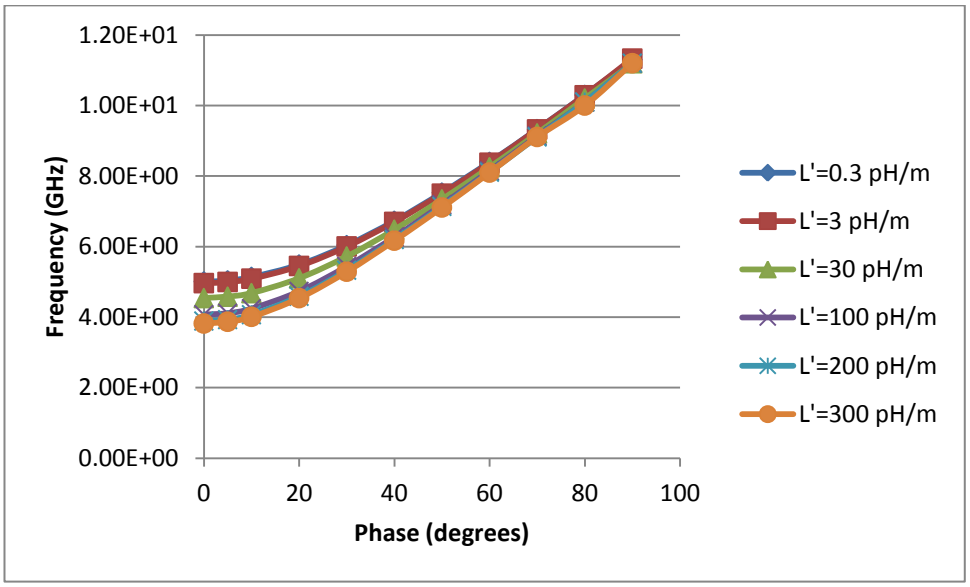

Figure 2.58: Dispersion curves from HFSS for Γ=1.5

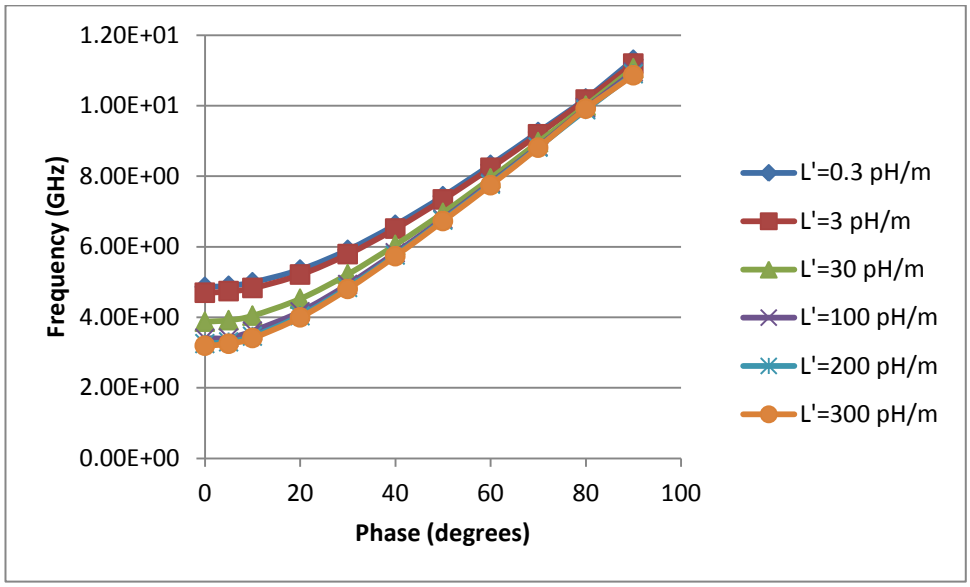

Figure 2.59: Dispersion curves from HFSS for Γ=3

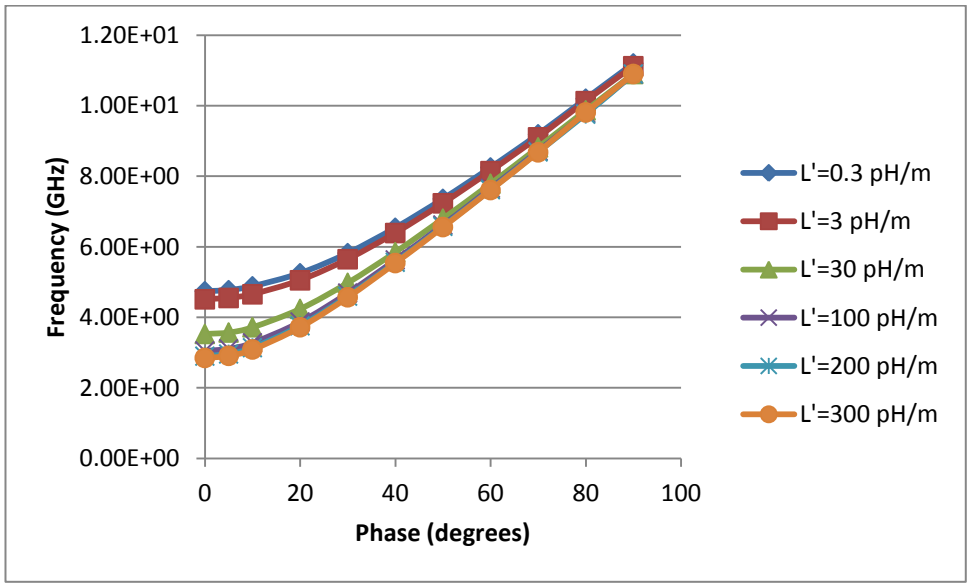

Figure 2.60: Dispersion curves from HFSS for Γ=6

The next three figures show the comparison between the predictions from our transverse resonance technique and the discrete values for the cut-off frequencies (shown in the preceding figures) from both CST Microwave Studio and HFSS for the respective values

of $\Gamma = 3,6,\frac{3}{2}$. One shortcoming on solely relying on the data from CST Microwave Studio and HFSS is that, being discrete, they are few and far between. In other words, it is imperative that we should use our method for calculated predictions in order to establish the proper shape of the design curves that follow.

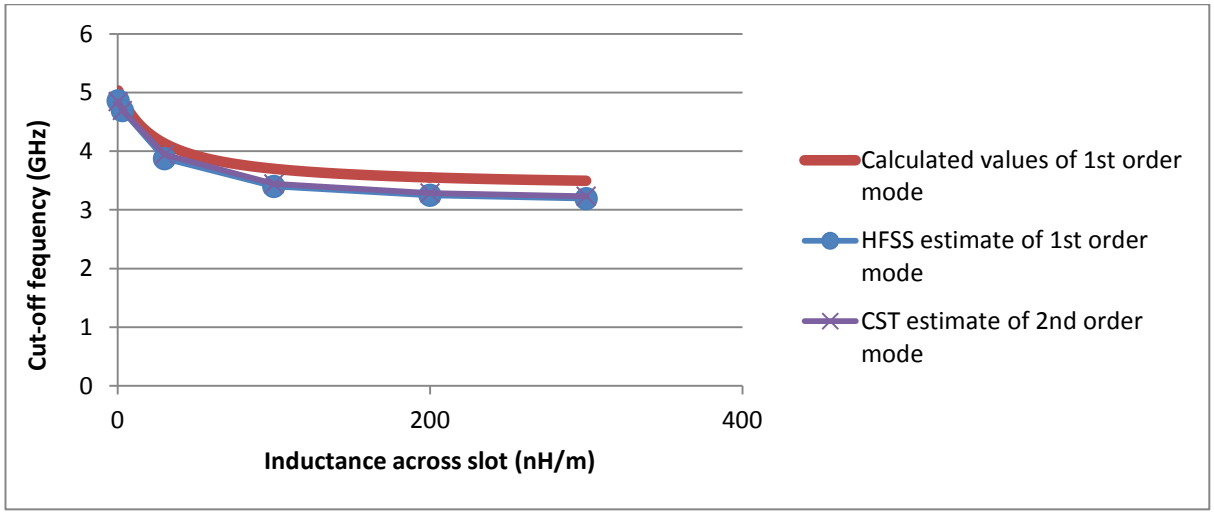

Figure 2.61: Cut-off frequency against inductance across slot in for Γ=3

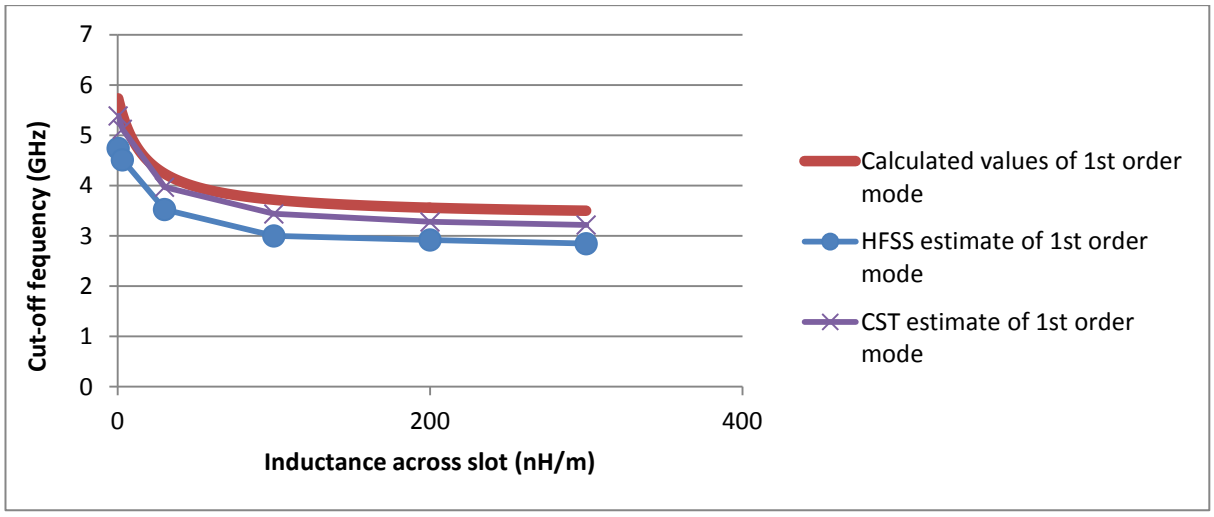

Figure 2.62: Cut-off frequency against inductance across slot in for Γ=6

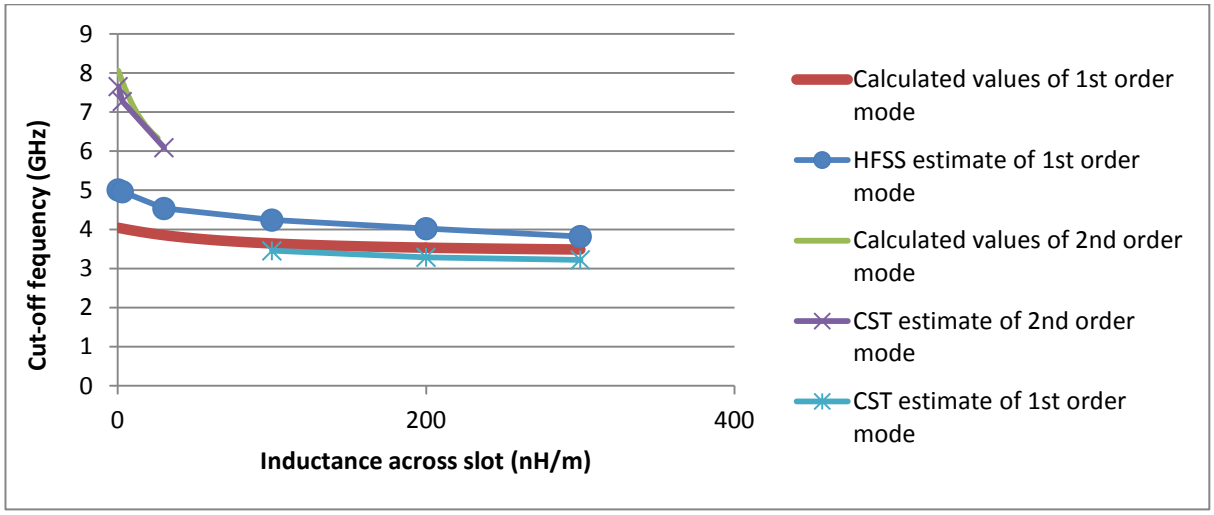

Figure 2.63: Cut-off frequency against inductance across slot in for Γ=1.5

Unlike the calculated forecasts which consider theoretically purely inductively loaded slots, the CST Microwave Studio results take into account that, in practice, the slot itself has a slight inherent capacitance. This explains why the cut-off frequency predictions obtained from simulations are slightly lower than those calculated from the transverse resonance technique. However, it is readily observed from the preceding graphs that this relatively small inherent capacitance of the slot has little effect, since there is appreciably close agreement between both categories of predictions.

Consider the case where $\Gamma = 1.5$. In this instance, the calculated predictions demonstrate that the first order mode applies for inductances per unit length which exceed approximately 25pH/m. For inductances per unit length below 25pH/m, our calculated predictions demonstrate that there is a higher order mode for which the cut-off frequency is in the range from 6-8GHz, which is readily apparent from the last graph. Both the existence and nature of this higher order mode is not so easily ascertained by using the data from CST Microwave studio alone. It may therefore be pointed out that this is an instance for which the calculated results can be used provide considerable assistance in effectively

interpreting the limited discrete data obtained from CST Microwave Studio and HFSS. The following graph shows the design curve predictions from our transverse resonance technique for the cut-off frequencies for the specified values of Γ over a range of inductances per unit length from 0.3 pH/m to 300pH/m.

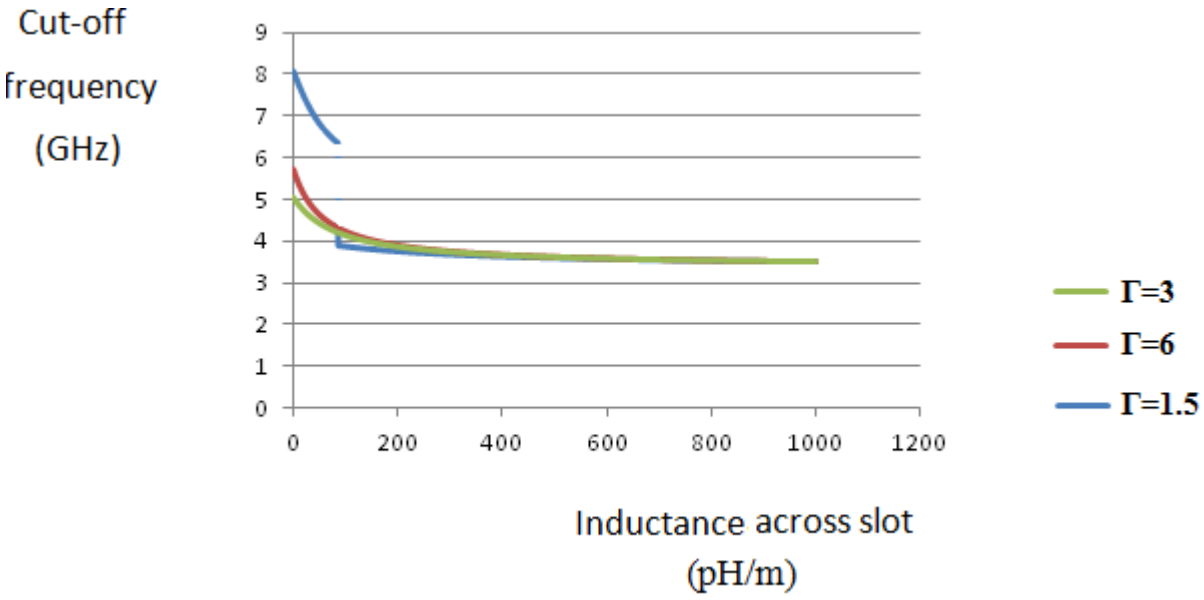

Figure 2.64: Predictions of cut-off frequency against inductance across slot from transverse resonance technique

We now consider looking at some field plots in a certain interesting case considered above, namely for $\Gamma = 3$ and L'=30pH/m at 4.25GHz (which is just above the cut-off frequency). The next figure shows the pattern of the component of electric field which travels from the top of the guide to its base. It is evident from this that the alternating electric field oscillates throughout the length of the guide.

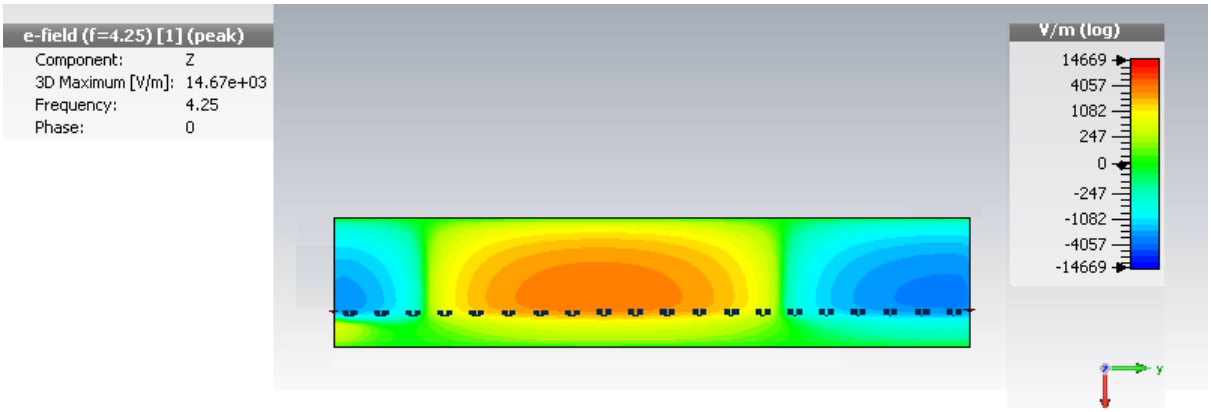

Figure 2.65: An aerial view field plot of when E_z is 0.4mm from the base of the guide for Γ=3 and a slot loaded with L' = 30 pH/m at 4.25 GHz

The following figure shows the alternating electric field vector pattern along the length of the waveguide.

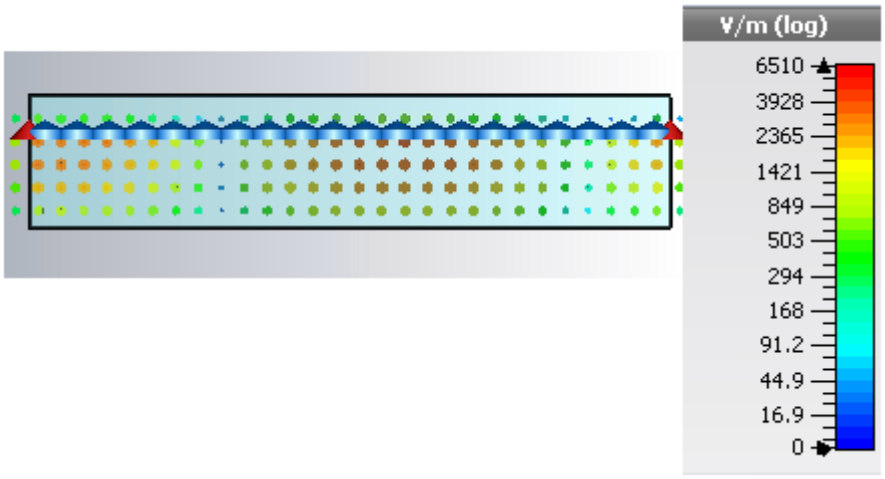

Figure 2.66: An aerial view E-field plot from the base of the guide for Γ=3 and a slot loaded with L' = 30 pH/m at 4.25 GHz

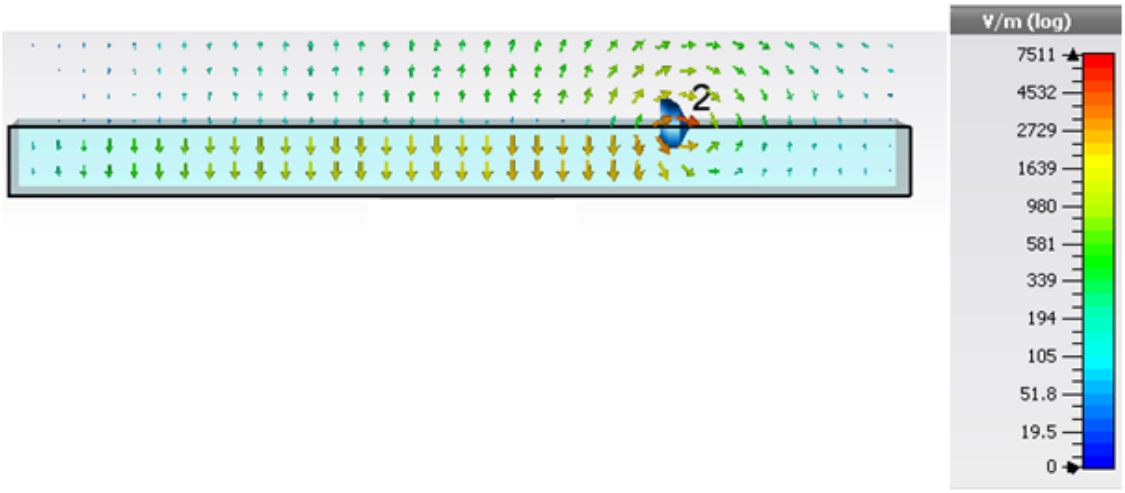

Figure 2.67: A cross sectional E-field plot 5mm inside the incident port of the guide for Γ=3 and a slot loaded with L' = 30 pH/m at 4.25GHz

From the above cross-sectional view of the incident port of the waveguide, it is evident that the electric field is largely centred around the slot.

It turns out that the field patterns do not significantly change so much at higher frequencies which are close to the next higher order mode.

2.15. Towards a bandpass waveguide filter

The cutoff frequencies of SIW structures are of paramount importance in the construction of filters, as shown in [19]-[26]. In this section, a structure which holds some characteristics of a rudimentary bandpass filter is designed by considering a slotted SIW of the same dimensions as those in the previous section with $\Gamma = 3$, except that each load element across the slot consists of an inductance of 1.4nH in series with a capacitance of 1.13pF. The load elements are places at a distance of 5mm apart, as before. The estimates from CST Microwave Studio for the S-parameters of this structure are shown below.

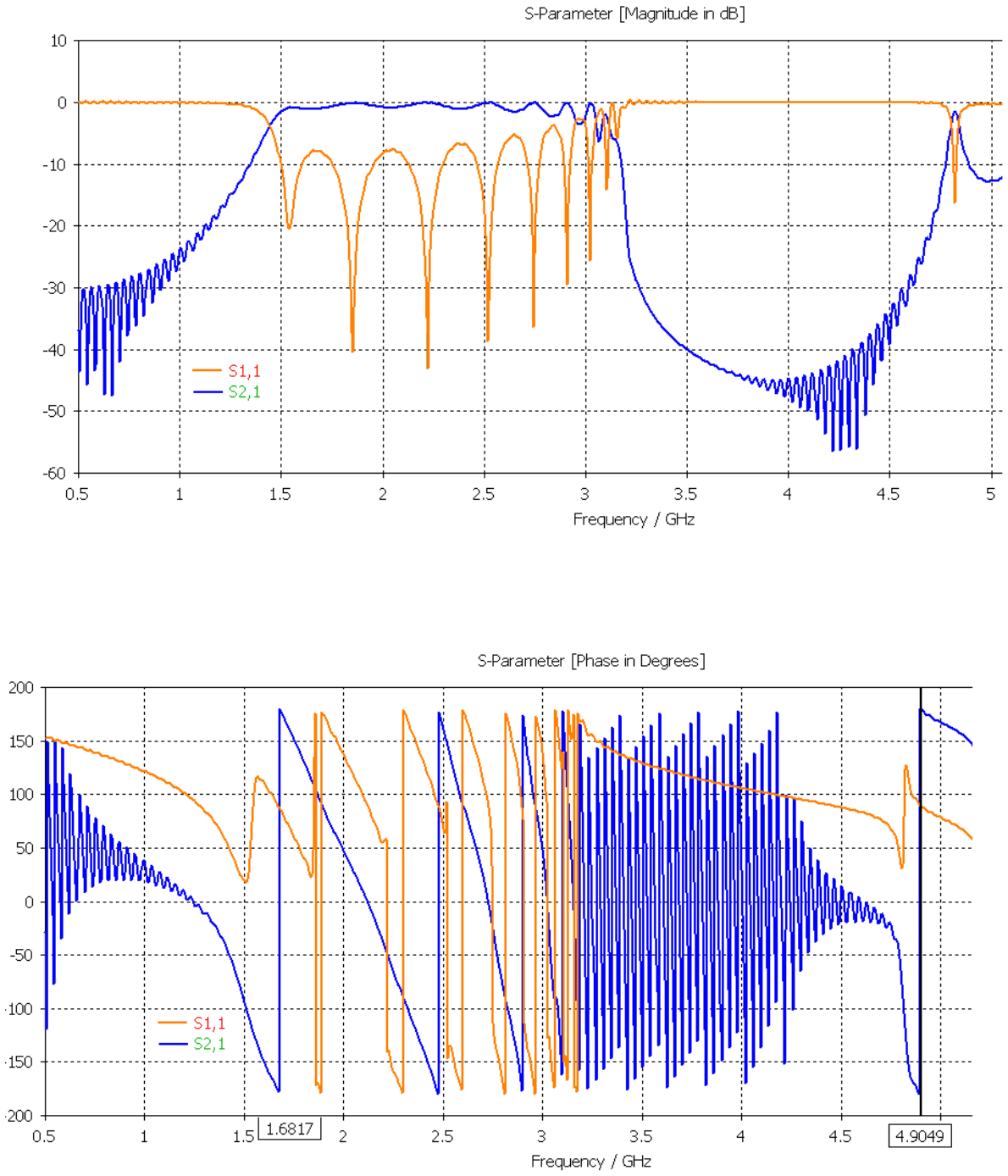

Figure 2.68: Magnitudes and phases of S-parameters for an unmatched bandpass waveguide filter structure

As exhibited in the S-parameter plots above, the waveguide filter has both lower and higher cut-off frequencies. These correspond to a capacitive cutoff for the lower frequency (at 1.68 GHz) and an inductive cut-off for the higher one (at 4.90 GHz). The lower cutoff frequency is capacitive because the load-element capacitance of 1.13pF is close to a capacitance per unit length $C' = 200$ pF/m (which corresponds to a load-element capacitance of 0.9pF from Fig. 2.11 in the previous section) for which the cutoff frequency is roughly 1.6 GHz according to the calculated predictions in Fig. 2.28. The upper cutoff frequency is inductive because the load-element inductance is 1.4nH which is close to an inductance per unit length $L' = 3$ pH/m (which corresponds to a inductance of 0.6nH from Fig. 2.39 in the previous section) for which the cut-off frequency is just under 5 GHz according to the calculated predictions in Fig. 2.52. This means that the load is predominantly capacitive for lower frequencies in the range of 1.7-3 GHz until it starts to become mostly inductive at frequencies approaching 5 GHz. There is a point where the impedance is zero (i.e. neither capacitive nor inductive) at resonance so that the guide is short circuited, resulting in a sharp dip in the magnitude of S_{21} in the range from 3-4 GHz just before it picks up again in the inductive region. By looking at these S-parameter characteristics, this structure appears to exhibit some characteristics of a novel bandpass filter that is constructed differently from other ways (as proposed in [19]-[23]). However, the excessive ripples in the S-parameter magnitudes indicate the guide is mismatched. In particular, in the range from 1.5 GHz to 3 GHz, the magnitude of S_{11} goes down to well under -5dB. Ideally, the magnitude of S_{11} should never be above -10dB over the entire frequency band in order for the structure to be properly matched. This major shortcoming demonstrates that this kind of structure is better suited for a narrow band device than for a bandpass filter.

It should also be noted from both the preceding S-parameter plots this ought to be regarded as a complicated waveguide structure which exhibits different regions of operation with important physical characteristics, rather than just a microwave device. It is evident from the last S-parameter phase plot that the phase constant β varies very rapidly with frequency in the region from 3.25 GHz to 4.25 GHz. As β varies very rapidly, the wavelength increases and the phase velocity decreases, so that the bandwidth from 3.25 GHz to 4.25 GHz corresponds to a slow mode region. This slow mode region occurs just before the

point of the upper cutoff frequency (due to the inductive load) at 4.9 GHz, as confirmed by the following HFSS plot, in which the phase φ varies very rapidly over a very small bandwidth when it is close to the inductive cutoff frequency.

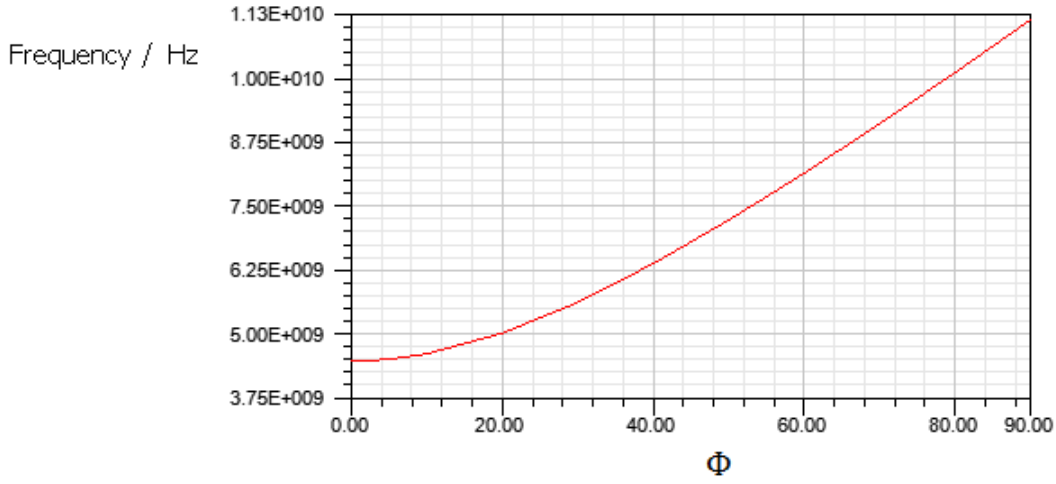

Figure 2.69: HFSS estimate of dispersion characteristics of slotted SIW with a 1.4nH load element inductance

This waveguide filter structure can be better matched by changing the load element capacitance to 0.5 pF and the load element inductance to 0.4 nH, and increasing the thickness *b* from 1.575mm to 30mm. The resulting S-parameter plots for this improved bandpass filter structure are shown as follows.

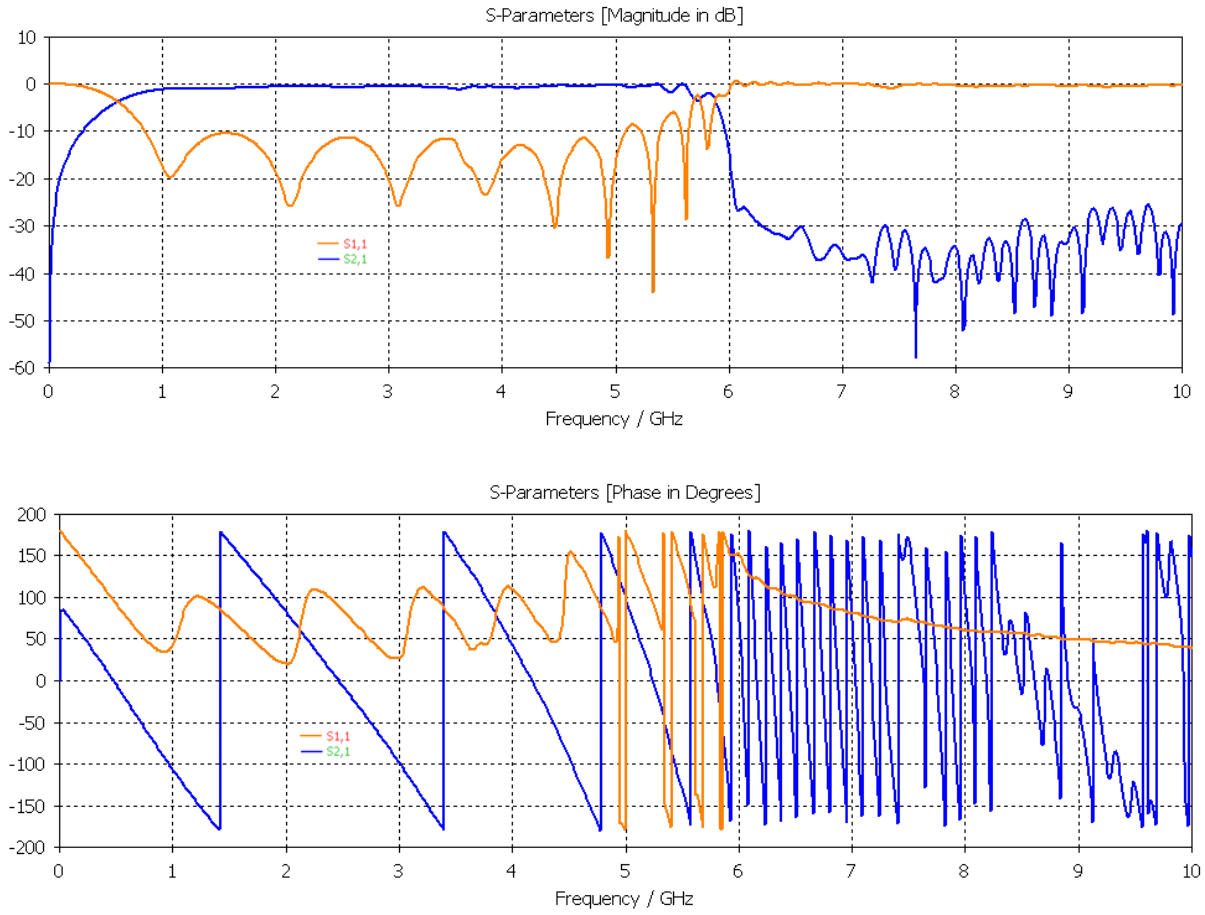

Figure 2.70: Magnitudes and phases of S-parameters for an improved bandpass waveguide filter structure

It can be observed from the above phase plot that there is a slow mode region from approximately 6 GHz to 8 GHz. It is worth noting that S_{11} remains below -10dB from 1 GHz to 5 GHz. It is therefore evident from the last plot of the S-parameter magnitudes that the new structure is better matched than in the previous case.

2.16. Two-port tuneable waveguide resonator

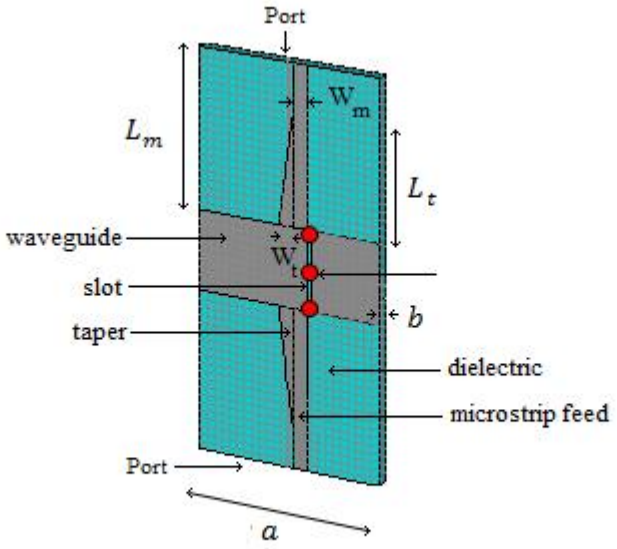

Figure 2.71: Structure of two-port SIW resonator

Cavity resonators are explained in detail in [1] and [2], and have been used to design microwave filters in [27] and [28]. The design for a tuneable waveguide resonator is provided in this section as follows. A slotted SIW structure is loaded with a series of lumped reactive elements across its slot. Each load element consists of an inductor and a capacitor in series with each other. As before, the horizontal distance from each sidewall to the boundary of the slot of width $w = 0.5$mm is given by L_1 and L_2 respectively, such that the longer cross-sectional length is denoted as L_1.

If the length of the waveguide (parallel to the direction of propagation) is excessively large, then unwanted higher order longitudinal resonances are produced. It is therefore necessary to reduce the length of the waveguide to avoid any such disturbances. For this reason, it has been found that the length of the waveguide should be set to be equal to 10mm. Since the distance between load elements is given by $d = 5$mm (as before), it follows that three load elements are used across the slot.

The design of this structure also involves using a rectangular microstrip feed joined to a triangular taper at both ends, as illustrated in the preceding figure. The feedlines and tapers are embedded in the dielectric substrate. The length and width of the microstrip

feed are denoted L_m and W_m, respectively. Similarly, the perpendicular length and maximum width of the taper are denoted L_t and W_t, respectively. The values for these parameters are selected (see the subsequent table) so that the characteristic impedance of the microstrip feed is very close to 50Ω. It is assumed without loss of generality that the cross-sectional distance from the left sidewall to the slot is given by L_1. The offset displacement r is defined to be the horizontal distance from the left sidewall to the end of the microstrip feed, i.e. the shortest distance between the slot and the microstrip feed is given by $L_1 - r$.

It transpires that if the offset displacement is sufficiently large, so that the microstrip feed is very close to the slot, then the structure becomes resonator at certain frequencies depending on the load elemental inductance and capacitance. The actual sizes of the measurements used to construct the two-port antenna are shown in the following table.

Parameter	Length (mm)
a	24
b	1.575
d	5
w	0.5
L_1	14.5
r	13.75
L_m	20
L_t	15
W_m	2
W_t	2

Figure 2.72: Measurements of parameters in two-port SIW resonator

The condition for resonance of the fundamental (i.e. first order) mode occurs at the lowest frequency for which that a standing electromagnetic wave is produced in the waveguide

structure. It follows that the resonant frequency corresponds to the point at which the S_{11} characteristic dips below at least 10dB and also when S_{21} is very close to zero.

The value for the load element inductance is permanently set to 0.9nH, as before in the previous section. The load element capacitance, which is placed in series with each load element inductance, is varied from 2.2pF down to 1.3 pF. In this way, the resonant frequency can be finely tuned from 1 GHz to almost 1.3 GHz, as shown in the following S-parameter plots predicted by CST Microwave Studio for an SIW with 3 load elements. Note that, in each of these subsequent plots, a marker is used to identify the unique fundamental resonant frequency for a given capacitance over a range of approximately 300MHz).

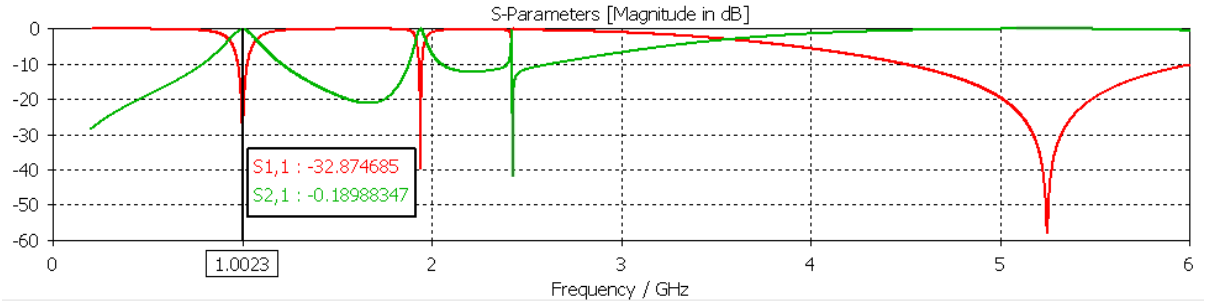

Figure 2.73: Magnitudes of S-parameters with a load element capacitance of 2.2pF

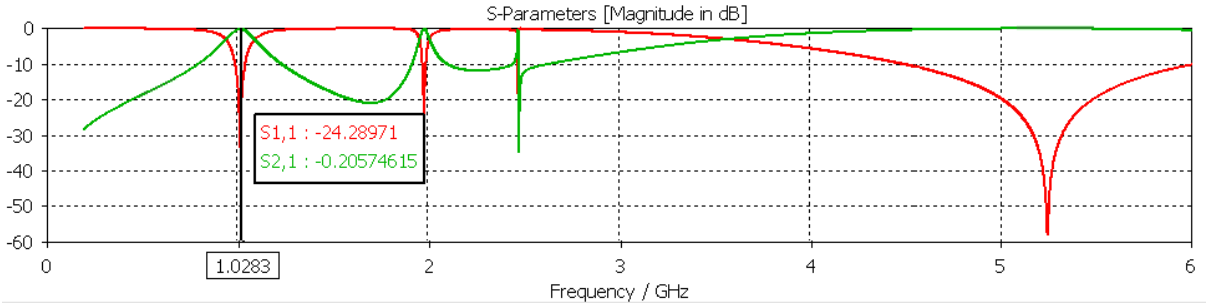

Figure 2.74: Magnitudes of S-parameters with a load element capacitance of 2.1pF

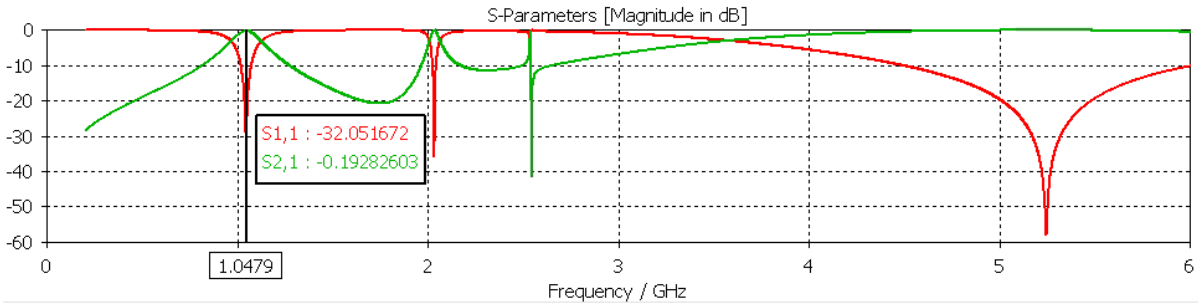

Figure 2.75: Magnitudes of S-parameters with a load element capacitance of 2.0pF

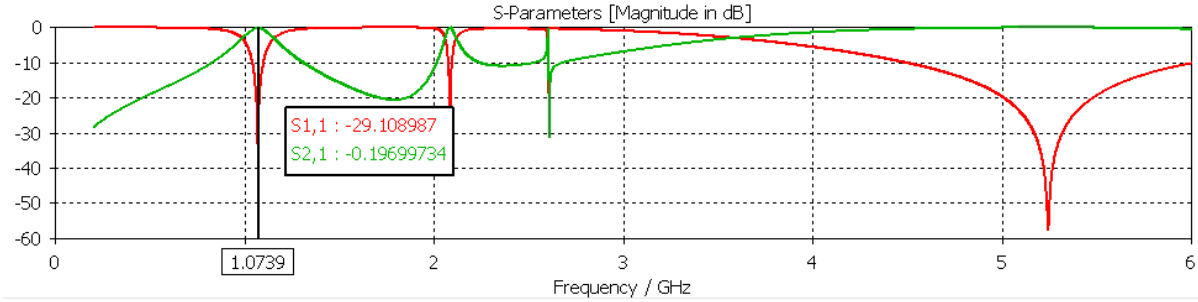

Figure 2.76: Magnitudes of S-parameters with a load element capacitance of 1.9pF

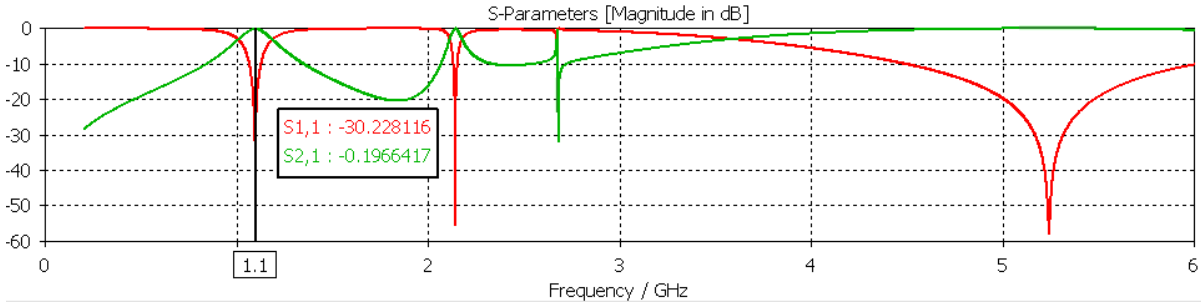

Figure 2.77: Magnitudes of S-parameters with a load element capacitance of 1.8pF

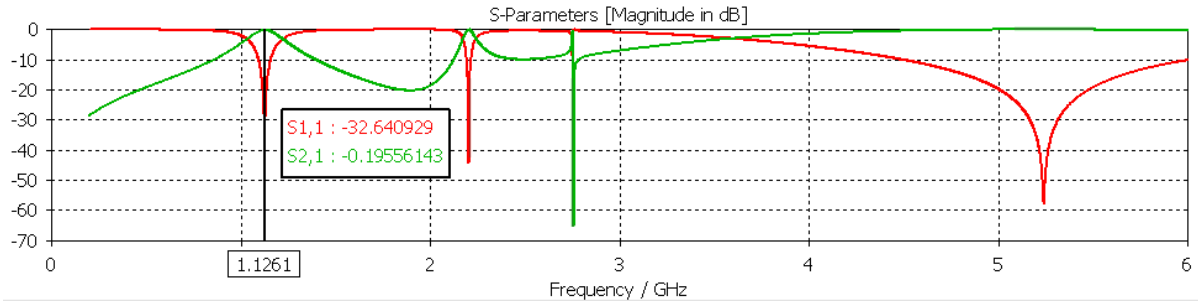

Figure 2.78: Magnitudes of S-parameters with a load element capacitance of 1.7pF

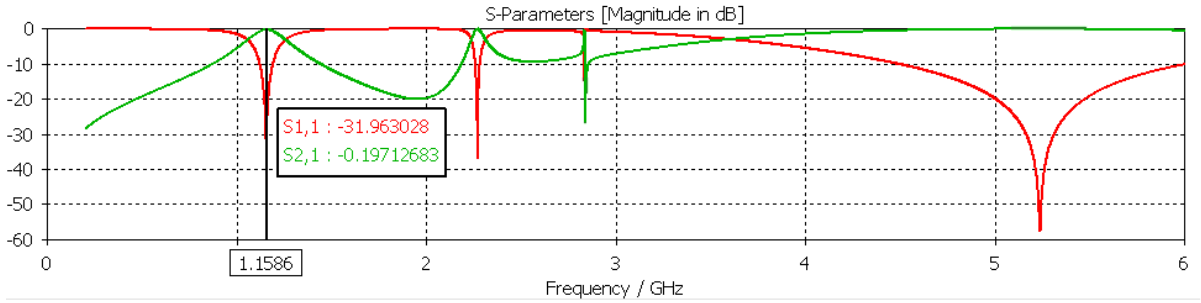

Figure 2.79: Magnitudes of S-parameters with a load element capacitance of 1.6pF

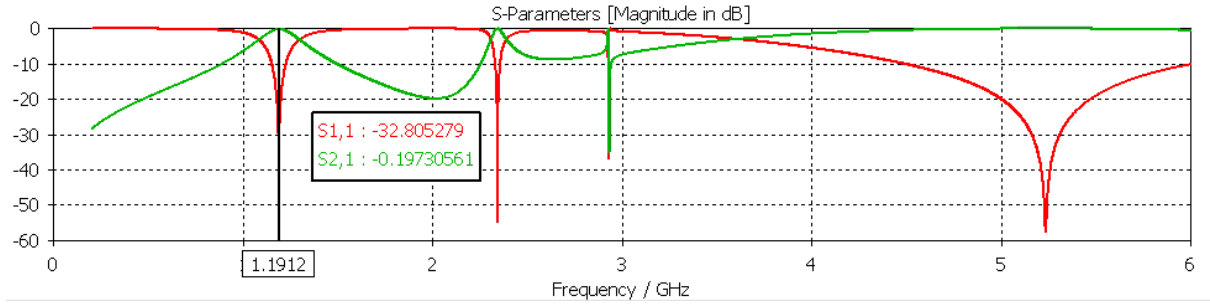

Figure 2.80: Magnitudes of S-parameters with a load element capacitance of 1.5pF

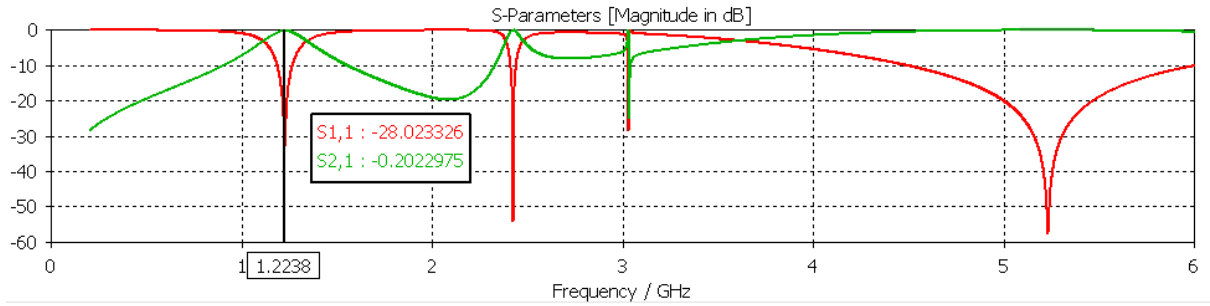

Figure 2.81: Magnitudes of S-parameters with a load element capacitance of 1.4pF

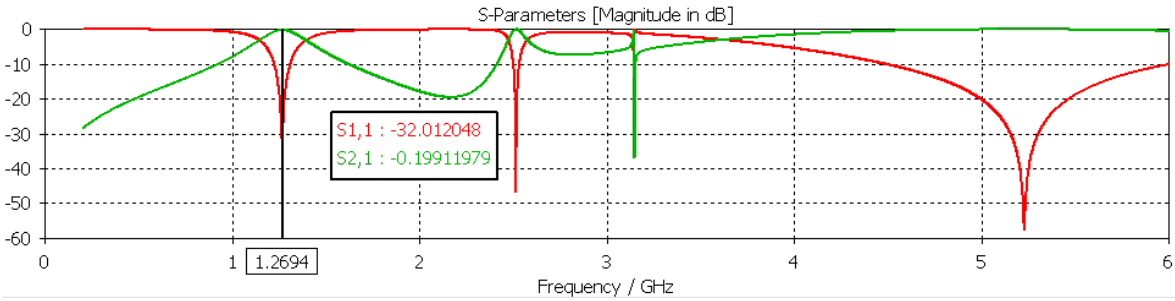

Figure 2.82: Magnitudes of S-parameters with a load element capacitance of 1.3pF

It was noted earlier that a longer waveguide containing more load elements would produce multiple longitudinal resonances. This is illustrated in the following plot, for which the length of the waveguide is doubled to 20 mm, so that the number of load elements (each of which consists of an inductor in series with a capacitance of the same specifications as before) is increased from three to five. It is easily observed from this plot with a longer waveguide that there exist three resonant frequencies between 1GHz to 2.2GHz, and that the envelope pattern that can be traced from these resonant peaks of the S_{21} curve forms the plateau of what would be the characteristic of a bandpass filter. However, as in the case of the previous section, this type of periodic structure falls short of being a workable bandpass filter, even though it shares some close similarities.

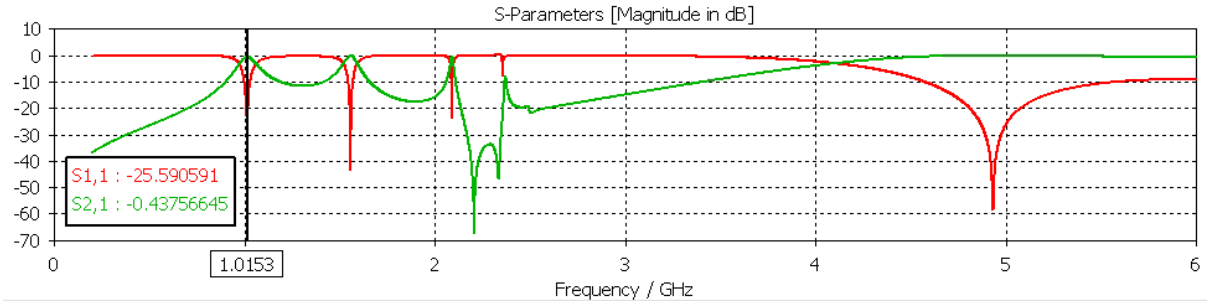

Figure 2.83: Magnitudes of S-parameters with a load element capacitance of 1.2pF in an SIW of length 20mm with 5 load elements

This tuneable resonator could be used in a feedback loop in a voltage controlled oscillator, which is a mandatory component in nearly all receivers and transmitters. Since this

resonator can be finely tuned with load capacitances, it follows that the oscillator frequency can be adjusted to a high degree of accuracy.

2.17. The difficulties associated with a two-port tuneable narrow-band antenna

The same structure that was used in the previous section (from Figures 2.61 and 2.62) is used again here with the waveguide length being 24mm, with the exception that the offset displacement of the microstrip feed, which is denoted as r, is much smaller. In other words, the microstrip feed and taper are placed further away from the slot and closer to the left waveguide wall. This allows the slot to radiate an electric field. It follows from Collier [29] that the S-parameters in a two-port network are given by

$$\begin{pmatrix} S_{11} & S_{12} \\ S_{21} & S_{21} \end{pmatrix} = \frac{1}{Y+2Y_0} \begin{pmatrix} -Y & 2Y_0 \\ 2Y_0 & -Y \end{pmatrix} , \quad (2.60)$$

where the characteristic admittance Y_0 must be equal to the shunt admittance Y for the network to be properly matched, in which case $S_{11} = -9.54$ dB and $S_{21} = -3.52$ dB. It follows that these S-parameter values need to be satisfied during resonance in order for the structure to behave as a properly matched antenna. However, it can be determined from all the remaining plots in this section that both these ideal S-parameter values cannot be simultaneously satisfied at the resonant frequency by using the afore-mentioned two-port tapered structure from Figure 2.61. It follows that a single-port structure is far better suited to being a matched antenna, because only one S-parameter would need to be satisfied. The following set of S-parameter plots show the fundamental resonant frequency when the load element capacitance is set to 1.3pF, whilst keeping the load element inductance at 0.9nH, and the offset displacement r (of the microstrip feed) is varied from 3.5 mm to 4.45 mm.

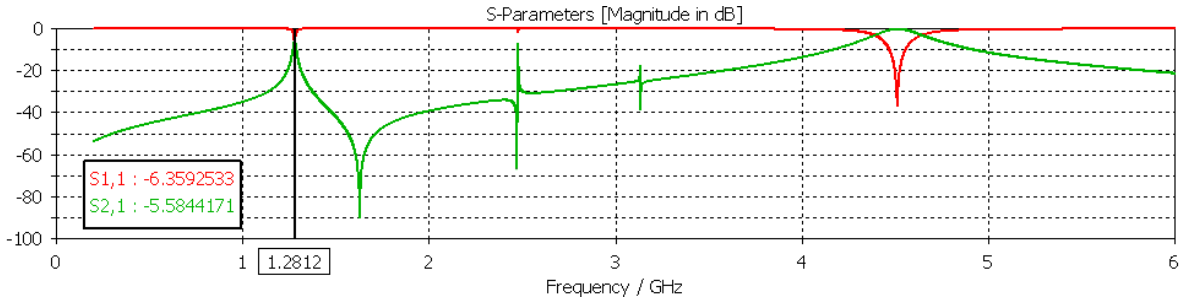

Figure 2.84: Magnitudes of S-parameters with a load element capacitance of 1.3pF with r=3.5 mm

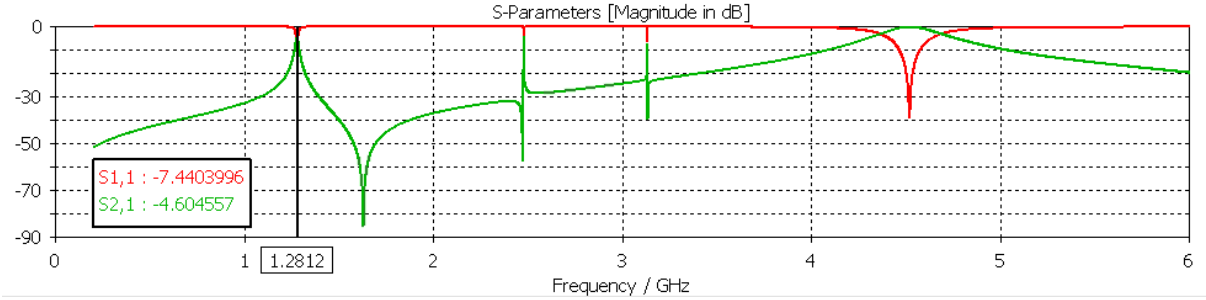

Figure 2.85: Magnitudes of S-parameters with a load element capacitance of 1.3pF with r=3.75 mm

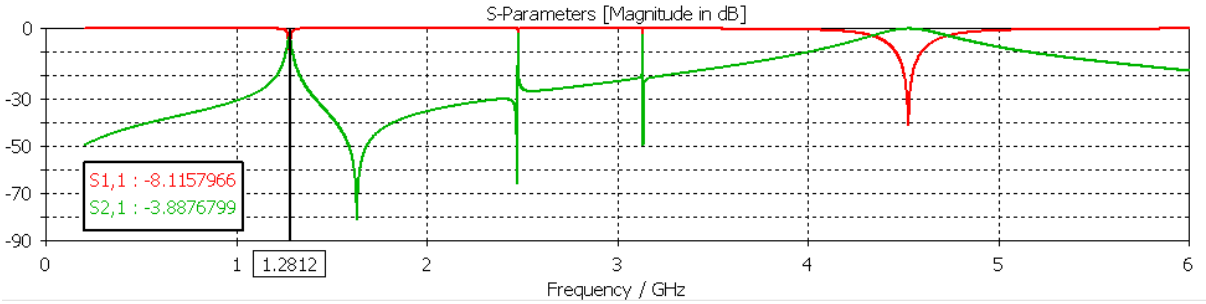

Figure 2.86: Magnitudes of S-parameters with a load element capacitance of 1.3pF with r=4 mm

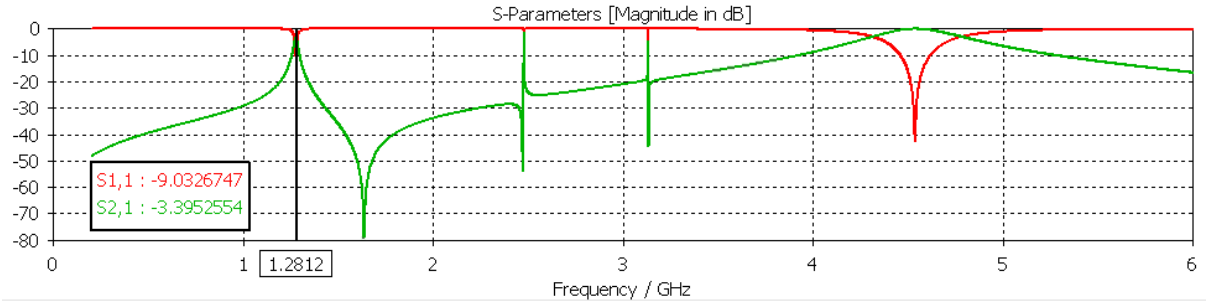

Figure 2.87: Magnitudes of S-parameters with a load element capacitance of 1.3pF with r=4.25 mm

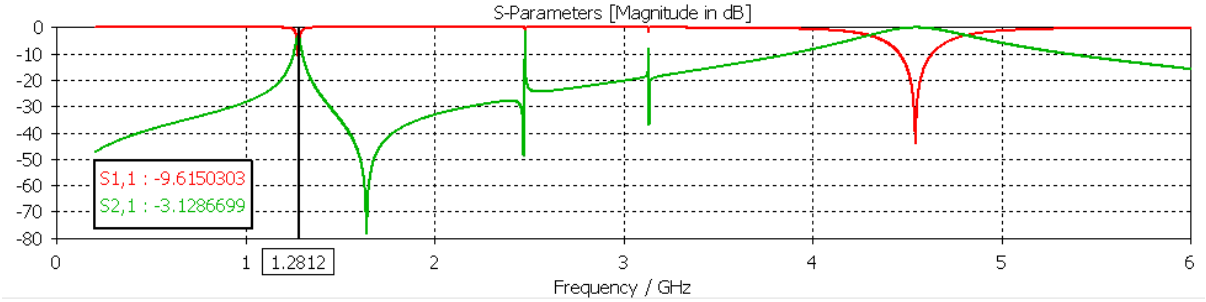

Figure 2.88: Magnitudes of S-parameters with a load element capacitance of 1.3pF with r=4.4 mm

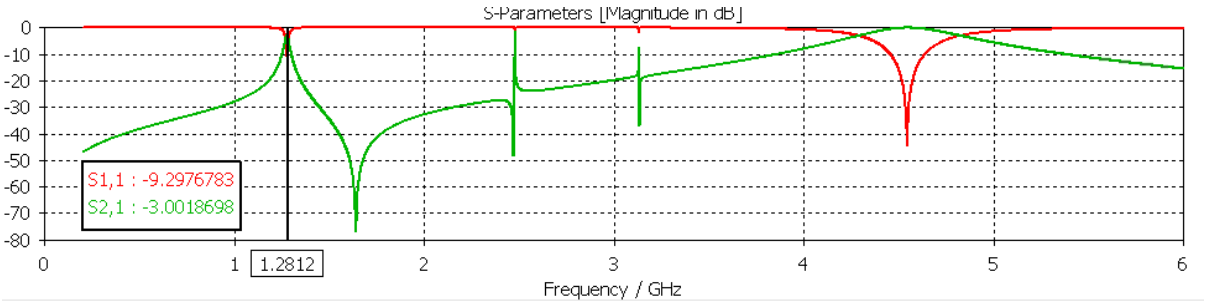

Figure 2.89: Magnitudes of S-parameters with a load element capacitance of 1.3pF with r=4.45 mm

It is easily seen from the last few S-parameter plots that the desired pair of S-parameter values is not quite achievable with a load element capacitance of 1.3pF. If the load element capacitance is varied from 1.2pF to 0.9 pF, the resonant frequency can continue to

be adjusted, but the desired valued of the S-parameters is not satisfactorily obtained, as shown in the following plots.

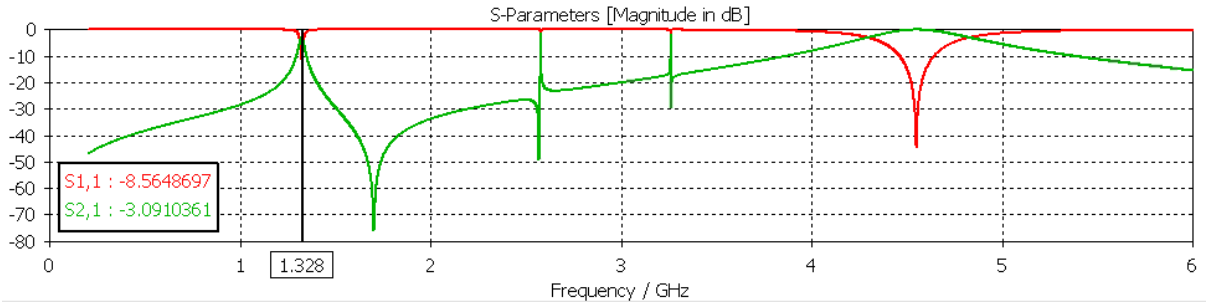

Figure 2.90: Magnitudes of S-parameters with a load element capacitance of 1.2pF with r=4.45 mm

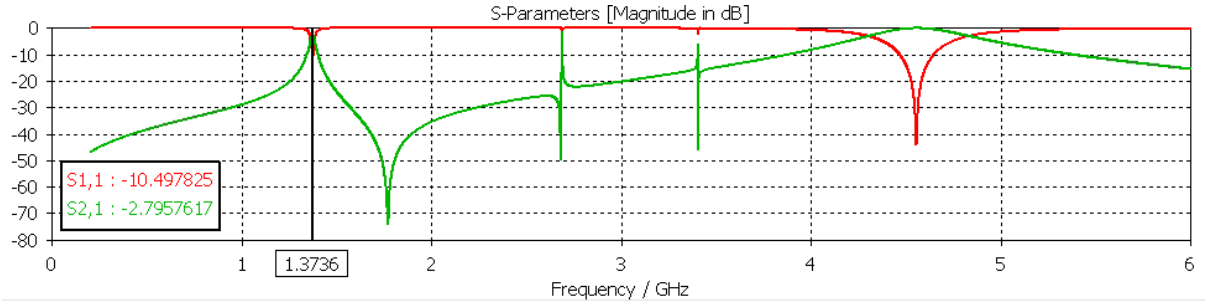

Figure 2.91: Magnitudes of S-parameters with a load element capacitance of 1.1pF with r=4.45 mm

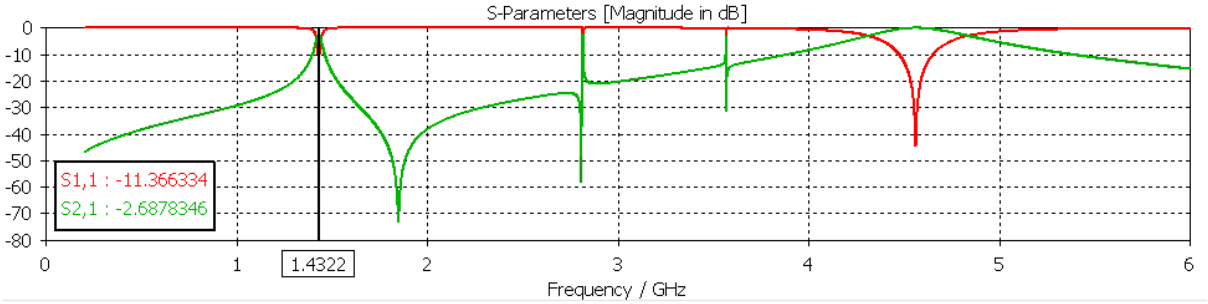

Figure 2.92: Magnitudes of S-parameters with a load element capacitance of 1pF with r=4.45 mm

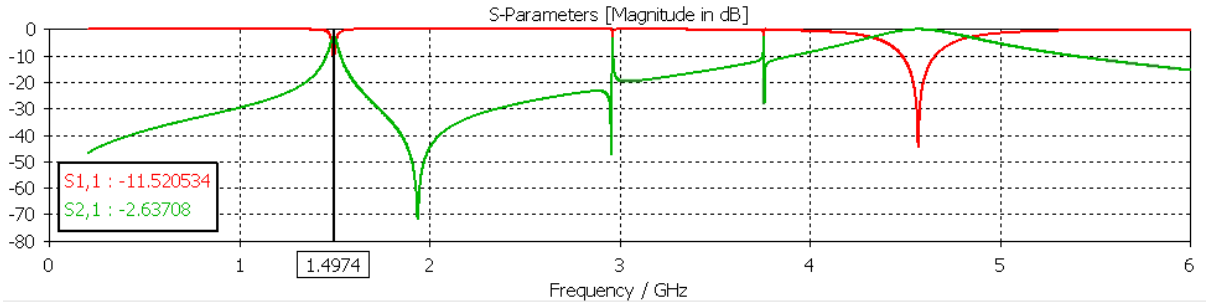

Figure 2.93: Magnitudes of S-parameters with a load element capacitance of 0.9pF with r=4.45 mm

If the offset displacement is increased slightly to 4.5mm and the load element capacitance is restored to 1.3pF, then the structure is almost matched, as shown by the S-parameters at the resonant frequency of 1.28GHz in the plot below.

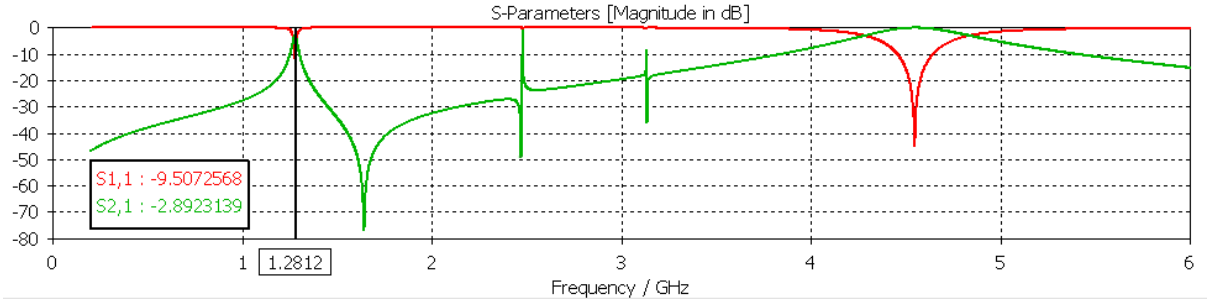

Figure 2.94: Magnitudes of S-parameters with a load element capacitance of 1.3pF with r=4.5 mm

It can be concluded from all the plots in this section that it is not possible to produce a matched tuneable antenna by simply adjusting the load capacitance in the proposed two-port structure.

2.18. A tuneable single-port narrow-band antenna

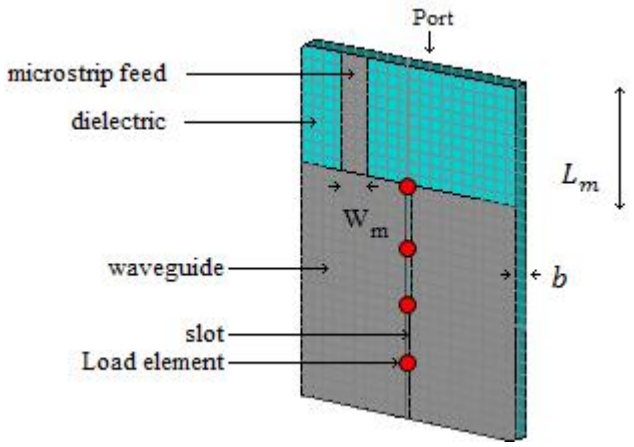

Figure 2.95: Structure of single-port antenna

Some recent SIW antenna applications are outlined in [30]-[34]. The design for a single-port waveguide is provided in this section is modelled with CST Microwave Studio as follows. Its structure, as shown in the preceding figure, is based on the two-port structure discussed earlier and is due to appear in a forthcoming paper. The slotted SIW structure is loaded with a series of lumped reactive elements across its slot so that. Each load element consists of a 0.9nH inductor and a capacitor in series with each other. The horizontal distance from each sidewall to the boundary of the slot of width $w = 0.4$mm is given by L_1 and L_2 respectively, such that the longer cross-sectional length $L_1 = 10.1$ mm.

The length of the waveguide z_L is set at 20mm in order to dispense with any unwanted higher order longitudinal resonances. Since the distance between load elements is given by $d = 5$mm (as before), it follows (see the preceding figure) that four load elements are used across the slot.

The principal modification of this structure also involves using only one single rectangular microstrip feed without any taper structure, as illustrated in the preceding figure. As before, the offset displacement r is defined to be the horizontal distance from the left sidewall to the end of the microstrip feed.

It transpires that if the microstrip feed is not close to the slot, then the structure radiates at certain frequencies. The offset displacement is set at r =5mm. The actual sizes of the measurements used to construct the two-port antenna are shown in the following table.

Parameter	Length (mm)
a	20
b	1.575
d	5
w	0.4
L_1	10.1
r	5
L_m	10
W_m	2.5
z_L	20

Figure 2.96: Measurements of parameters in tuneable single port SIW antenna

It was pointed out in the previous section that it is easier to match a device with one port. In other words, it is necessary to ensure that S_{11} reaches a value below -10 dB in order for the structure to be properly matched. This requirement is satisfied by using loaded capacitances varying from 0.5pF to 1.2pF to finely tune a very large range of resonant frequencies from approximately 3GHz to 3.8GHz, as shown in the subsequent plots.

As an initial example, consider the structure with a loaded capacitance of 0.5pF for which the following S-parameter plot from CST Microwave Studio indicates the cutoff frequency is 3.8462 GHz. This fundamental resonant frequency is obtained in exactly the same manner as before with the resonator example, so that it is the smallest frequency for which the magnitude of S_{11} dips to its lowest value. The 10dB operational bandwidth of the antenna is determined by finding the difference of the two boundary values of the frequency (between which the point of cutoff exists) for which S_{11} reaches -10 dB. In the case of the following plot (for which the loaded capacitance is 0.5 pF), these two boundary values are given by 3.7906 GHz and 3.9013 GHz , so that the operational bandwidth,

which is equal to their difference, is given by 0.1107 GHz . All these values of frequency are listed in the subsequent table.

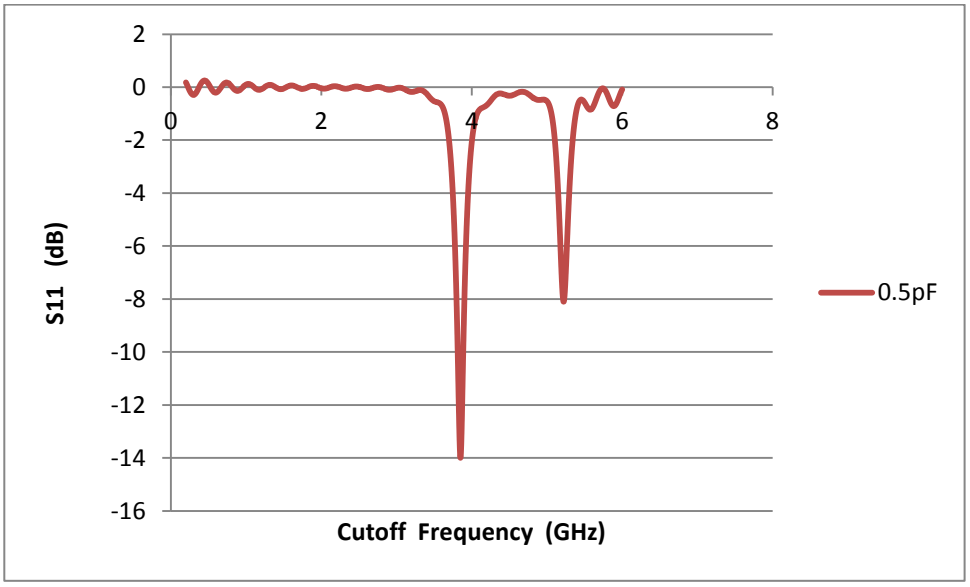

Figure 2.97: Magnitudes of S-parameters with a load element capacitance of 0.5pF

The next figure shows a how the S_{11} parameter varies with load element capacitances from 0.5 pF to 1.2pF. The cutoff frequency (i.e. the resonant frequency at which the waveguide antenna radiates) of the waveguide structure is tuneable over the range from 3GHz to 3.8GHz. This is an exceptionally large range for a tuneable antenna and it is appreciably close to the standard wi-fi channel frequency at 2.5GHz. The fact that the S_{11} parameter at each of the fundamental cutoff frequencies is less than -10dB (as shown in the following plot) is a mandatory requirement, so that the reflection is sufficiently small in order for enough energy to be radiated by the antenna.

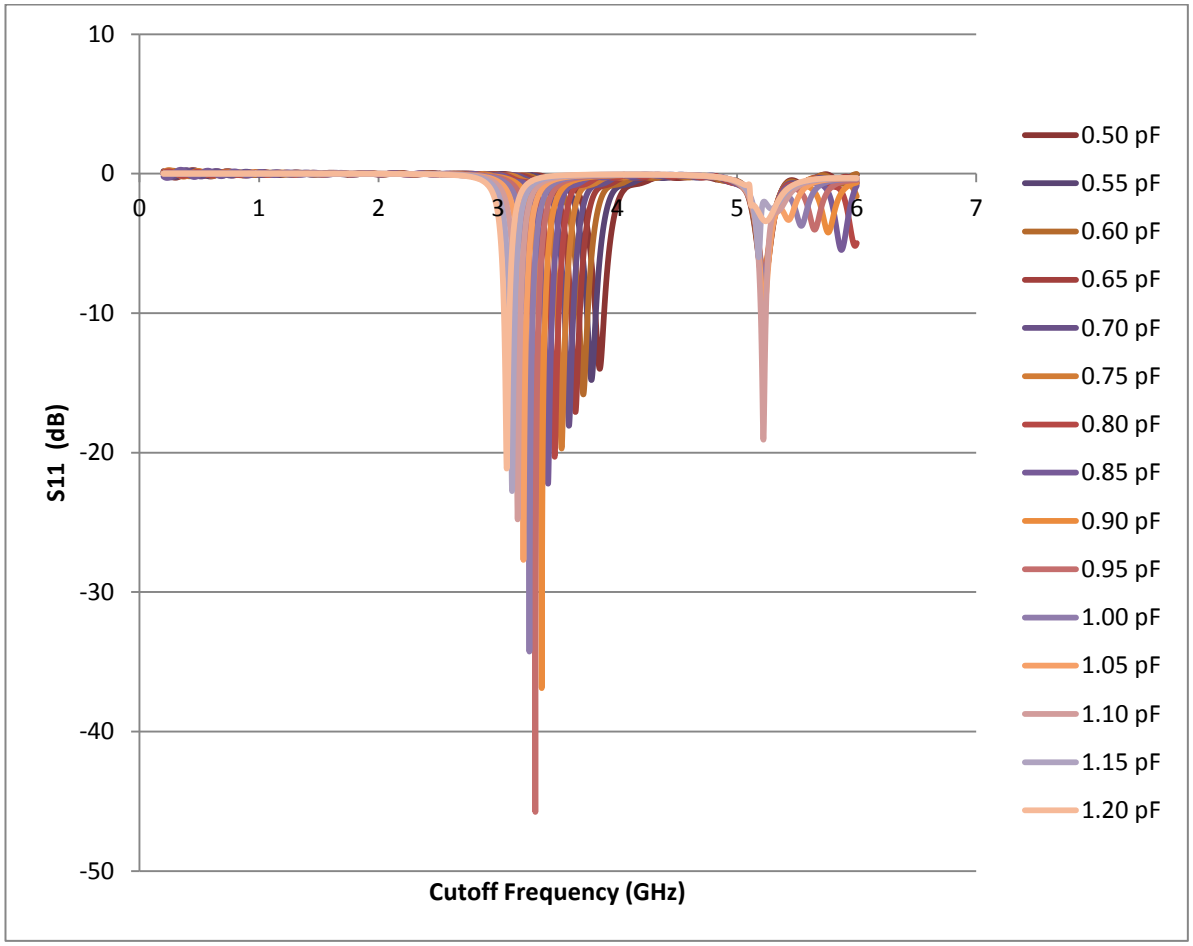

Figure 2.98: Magnitudes of S-parameters for various load element capacitances

It is important for a tuneable antenna to have a narrow band of operation. A conventional system usually consists of a broadband antenna followed by a tuneable filter, so that it is possible to select the desirable resonant frequency which is required by the antenna. However, this novel antenna structure has the facility to perform the tuning without using an additional filter. This tuneable novel antenna therefore allows for the specific choice of one of several different channels over a range of almost 1GHz. It is clear from the subsequent table that the 10dB operational frequency bandwidth (i.e. the width of the resonant peak of the S_{11} parameter at -10dB) is tens of MHz.

Load element capacitance across slot (pF)	Lower Fundamental 10dB Frequency (GHz)	Cutoff Frequency of Fundamental Mode (GHz)	Upper Fundamental 10dB Frequency (GHz)	10dB Operational Frequency Bandwidth (GHz)
0.50	3.7906	3.8462	3.9013	0.1107
0.55	3.7189	3.7746	3.8296	0.1107
0.60	3.6537	3.7029	3.7515	0.0978
0.65	3.5886	3.6378	3.6863	0.0977
0.70	3.5365	3.5821	3.6342	0.0977
0.75	3.4779	3.5235	3.5625	0.0846
0.80	3.4192	3.4583	3.5039	0.0847
0.85	3.3606	3.4062	3.4453	0.0847
0.90	3.3215	3.3576	3.3866	0.0651
0.95	3.2694	3.3020	3.3310	0.0616
1.00	3.2173	3.2498	3.2694	0.0621
1.05	3.1717	3.1977	3.2238	0.0621
1.10	3.1261	3.1521	3.1717	0.0456
1.15	3.0805	3.1065	3.1261	0.0456
1.20	3.0349	3.0609	3.0805	0.0456

Figure 2.99: Operational frequency table over range of load element capacitances

The following graphs use the data from the table to illustrate that both the operational frequency bandwidth and the resonant frequency decrease as the capacitance is increased over a range from 0.5pF to 1.2 pF.

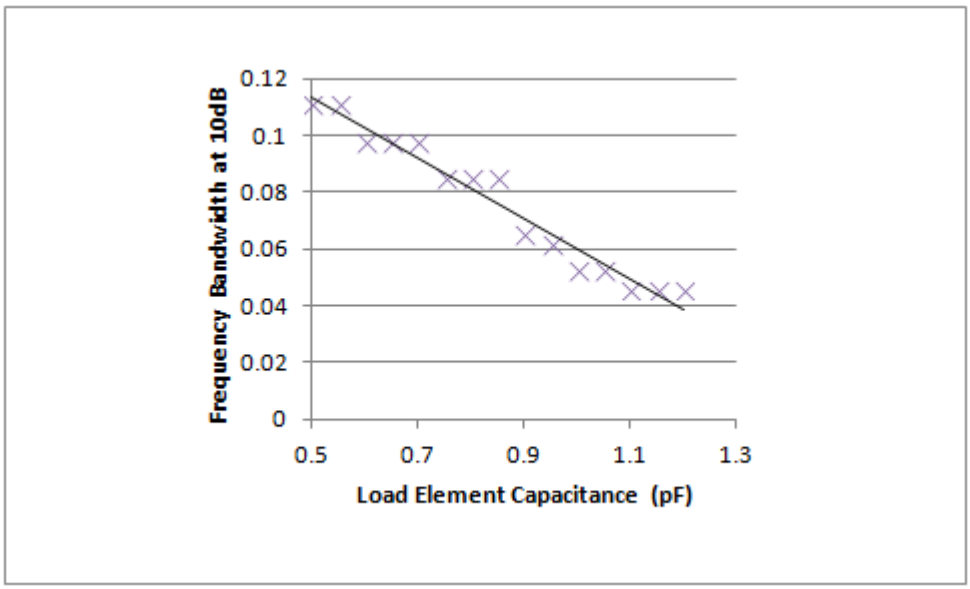

Figure 2.100: Operational frequency bandwidth vs. load element capacitance

A straight line of best fit is used to show that the operational frequency bandwidth of the antenna falls rather rapidly over a relatively small range of load element capacitances.

It is evident that the relationship between the resonant frequency and the load element capacitance is very close to being a linear one. This demonstrates that it relatively easy to finely tune the resonant frequency at which the antenna radiates.

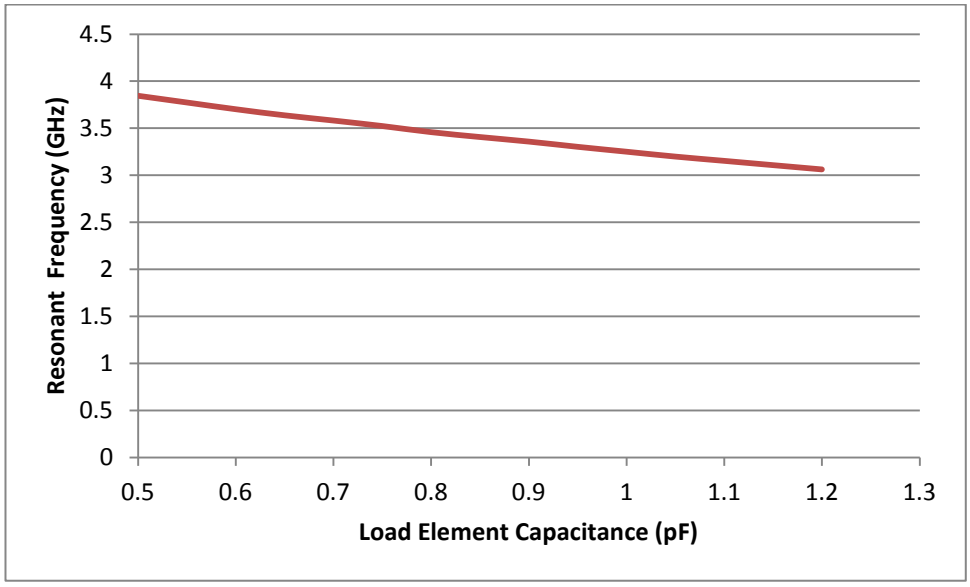

Figure 2.101: Operational frequency bandwidth vs. load element capacitance

The following field plot at the resonant frequency of 3.06 GHz illustrates an aerial view of the electric field at a position roughly equidistant from the top and base of the waveguide when the load element capacitance is 1.2pF.

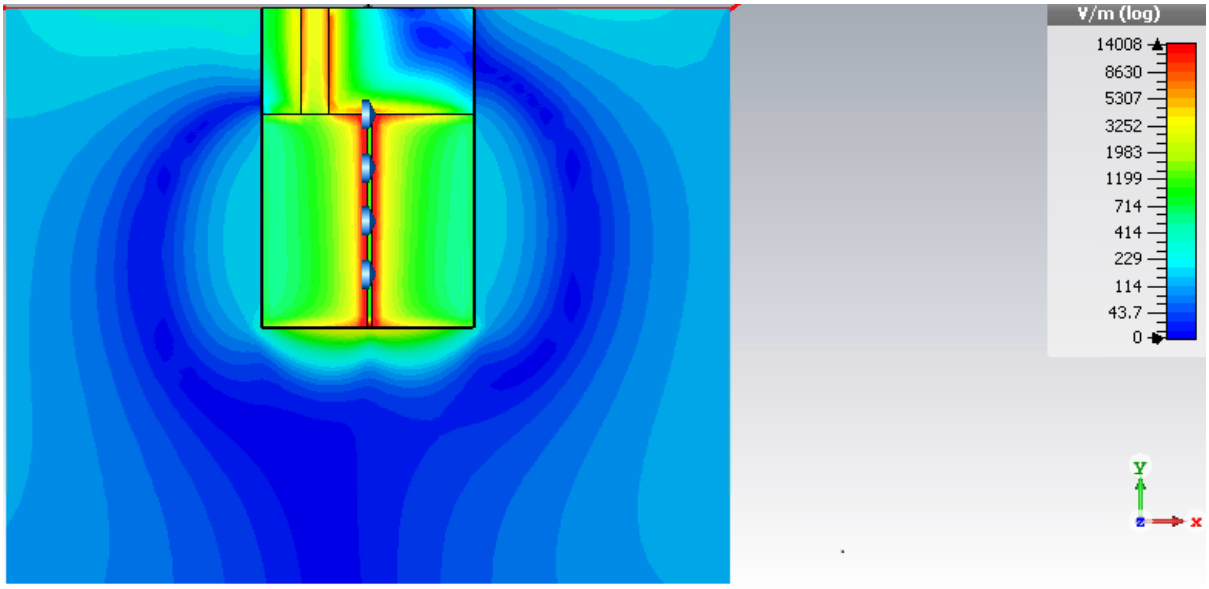

Figure 2.102: Aerial view field plot (at cutoff) of the magnitude of the E-field at a position 0.7mm above the base of SSIW antenna with a load element capacitance of 1.2pF.

The subsequent cross-sectional plot shows the electric field vector at the resonant frequency of the same SSIW structure, for which the load element capacitance is 1.2pF.

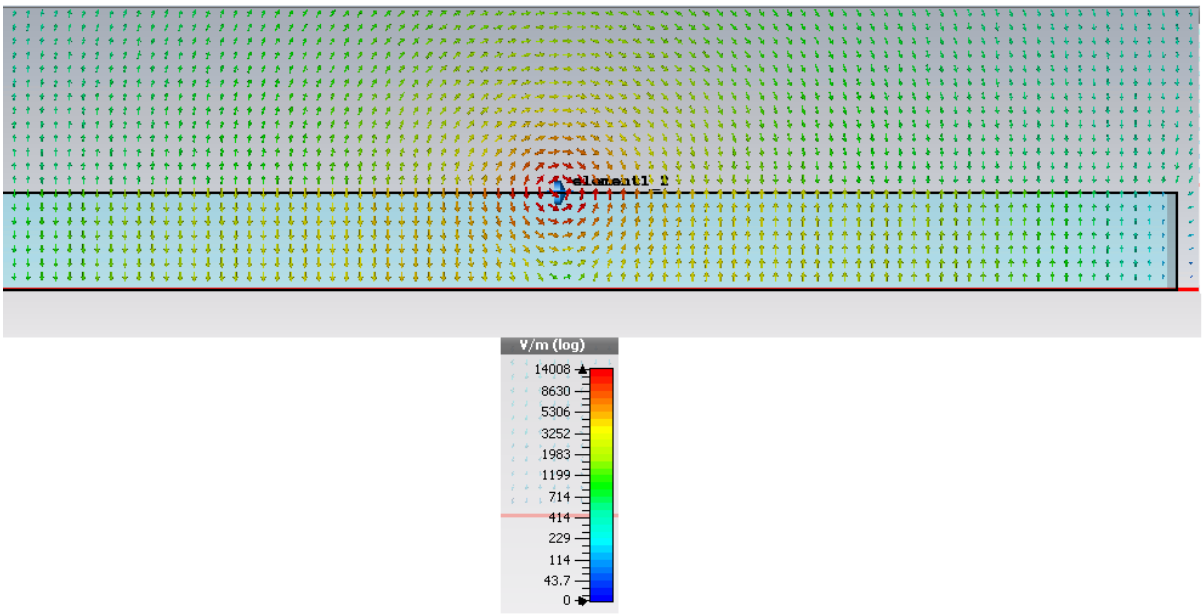

Figure 2.103: Cross-sectional vector plot (at cutoff) of E-field in the SSIW antenna with a load element capacitance of 1.2pF.

Both the preceding field plots demonstrate that the electric field is concentrated across the slot region at resonance. The next figure is a farfield plot of the electric field in the same SSIW antenna structure at the resonant frequency. The total efficiency of the antenna is given by the proportion of the radiated power with respect to the input power. It is evident from this farfield plot that both the total and radiation efficiency are close to -3dB, so that the antenna is reasonably efficient.

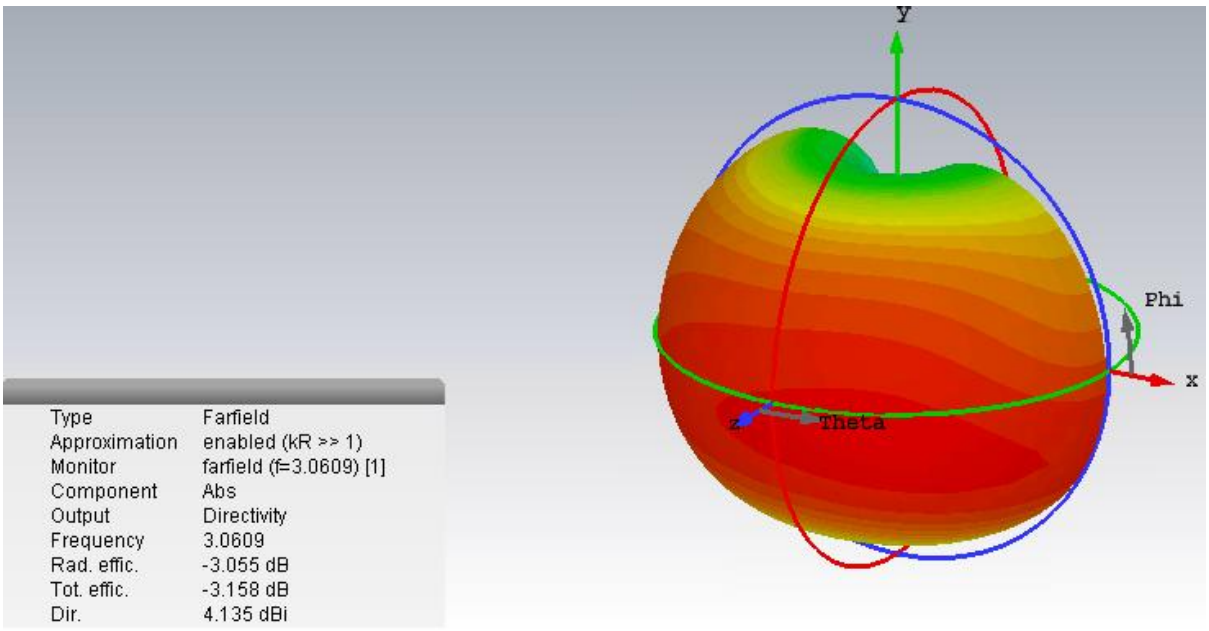

Figure 2.104: Farfield plot at cutoff of the magnitude of the E-field in the SSIW antenna with a load element capacitance of 1.2pF.

If the load element capacitance is reduced to 0.5pF, the SSIW antenna is even more efficient because both the total and radiation efficiency are roughly -2dB. Any load capacitance over the specified range between 0.5pF and 1.2pF corresponds to efficiencies between -2dB and -3dB. Also, any value of efficiency which does not dip below -6dB is desirable, though technically, an antenna with low efficiency may be compensated by using a larger value of input power.

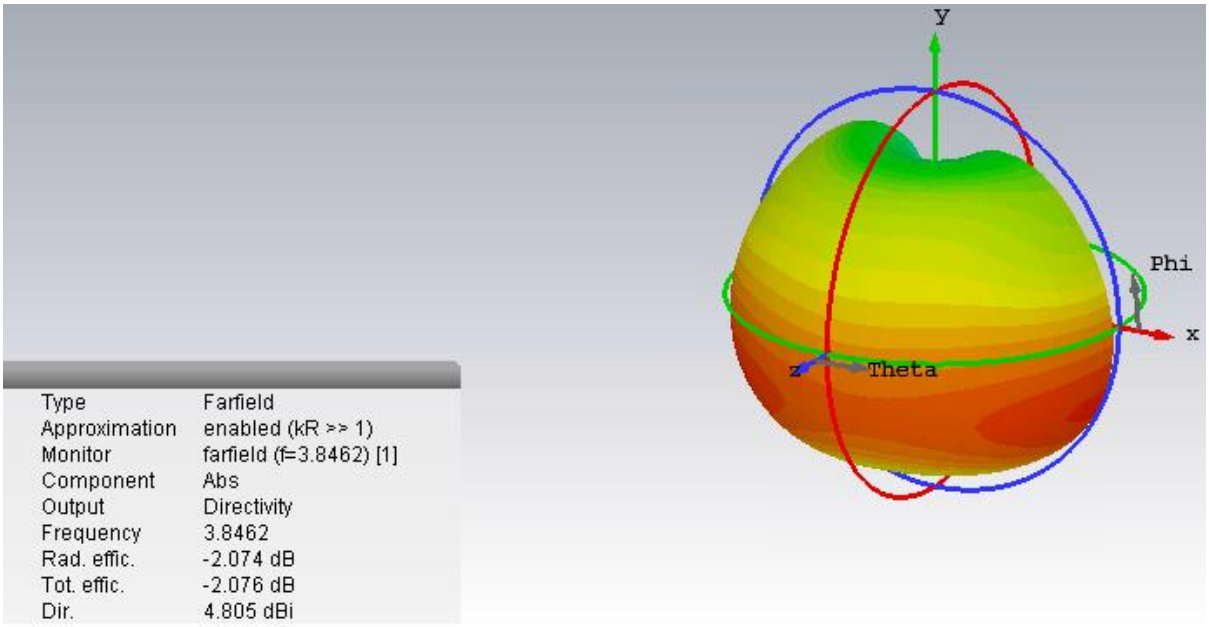

Figure 2.105: Farfield plot at cutoff of the magnitude of the E-field in the SSIW antenna with a load element capacitance of 0.5pF.

The next field plot at the resonant frequency of 3.85 GHz illustrates an aerial view of the electric field at a position roughly equidistant from the top and base of the waveguide when the load element capacitance is reduced 0.5pF.

This plot suggests that the field becomes less concentrated if the load element capacitance is reduced.

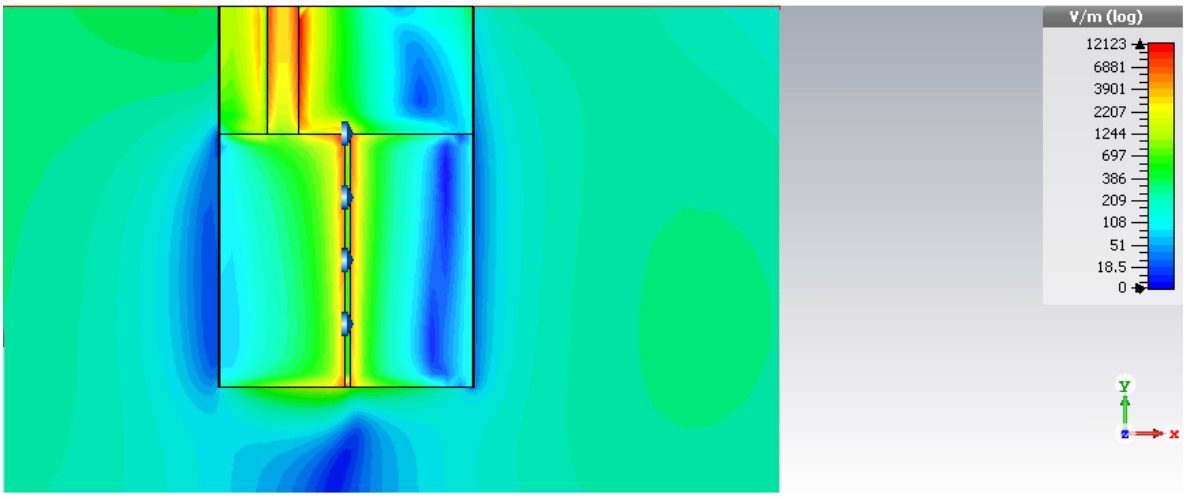

Figure 2.106: Aerial view field plot (at cutoff) of the magnitude of the E-field at a position 0.7mm above the base of SSIW antenna with a load element capacitance of 0.5pF.

Bearing in mind that a capacitor stores an electric field so that, with two parallel plates, it is similar to a patch antenna, it follows that any capacitance radiates to a certain extent. It is evident from this that the field becomes more concentrated if the load element capacitance is increased. This explains why the SSIW antenna structure does not radiate as efficiently for larger capacitances. It follows that the tuneable SSIW antenna loses bandwidth and efficiency if the load element capacitance is too large. Consequently, there is an inevitable a trade off between tuneability and efficiency.

2.19. Summary

It has been established that a transverse resonance technique can be used to understand the characteristics of the cutoff frequencies for the first several modes over the full range of normalized loaded capacitances and inductances for slotted SIW structures. In particular, this technique has been used to assist with the explanation of the calculations for cutoff frequencies when very large and very small inductances and capacitances are used to load the slot.

This transverse resonance technique is then used to calculate specific cutoff frequencies of the fundamental mode for slotted SIWs loaded with a range of actual capacitances and

inductances. These estimates of cutoff frequencies compare well with those from simulations in both CST Microwave Studio and HFSS, for which the cutoff frequency is found by using the group delay definition from S-parameters and setting the phase to zero, respectively. The transverse resonance technique is of great importance because it can provide a whole range of cutoff frequencies as a continuous function, unlike the simulation packages which can only evaluate discrete cutoff frequencies one at a time.

It is clear from the S-parameter plots (from CST Microwave Studio) of these waveguide structures are much better suited to the design of narrow band devices. Dispersion curves obtained from HFSS illustrate the relationship between the phase and the corresponding frequency, and it is evident from these results that the frequencies for sufficiently large phase values are changed much more by load capacitances than by load inductances, especially when the slot is closer to the centre of the waveguide. It is also apparent from these dispersion characteristics that the cutoff frequencies (which correspond to a phase value of zero) are closer to one another for SIWs loaded with inductances rather than with capacitances, particularly when the slot is closer to the centre of the waveguide.

This work on establishing cutoff frequency is subsequently used to attempt to design a slotted SIW structure (with a load capacitance and load inductance in series) which exhibits distinctive features of a bandpass waveguide filter, which is better matched by increasing the thickness of the SIW to 3mm. However, the associated S-parameter phase plots are useful in providing greater understanding of the behaviour of this structure in terms of fast modes and slow modes. This confirms earlier S-parameter plots from CST Microwave Studio that loaded SIWs are better suited for the construction of narrow band devices.

This provides the motivation for the novel design of two devices, namely a two-port tuneable waveguide resonator which can be adjusted over a frequency interval of 300 GHz, and a single port tuneable narrow band antenna which functions over a large operational bandwidth of almost 1 GHz. It is also explained why a two port tuneable antenna cannot be designed with these types of loaded SIWs. Both these narrow band devices are finely tuned by using loaded capacitances. This antenna in particular is the subject of a forthcoming publication.

2.20. References

1. D.M. Pozar, "Microwave Engineering," 2nd edition, Wiley, New York, 1998.
2. R.E. Collin, "Foundations for Microwave Engineering," 2nd edition, IEEE Press, 2001.
3. R.E. Collin, "Field Theory of Guided Waves," McGraw-Hill, 1960.
4. N. Marcuvitz, "Waveguide Handbook," McGraw-Hill, 1951.
5. L. Lewin, "Advanced Theory of Waveguides" Iliffe, 1951
6. Y.K. Cho, "On the equivalent circuit representation of the slitted parallel-plate filled with dielectric," IEEE Trans. Antennas Propag., Vol.37, no.9, 1193-1200, 1989.
7. A.J. Farrall and P.R. Young, "Integrated waveguide slot antennas," Electron.Lett., vol.40, No.16, August 2004, pp.974-975.
8. H.S. Wu and C.-K. C. Tzuang, "Miniaturized synthetic rectangular waveguide," in 2003 IEEE MTT-S Int. Microwave Symp. Dig., Philadelphia, PA, Jun. 8–13, pp. 1099–1102, 2003.
9. S. Pioch and J.-M. Laheurte, "Size reduction of microstrip antennas by means of periodic metallic patterns," Electron. Lett., vol. 39, no. 13, pp. 959–961, Jun. 2003.
10. Q.H. Lai, W. Hong, Z.Q. Kuai, Y.S. Zhang and K. Wu, "Half-Mode Substrate Integrated Waveguide Transverse Slot Array Antennas," IEEE Transactions on Antennas and Propagation, Vol. 57, No. 4, 2009.
11. Q.H. Lai, W. Hong, Z.Q. Kuai, Y.S. Zhang and K. Wu, "Half-mode substrate Integrated waveguide transverse slot array antennas," IEEE Transactions on Antennas and Propagation, Vol. 57, No. 4, 2009.
12. Sellal K., Talbi L., Denidni, T.A. and Lebel J., "Design and implementation of a substrate integrated waveguide phase shifter," IET Microw. Antennas Propag., vol. 2, no. 2, pp. 194-199, 2008.
13. Sellal K., Talbi L., Denidni, T.A., and Lebel J., "Design and implementation of a substrate integrated waveguide phase shifter," IET Microw. Antennas Propag., vol. 2, no. 2, pp. 194-199, 2008.
14. Z. Jin, S. Ortiz, and A. Mortazawi, " Design and performance of a new digital phase shifter at X-band," IEEE Microwave Wireless Comp. Lett., vol.14, no.9, pp.428-430, 2004.
15. S. Cheng, E. Öjefors, P. Hallbjörner, and A. Rydberg, "Compact reflective microstrip phase shifter for traveling wave antenna applications," IEEE Microwave Wireless Comp. Lett., vol.16, no.7, pp.413 433, 2006.
16. Elisa Sbarra, Luca Marcaccioli, Roberto Vincenti Gatti and Roberto Sorrentino, "Ku-band analogue phase shifter in SIW technology," in 39th European Microwave Conference, pp. 264-267, 2009.
17. Cheng Y. J., Hong W. and Wu K., Broadband Self-Compensating Phase Shifter Combining Delay Line and Equal-Length Unequal-Width Phaser," IEEE Trans. Microwave Theory and Tech., Vol 58 , Issue 1, pp. 203 – 210, 2010. 161

18. Sellal K., Talbi L., Denidni, T.A. and Lebel J., "Design and implementation of a substrate integrated waveguide phase shifter," IET Microw. Antennas Propag., vol. 2, no. 2, pp. 194-199, 2008.
19. R. Wang, L.S. Wu and X.-L. Zhou, "Compact folded substrate integrated waveguide cavities and bandpass filters" Progress in Electromagnetics Research, PIER 84, 135-147, 2008.
20. R. Wang, L.S. Wu and X.-L. Zhou, "Compact folded substrate integrated waveguide cavities and bandpass filters" Progress in Electromagnetics Research, PIER 84, 135-147, 2008.
21. Y.Q. Wang, W. Hong, Y.D. Dong, B. Liu, H.J. Tang, J.X. Chen, X.X Yin and K. Wu, "Half mode substrate integrated waveguide (HMSIW) bandpass filter," IEEE Microw. Wireless Compon. Lett, Vol. 17, no.4, pp.265-267, 2007.
22. H. Xin, A. Higgins, J. Hacker,M. Kim, and M. Rosker, "Electromagnetic crystal (EMXT) waveguide band-stop filter," IEEE Microwave Wireless Comp. Lett., vol. 13, no. 3, pp. 108–110, Mar. 2003.
23. H. Xin, A. Higgins, and M. Kim, "Tunable millimeter-wave band-stop filter using electromagnetic crystal (EMXT) surfaces," in *2003 IEEE AP-S Int. Microwave Symp. Dig.*, pp. 1107–1110, 2003
24. D. Deslandes and K. Wu, "Single-substrate integration technique of planar circuits and waveguide filters," IEEE Trans. Microwave Theory Tech., vol. 51, no. 2, pp. 593–596, Feb. 2003.
25. A. Ismail, M.S. Razalli, "X-band and trisection substrate integrated waveguide quasi-elliptic filter," Progress in Electromagnetics Research, PIER 85, 133-145, 2008.
26. H.J. Tang, W. Hong, J.-X. Chen, G.Q. Luo, and K. Wu, "Development of millimetre-wave diplexers based on complementary characters of dual-mode substrate integrated waveguide filters with circular and elliptic cavities," IEEE Progress in Electromagnetics Research Letters, Vol. 10, 2009.
27. D. D. Zhang, L. Zhou, L-S Wu, L-F Qiu, W-Y Yin and J-F Mao, "Novel bandpass filters by using cavity-loaded dielectric resonators in a substrate integrated waveguide," IEEE Trans. Microwave Theory and Techniques, vol. 62, pp. 1173-1182, 2014.
28. M. J. Hill, R. W. Ziolkowski and J. Papapolymerou, "Simulated and measured results from a duroid-based MBG planar cavity resonator filter," Microwave and Guided Wave Lett., IEEE, vol.10, pp. 528-530, 2000.
29. R. Collier, "Transmission Lines, Equivalent Circuits, Electromagnetic Theory and Photons," Cambridge University Press, 2013.
30. Y. J. Cheng, W. Hong, K. Wu, "Millimetre-Wave Substrate Integrated Waveguide Frequency Scanning Antenna with Quadri-Polarization," IEEE Trans. Antennas Propag., Vol.59, no.6, pp.1848-1855-139, 2010.
31. R. Coccioli, F.-R. Yang, K.-P.Ma, and T. Roh, "Aperature-coupled patch antenna on UC-PBG substrate," IEEE Trans. Microwave Theory Tech., vol. 47, no. 11, pp. 2123–2130, Nov. 1999.
32. S. Maci, R. Magliacani, and A. Cucini, "Leaky-wave antennas realized by using artificial surfaces," in Proc. IEEE Antennas Propag. Int. Symp., pp. 1099–1102, 2003.
33. K.C. Chen, Y. Qian, C.K.C. Tzuang, and T. Itoh, "A periodic microstrip radial antenna array with a conical beam," IEEE Trans. Antennas Propag., vol. 51, no. 4, pp. 756–765, Apr. 2003.

34. C.K. Wu, Y.C. Chen, and C.K.C. Tzuang, “Compressed-width leaky EH mode PBG antenna,” IEEE Microwave Wireless Comp. Lett., vol. 13, no. 8, pp. 343–344, Aug. 2003.

3. Transverse Resonance Technique for slotted HMSIW

3.1. Introduction

In this chapter, the transverse resonance technique is applied to the slotted half mode substrate integrated waveguide (HMSIW) to determine its cutoff frequency. As it will be seen, the design and operation of the HMSIW is related to the full rectangular SIW. However, as before, it is much easier to consider its equivalent circuit model for its design analysis, rather than to use analytic techniques involving electric field calculations that appear in the standard textbooks [1]-[5] on the subject. Ever since its introduction in 2006 [6], the versatility of the HMSIW has created the opportunity for it to be easily employed in many different applications. Such devices include antennas [7]-[12], circular cavities [13]-[14], couplers [15]-[16], filters [17]-[18] and switches [19].

The format of this chapter resembles that of the previous one. However many of the results for the HMSIW are shown to exhibit contrasting characteristics which correspond to that of the SIW.

3.2. Background theory

By considering the equivalent circuit model of the slotted HMSIW (shown as follows), it is assumed that the transmission line is terminated with an open circuit at one end.

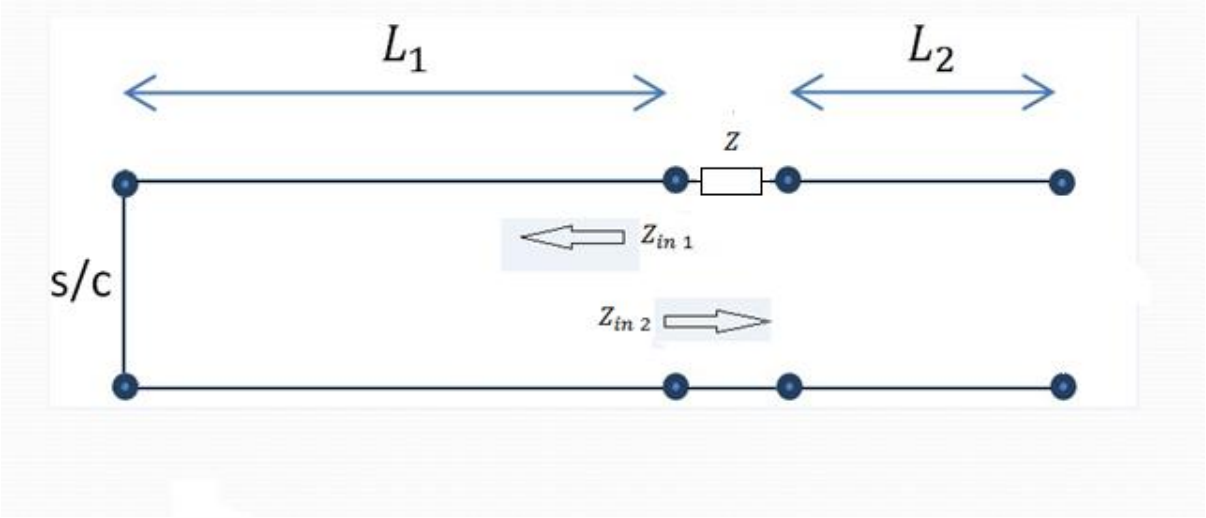

Figure 3.1: Equivalent circuit model of slotted HMSIW

In other words, consider assigning $Z_{Load\,1} = 0$ for the end where the input impedance is $Z_{in\,1}$ and set $Z_{Load\,2} \to \infty$ for the other end where the input impedance is $Z_{in\,2}$.

By using the fact that the input impedance of a lossless terminated line is given by

$$Z_{in} = Z_0 \cdot \frac{Z_{Load} + jZ_0 \tan k_x L_0}{Z_0 + jZ_{Load} \tan k_x L_0} \ , \quad (3.1)$$

it follows that

$$Z_{in\,1} = j\, Z_0\, tan\, k_x L_1 \ , \quad (3.2)$$

$$Z_{in\,2} = Z - \frac{jZ_0}{tan\, k_x L_2} \ . \quad (3.3)$$

Since $$Z_{in\,1} = -Z_{in\,2} \ , \quad (3.4)$$

it may be deduced that

$$jZ_0\ tan\, k_x L_1 = -Z + \frac{jZ_0}{tan\, k_x L_2} \ . \quad (3.5)$$

If $Z = jX$, then

$$tan\ k_x L_1 = -\frac{X}{Z_0} + \frac{1}{tan\ k_x L_2}\ . \qquad (3.6)$$

Note that if the slot is being modelled by a capacitance C , then set

$$X = -\frac{1}{\omega C}\ . \qquad (3.7)$$

Note that if the slot is being modelled by an inductance L , then set

$$X = \omega L\ . \qquad (3.8)$$

By substituting (2.10) and (3.7) into (3.6), it follows that the cut-off equation for a capacitive impedance is given by

$$tan\ \omega L_1\sqrt{\mu\varepsilon} = \frac{1}{\omega C Z_0} + \frac{1}{tan\ \omega L_2\sqrt{\mu\varepsilon}}\ , \qquad (3.9)$$

and, by substituting (2.10) and (3.8) into (3.6), it follows that the cut-off equation for an inductive impedance is given by

$$tan\ \omega L_1\sqrt{\mu\varepsilon} = -\frac{\omega L}{Z_0} + \frac{1}{tan\ \omega L_2\sqrt{\mu\varepsilon}}\ . \qquad (3.10)$$

3.3. Capacitive cutoff equation for a HMSIW

Let C' be the capacitance per unit length. Then for a distance d along the length of the slot, the total capacitance and total inductance across the slot is given by

$$C = C'd\ , \qquad (3.11)$$

and

$$L = L'd\ , \qquad (3.12)$$

for the purely capacitively and inductively loaded HMSIWs respectively.

Then, by substituting (2.23) into (3.9) and into (3.10), the cut-off equations for a purely capacitive and purely inductive impedance in a HMSIW are given by

$$tan\ \omega L_1\sqrt{\mu\varepsilon} = \frac{1}{\omega C' b\sqrt{\frac{\mu}{\varepsilon}}} + \frac{1}{tan\ \omega L_2\sqrt{\mu\varepsilon}}\ , \qquad (3.13)$$

and

$$tan\ \omega L_1\sqrt{\mu\varepsilon} = -\frac{\omega L'}{b\sqrt{\frac{\mu}{\varepsilon}}} + \frac{1}{tan\ \omega L_2\sqrt{\mu\varepsilon}}\ , \qquad (3.14)$$

respectively, where the angular cut-off frequency is given by ω.

The respective cut-off equations for a purely capacitive and purely inductive impedance can be rewritten by substituting (2.28), (2.29) and (2.30) into both (3.13) and (3.14), and are given by

$$tan\ \theta - \frac{1}{tan\frac{\theta}{\Gamma}} = \frac{1}{\hat{C}\theta}\ , \qquad (3.15)$$

$$tan\ \theta - \frac{1}{tan\frac{\theta}{\Gamma}} = -\hat{L}\theta\ , \qquad (3.16)$$

where $\Gamma = \frac{L_1}{L_2}$, and θ, $\hat{C}$, $\hat{L}$ represent normalized parameters of frequency, capacitance and inductance, respectively. Since these cut-off equations for the HMSIW are transcendental, they can only be solved numerically. In order to find the solutions of this equation, it is necessary to locate intervals of θ inside which possible solutions may exist.

3.4. Normalized solutions of the capacitive cut-off equation for the HMSIW

Maple software has been used once again to calculate the solutions of θ for the first five modes over a suitable range of $\hat{C}$ for values of $\Gamma = 3,4,5,6$. These results are presented below as theoretical design curves. In order to see the results over a suitably large ranges of $\hat{C}$ and $\hat{L}$, a logarithmic scale is employed.

By considering the capacitive cut-off equation for a HMSIW, the vertical axis of each design curve, being in units of $\frac{\theta}{\pi}$, is proportional to the angular cut-off frequency ω by (2.28). The horizontal axis of each design curve is given by the reciprocal of either $\hat{C}$ or $\hat{L}$, which is

regarded as normalized elastance or reluctance, respectively. Some explanations for these design curves are provided in the subsequent sections.

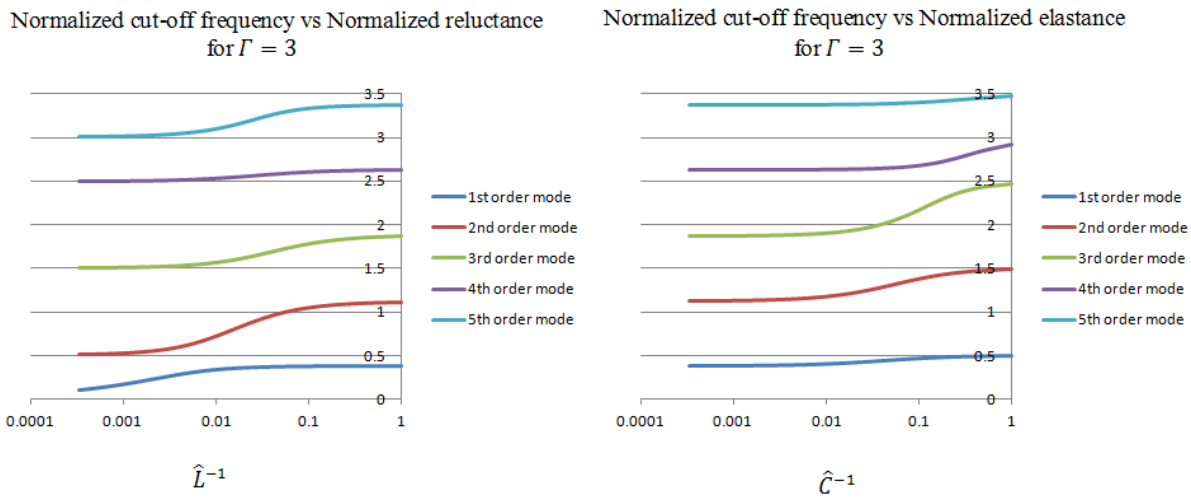

Figure 3.2: HMSIW design curves for loaded capacitances and inductances for Γ=3

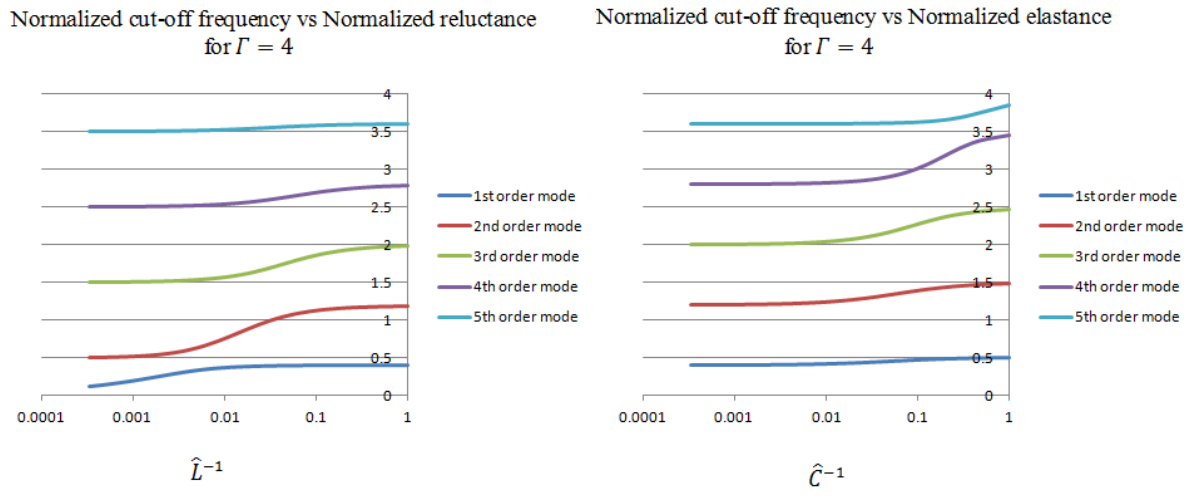

Figure 3.3: HMSIW design curves for loaded capacitances and inductances for Γ=4

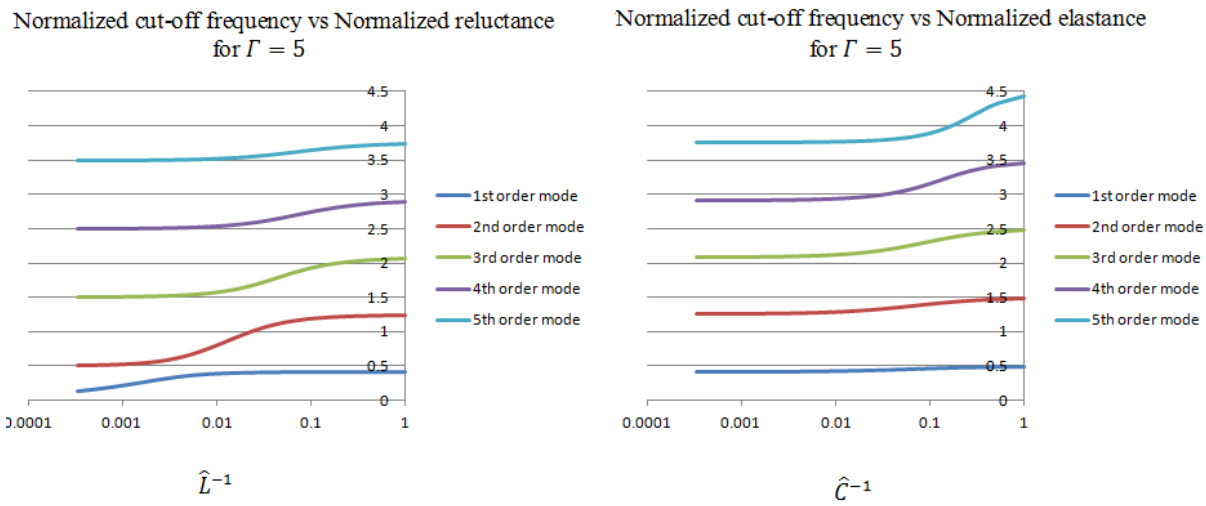

Figure 3.4: HMSIW design curves for loaded capacitances and inductances for Γ=5

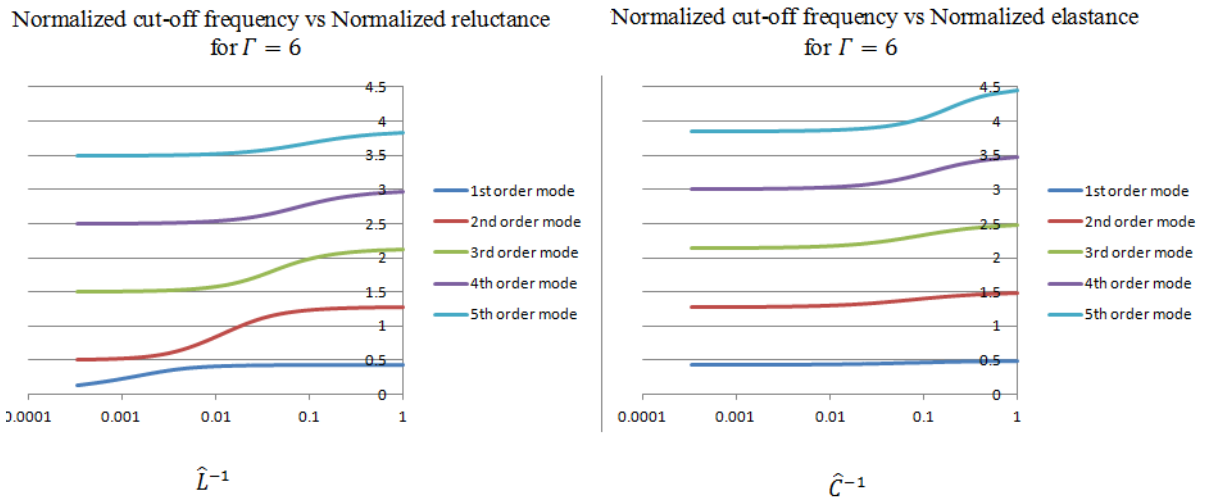

Figure 3.5: HMSIW design curves for loaded capacitances and inductances for Γ=6

3.5. Small capacitances for the capacitive cut-off equation

If the capacitance is very small, it is equivalent to an open circuit. It follows that the HMSIW slotted with a very small capacitance has the cut-off frequency of a standard half mode

waveguide. This is shown in the graphs above where $\theta \to \frac{\pi}{2}$, $\theta \to \frac{3\pi}{2}$ and $\theta \to \frac{5\pi}{2}$ as the capacitance $C \to 0$ for the 1st , 2nd and 3rd order modes respectively, for any value of Γ.

3.6. Large capacitances for the capacitive cut-off equation

If the capacitance is sufficiently large it behaves more like a short circuit.

Therefore, the HMSIW slotted with a sufficiently large capacitance is equivalent to a standard half mode waveguide.

As the capacitance is increased, the cut-off frequency of the 1st order mode decreases to almost zero until eventually the E-field concentrates itself around the slot, at which point the mathematics of our transverse resonance technique breaks down.

Consider the quarter cosine waveform which envelopes the electric field pattern of the 1st order mode in the standard half mode waveguide, as shown in Figure 2.10.

It follows that the cut-off frequency of the n^{th} order mode in the SIW slotted with a sufficiently large capacitance is equivalent to the cut-off frequency of the $(2n-1)^{\text{th}}$ order mode in a half mode waveguide, where $n = 1,2, \ldots$. For simplicity, the non-existent even order modes are counted as modes of the standard half mode waveguide by definition.

Defining x to be the transverse axis of the SIW slotted with a sufficiently large capacitance, the standard condition at cut-off for this SIW is then given by $\theta = k_x L_1 a = (2n-1)\frac{\pi}{2} L_1$, where $n = 1,2, \ldots$, where θ is given by (2.28), and where the wave number k_x is defined in (2.2) and $a = L_1 + L_2$ (since the slot width is negligible in comparison to the guide width a).

Then the condition at cut-off is given by

$$\theta = \frac{(2n-1)\frac{\pi}{2} L_1}{L_1 + L_2} = \frac{(2n-1)\frac{\pi}{2}}{\left(1 + \frac{1}{\Gamma}\right)} \quad . \qquad (3.17)$$

For example, if $n = 2$ (i.e. considering the 2nd order mode), then it follows from the last equation that for $\Gamma = 3$, $\theta \to \frac{9}{8}\pi$ for very large capacitances. Also, if $n = 2$, then for $\Gamma = 4$, $\theta \to \frac{12}{10}\pi$ for very large capacitances. This is in agreement with the 2nd order mode solution

(when $\Gamma = 3,4$ respectively) design curve values for normalized frequency for very large capacitances. By the above equation, we can see, for the 2nd order mode, that as Γ becomes sufficiently large, then, theoretically, $\theta \to \frac{3\pi}{2}$ for very large capacitances.

3.7. Large inductances for the inductive cut-off equation

If the inductance is very large it behaves more like an open circuit. For $n = 2,3, \dots$, the n^{th} order mode of the HMSIW loaded with a large inductance has the cut-off frequency of the $(n-1)^{\text{th}}$ mode in in a conventional half mode waveguide. As the inductance is increased, the cut-off frequency of the 1st mode decreases to almost zero until eventually the E-field concentrates itself around the slot, at which point the mathematics of our transverse resonance technique breaks down.

The results for inductance in the graphs above can therefore be confirmed by considering the corresponding modes in the basic half mode waveguide.

For instance $\theta \to 0$ as the inductance $L \to 0$ for the 1st order modes of the slotted HMSIW, irrespective of the choice of Γ. Also $\theta \to \frac{\pi}{2}$ and $\theta \to \frac{3\pi}{2}$ as the inductance $L \to 0$ for the 2nd and 3rd order modes of the slotted HMSIW respectively, and this is independent of Γ.

3.8. Small inductances for the inductive cut-off equation

If the inductance is very small, it is equivalent to a short circuit. Therefore, the HMSIW slotted with a sufficiently small inductance is equivalent to a standard half mode waveguide.

Consider, as was done in the case for HMSIW slotted with a very large capacitance, the quarter cosine waveform which envelopes the electric field pattern of the 1st order mode in the standard half mode waveguide. It follows that the cut-off frequency of the n^{th} order mode in the SIW slotted with a sufficiently small inductance is equivalent to the cut-off frequency of the $(2n-1)^{\text{th}}$ order mode in a half mode waveguide, where $n = 1,2, \dots$. For simplicity, by our definition we have counted the non-existent even order modes as modes of the standard half mode waveguide.

Defining x to be the transverse axis of the inductively slotted HMSIW, the standard condition at cut-off for this inductively slotted HMSIW is then given by $\theta = k_x L_1 a = (2n-1)\frac{\pi}{2}$, where $n \epsilon \{1,2,...\}$. Then this condition at cut-off is given by (3.17).

For example, if $n = 1$ (i.e. considering the 1st order mode), then it follows from the last equation that for $\Gamma = 3,\ \theta \to \frac{3}{4}\cdot\frac{1}{2}\pi = \frac{3}{8}\pi$ for very small inductances. Also, if $n = 2$, then for $\Gamma = 4,\ \theta \to \frac{4}{5}\cdot\frac{3}{2}\pi = \frac{6}{5}\pi$ for very small inductances. These calculations are in agreement with the 1st and 2nd order mode solutions from the the design curve value for normalized frequency for very small inductances when $\Gamma = 3,4$ respectively. By the above equation, we can see that as Γ becomes sufficiently large, then, theoretically, $\theta \to (2n-1)\frac{\pi}{2}$ for the n^{th} order mode for very small inductances for $n = 1,2,3$.

3.9. Modelling specific capacitances across a slot in a HMSIW

We recall that the cut-off equation for a purely capacitive slot with capacitance C' per unit length is given by

$$tan\ \omega L_1\sqrt{\mu\varepsilon} = \frac{1}{\omega C' b\sqrt{\frac{\mu}{\varepsilon}}} + \frac{1}{tan\ \omega L_2\sqrt{\mu\varepsilon}}\ , \qquad (3.18)$$

which, by using the fact that $k_x = \omega\sqrt{\mu\varepsilon}$, may be rewritten as

$$tan\ k_x L_1 = \frac{1}{\omega C' b\sqrt{\frac{\mu}{\varepsilon}}} + \frac{1}{tan\ k_x L_2}\ . \qquad (3.19)$$

Since $\Gamma = \frac{L_1}{L_2}$, it follows that

$$tan\ \theta - cot\ \frac{\theta}{\Gamma} = \frac{1}{\omega C' b\sqrt{\frac{\mu}{\varepsilon}}}\ , \qquad (3.20)$$

where $\theta = k_x L_1$ by (2.36).

By recalling from (2.37) that

$$\frac{1}{\omega C' b\sqrt{\frac{\mu}{\varepsilon}}} = \frac{L_1}{\hat{C}\theta} \ , \tag{3.21}$$

where $\hat{C} = \frac{C'b}{\varepsilon}$ from (2.29), it now follows easily that

$$tan\,\theta + cot\,\frac{\theta}{\Gamma} = \frac{L_1}{\hat{C}\theta} \ , \tag{3.22}$$

from which it is possible to determine θ for suitable values of C'.

As in the previous chapter, (2.39)-(2.41) are used to obtain calculated predictions for the cut-off frequency f_c of the first mode over a suitable range of values of C' which is, in practice, at least 20pF/m (from [20]). These predictions will now be compared with those from CST Microwave Studio.

The corresponding values of C_{load} for C', which are used to model the specific slotted waveguide structures in CST Microwave Studio, are exactly the same as in the previous chapter and can be found in Figure 2.13 in Section 2.8.

CST Microwave Studio is used to predict the cut-off frequencies from the values for C' in the table above in exactly the same manner as before. Exactly the same waveguide dimensions, where $\Gamma = \frac{3}{2}, 3, 6$, are considered as before. Some S-parameter plots from CST Microwave Studio are shown in the following figures with the corresponding cutoff frequencies.

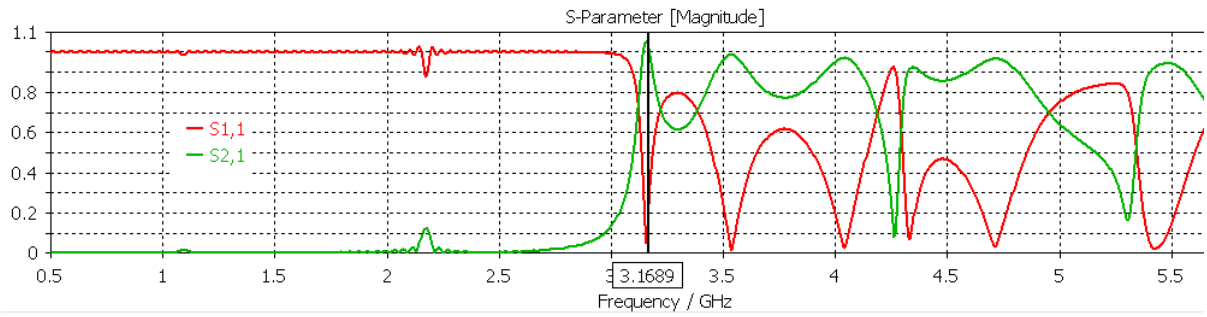

Figure 3.6: Magnitudes of S-parameters for Γ=3, C' = 20 pF/m

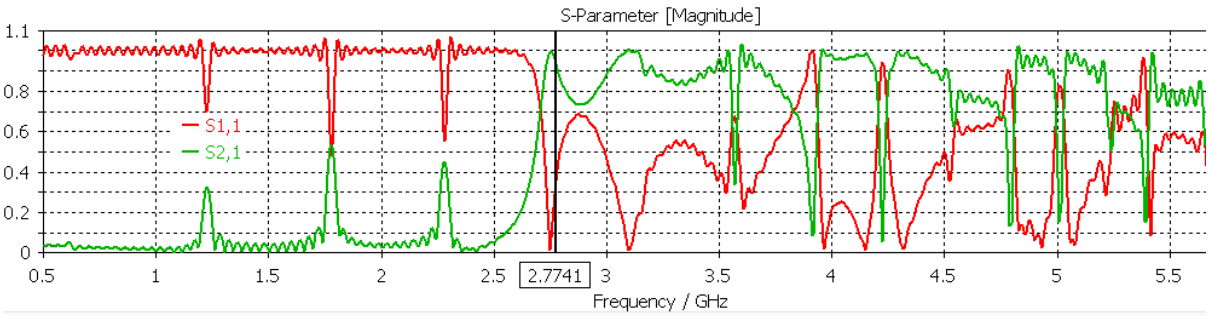

Figure 3.7: Magnitudes of S-parameters for Γ=3, C' = 200 pF/m

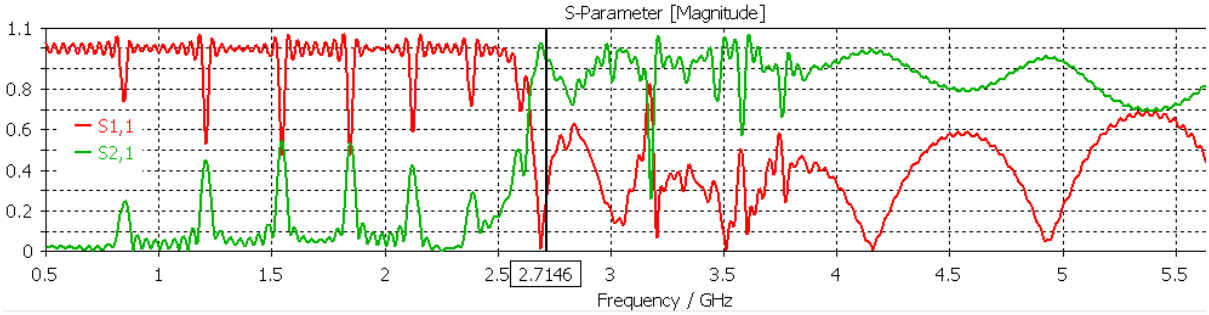

Figure 3.8: Magnitudes of S-parameters for Γ=3, C' = 500 pF/m

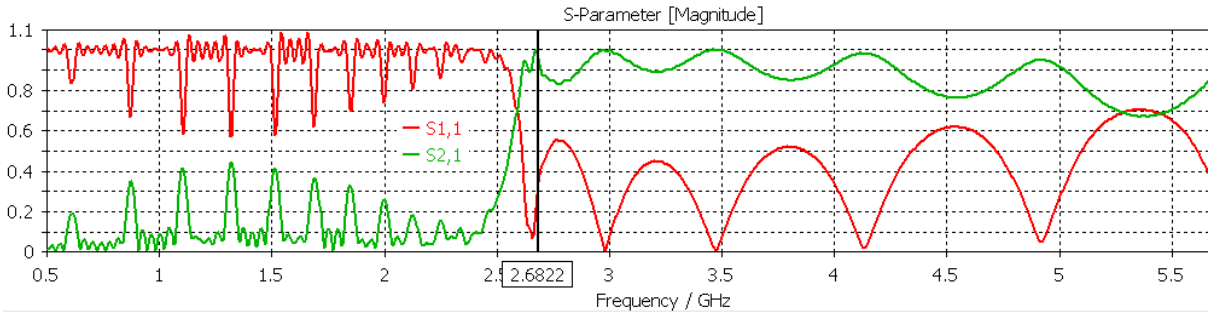

Figure 3.9: Magnitudes of S-parameters for Γ=3, C' = 1000 pF/m

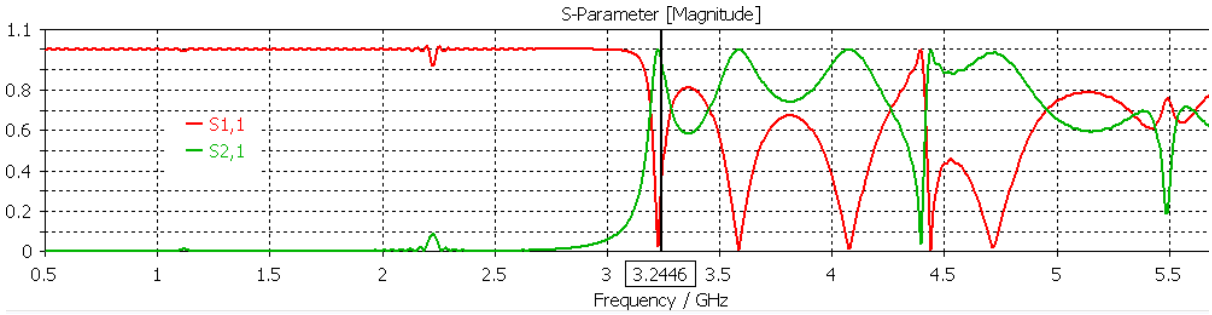

Figure 3.10: Magnitudes of S-parameters for Γ=6, C' = 20 pF/m

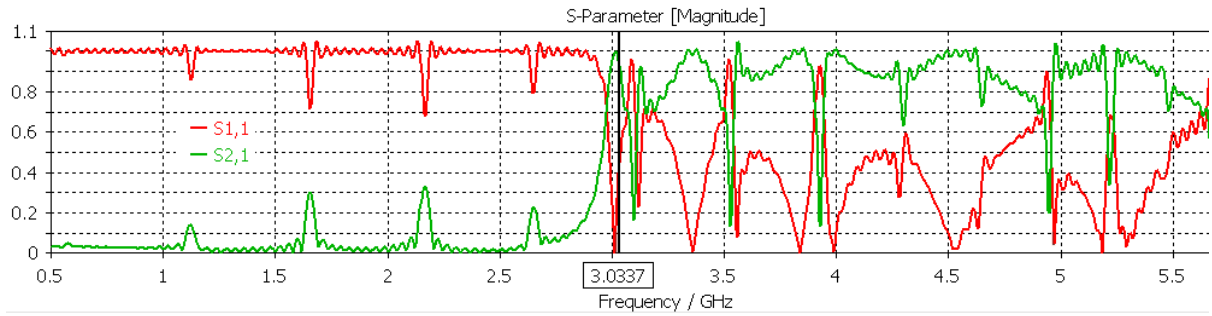

Figure 3.11: Magnitudes of S-parameters for Γ=6, C' = 200 pF/m

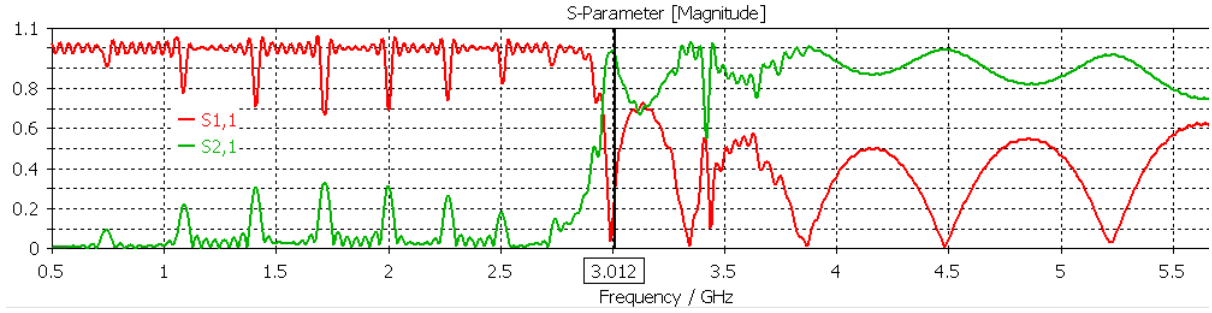

Figure 3.12: Magnitudes of S-parameters for Γ=6, C' = 500 pF/m

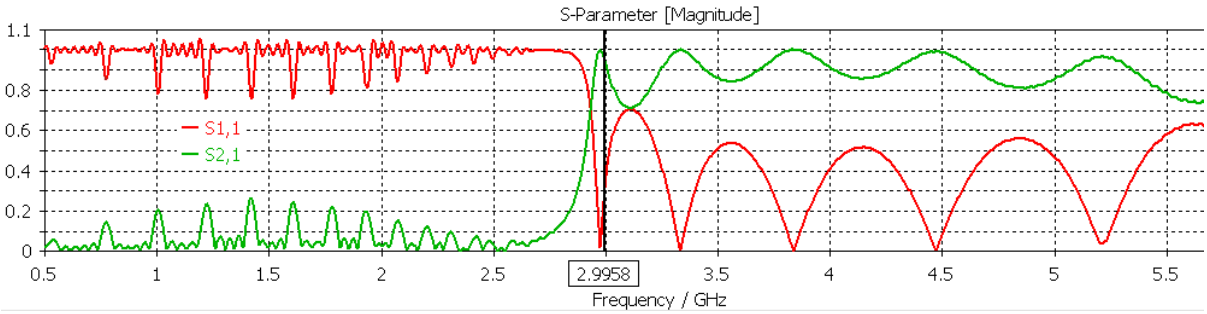

Figure 3.13: Magnitudes of S-parameters for Γ=6, C' = 1000 pF/m

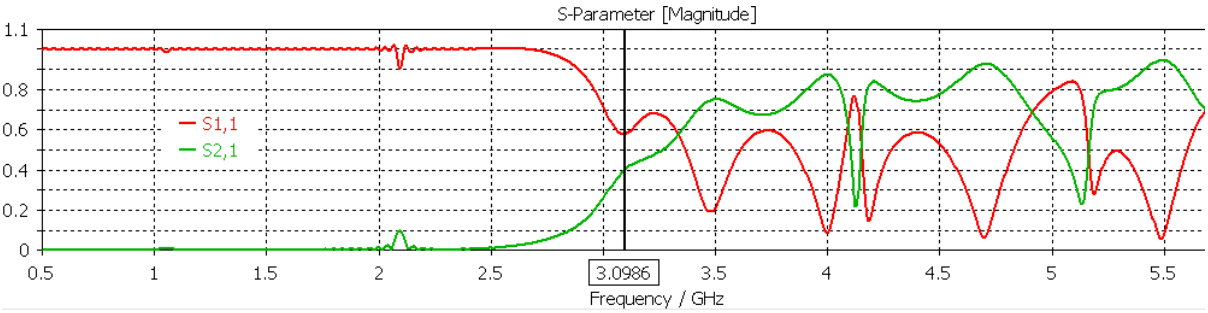

Figure 3.14: Magnitudes of S-parameters for Γ=1.5, C' = 20 pF/m

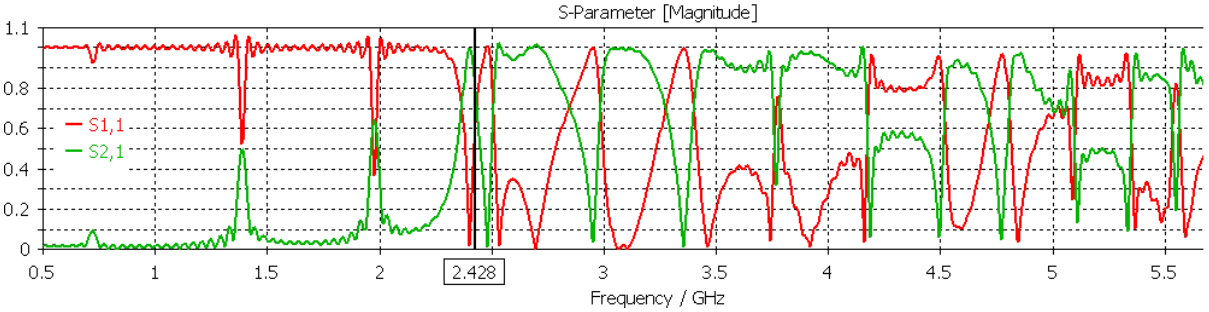

Figure 3.15: Magnitudes of S-parameters for Γ=1.5, C' = 200 pF/m

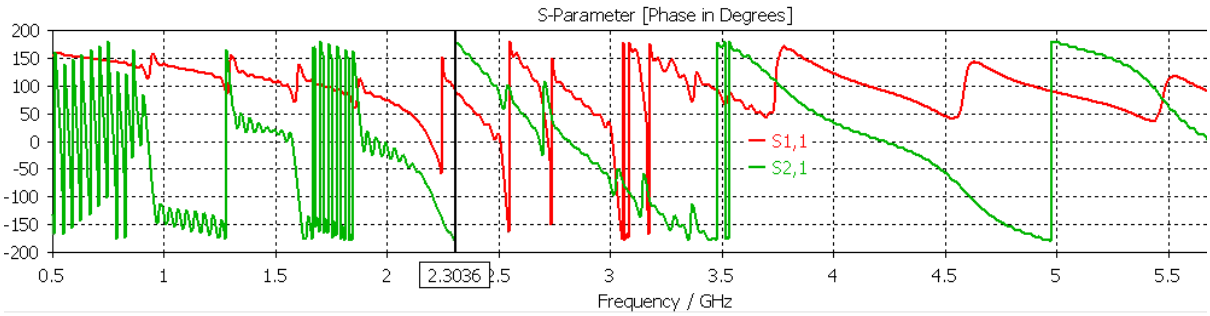

Figure 3.16: Magnitudes of S-parameters for Γ=1.5, C' = 500 pF/m

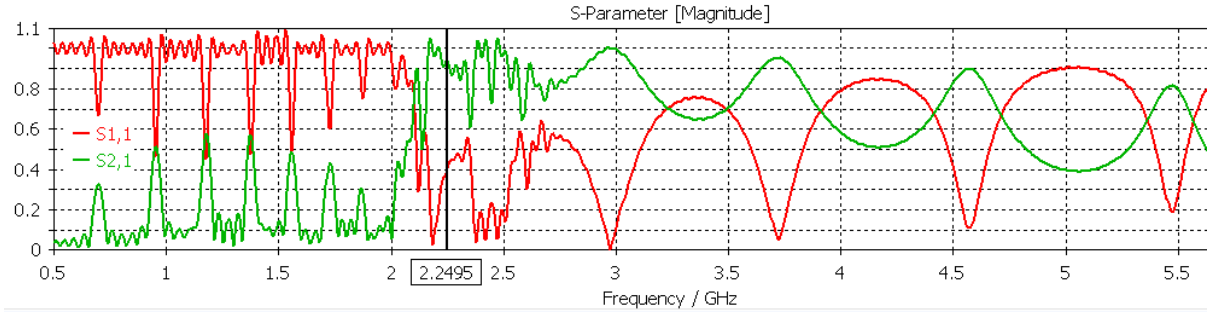

Figure 3.17: Magnitudes of S-parameters for Γ=1.5, C' = 1000 pF/m

The following dispersion curves from HFSS indicate that the frequencies for the HMSIW structures are much closer together than for the SIW structures, and even more so for larger values of Γ as the slot is further away from the centre of the waveguide. This demonstrates that the cutoff frequency varies much less with the load capacitance in the case of HMSIW structures as compared with full SIW structures.

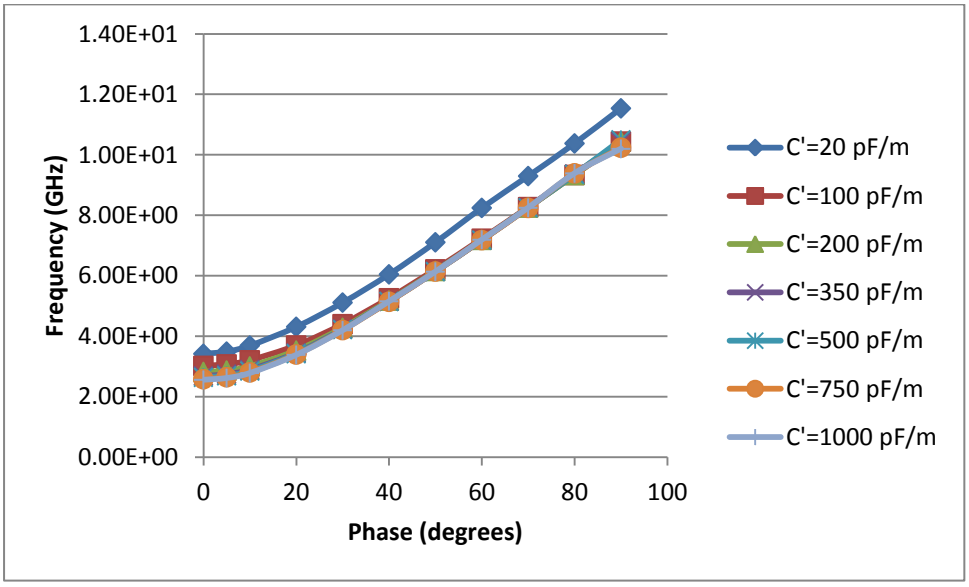

Figure 3.18: Dispersion curve from HFSS for HMSIW with Γ=1.5

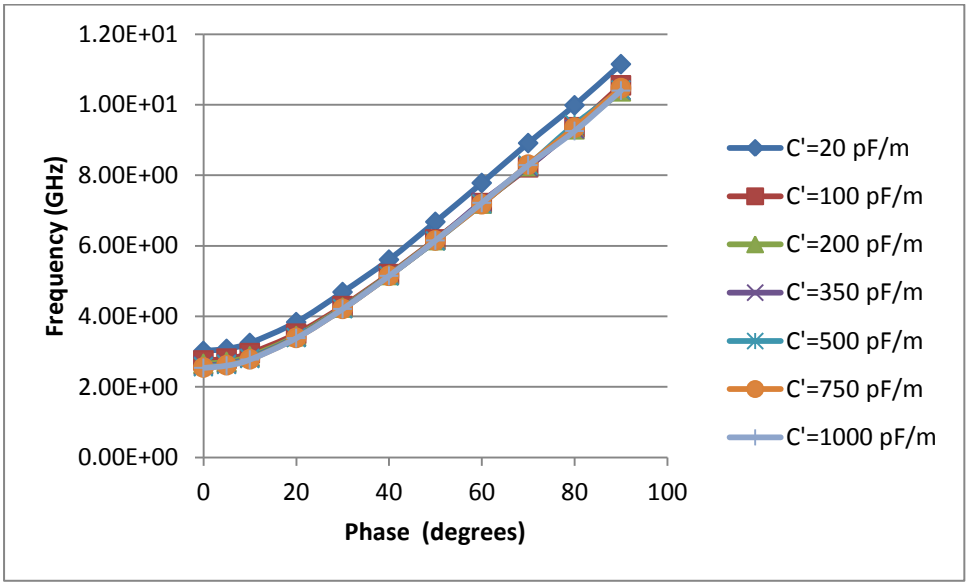

Figure 3.19: Dispersion curve from HFSS for HMSIW with Γ=3

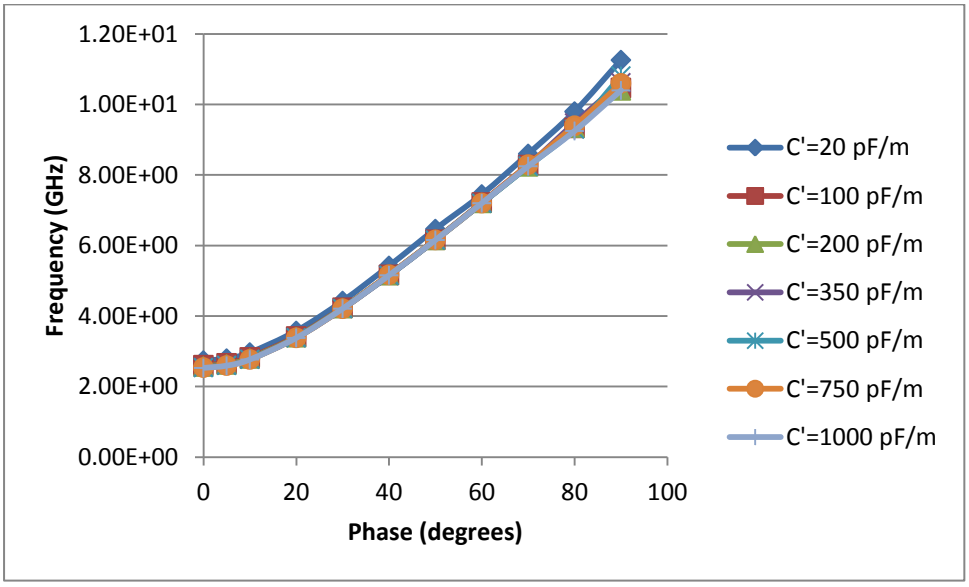

Figure 3.20: Dispersion curve from HFSS for HMSIW with Γ=6

The next three figures show the comparison between the predictions for the cut-off frequencies of the first mode from our transverse resonance technique and the discrete values for the cut-off frequencies (shown in the preceding figures) from CST Microwave Studio for the respective values of $\Gamma = 3,6,\frac{3}{2}$. The agreement between these two sets of results is stronger when the slot is closer to the centre of the waveguide (i.e. for smaller values of Γ). There is also better agreement between both sets of predictions when the loaded capacitance is relatively small.

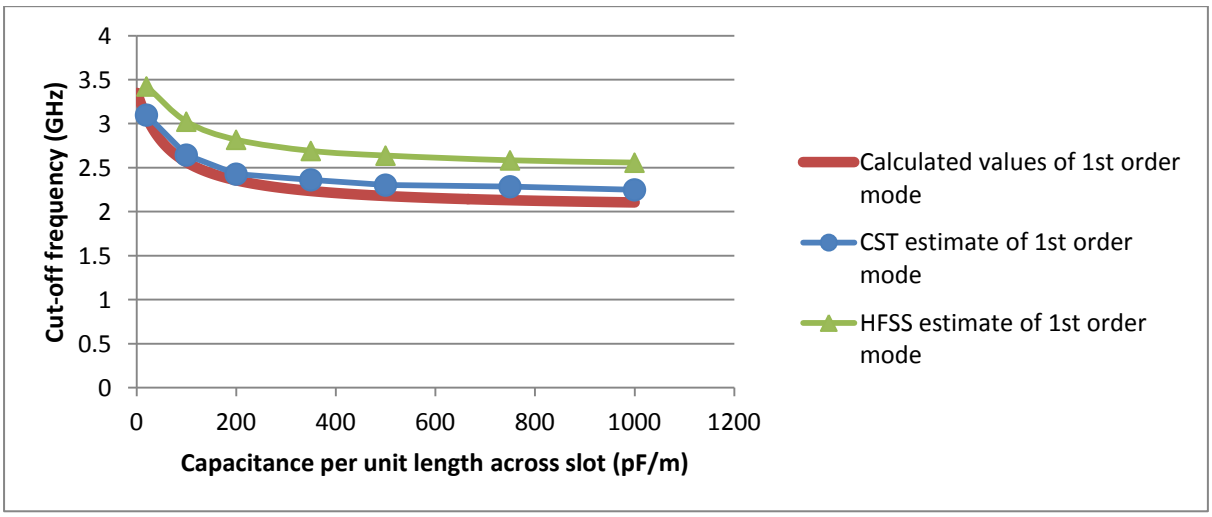

Figure 3.21: Cut-off frequency against capacitance across slot in for Γ=1.5

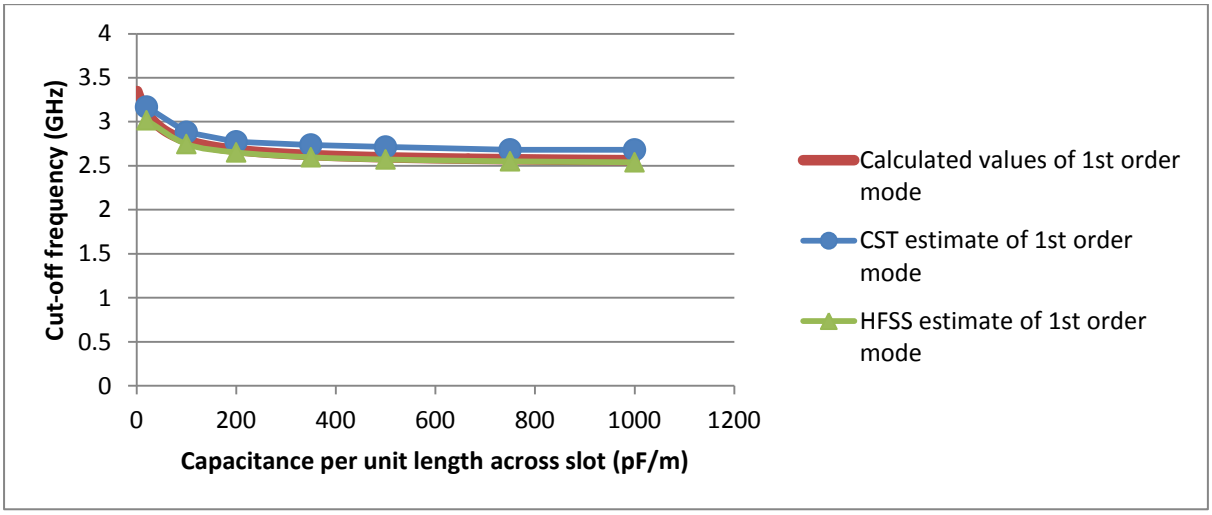

Figure 3.22: Cut-off frequency against capacitance across slot in for Γ=3

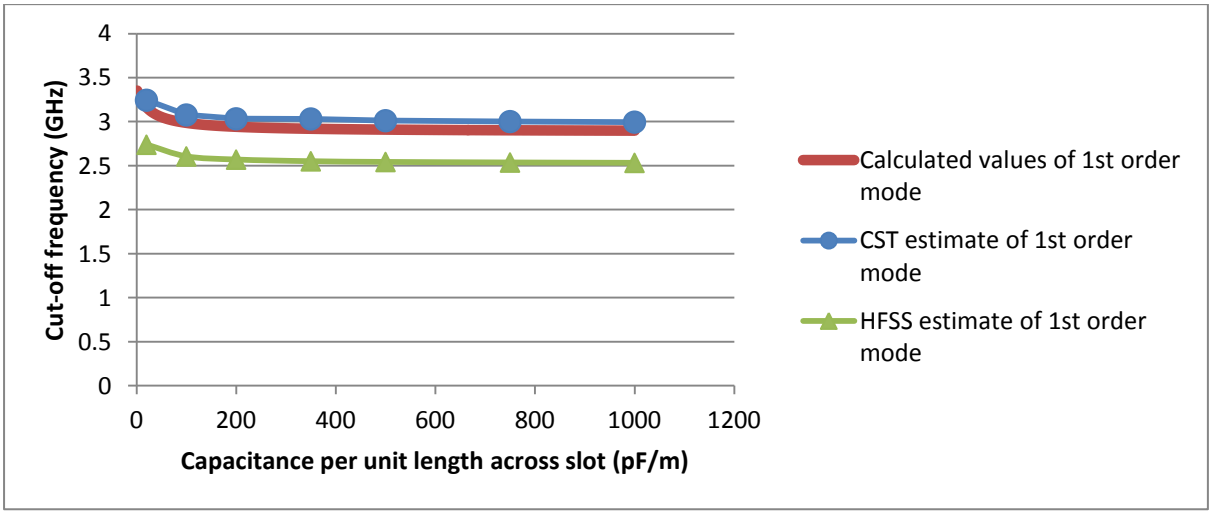

Figure 3.23: Cut-off frequency against capacitance across slot in for Γ=6

The following graph shows the design curve predictions from the transverse resonance technique for the cut-off frequencies for the earlier specified values of Γ over a range of capacitances per unit length from 1 pF/m to 1nF/m.

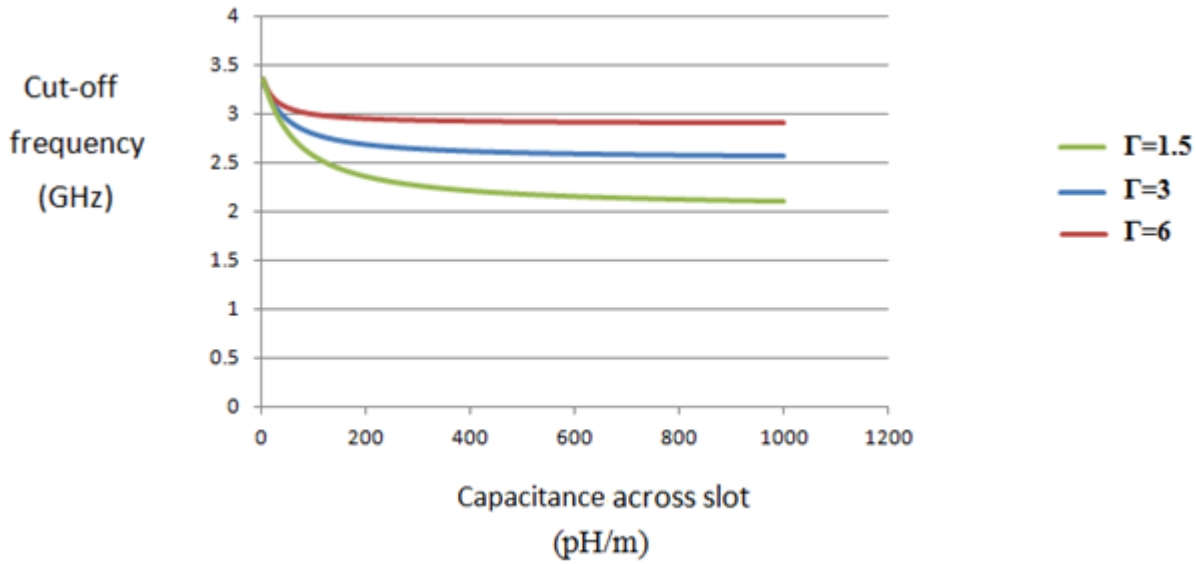

Figure 3.24: Predictions of cut-off frequency against capacitance across slot from transverse resonance technique

Now consider looking at field plots in a certain interesting case considered above, namely for $\Gamma = 3$ and C'=500pF/m at 3.25GHz (which is just above the cut-off frequency). The next figure shows the pattern of the component of electric field which travels from the top of the guide to its base. It is evident from this that the alternating electric field oscillates throughout the length of the guide, but it is not as strong as in the analogous capacitively loaded full guide case looked at before.

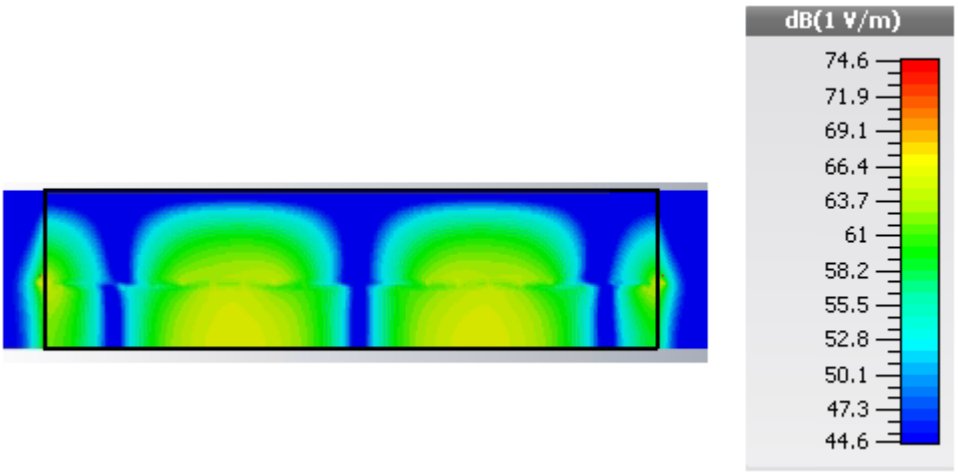

Figure 3.25: An aerial view field plot of E_z 0.4mm from the base of the HMSIW for Γ=3 and a slot loaded with C' = 500 pF/m at 3.25GHz

The following cross-sectional plot of the electric field on the incident port of the waveguide indicates that the field pattern is dominated by the part of the guide that is on the left hand side of the slot (i.e. the larger section of waveguide corresponding to the cross-sectional length L_1 for which the field is maximal when closest to the slot). The smaller part of this cross-section corresponding to the length L_2 is swamped with the largest values of electric field. This demonstrates that the model from CST Microwave Studio may have difficulty in calculating results for the HMSIW, particularly when the length L_2 is relatively small (as was demonstrated in the comparisons made earlier with both the analytical method and the HFSS simulations).

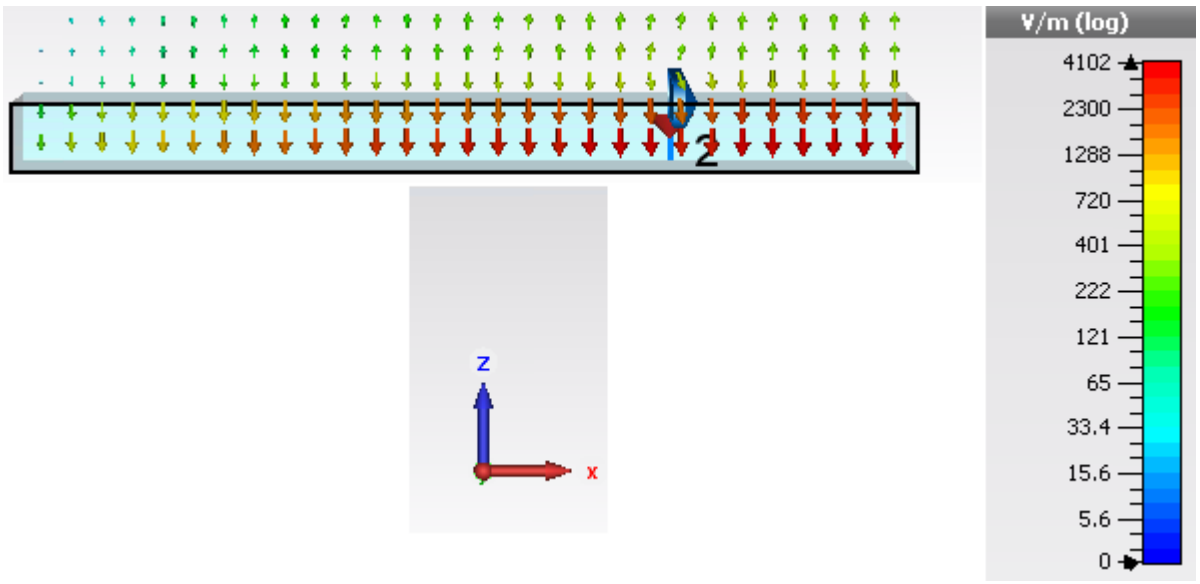

Figure 3.26: A cross-sectional E-field plot at the edge of the longitudinal side of the guide for Γ=3 and a slot loaded with C' = 500 pF/m at 3.25GHz

It transpires that the field patterns do not significantly change so much at higher frequencies which are close to the next higher order mode.

3.10. Modelling an inductively loaded slot in an HMSIW

By using the fact that $k_x = \omega\sqrt{\mu\varepsilon}$, the cut-off equation for a purely inductive slot with inductance L' per unit length is given by (3.14) may be rewritten as

$$tan\ k_x L_1 = -\frac{\omega L'}{b\sqrt{\frac{\mu}{\varepsilon}}} + cot\ k_x L_2\ . \qquad (3.23)$$

Since $\Gamma = \frac{L_1}{L_2}$, it follows that

$$tan\ \theta - cot\ \frac{\theta}{\Gamma} = -\frac{\omega L'}{b\sqrt{\frac{\mu}{\varepsilon}}}\ , \qquad (3.24)$$

where $\theta = k_x L_1$ by (2.36).

By noticing from (2.55) that

$$\frac{\omega L'}{b\sqrt{\frac{\mu}{\varepsilon}}} = \frac{\hat{L}\theta}{L_1}, \qquad (3.25)$$

where $\hat{L} = \frac{L'}{b\mu}$ from (2.30), it is easily observed that

$$tan\,\theta - cot\,\frac{\theta}{\Gamma} = -\frac{\hat{L}\theta}{L_1}\ , \qquad (3.26)$$

from which it is possible to determine θ for suitable values of L'.

By considering (2.39)-(2.41) and (3.26), it is possible to obtain the cut-off frequency f_c over an appropriate range of values of L'. This allows for calculated predictions for the cut-off frequency f_c over an appropriate range of values of L' from 0.3 pH/m to 300pH/m. These calculated estimates can now be compared with those from CST Microwave Studio and HFSS.

The slot is loaded in exactly the same way with the same inductances as before in the case of the full waveguide (see Figure 2.42).

Both CST Microwave Studio and HFSS used, with one side of the waveguide represented by an H plane, to predict the cut-off frequencies from the same values for L' as before. Once again, we consider slotted SIW structures with width $L_1 = 15$ mm, height $b = 1.575$ mm and relative permittivity $\varepsilon_r = 2.2$. The same three waveguide structures are considered, namely those with $\Gamma = 3,6,\frac{3}{2}$. Selected plots of S-parameters are shown with corresponding estimates for cutoff frequencies in the subsequent CST plots.

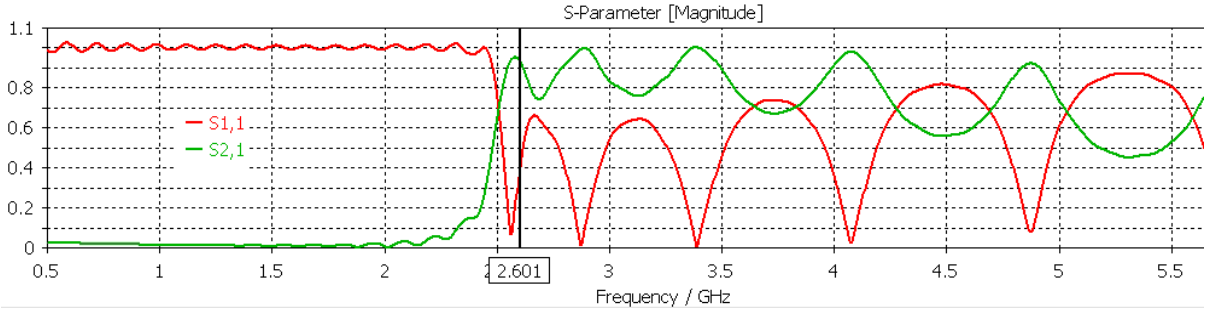

Figure 3.27: Magnitudes of S-parameters for Γ=3, L' = 0.3 pH/m

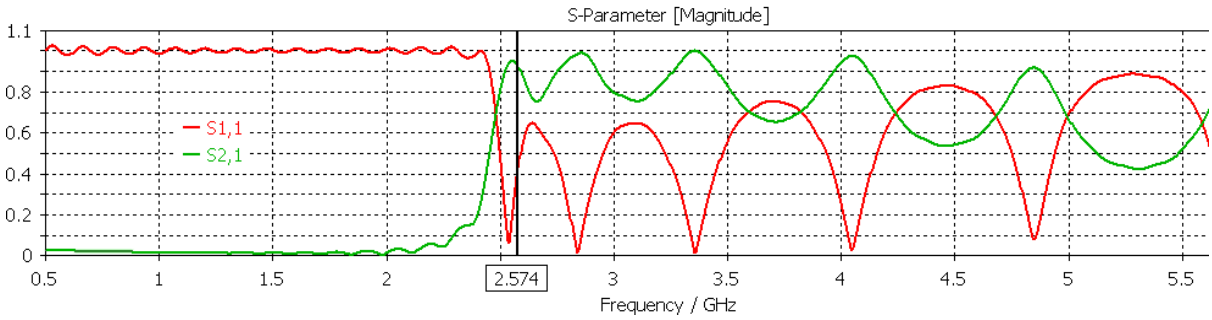

Figure 3.28: Magnitudes of S-parameters for Γ=3, L' = 3 pH/m

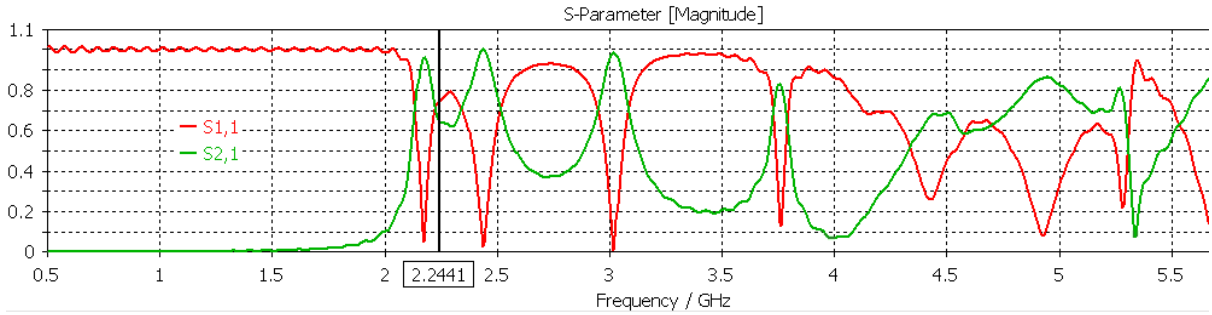

Figure 3.29: Magnitudes of S-parameters for Γ=3, L' = 30 pH/m

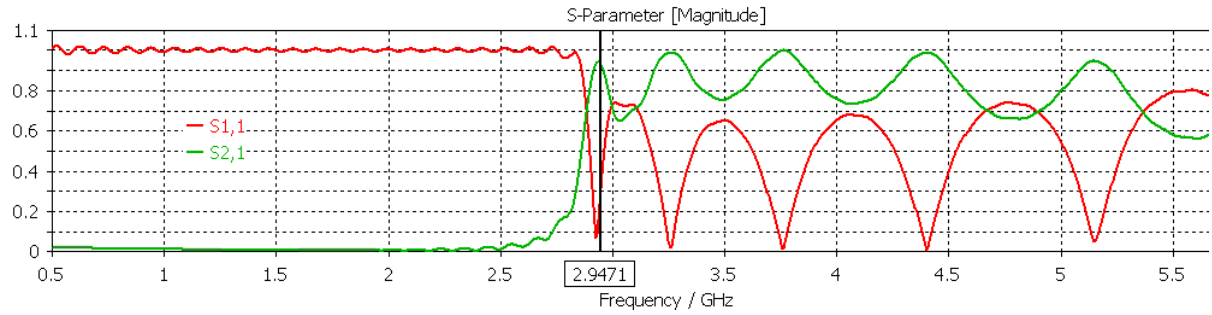

Figure 3.30: Magnitudes of S-parameters for Γ=6, L' = 0.3 pH/m

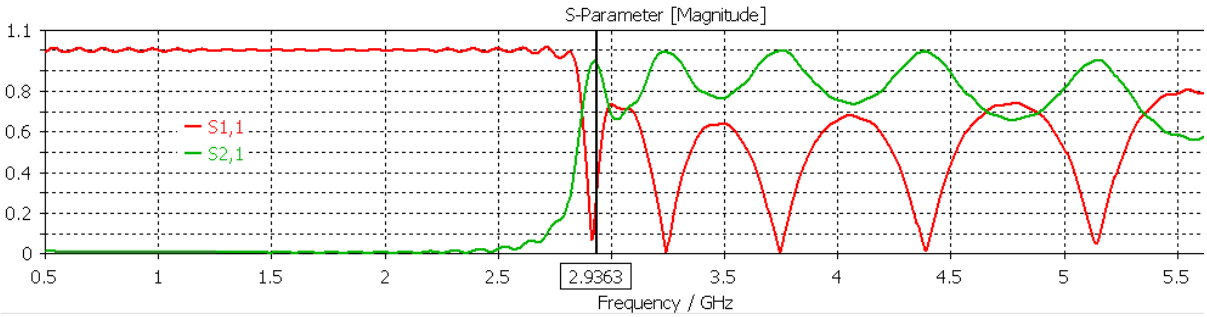

Figure 3.31: Magnitudes of S-parameters for Γ=6, L' = 3 pH/m

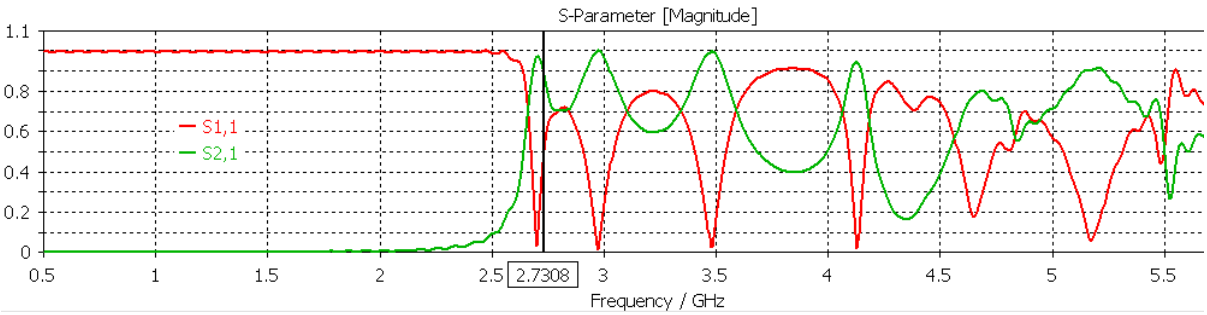

Figure 3.32: Magnitudes of S-parameters for Γ=6, L' = 30 pH/m

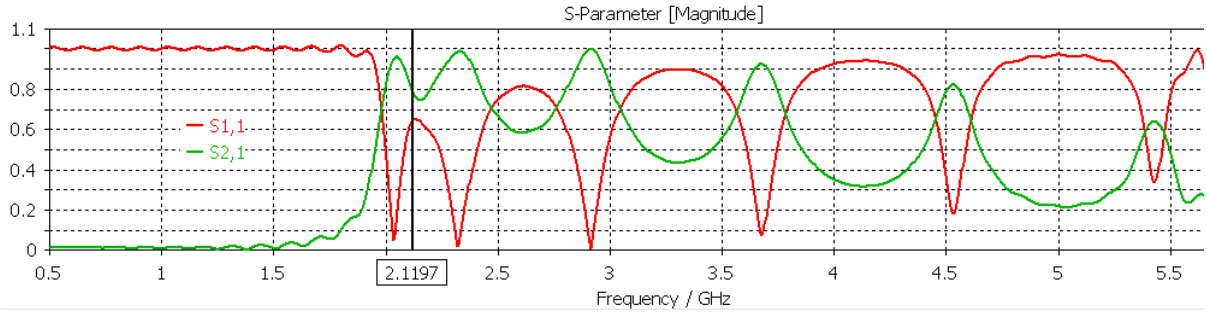

Figure 3.33: Magnitudes of S-parameters for Γ=1.5, L' = 0.3 pH/m

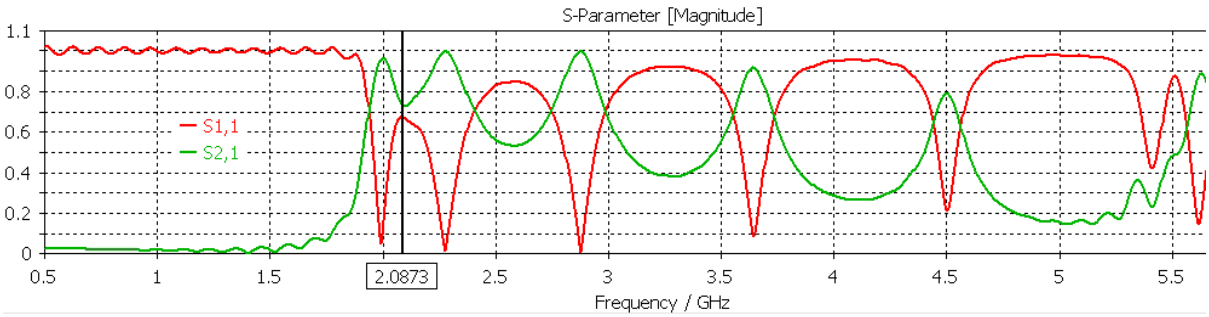

Figure 3.34: Magnitudes of S-parameters for Γ=1.5, L' = 3 pH/m

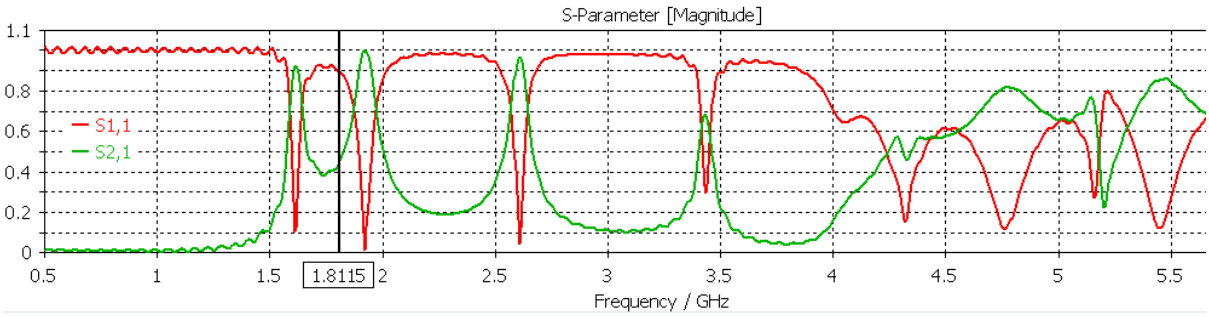

Figure 3.35: Magnitudes of S-parameters for Γ=1.5, L' = 30 pH/m

The following dispersion curves from HFSS indicate that the frequencies for the inductively loaded HMSIW structures vary significantly less than for the corresponding SIW structures, especially for larger values of Γ. However the range of cutoff frequencies (at $\beta = 0$) for inductively loaded HMSIW is roughly 1-1.5GHz, and it increases for smaller values of Γ (as the slot is closer to the centre of the waveguide). This range of cutoff frequencies is much larger than for the purely capacitive loaded HMSIW structures for larger values of Γ (for which the corresponding range is approximately 0.2-1GHz.

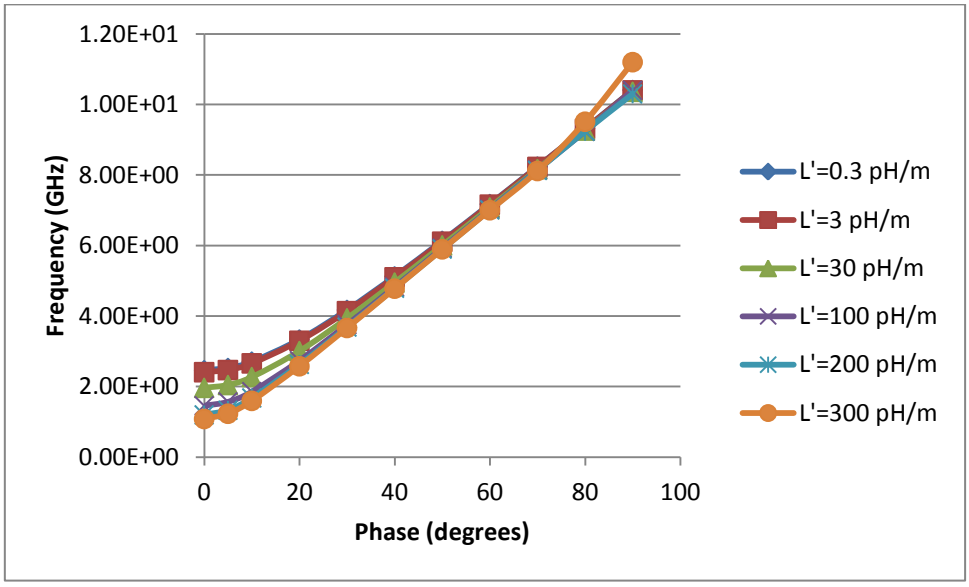

Figure 3.36: Dispersion curve from HFSS for HMSIW with Γ=1.5

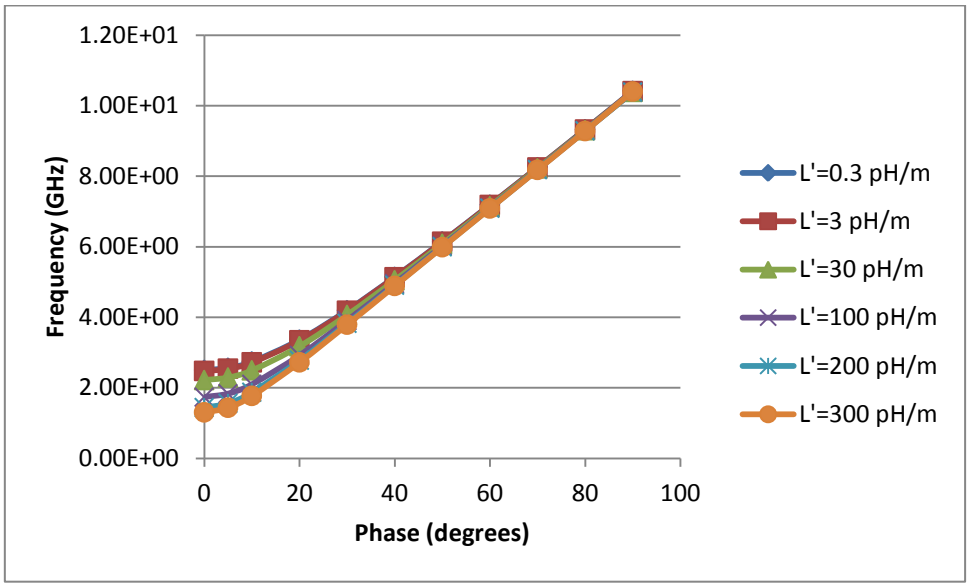

Figure 3.37: Dispersion curve from HFSS for HMSIW with Γ=3

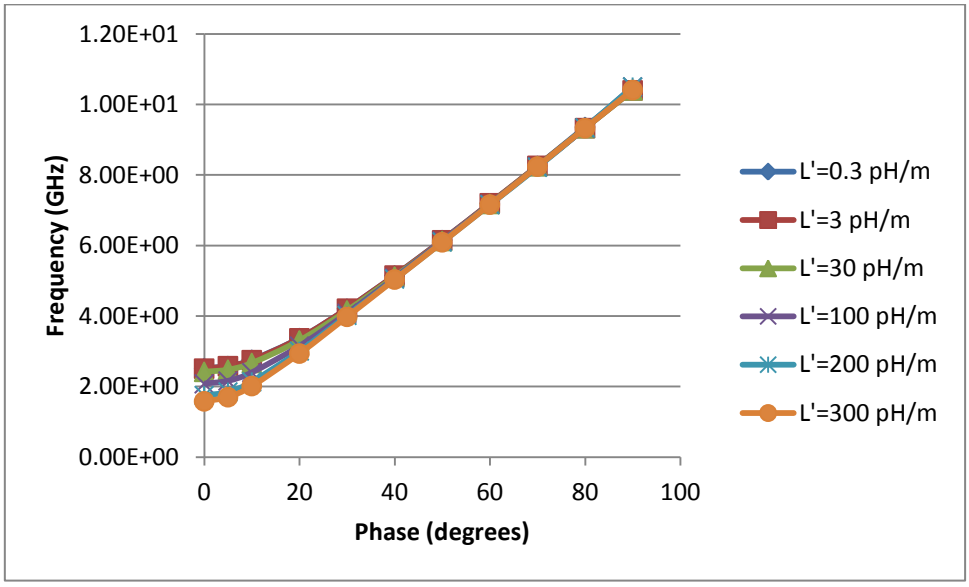

Figure 3.38: Dispersion curve from HFSS for HMSIW with Γ=6

The next three figures show the comparison between the predictions from the transverse resonance technique and the discrete values for the cut-off frequencies (shown in the preceding figures) of the first mode from CST Microwave Studio and HFSS for the respective values of $\Gamma = \frac{3}{2}, 3, 6$. Unlike the calculated forecasts which implicitly assume theoretically purely inductively loaded slots, the results from the simulations take into account that, in practice, the slot itself has a slight inherent capacitance. This explains why the cut-off frequency predictions obtained from simulations are lower than those calculated from the transverse resonance technique. However, it is readily observed from the following graphs that there is very close agreement between both categories of predictions only when Γ is not too large so that the slot is close to the centre of the guide.

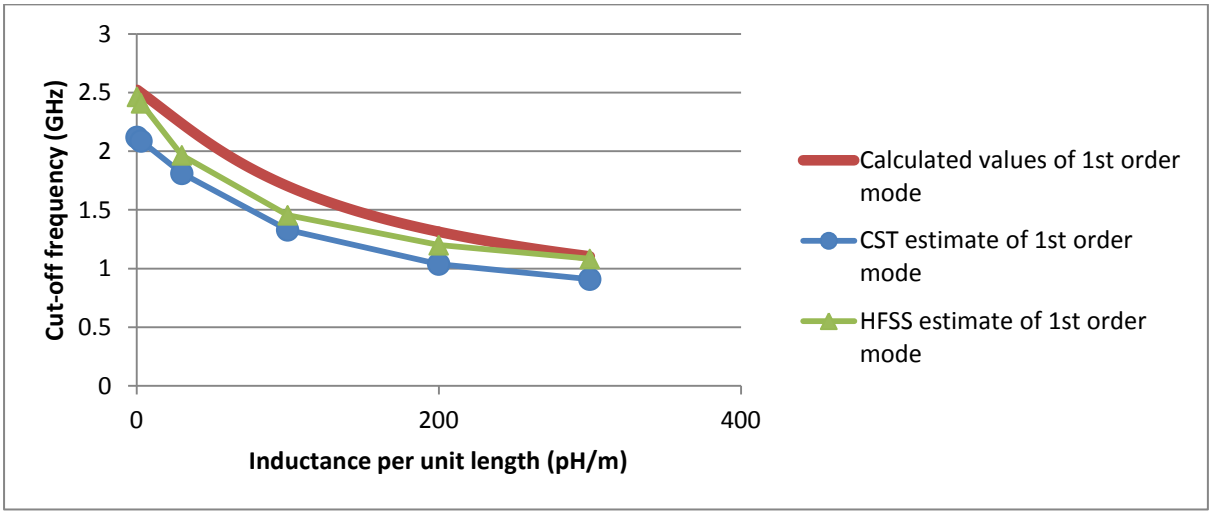

Figure 3.39: Cut-off frequency against inductance across slot in for Γ=3

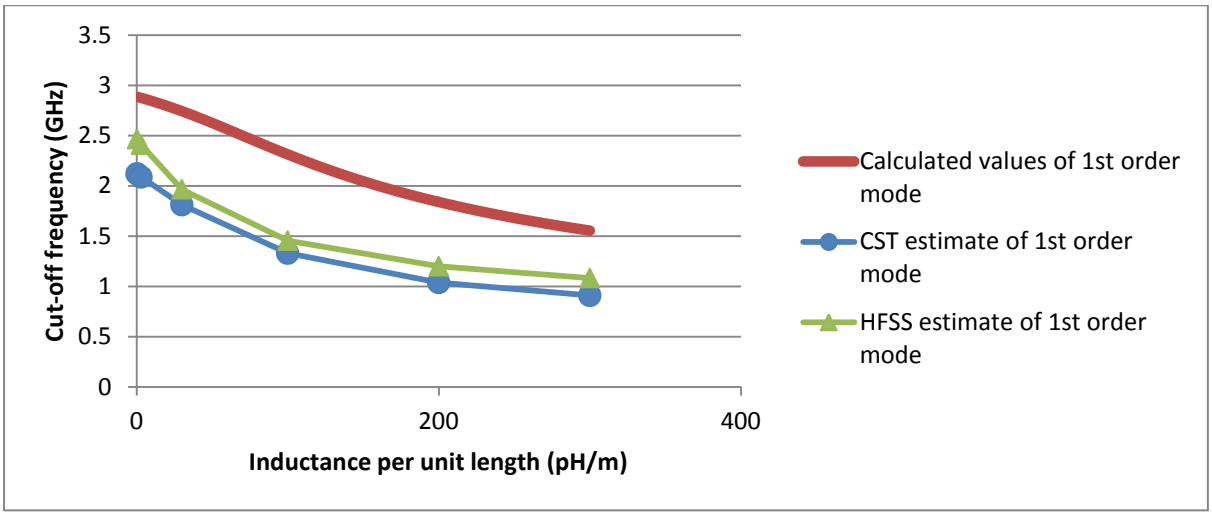

Figure 3.40: Cut-off frequency against inductance across slot in for Γ=6

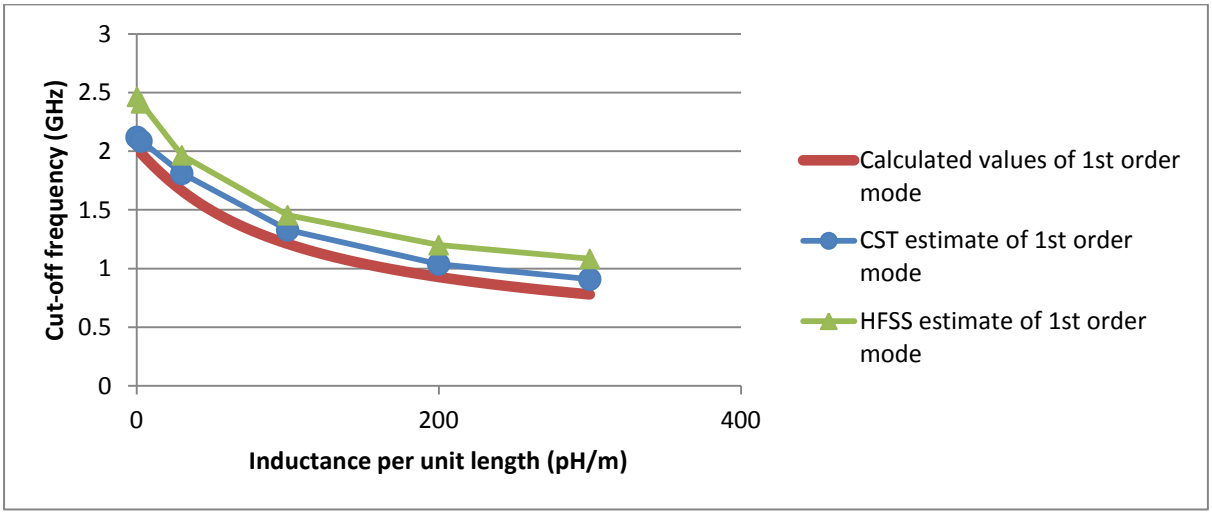

Figure 3.41: Cut-off frequency against inductance across slot in for Γ=1.5

It is apparent from the subsequent figure that the cut-off frequencies become less dependent on the inductance applied across the slot as Γ becomes sufficiently large, as the slot is closer to the H-plane of the HMSIW.

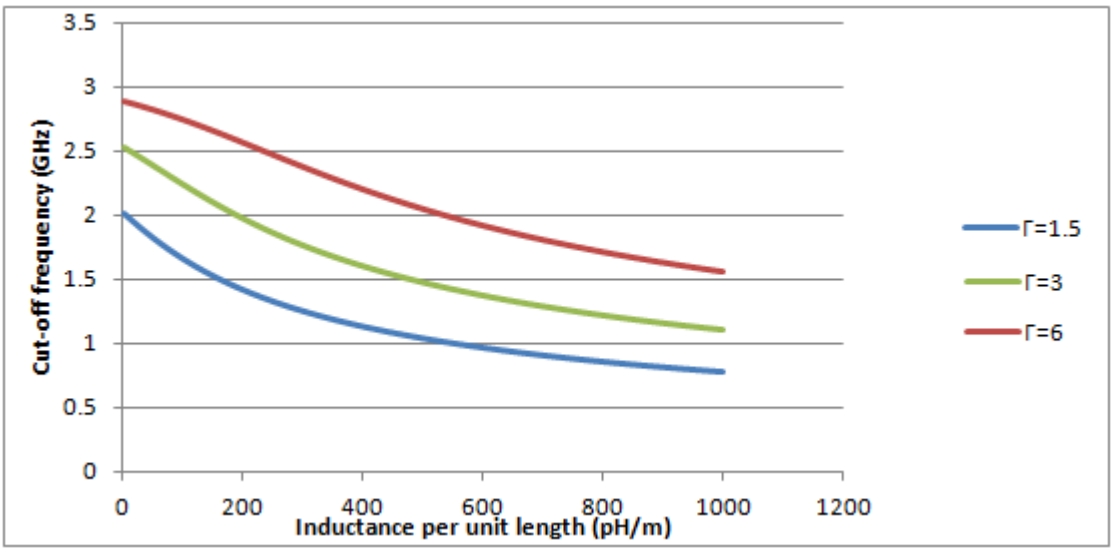

Figure 3.42: Transverse resonance technique predictions for cut-off frequency against inductance across slot

The subsequent figures are field plots in a special case considered above, namely for $\Gamma = 3$ and C'=30nH/m at 2.5GHz (which is just above the cut-off frequency). The next field plot shows the pattern of the component of electric field which travels from the top of the guide to its base. It is evident from this that the electric field oscillations along the length of the guide are less frequent. The electric field it is not as strong as in the analogous inductively loaded full guide case looked at before.

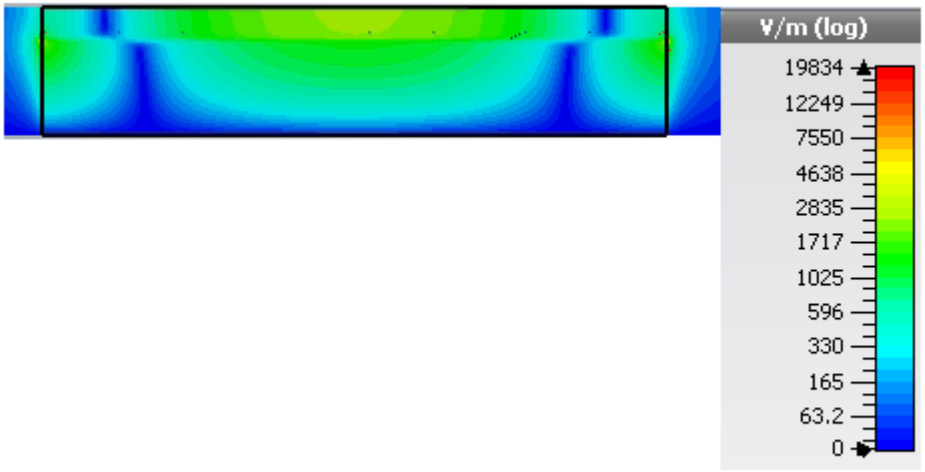

Figure 3.43: An aerial view field plot of E_z 0.88mm from the base of the HMSIW for Γ=3 and a slot loaded with L' = 30 nH/m at 2.5GHz

The following cross-sectional plot of the electric field on the incident port of the waveguide indicates that the field pattern is dominated by the part of the guide that is on the left hand side of the slot (i.e. the larger section of waveguide corresponding to the cross-sectional length L_1 for which the field is maximal when closest to the slot). The smaller part of this cross-section corresponding to the length L_2 is affected more significantly as most of it manages to avoid receiving much electric field. This demonstrates that the model from CST Microwave Studio may have difficulty in calculating results for the HMSIW, particularly

when the length L_2 is relatively large (as was demonstrated in the comparison with the analytical transverse resonance method).

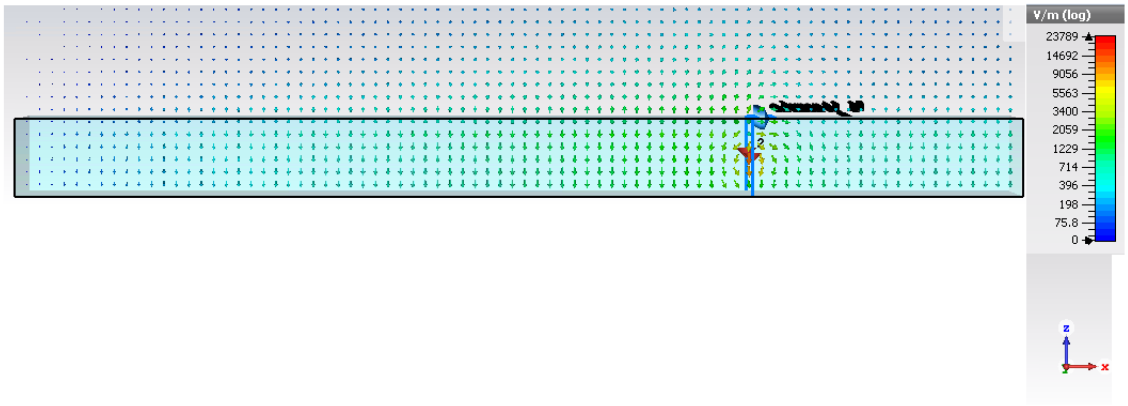

Figure 3.44: A cross-sectional E-field plot at the edge of the longitudinal side of the guide for Γ=3 and a slot loaded with L' = 30 nH/m at 2.5GHz

It turns out that the field patterns do not significantly change so much at higher frequencies which are close to the next higher order mode.

3.11. Summary

A transverse resonance technique is be used to understand the characteristics of the cutoff frequencies for the first several modes over the full range of normalized loaded capacitances and inductances for slotted HMSIW structures. Limiting cases, for which very large and very small inductances and capacitances are used to load the slot cutoff frequencies, are explained in detail, as in the previous chapter.

Estimates of cutoff frequencies for slotted HMSIWs loaded with a range of actual capacitances and inductances are then calculated. These compare well with those from simulations in both CST Microwave Studio and HFSS. Dispersion curves obtained from HFSS illustrate that the frequencies for sufficiently large phase values for HMSIWs are

affected much less by loaded capacitances and inductances than for SIWs in the previous chapter. It is also apparent from these dispersion characteristics that the cutoff frequencies (which correspond to a phase value of zero) are very much closer to one another for HMSIWs loaded with capacitances rather than inductances, especially when the slot is further way from the centre of the guide. These dispersion characteristics are the opposite to the corresponding behaviour exhibited by the SIW structures in the previous chapter.

The fact that the cutoff frequencies for capacitively loaded HMSIWs are so close to each other demonstrates that the transverse resonance technique is very accurate for the capacitively loaded HMSIWs and SIWs. Because it does not take into consideration that in practice the slot itself has an inherent capacitance of 20pF /m in parallel with a possible load inductance, the transverse resonance technique does not compare as well with the simulated results for inductively loaded waveguides when the slot is further away from the centre of the guide.

It is also evident from the dispersion curves that the frequencies corresponding to sufficiently large values of phase are convergent in the case of both inductively loaded SIWs and HMSIWs, irrespective of the value of load inductance. This is of particular interest, since it has also been established that the cutoff frequencies (corresponding to a phase value of zero) are convergent in the case of both capacitively loaded HMSIWs (but not for SIWs).

.

3.12. References

1. D.M. Pozar, "Microwave Engineering," 2nd edition, Wiley, New York, 1998.
2. R.E. Collin, "Foundations for Microwave Engineering," 2nd edition, IEEE Press, 2001.
3. R.E. Collin, "Field Theory of Guided Waves," McGraw-Hill, 1960.
4. N. Marcuvitz, "Waveguide Handbook," McGraw-Hill, 1951.
5. L. Lewin, "Advanced Theory of Waveguides" Iliffe, 1951
6. W. Hong, B. Liu, Y.Q. Wang, Q.H. Lai and K.Wu, "Half Mode Substrate Integrated Waveguide: A New Guided Wave Structure for Microwave and Millimetre Wave Application," (Keynote Talk), Joint 31st Int. Conf. On Infrared and Millimetre Waves and 14th Int. Conf. On Terahertz Electronics, Shanghai, September 2006.
7. J. Xu, W. Hong, H. Tang, Z. Kuai and K. Wu, "Half mode substrate integrated waveguide (HMSIW) Leaky-Wave Antenna for Millimetre-Wave Applications," IEEE Antennas and Wireless Propag. Lett., vol. 7, 2008.
8. Q.H. Lai, W. Hong, Z.Q. Kuai, Y.S. Zhang and K. Wu, "Half-Mode Substrate Integrated Waveguide Transverse Slot Array Antennas," IEEE Transactions on Antennas and Propagation, Vol. 57, No. 4, 2009.
9. G.V. Krishna Reddy, S. Mukherjee and A. Biswas, "Design of HMSIW fed dual frequency microstrip patch antenna for X-band applications," IEEE International Symposium on Antennas and Propagation, pp. 203-204, 2016.
10. S. Revathy, H. Umma Habiba and A.E. Ramanujan, "Low profile HMSIW rectenna for wireless power transmission," International Conf. on Wireless Comm., Signal Processing and Networking, pp.1971-1974, 2016.
11. S. Banerjee, T. Mohanty, S. Das and B. Rana, "Slot-loaded compact HMSIW triangular antenna," International Conf. on Microelectronics, Computing and Communications, pp.1-4, 2016.
12. P. Hubka and J. Lacik, "Polarization reconfigurable HMSIW U-slot antenna," International Conference on Microwave, Radar and Wireless Communications, pp.1-4, 2016.
13. H.J. Tang, W. Hong, J.-X. Chen, G.Q. Luo, and K. Wu, "Development of millimetre-wave diplexers based on complementary characters of dual-mode substrate integrated waveguide filters with circular and elliptic cavities," IEEE Progress in Electromagnetics Research Letters, Vol. 10, 2009.
14. J. Gu, Y. Fan, Y. Zhang and D. Wu, "A novel 3-D transition and power divider based on half mode SICC structure," Progress in Electromagnetics Research Letters, Vol.10, 125-133, 2009.
15. B. Liu, W. Hong, Y-Q. Wang, Q-H . Lai and K. Wu, "Half mode substrate integrated waveguide (HMSIW) 3-db coupler," IEEE Microwave and Wireless Components Letters, Vol.17, No. 1, 22, 2007.
16. Z. Zhang, Y. Fang, Y. Cheng and Y. Zhang "A novel multilayer e-plane HMSIW 3-db coupler with improved out-of-band rejection," Progress in Electromagnetic Research Symposium, pp.1088-1091, 2016.

17. Y.Q. Wang, W. Hong, Y.D. Dong, B. Liu, H.J. Tang, J.X. Chen, X.X Yin and K. Wu, "Half mode substrate integrated waveguide (HMSIW) bandpass filter," IEEE Microw. Wireless Compon. Lett, Vol. 17, no.4, pp.265-267, 2007.
18. R.-S. Chen, S.W. Wong, Z.-C. Guo, K. Wang and Q.-Z. Chu, "Wideband bandpass filter based on SIW and HMSIW cavities," IEEE International Wireless Symposium, pp.1-4, 2015.
19. H. Chen, W. Che, T. Zhang, Y. Chao and W. Feng, "SIW SPDT switch based on switchable HMSIW units," IEEE International Workshop on Electromagnetics, pp. 1-3, 2016.
20. Y.K. Cho, "On the equivalent circuit representation of the slotted parallel-plate filled with dielectric," IEEE Trans. Antennas Propag., Vol.37, no.9, 1193-1200, 1989.

4. Transverse Resonance Analysis for slotted Parallel plate SIWs

In this chapter a transverse resonance technique is applied to the slotted parallel plate substrate integrated waveguide. This is meant to be regarded as an extension of the earlier work which is of purely theoretical interest, rather than a topic of practical significance. Also, because of the difficulties with CST Microwave Studio mentioned in the case of the HMSIW, no simulation software for the parallel plate SIW. The transverse resonance technique used here is a simple alternative method for estimating the cutoff frequency of the parallel plate SIW, as compared with more complicated approaches based on methods from standard treatises like [1]-[5] which consider field analysis. Due to the nature of the results in this chapter, the mathematical reasoning in this section is significantly deeper than in the earlier work of this thesis.

4.1. Background theory

By considering the equivalent circuit model of the slotted parallel plate SIW (as shown in the next figure), the transmission line is terminated with an open circuit at both ends.

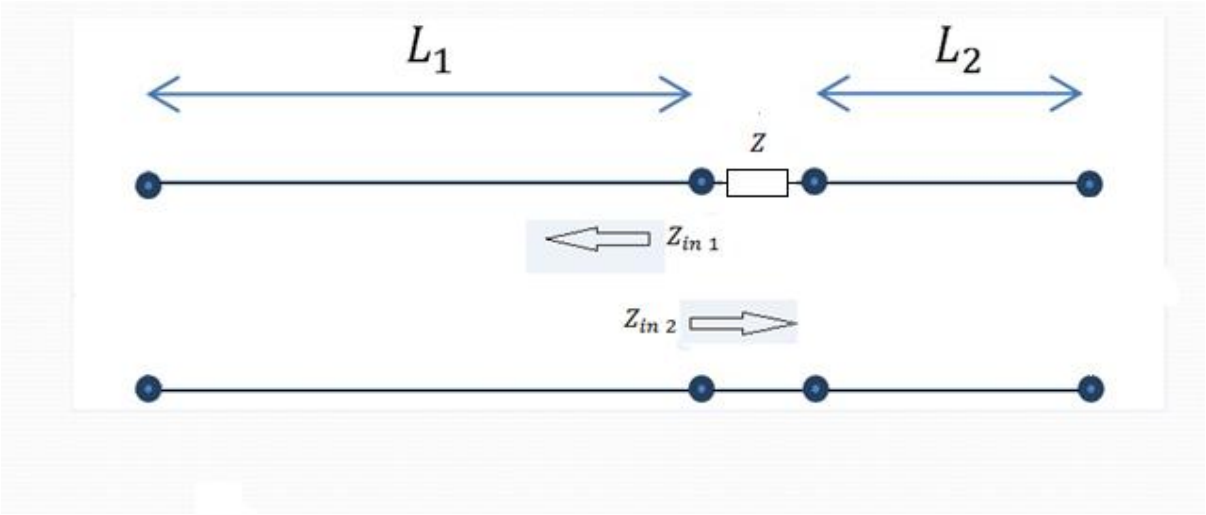

Figure 4.1: Equivalent circuit model for a loaded parallel plate SIW

In other words, set $Z_{Load\,1} \to \infty$ for the end where the input impedance is $Z_{in\,1}$ and set $Z_{Load\,2} \to \infty$ for the other end where the input impedance is $Z_{in\,2}$.

By using the fact that the input impedance of a lossless terminated line is given by

$$Z_{in} = Z_0 \cdot \frac{Z_{Load} + jZ_0 \tan k_x L_0}{Z_0 + jZ_{Load} \tan k_x L_0} \ , \qquad (4.1)$$

so that

$$Z_{in\,1} = -\frac{jZ_0}{tan\ k_x L_2} \ , \qquad (4.2)$$

and

$$Z_{in\,2} = Z - \frac{jZ_0}{tan\ k_x L_2} \ . \qquad (4.3)$$

Since, at resonance,

$$Z_{in\,1} = -Z_{in\,2} \ , \qquad (4.4)$$

it may be deduced that

$$-\frac{jZ_0}{tan\ k_x L_2} = -Z + \frac{jZ_0}{tan\ k_x L_2} \ . \qquad (4.5)$$

If $Z = jX$, then

$$\frac{1}{tan\ k_x L_1} = \frac{X}{Z_0} - \frac{1}{tan\ k_x L_2} \ . \qquad (4.6)$$

Note that if the slot is being modelled by a capacitance C , then set

$$X = -\frac{1}{\omega C} \ . \qquad (4.7)$$

On the other hand, if the slot is being modelled by an inductance L , then set

$$X = \omega L \ . \qquad (4.8)$$

Since

$$k_x = \omega\sqrt{\mu\varepsilon} \ , \qquad (4.9)$$

it follows from (4.6) that

$$\frac{1}{tan\ \omega L_1\sqrt{\mu\varepsilon}} = -\frac{1}{\omega C Z_0} - \frac{1}{tan\ \omega L_2\sqrt{\mu\varepsilon}} \qquad (4.10)$$

for a capacitive impedance,

and

$$\frac{1}{tan\ \omega L_1\sqrt{\mu\varepsilon}} = \frac{\omega L}{Z_0} - \frac{1}{tan\ \omega L_2\sqrt{\mu\varepsilon}} \qquad (4.11)$$

for an inductive impedance.

4.2. Capacitive Cut-off Equation

Let C' be the capacitance per unit length which could be taken to be in the range of anything from 0.1 pF/m to 100 pF/m. Then for a distance d along the slot, the total capacitance is given by

$$C = C'd\ , \qquad (4.12)$$

so that, because $Z_0 = \frac{b}{d}\sqrt{\frac{\mu}{\varepsilon}}$, it follows that

$$Z_0 C = C'b\sqrt{\frac{\mu}{\varepsilon}}\ , \qquad (4.13)$$

So that the capacitive cut-off equation (4.10) may be rewritten as

$$\frac{1}{tan\ \omega L_1\sqrt{\mu\varepsilon}} = -\frac{1}{\omega C'b\sqrt{\frac{\mu}{\varepsilon}}} - \frac{1}{tan\ \omega L_2\sqrt{\mu\varepsilon}}\ . \qquad (4.14)$$

Recall that that the angular cut-off frequency is given by ω.

By setting

$$\theta = \omega L_1\sqrt{\mu\varepsilon}\ , \qquad (4.15)$$

and

$$\hat{C} = \frac{C\prime b}{\varepsilon} \ , \qquad (4.16)$$

(4.14) can be rewritten as

$$\frac{1}{tan\,\theta} + \frac{1}{tan\frac{\theta}{\Gamma}} = -\frac{1}{\hat{C}\theta} \ , \qquad (4.17)$$

where $\Gamma = \frac{L_1}{L_2}$.

4.3. Normalized solutions of the capacitive cut-off equation

Maple is used to calculate the solutions of θ for the first six modes over a suitable range of $\hat{C}$ for values of $\Gamma = 3{,}4$. These results are presented below as theoretical design curves. A logarithmic scale to see the results over a suitably large range of $\hat{C}$, which is represented by integers ranging from from 1 to 3000.

By considering the capacitive cut-off equation for a parallel plate SIW, the y-axis of each design curve, being in units of $\frac{\theta}{\pi}$, is proportional to the angular cut-off frequency ω. Similarly, the x-axis of each design curve, being in units of $\hat{C}$, is proportional to the capacitance. Therefore, these design curves show a plot of normalized frequency against normalized capacitance. Explanations for these design curves are provided in the subsequent sections.

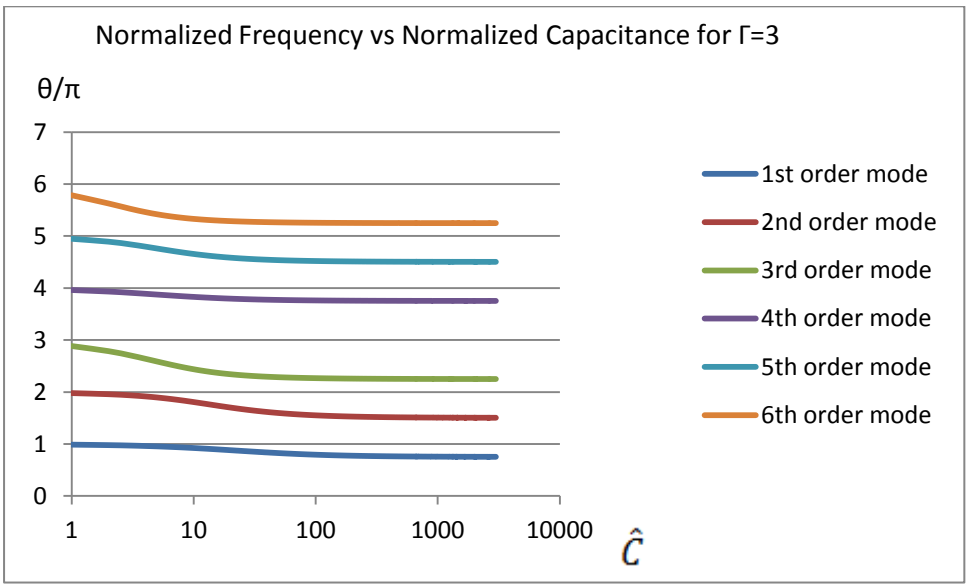

Figure 4.3: Design curves for loaded capacitances for Γ=3

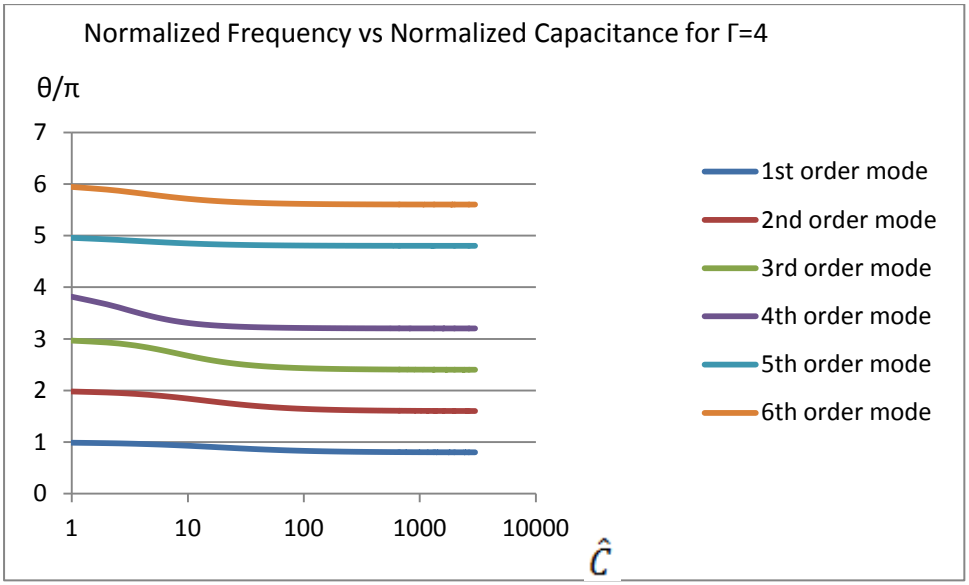

Figure 4.4: Design curves for loaded capacitances for Γ=4

4.4. Small capacitances for the capacitive cut-off equation

If the capacitance is very small, it is equivalent to an open circuit. Therefore, the parallel plate SIW slotted with a sufficiently small capacitance is equivalent to a standard parallel plate waveguide. By considering the left and right hand side terms of the corresponding capacitive cut-off equation (4.17) graphically, as in the Cartesian plot for $\Gamma = 3$ below, it is evident that solutions of θ for the cut-off equation for very small capacitances (for which $y \to -\infty$ as in the case of $\Gamma = 3$ in the Cartesian plot below) get closer and closer to the asymptotes of the function $y = \frac{1}{\tan\theta} + \frac{1}{\tan\frac{\theta}{\Gamma}}$, for $\theta > 0$.

Therefore, as $C \to 0$, $\theta \to r\pi$ for the corresponding r^{th} order mode of the parallel plate slotted SIW, where $r = 1,2,3, \ldots$. Note that this is independent of the choice for Γ. This is confirmed by the above design curves showing normalized frequency versus normalized capacitance.

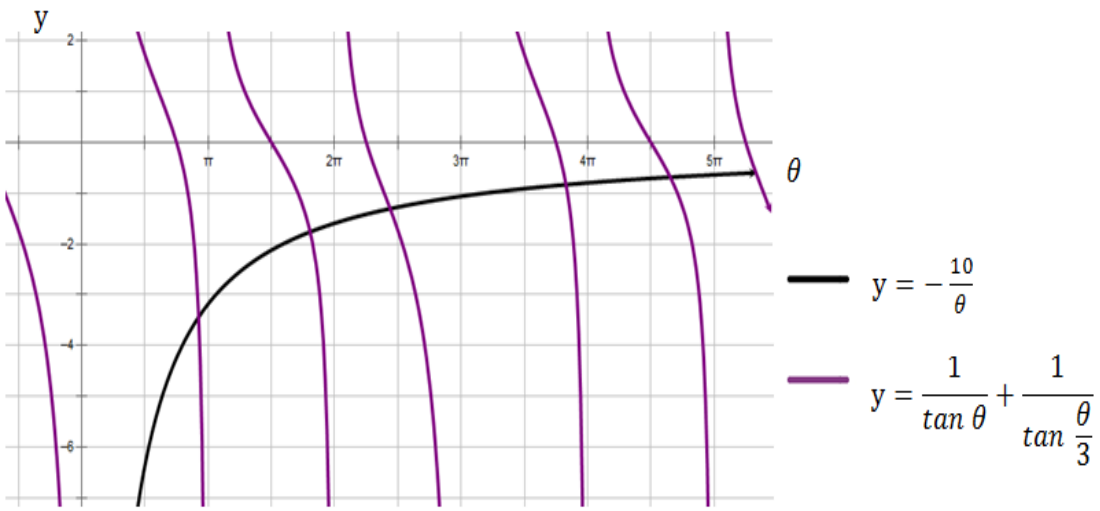

Figure 4.5: Left and right hand side functions of the capacitive cut-off equation for the parallel plate slotted SIW with normalized capacitance of 10 and Γ=3.

4.5. Large capacitances for the capacitive cut-off equation

If the capacitance is very large, it is equivalent to a short circuit. Therefore, the parallel plate SIW slotted with a sufficiently large capacitance should be equivalent to a standard parallel plate waveguide. So it may be assumed that the n^{th} order mode in the parallel plate SIW slotted with a sufficiently large capacitance is equivalent to the n^{th} order mode in a standard parallel plate waveguide for $n \in \{1,2, \ldots\}$.

Defining x to be the transverse axis of the parallel plate SIW slotted with a very large capacitance, it follows from this assumption that the condition at cut-off for this slotted waveguide is then given by $k_x a = n\pi$, where $n \in \{2,3, \ldots\}$, where the wave number $k_x = \omega\sqrt{\mu\varepsilon}$ as in (2.2).

In this case $\theta = k_x L_1$ and $a = L_1 + L_2$.

Then the condition at cut-off for the $(n-1)^{\text{th}}$ order mode of the SIW slotted with a sufficiently large capacitance, where $\in \{2,3, \ldots\}$, is given by

$$\theta = \frac{n\pi L_1}{L_1+L_2} = \frac{n\pi L_1}{L_1\left(1+\frac{1}{\Gamma}\right)} = \frac{n\pi}{\left(1+\frac{1}{\Gamma}\right)} \ . \qquad (4.18)$$

Now consider the instance when $\Gamma = 3$.

If $n = 1$ (i.e. considering the 1st order mode), then it follows from the last equation that for $\Gamma = 3,\ \theta \to \frac{3}{4}\pi$ for very large capacitances. If $n = 2$ (i.e. considering the 2nd order mode), then it follows from the last equation that for $\Gamma = 3,\ \theta \to \frac{3}{2}\pi$ for very large capacitances. If $n = 3$ (i.e. considering the 3rd order mode), then it follows from the last equation that for $\Gamma = 3,\ \theta \to \frac{9}{4}\pi$ for very large capacitances.

These three calculations are in agreement with the 1st, 2nd and 3rd order mode solutions from the the design curve values for normalized frequency for very small inductances when $\Gamma = 3$.

If $n = 4$, then it follows from the last equation that for $\Gamma = 3,\ \theta \to 3\pi$ for very large capacitances. However, for this particular case with $\Gamma = 3$, setting $n = 4$ does not correspond to the 2nd order mode of the SIW slotted with a small inductance in the corresponding design curve (showing normalized frequency versus normalized inductance) above.

This is because $\theta = 3\pi$ cannot be regarded as a solution of any mode of the parallel plate waveguide slotted with a very large capacitance

A Cartesian plot of the terms in the corresponding capacitive cut-off equation for $\Gamma = 3$ (as shown as follows with $\hat{C} \to \infty$) demonstrates that $\theta = 3\pi$ is in fact an asymptote. It follows that the condition that $cot\,\theta + cot\,\frac{\theta}{3} \to -\frac{1}{\hat{C}\theta}$ as $\theta \to 3\pi$ is satisfied only as $\hat{C} \to 0$ (as confirmed in the previous section), and not when $\hat{C}$ is very large (as $\hat{C} \to \infty$, $y = -\frac{1}{\hat{C}\theta}$ coincides with the θ-axis in the Cartesian plot below). Therefore, for the case where $\Gamma = 3$, there exists no mode of a parallel plate slotted SIW slotted with a sufficiently large capacitance for which $\theta = 3\pi$.

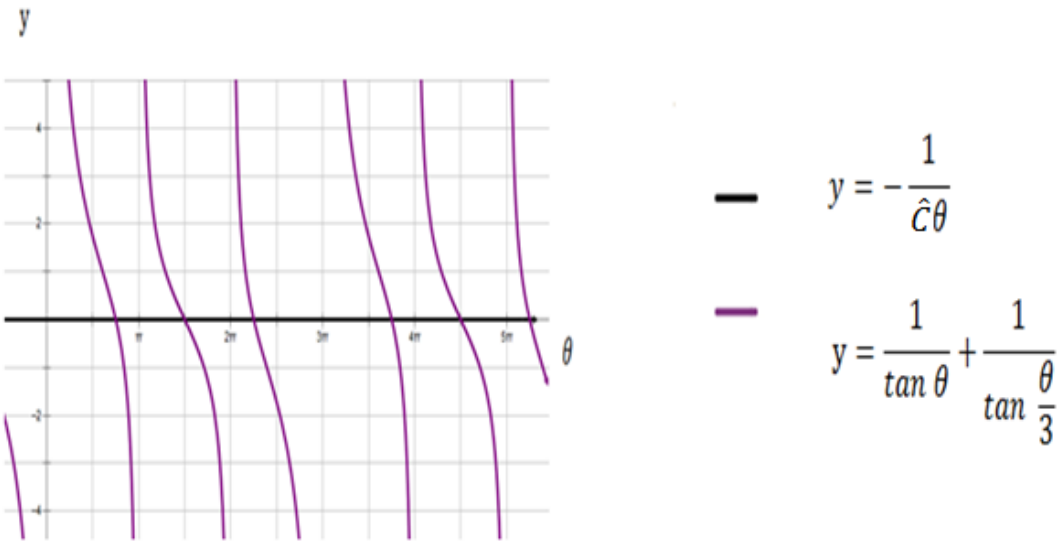

Figure 4.6: Cartesian plot of left and right hand side terms of the capacitive cut-off equation of the parallel plate SIW for Γ=3 and sufficiently large capacitance.

Therefore, for $\Gamma = 3$, the instance where $n = 4$ for the parallel plate SIW slotted with a very large capacitance must be neglected.

If $n = 5,6,7$ (i.e. considering the 4th, 5th and 6th order modes), then it follows from the last equation that for $\Gamma = 3$, $\theta \to \frac{15}{4}\pi$, $\frac{9}{2}\pi$, $\frac{21}{4}\pi$ respectively for very large capacitances. These three calculations are in agreement with the 4th, 5th and 6th order mode solutions from the the design curve values for normalized frequency for very large capacitances when $\Gamma = 3$, respectively.

All the limiting cases for θ given by $\theta = \frac{n\pi}{\left(1+\frac{1}{\Gamma}\right)}$, where $n = \{1,2,3, \ldots\}$, (except for those of the form $\theta = \Gamma n\pi,$ which instead correspond to the asymptotes of the function $y = \frac{1}{\tan\theta} + \frac{1}{\tan\frac{\theta}{\Gamma}}$ as discussed earlier) are the same as those values of θ for large capacitances in the design curves of the parallel plate slotted SIW showing normalized frequency versus normalized capacitance. It follows that when these particular values of θ are the zeros of the function $y = \frac{1}{\tan\theta} + \frac{1}{\tan\frac{\theta}{\Gamma}}$ (see the last Cartesian plot above).

It shall now mathematically proved that the individual numerical values of

$\theta = \frac{n\pi}{\left(1+\frac{1}{\Gamma}\right)}$, such that $\theta \neq \Gamma n\pi$ and $n = \{1,2,3, \ldots\}$, are zeros of the function $y = \frac{1}{tan\,\theta} + \frac{1}{tan\,\frac{\theta}{\Gamma}}$

.

Consider

$$cot\,\theta = \frac{cos\,\theta}{sin\,\theta} = \frac{sin\,\left(\frac{\pi}{2} - \theta\right)}{cos\,\left(\frac{\pi}{2} - \theta\right)} = tan\,\left(\frac{\pi}{2} - \theta\right) .$$

Then the function $y = \frac{1}{tan\,\theta} + \frac{1}{tan\,\frac{\theta}{\Gamma}}$ may be rewritten as

$$y = tan\,\left(\frac{\pi}{2} - \theta\right) + tan\,\left(\frac{\pi}{2} - \frac{\theta}{\Gamma}\right) .$$

Substituting $\theta = \frac{n\pi}{\left(1+\frac{1}{\Gamma}\right)} = \frac{\Gamma}{\Gamma+1} n\pi$ into the last formula yields

$$\Leftrightarrow y = tan\left(\frac{\pi}{2} - \frac{\Gamma}{\Gamma+1} n\pi\right) + tan\left(\frac{\pi}{2} - \frac{1}{\Gamma+1} n\pi\right)$$

$$\Leftrightarrow y = tan[(1-\mathrm{n})\pi] \left[1 - cot\left(\frac{\Gamma}{\Gamma+1} n\pi\right) cot\left(\frac{1}{\Gamma+1} n\pi\right)\right],$$

by using the trigonometric addition formula for tangents.

Then $y = 0 \;\; iff \;\; n$ is not an integer multiple of $\Gamma + 1$,

i.e. $y = 0$ for $\theta \neq \Gamma n\pi, \;\; n = \{1,2,3, \ldots\}$,

since $tan[(1-\mathrm{n})\pi] = 0$.

4.6. Inductive cut-off equation for a parallel plate SIW

Let L' be the inductance per unit length. Then for a slot width w , we have

$$L = L'd \,, \qquad (4.19)$$

so that, because $Z_0 = \frac{b}{d}\sqrt{\frac{\mu}{\varepsilon}}$, it follows that

$$\frac{\omega L}{Z_0} = \frac{\omega L'}{b\sqrt{\frac{\mu}{\varepsilon}}} \ . \qquad (4.20)$$

Then the cut-off equation for an inductive impedance in a parallel plate waveguide is given by

$$\frac{1}{tan\ \omega L_1\sqrt{\mu\varepsilon}} = \frac{\omega L' w^2}{b\sqrt{\frac{\mu}{\varepsilon}}} - \frac{1}{tan\ \omega L_2\sqrt{\mu\varepsilon}} \ . \qquad (4.21)$$

Note that the angular cut-off frequency is given by ω.

Set

$$\widehat{L} = \frac{L'}{b\mu} \ , \qquad (4.22)$$

and

$$h' = \hat{L} \ , \qquad (4.23)$$

The cut-off equation for an inductive impedance can then be rewritten as

$$\frac{1}{tan\ \theta} + \frac{1}{tan\frac{\theta}{\Gamma}} = \hat{L}\theta \ , \qquad (4.24)$$

where $\Gamma = \frac{L_1}{L_2}$.

4.7. Frequency intervals for the inductive cut-off equation

Since the inductive cut-off equation is a transcendental equation, it can only be solved numerically. The trigonometric terms in this inductive cut-off equation for the parallel plate slotted SIW are identical to those of the capacitive cut-off equation for the capacitively slotted parallel plate. Therefore both cut-off equations share the same frequency intervals inside which the solutions of θ exist.

4.8. Normalized solutions of the inductive cut-off equation

Maple is used to calculate the solutions of θ for the first four modes over the full range of $\hat{L}$ over which the frequency significantly varies for values of $\Gamma = 3{,}4$. These results are

presented below as theoretical design curves. Since the results are over a suitably large range of $\hat{L}$, a logarithmic scale is used in the plots. $\hat{L}$ ranges from 0.01 to 30 at intervals of 0.01.

By considering the cut-off equation, the y-axis of each design curve, being in units of $\frac{\theta}{\pi}$, is proportional to the angular cut-off frequency ω. Similarly, the x-axis of each design curve, being in units of $\hat{L}$, is proportional to the inductance. Therefore, these design curves show a plot of normalized frequency against normalized inductance.

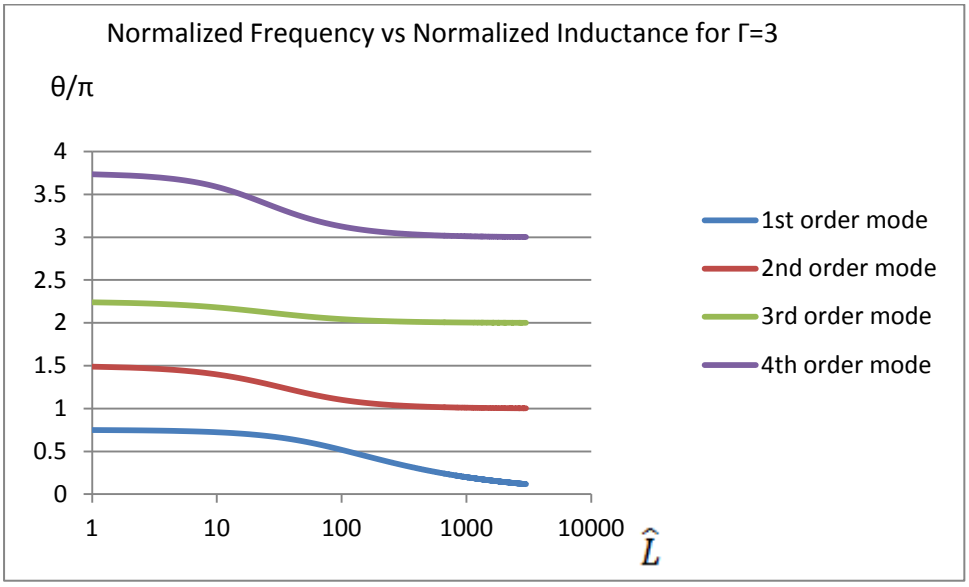

Figure 4.7: Design curves for loaded inductances for Γ=3

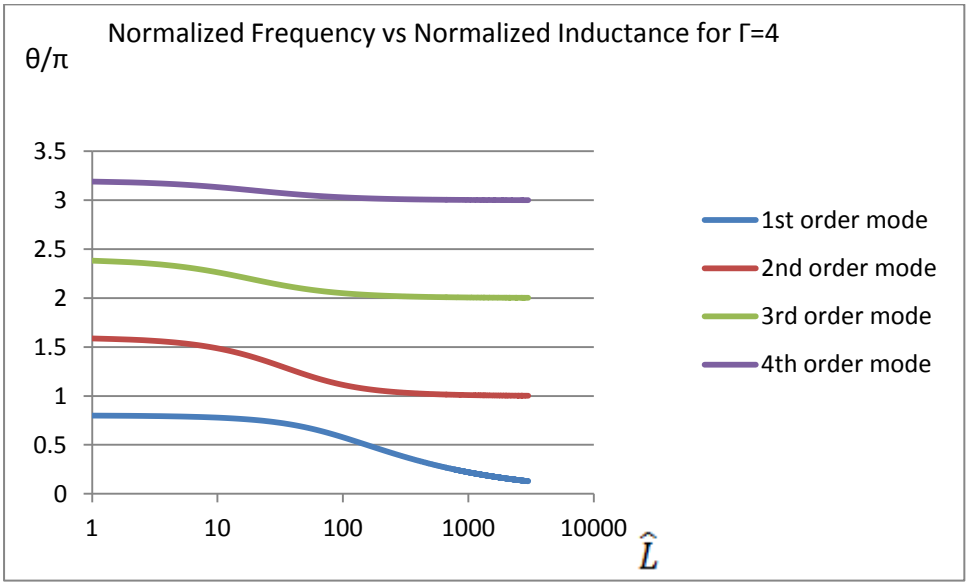

Figure 4.8: Design curves for loaded inductances for Γ=4

4.9. Large inductances for the inductive cut-off equation

If the inductance is very large, it is equivalent to an open circuit. As the inductance is increased, the cut-off frequency decreases (as demonstrated in the graphs above) until eventually the electric field concentrates itself around the slot, at which point the mathematics of the transverse resonance technique breaks down. In particular, the cut-off frequency of the 1st order mode in the SIW slotted with a sufficiently large inductance decreases to almost zero.

It follows that the cut-off frequency of the n^{th} order mode in the parallel plate SIW slotted with a sufficiently large inductance is equivalent to the cut-off frequency of the $(n-1)^{th}$ order mode in a standard parallel plate waveguide, where $n = 2,3, \ldots$.

By considering the left and right hand side terms of the corresponding inductive cut-off equation graphically, as in the Cartesian plot for $\Gamma = 3$ below, it is evident that solutions of θ for the cut-off equation for very large inductances (for which $y \to \infty$ as in the case of $\Gamma = 3$ in the Cartesian plot below) get closer and closer to the asymptotes of the function

$y = \frac{1}{\tan\theta} + \frac{1}{\tan\frac{\theta}{\Gamma}}$, for $\theta > 0$.

Therefore, as $\hat{L} \to \infty$, $\theta \to (r-1)\pi$ for the corresponding r^{th} order mode of the parallel plate inductively slotted SIW, where $r = 1,2,3, \ldots$. Note that this is independent of the choice for Γ. This is confirmed by the above design curves showing normalized frequency versus normalized inductance.

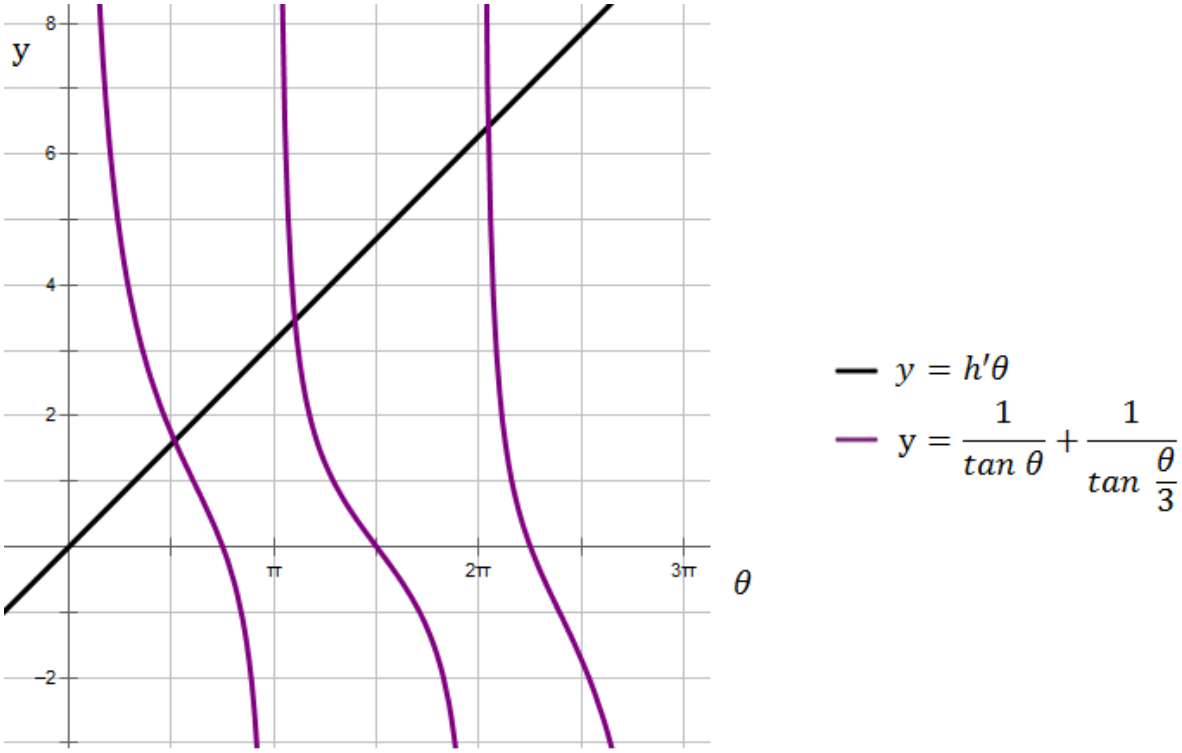

Figure 4.9: Left and right hand side functions of the inductive cut-off equation for the parallel plate slotted SIW for h'=1 and Γ=3.

4.10. Small inductances for the inductive cut-off equation

If the inductance is very small it behaves more like a short circuit. Therefore, the parallel plate SIW slotted with a sufficiently small inductance should be equivalent to a standard parallel plate waveguide. By considering the left and right hand side functions of the inductive cut-off equation graphically with (4.23), as in the case of $\Gamma = 3$ in the Cartesian

plot above, it is evident that as $h' \to 0$ (i.e. as $\hat{L} \to 0$), then the solutions of θ lie on the horizontal axis.

Therefore the solutions of θ are the zeros of the function $= \frac{1}{tan\,\theta} + \frac{1}{tan\frac{\theta}{\Gamma}}$, such that $\theta > 0$.

But this was also the case for the solutions of θ for the parallel plate SIW slotted with very a large capacitance.

Therefore the parallel plate SIW slotted with a very small inductance is equivalent to the parallel plate SIW slotted with a very large capacitance.

It follows in both these cases that $\theta = \frac{n\pi}{\left(1+\frac{1}{\Gamma}\right)}$, such that $\theta \neq \Gamma n\pi$, where $n = \{1,2,3, \ldots\}$ for each successive mode respectively.

This is confirmed by all the design curves in this chapter showing normalized frequency against the normalized inductance and normalized capacitance.

4.11. References

1. D.M. Pozar, "Microwave Engineering," 2nd edition, Wiley, New York, 1998.
2. R.E. Collin, "Foundations for Microwave Engineering," 2nd edition, IEEE Press, 2001.
3. R.E. Collin, "Field Theory of Guided Waves," McGraw-Hill, 1960.
4. N. Marcuvitz, "Waveguide Handbook," McGraw-Hill, 1951.
5. L. Lewin, "Advanced Theory of Waveguides" Iliffe, 1951

5. Modal Analysis of loaded composite SIW structures

5.1. Introduction

The classical theory of waveguide discontinuities is detailed in [1]-[5]. Modal analysis, which is also known as mode matching, is an established technique that has been applied to electromagnetic problems for several decades. It is explained comprehensively in the classic treatise by Mittra and Lee [4]. In this chapter, a generalized modal analysis technique is used to determine the S-parameters for a large class of hybrid waveguide structures with discontinuities. This mode matching method extends and improves ideas from [6] and [7]. These results are compared with those from HFSS for specific examples of practical significance. It is later reasoned that these operational characteristics can be used to model slotted SIWs (SSIWs) which are instrumental in the novel design of different types of microwave devices.

Modal analysis has been used to to solve for the scattering problem when dealing with discontinuities within waveguides [8-9], finlines [10] and microstrip [11-13]. It has also been used to study composite structures which consists of E-planes [14-19] and H-planes [20]. Mode matching methods have been applied to the design of a variety of devices, including E-plane filters [14-15] and power dividers [16]. Some basic structures involving E-planes and H-planes will be considered in the latter sections of this chapter.

5.2. Background theory

Consider a rectangular waveguide structure of width a_1 in the transverse plane which is fed into a second waveguide structure of width a_2, where $a_1 \neq a_2$, which is in turn fed into a third guided structure of width a_1. According to Clarricoats [7], setting the middle section with width $a_2 < a_1$ can be used to model a slotted SIW (SSIW). For the purposes in this section, the initial, middle and final sections are denoted as regions A, B, C with surfaces denoted as S_1, S_2, S_3 respectively. By considering the standard rectangular coordinates given by x, y, z, the junctions between these three guides are defined to exist at $z = 0$ and $z = L$. Then it is clear that $z < 0$ for any point along guide A. Similarly, it is evident that $0 < z < L$ for any

point along guide B, and $z \geq L$ for any point along guide C. It is assumed that only the fundamental TE_{10} mode is propagating in guide A, and that this mode is incident on the junction from $z < 0$. It is also assumed that no modes are propagating in guide B or C. Because of the discontinuity at $z = 0$, all guides consist of reflected and transmitted waves consisting of infinite sets of TE_{n0} modes. Since only the TE_{10} mode propagates in guide A, the higher order modes account for stored energy localized near $z = 0$. It is also assumed that there does not exist any y-variation introduced by the discontinuities at $z = 0$ and $z = L$. It follows that the TE_{nm} modes, where both m and n are positive integers, and the TM modes are not excited.

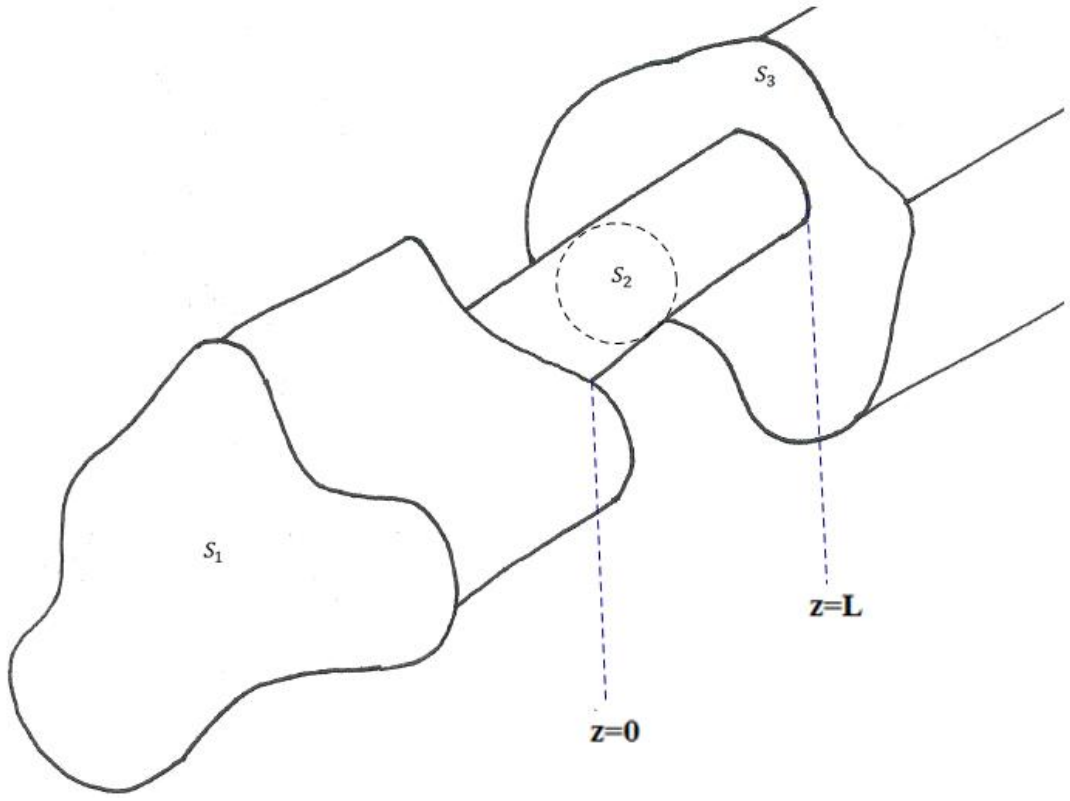

Figure 5.1 : Schematic of an arbitrary composite waveguide structure.

Define the propagation constant and the wave impedance of the TE_{n0} mode of guides A and B to be given by

$$\gamma_n^A = \sqrt{{k_{x_n}^A}^2 - \epsilon_r {k_0}^2}\,, \qquad (1)$$

$$\gamma_n^B = \sqrt{{k_{x_n}^B}^2 - \epsilon_r {k_0}^2}\,. \qquad (2)$$

Note that $\gamma_n^A = j\beta_n^A$ if ${k_{x_n}^A}^2 < \epsilon_r {k_0}^2$, and $\gamma_n^A = \alpha_n^A$ if ${k_{x_n}^A}^2 > \epsilon_r {k_0}^2$.

Similarly, we have $\gamma_n^B = j\beta_n^B$ if ${k_{x_n}^B}^2 < \epsilon_r {k_0}^2$, and $\gamma_n^B = \alpha_n^B$ if ${k_{x_n}^B}^2 > \epsilon_r {k_0}^2$, so that the impedances in regions A and B are given by

$$Z_n^A = \frac{jk_0\eta_0}{\gamma_n^A}\,, \qquad (3)$$

$$Z_n^B = \frac{jk_0\eta_0}{\gamma_n^B}\,, \qquad (4)$$

respectively, where $\eta_0 = \sqrt{\frac{\mu_0}{\varepsilon_0}} \approx 120\pi$ and $k_0 = \omega\sqrt{\mu_0\varepsilon_0}$. Suppose that the unit vectors in the x, y, z directions are represented by $\boldsymbol{i}, \boldsymbol{j}, \boldsymbol{k}$ respectively. Then the transverse components of the incident TE_{n0} mode in region A may be given by

$$\boldsymbol{E}_n^A = {f_n}^A(x)\ \boldsymbol{j}, \qquad (5)$$

$$\boldsymbol{H}_n^A = -\frac{1}{Z_n^A}{f_n}^A(x)\ \boldsymbol{i}, \qquad (6)$$

where ${f_n}^A(x)$ is a sinusoidal function of x (for the n^{th} mode in waveguide A) which vanishes at the maximum and minimum boundary values of x for the surface S_1 for which we have $z < 0$. Similarly, the transverse components of the incident TE_{n0} mode in region B may be given by

$$\boldsymbol{E}_n^B = {f_n}^B(x)\boldsymbol{j}, \qquad (7)$$

$$\boldsymbol{H}_n^B = -\frac{1}{Z_n^B}{f_n}^B(x)\ \boldsymbol{i}, \qquad (8)$$

where ${f_n}^B(x)$ is a sinusoidal function of x (for the n^{th} mode in waveguide B) which vanishes at the maximum and minimum boundary values of x for the surface S_2 for which we have $0 < z < L$. The fields are independent of the variation in y coordinates. Then, by multiplying by the waveguide height b (since there is no y-variation) and integrating over the surface in the x-z plane where the incremental area element $d\mathbf{s}$ is given by $d\mathbf{s} = \mathrm{dx} \cdot \boldsymbol{k}$, the complex power flow from solely the fields for the n^{th} mode in region A is given by

$$\boldsymbol{P}_n^A = \int_{S_1} \boldsymbol{E}_n^A \times \boldsymbol{H}_n^{A^*} \cdot \mathbf{ds} = \frac{b}{Z_n^{A^*}} \int_{S_1} {f_n}^A(x) {f_n}^{A^*}(x) \cdot dx\, \boldsymbol{k}$$

$$= \frac{b}{Z_n^{A^*}} \int_{\frac{-a_1}{2}}^{\frac{a_1}{2}} cos^2\, k_{x_n}^A\, x\, dx\,. \qquad (9)$$

Similarly, the complex power flow from solely the fields fields for the n^{th} mode inside region B is given by

$$\boldsymbol{P}_n^B = \int_{S_2} \boldsymbol{E}_n^B \times \boldsymbol{H}_n^{B^*} \cdot \mathbf{ds} = \frac{b}{Z_n^{B^*}} \int_{S_2} {f_n}^B(x) {f_n}^{B^*}(x) \cdot dx\, \boldsymbol{k}\,. \qquad (10)$$

The complex power flow from the magnetic field fields for the m^{th} mode in region A and the electric field fields for the n^{th} mode in region B is given by

$$\boldsymbol{P}_{nm}^{BA} = \int_{S_2} \boldsymbol{E}_n^B \times {\boldsymbol{H}_m^A}^* \cdot \mathbf{ds} = \frac{b}{Z_m^{A^*}} \int_{\frac{-a_2}{2}}^{\frac{a_2}{2}} {f_n}^{A^*}(x)\, {f_n}^B(x)\; dx\, \boldsymbol{k}\,. \qquad (11a)$$

Similarly, it may be deduced that

$$\boldsymbol{P}_{mn}^{AB} = \int_{S_2} \boldsymbol{E}_m^A \times \boldsymbol{H}_n^{B^*} \cdot \mathbf{ds}\;. \qquad (11b)$$

Now consider the reflected and transmitted electric and magnetic waves at the discontinuities $z = 0$ and $z = L$. At $z = 0$, the superposition of the incident wave of the 1^{st} mode and the transmitted waves of all the modes (for which the n^{th} mode amplitude is denoted as A_n) from

the first boundary at $z = 0$ which are reflected from the boundary at $z = L$ are equal to the forwards and backwards waves propagating in region B, i.e. it follows that at $z = 0$

$$\boldsymbol{E}_1^A + \sum_{n=1}^{\infty} A_n \boldsymbol{E}_n^A = \sum_{n=1}^{\infty} B_n^+ \boldsymbol{E}_n^B + \sum_{n=1}^{\infty} B_n^- \boldsymbol{E}_n^B , \tag{12}$$

$$\boldsymbol{H}_1^A - \sum_{n=1}^{\infty} A_n \boldsymbol{H}_n^A = \sum_{n=1}^{\infty} B_n^+ \boldsymbol{H}_n^B - \sum_{n=1}^{\infty} B_n^- \boldsymbol{H}_n^B , \tag{13}$$

for which the n^{th} mode amplitude of the forwards and backwards waves in region B is denoted as B_n^+ and B_n^- respectively).

Similarly, at $z = L$, it follows that

$$\sum_{n=1}^{\infty} B_n^+ e^{-\gamma_n L} \boldsymbol{E}_n^B + \sum_{n=1}^{\infty} B_n^- e^{\gamma_n L} \boldsymbol{E}_n^B = \sum_{n=1}^{\infty} C_n \boldsymbol{E}_n^A , \tag{14}$$

$$\sum_{n=1}^{\infty} B_n^+ e^{-\gamma_n L} \boldsymbol{H}_n^B - \sum_{n=1}^{\infty} B_n^- e^{\gamma_n L} \boldsymbol{H}_n^B = \sum_{n=1}^{\infty} C_n \boldsymbol{H}_n^A , \tag{15}$$

where γ_n is the propagation constant of the n^{th} mode in region B and the n^{th} mode amplitude in region C is denoted as C_n.

In this section, an analytical method is designed to determine the amplitude coefficients A_n, B_n^+, B_n^-, C_n. Post-multiply (12) by $\boldsymbol{H}_m^{A^*}$ and integrate over the waveguide surface S_1, so that

$$\int_{S_1} \boldsymbol{E}_1^A \times \boldsymbol{H}_m^{A^*} \cdot \mathbf{ds} + \sum_{n=1}^{\infty} A_n \int_{S_1} \boldsymbol{E}_n^A \times \boldsymbol{H}_m^{A^*} \cdot \mathbf{ds} = \sum_{n=1}^{\infty} B_n^+ \int_{S_2} \boldsymbol{E}_n^B \times \boldsymbol{H}_m^{A^*} \cdot \mathbf{ds} + \sum_{n=1}^{\infty} B_n^- \int_{S_2} \boldsymbol{E}_n^B \times \boldsymbol{H}_m^{A^*} \cdot \mathbf{ds}$$

for which, by using (9) , it follows that

$$\int_{S_1} \boldsymbol{E}_n^A \times \boldsymbol{H}_m^{A\,*} \cdot \mathbf{ds} = \begin{cases} \boldsymbol{P}_n^A & if\ n = m. \\ 0 & if\ n \neq m. \end{cases}$$

Consider two cases which both have the structure in the figure given above. All the boundaries of both the surfaces S_1 and S_3 at both $z = 0$ and $z = L$ are E-planes and H-planes in each of these respective cases.

5.3. E-plane case

Note that the latter condition in the above expression follows directly from orthogonality relations. It follows from the last two expressions and from (11) that

$$\delta_{1m}\boldsymbol{P}_1^A + \boldsymbol{A_m}\boldsymbol{P}_m^A = \sum_{n=1}^{\infty} B_n^+ \ \boldsymbol{P}_{nm}^{BA} + \sum_{n=1}^{\infty} B_n^- \ \boldsymbol{P}_{nm}^{BA} \quad , \qquad (16)$$

where the standard Kronecker delta symbol is used so that $\delta_{1m} = 1$ iff $m = 1$, and $\delta_{1m} = 0$ for any other value of m. Note that

$$\int_{S_2} \boldsymbol{E}_n^B \times \boldsymbol{H}_m^{B\,*} \cdot \mathbf{ds} = \begin{cases} \boldsymbol{P}_n^B & if\ n = m. \\ 0 & if\ n \neq m. \end{cases}$$

On the E-plane boundaries between A and B, which are represented by $S_1 - S_2$ at $z = 0$, it is evident that

$$\boldsymbol{E}_1^A - \sum_{n=1}^{\infty} A_n \, \boldsymbol{E}_n^A = 0 \ .$$

On the E-plane boundaries (between B and C) at $z = L$, it follows that

$$\sum_{n=1}^{\infty} C_n \, \boldsymbol{E}_n^A = 0 \ .$$

These two boundary conditions are implicitly assumed for the establishment of the subsequent derivations.

Premultiply (13) by $\boldsymbol{E}_m^{B\,*}$ and integrate over the waveguide surface, so that

$$\int_{S_1} \boldsymbol{E}_m^{B\,*} \times \boldsymbol{H}_1^A \cdot \mathbf{ds}$$

$$- \sum_{n=1}^{\infty} A_n \int_{S_2} \boldsymbol{E}_m^{B\,*} \times \boldsymbol{H}_n^A \cdot \mathbf{ds}$$

$$= \sum_{n=1}^{\infty} B_n^+ \int_{S_2} \boldsymbol{E}_m^{B\,*} \times \boldsymbol{H}_n^B \cdot \mathbf{ds} - \sum_{n=1}^{\infty} B_n^- \int_{S_2} \boldsymbol{E}_m^{B\,*} \times \boldsymbol{H}_n^B \cdot \mathbf{ds}$$

By taking the conjugate expressions of (10) and (11), it follows that

$$\int_{S_2} \boldsymbol{E}_m^{B\,*} \times \boldsymbol{H}_n^B \cdot \mathbf{ds} = \begin{cases} \boldsymbol{P}_m^{B\,*} & if\ n = m. \\ 0 & if\ n \neq m. \end{cases}$$

and

$$\int_{S_2} \boldsymbol{E}_n^{B\,*} \times \boldsymbol{H}_m^A \cdot \mathbf{ds} = \boldsymbol{P}_{nm}^{BA\,*}$$

Combining the last three expressions implies that

$$\boldsymbol{P}_{m1}^{BA\,*} - \sum_{n=1}^{\infty} A_n \boldsymbol{P}_{mn}^{BA\,*} = B_m^+ \boldsymbol{P}_m^{B\,*} - B_m^- \boldsymbol{P}_m^{B\,*} \quad . \tag{17}$$

Post-multiply (14) by $\boldsymbol{H}_m^{A\,*}$ and integrate over the waveguide surface, so that

$$\sum_{n=1}^{\infty} B_n^+ e^{-\gamma_n L} \int_{S_2} \boldsymbol{E}_n^B \times \boldsymbol{H}_m^{A\,*} \cdot \mathbf{ds} + \sum_{n=1}^{\infty} B_n^- e^{\gamma_n L} \int_{S_2} \boldsymbol{E}_n^B \times \boldsymbol{H}_m^{A\,*} \cdot \mathbf{ds}$$

$$= \sum_{n=1}^{\infty} C_n \int_{S_1} \boldsymbol{E}_n^A \times \boldsymbol{H}_m^{A\,*} \cdot \mathbf{ds}\,.$$

Thus, by applying the same procedure that was used to obtain (16), the last expression may be rewritten as

$$\sum_{n=1}^{\infty} B_n^+ e^{-\gamma_n L}\, \boldsymbol{P}_{nm}^{BA} + \sum_{n=1}^{\infty} B_n^- e^{\gamma_n L}\, \boldsymbol{P}_{nm}^{BA} = C_m \boldsymbol{P}_m^A \quad . \tag{18}$$

Pre-multiply (15) by $\boldsymbol{E}_m^{B\,*}$ and integrate over the waveguide surface, so that

$$\sum_{n=1}^{\infty} B_n^+ e^{-\gamma_n L} \int_{S_2} \boldsymbol{E}_m^{B\,*} \times \boldsymbol{H}_n^B \cdot \mathbf{ds} + \sum_{n=1}^{\infty} B_n^- e^{\gamma_n L} \int_{S_2} \boldsymbol{E}_m^{B\,*} \times \boldsymbol{H}_n^B \cdot \mathbf{ds}$$

$$= \sum_{n=1}^{\infty} C_n \int_{S_2} \boldsymbol{E}_m^{B\,*} \times \boldsymbol{H}_n^A \cdot \mathbf{ds}\,.$$

Thus, by applying the same procedure that was used to obtain (16), the last expression may be rewritten as

$$B_m^+ e^{-\gamma_m L} \boldsymbol{P}_m^{B\,*} - B_m^- e^{\gamma_m L} \boldsymbol{P}_m^{B\,*} = \sum_{n=1}^{\infty} C_n\, \boldsymbol{P}_{mn}^{BA\,*} \quad . \tag{19}$$

By truncating the above equations so that both n and m are given values from 1 to N, it is possible obtain a general equation in terms of matrices which is equivalent to all four of the equations (16)-(19) (as explained below) given by

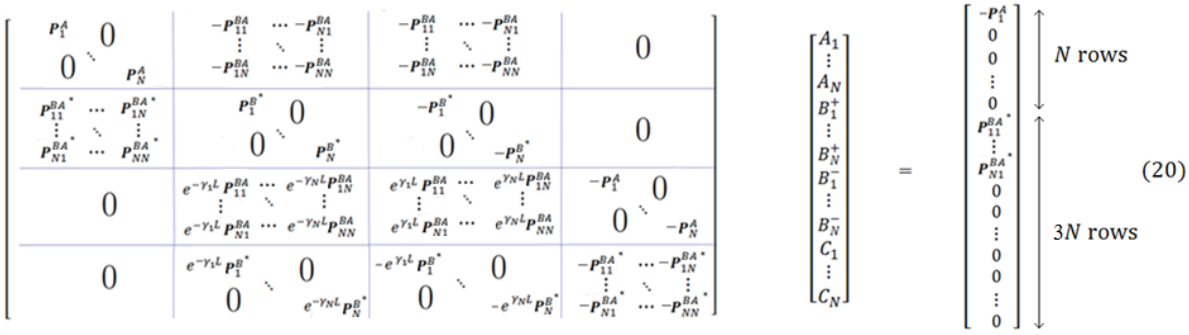

(20)

from which the $4N$ x 1 column matrix consisting of the amplitude coefficients $A_1, \ldots, A_N$, $B_1^+, \ldots, B_N^+$, $B_1^-, \ldots, B_N^-$, $C_1, \ldots, C_N$ can easily be obtained. The $4N$ x $4N$ square matrix has been partitioned into sixteen blocks of N x N matrices in order to clearly show that the equation contained in (20) involving each of the four rows of these N x N matrices corresponds to each one of the respective equations (16)-(19) in their truncated form.

5.4. H-plane case

On the H-plane boundaries between A and B, which are represented by $S_1 - S_2$ at $z = 0$, it follows that

$$\boldsymbol{H}_1^A - \sum_{n=1}^{\infty} A_n \boldsymbol{H}_n^A = 0 \ . \tag{21}$$

On the H-plane boundaries (between B and C) at $z = L$, it is evident that

$$\sum_{n=1}^{\infty} C_n \boldsymbol{H}_n^A = 0 \ . \tag{22}$$

Postmultiply (12) by $\boldsymbol{H}_m^{B\,*}$, so that

$$\int_{S_2} \boldsymbol{E}_1^A \times \boldsymbol{H}_m^{B\,*} \cdot \mathbf{ds} + \sum_{n=1}^{\infty} A_n \int_{S_2} \boldsymbol{E}_n^A \times \boldsymbol{H}_m^{B\,*} \cdot \mathbf{ds} = \sum_{n=1}^{\infty} (B_n^+ - B_n^-) \int_{S_2} \boldsymbol{E}_n^B \times \boldsymbol{H}_m^{B\,*} \cdot \mathbf{ds} \ ,$$

i.e.

$$\boldsymbol{P}_{1m}^{AB} + \sum_{n=1}^{\infty} A_n \boldsymbol{P}_{nm}^{BA} = B_m^{+}\boldsymbol{P}_m^{B} - B_m^{-}\boldsymbol{P}_m^{B} \quad . \tag{23}$$

Premultiply (13) by $\boldsymbol{E}_m^{A\,*}$, so that

$$\int_{S_2} \boldsymbol{E}_m^{A\,*} \times \boldsymbol{H}_1^{A} \cdot \mathbf{ds} - \sum_{n=1}^{\infty} A_n \int_{S_2} \boldsymbol{E}_m^{A\,*} \times \boldsymbol{H}_n^{A} \cdot \mathbf{ds} = \sum_{n=1}^{\infty} (B_n^{+} - B_n^{-}) \int_{S_2} \boldsymbol{E}_m^{A\,*} \times \boldsymbol{H}_n^{B} \cdot \mathbf{ds} \quad .$$

If both sides of the last equation are added to

$$\int_{S_1 - S_2} \boldsymbol{E}_m^{A\,*} \times \left(\boldsymbol{H}_1^{A} - \sum_{n=1}^{\infty} A_n \boldsymbol{H}_n^{A} \right) \cdot \mathbf{ds} \ ,$$

which, from (21), is zero, then it is possible to take the integrals on the left hand side of the last equation to be over S_1 instead of S_2 so that

$$\delta_{m1}\boldsymbol{P}_1^{A^*} + \boldsymbol{A_m}\boldsymbol{P}_m^{A\,*} = \sum_{n=1}^{\infty} B_n^{+} \ \boldsymbol{P}_{mn}^{AB\,*} + \sum_{n=1}^{\infty} B_n^{-} \ \boldsymbol{P}_{mn}^{AB\,*} \quad . \tag{24}$$

Postmultiply (14) by $\boldsymbol{H}_m^{B\,*}$ and integrate over S_2 , so that

$$\sum_{n=1}^{\infty} (B_n^{+} e^{-\gamma_n L} + B_n^{-} e^{\gamma_n L}) \int_{S_2} \boldsymbol{E}_n^{B} \times \boldsymbol{H}_m^{B\,*} \cdot \mathbf{ds} = \sum_{n=1}^{\infty} C_n \int_{S_2} \boldsymbol{E}_n^{A} \times \boldsymbol{H}_m^{B\,*} \cdot \mathbf{ds} \ ,$$

i.e.

$$B_m^{+} e^{-\gamma_m L} \boldsymbol{P}_m^{B} - B_m^{-} e^{\gamma_m L} \boldsymbol{P}_m^{B} = \sum_{n=1}^{\infty} C_n \boldsymbol{P}_{nm}^{AB} \quad . \tag{25}$$

Premultiply (15) by $\boldsymbol{E}_m^{A\,*}$ and integrate over S_2, so that

$$\sum_{n=1}^{\infty}(B_n^+ e^{-\gamma_n L} - B_n^- e^{\gamma_n L}) \int_{S_2} \boldsymbol{E}_m^{A\,*} \times \boldsymbol{H}_n^B \cdot \mathbf{ds} = \sum_{n=1}^{\infty} C_n \int_{S_2} \boldsymbol{E}_m^{A\,*} \times \boldsymbol{H}_n^A \cdot \mathbf{ds} \ .$$

If both sides of the last equation are added to

$$\int_{S_1 - S_2} \boldsymbol{E}_m^{A\,*} \times \left(\sum_{n=1}^{\infty} C_n \boldsymbol{H}_n^A \right) \cdot \mathbf{ds} \ ,$$

which, from (22), is zero, then the integral on the right hand side of the last equation can be taken to be over S_1 instead of S_2 so that

$$\sum_{n=1}^{\infty} B_n^+ e^{-\gamma_n L} \boldsymbol{P}_{mn}^{AB\,*} - \sum_{n=1}^{\infty} B_n^- e^{\gamma_n L} \boldsymbol{P}_{mn}^{AB\,*} = C_m \boldsymbol{P}_m^{A\,*} \quad . \tag{26}$$

By truncating the above equations so that both n and m are given values from 1 to N, a general equation can be obtained in terms of matrices which is equivalent to all four of the equations (23)-(26) (as explained below) given by

$$\begin{bmatrix} -P_{11}^{AB} & \cdots & -P_{N1}^{AB} \\ \vdots & \ddots & \vdots \\ -P_{1N}^{AB} & \cdots & -P_{NN}^{AB} \end{bmatrix} \quad \begin{bmatrix} P_1^B & & 0 \\ & \ddots & \\ 0 & & P_N^B \end{bmatrix} \quad \begin{bmatrix} P_1^B & & 0 \\ & \ddots & \\ 0 & & P_N^B \end{bmatrix} \quad \begin{bmatrix} 0 \end{bmatrix}$$

$$\begin{bmatrix} -P_1^{A^*} & & 0 \\ & \ddots & \\ 0 & & -P_N^{A^*} \end{bmatrix} \quad \begin{bmatrix} -P_{11}^{AB^*} & \cdots & -P_{1N}^{AB^*} \\ \vdots & \ddots & \vdots \\ -P_{N1}^{AB^*} & \cdots & -P_{NN}^{AB^*} \end{bmatrix} \quad \begin{bmatrix} P_{11}^{AB^*} & \cdots & P_{1N}^{AB^*} \\ \vdots & \ddots & \vdots \\ P_{N1}^{AB^*} & \cdots & P_{NN}^{AB^*} \end{bmatrix} \quad \begin{bmatrix} 0 \end{bmatrix}$$

$$\begin{bmatrix} 0 \end{bmatrix} \quad \begin{bmatrix} e^{-\gamma_1 L} P_1^B & & 0 \\ & \ddots & \\ 0 & & e^{-\gamma_N L} P_N^B \end{bmatrix} \quad \begin{bmatrix} e^{\gamma_1 L} P_1^B & & 0 \\ & \ddots & \\ 0 & & e^{\gamma_N L} P_N^B \end{bmatrix} \quad \begin{bmatrix} -P_{11}^{AB} & \cdots & -P_{N1}^{AB} \\ \vdots & \ddots & \vdots \\ -P_{1N}^{AB} & \cdots & -P_{NN}^{AB} \end{bmatrix}$$

$$\begin{bmatrix} 0 \end{bmatrix} \quad \begin{bmatrix} e^{-\gamma_1 L} P_{11}^{AB^*} & \cdots & e^{-\gamma_N L} P_{1N}^{AB^*} \\ \vdots & \ddots & \vdots \\ e^{-\gamma_1 L} P_{N1}^{AB^*} & \cdots & e^{-\gamma_N L} P_{NN}^{AB^*} \end{bmatrix} \quad \begin{bmatrix} -e^{\gamma_1 L} P_{11}^{AB^*} & \cdots & -e^{\gamma_N L} P_{1N}^{AB^*} \\ \vdots & \ddots & \vdots \\ -e^{\gamma_1 L} P_{N1}^{AB^*} & \cdots & -e^{\gamma_N L} P_{NN}^{AB^*} \end{bmatrix} \quad \begin{bmatrix} -P_1^{A^*} & & 0 \\ & \ddots & \\ 0 & & -P_N^{A^*} \end{bmatrix}$$

$$\begin{bmatrix} A_1 \\ \vdots \\ A_N \\ B_1^+ \\ \vdots \\ B_N^+ \\ B_1^- \\ \vdots \\ B_N^- \\ C_1 \\ \vdots \\ C_N \end{bmatrix} = \begin{bmatrix} P_{11}^{AB} \\ \vdots \\ P_{1N}^{AB} \\ -P_1^{A^*} \\ 0 \\ 0 \\ \vdots \\ 0 \end{bmatrix} \begin{matrix} \uparrow \\ \vdots \\ \downarrow \\ \uparrow \\ \vdots \\ \downarrow \end{matrix} \begin{matrix} N \text{ rows} \\ \\ \\ 3N \text{ rows} \end{matrix} \tag{27}$$

from which the $4N$ x 1 column matrix consisting of the amplitude coefficients $A_1, \ldots, A_N$, $B_1^+, \ldots, B_N^+$, $B_1^-, \ldots, B_N^-$, $C_1, \ldots, C_N$ can easily be obtained. As before, we have partitioned the $4N$ x $4N$ square matrix into sixteen blocks of N x N matrices in order to clearly show that each equation contained in (20) contained in one of the four rows of these N x N matrices corresponds to one of the respective equations (23)-(26) in their truncated form.

5.5. Comparisons of practical examples with HFSS

Now consider a special instance of the above structure with its three regions A, B, C. The composite structure in which regions A and C are represented by rectangular SIWs and region B is a slotted SIW with E-plane and H-plane boundaries respectively. This composite structure is equivalent to modelling another in which all regions A, B, C are regarded as rectangular SIWs, where the middle region B has a smaller width than the other two so that it forms a single E-plane / H-plane step. This is illustrated in the schematic figure below. The line segment O_1O_3 is used to portray an H-plane and the line segments O_1O_2 and O_3O_4 either both characterize a pair of E-planes or both represent a pair of H-planes in the respective cases. In this way, we consider two different manifestations of the structure in the figure below, namely an E-plane case and an H-plane case. We make use of an offset perpendicular distance from $x = 0$ to the line segment O_1O_3, which is denoted as X.

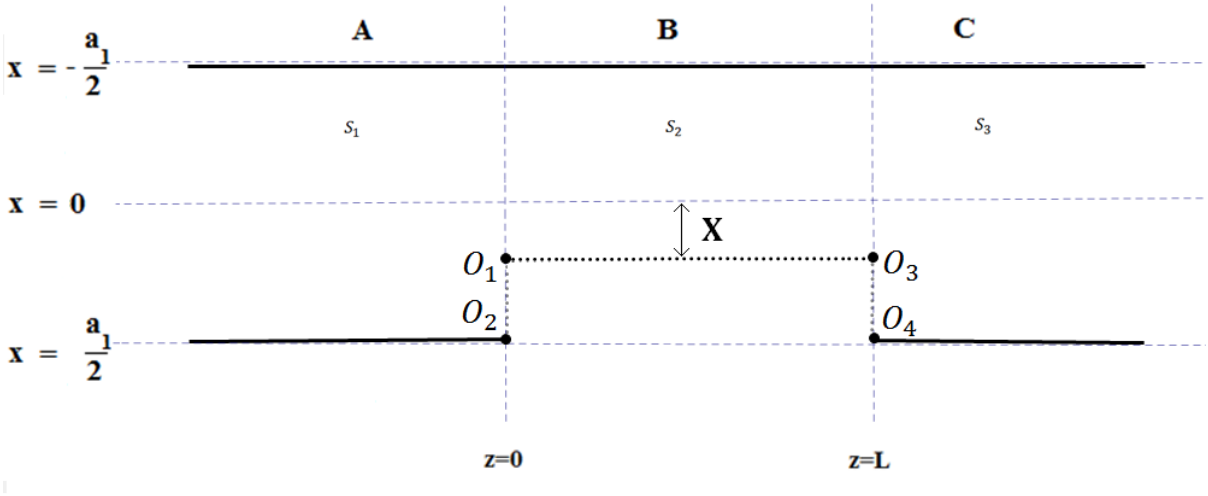

Figure 5.2: Schematic of a specific composite waveguide structure.

The wave numbers of the waveguide regions A and B are represented by $k_{x_n}^A = \frac{(2n-1)\pi}{a_1}$ and $k_{x_n}^B = \frac{(2n-1)\pi}{a_2}$ respectively, so that

$$f_n{}^A(x) = \begin{cases} cos\, k_{x_n}^A\, x\ , & n = 1,3,5\ldots \\ sin\, k_{x_n}^A\, x\ , & n = 2,4,6,\ldots \end{cases} \tag{28}$$

$$f_n{}^B(x) = cos\, k_{x_n}^B\,(x - X)\,, \tag{29}$$

where, by using the fact that $L_1 = \frac{a_1}{2} + X$,

$$k_{x_n}^B = \frac{(2n-1)\pi}{2\left(\frac{a_1}{2} + X\right)} \quad . \tag{30}$$

Then (28) may be substituted into (9) to obtain the complex power flow from solely the fields for the n^{th} mode inside region A, which is given by

$$\boldsymbol{P}_n^A = \int_{S_1} \boldsymbol{E}_n^A \times \boldsymbol{H}_n^{A^*} \cdot \mathbf{ds} = \frac{b}{Z_n^{A^*}} \int_{\frac{-a_1}{2}}^{\frac{a_1}{2}} f_n{}^A(x) f_n{}^{A^*}(x)\, dx\, \boldsymbol{k} = \frac{b a_1}{2 Z_n^{A^*}}\,. \tag{31}$$

Similarly, by substituting (29) into (10) , it follows that the complex power flow from solely the fields for the n^{th} mode inside region B is given by

$$\boldsymbol{P}_n^B = \int_{S_2} \boldsymbol{E}_n^B \times \boldsymbol{H}_n^{B^*} \cdot \mathbf{ds} = \frac{b}{Z_n^{B^*}} \int_{S_2} f_n{}^B(x) f_n{}^{B^*}(x) \cdot dx\, \boldsymbol{k}$$

$$= \frac{b}{Z_n^{B^*}} \int_{\frac{-a_2}{2}}^{X} cos^2\, k_{x_n}^B\,(x - X) dx = \frac{\left(\frac{a_1}{4} + \frac{X}{2}\right) b}{Z_n^{B^*}}\,. \tag{32}$$

$$\boldsymbol{P}_{nm}^{BA} = \int_{S_2} \boldsymbol{E}_n^B \times \boldsymbol{H}_m^{A^*} \cdot \mathbf{ds} = \frac{b}{Z_m^{A^*}} \int_{\frac{-a_2}{2}}^{X} f_m{}^A(x)\, f_n{}^{B^*}(x)\ dx$$

$$= \frac{b}{Z_m^{A^*}} \int_{\frac{-a_2}{2}}^{X} cos\, k_{x_n}^B x \;\; cos\, k_{x_m}^A x \, dx$$

$$= \frac{b}{Z_m^{A^*}} \int_{\frac{-a_2}{2}}^{X} \cos\frac{\left(k_{x_n}^B + k_{x_m}^A\right)}{2} x \;\; \cos\frac{\left(k_{x_n}^B - k_{x_m}^A\right)}{2} x \, dx$$

$$= \frac{b}{Z_m^{A^*}} \left[\frac{\sin\left(k_{x_n}^B + k_{x_m}^A\right)x}{2\left(k_{x_n}^B + k_{x_m}^A\right)} + \frac{\sin\left(k_{x_n}^B - k_{x_m}^A\right)x}{2\left(k_{x_n}^B - k_{x_m}^A\right)} \right]_{-\frac{a_2}{2}}^{X}$$

$$= \frac{b}{Z_m^{A^*}} \left[\frac{\sin\left(k_{x_n}^B + k_{x_m}^A\right)(2X + a_2)}{4\left(k_{x_n}^B + k_{x_m}^A\right)} + \frac{\sin\left(k_{x_n}^B - k_{x_m}^A\right)(2X + a_2)}{4\left(k_{x_n}^B - k_{x_m}^A\right)} \right], \qquad (33)$$

where $k_{x_n}^A \neq k_{x_m}^B$.

By considering (31)-(33), the necessary complex power flow integrals is substituted into (20) and (27) to obtain the amplitude coefficients for E-plane and H-plane cases respectively. Only the first mode is of particular interest. In other words, the objective is to extract the amplitude coefficients A_1 and C_1 because they are equivalent to the S-parameters S_{11} and S_{21} respectively.

This modal analytic technique is implemented in Matlab to obtain the S-parameters in both the E-plane and H-plane cases over suitable range of frequency. In all the subsequent numerical examples, $a_1 = 61$ mm, waveguide height $b = 1$ mm and $\varepsilon_r = 2.2$. It has been found that if the total number of modes considered is given by $N = 50$, then the most accurate results are obtained from this modal analysis technique. The following three figures show results for the E-plane case, and they suggest that the agreement with the HFSS simulations is appreciably close when the azimuthal length of the middle section is close to the width a_1 of the feeder guides in the outer sections. It was also found from HFSS that the distance X (which is proportional to the width of the middle section) should be significantly less than half of a_1 in order for a significantly large electric field to propagate (as indicated

by a sharp fall / climb in the magnitude of S_{11} / S_{21} respectively during operation) over a frequency above cutoff from roughly 2.2-3.5 GHz.

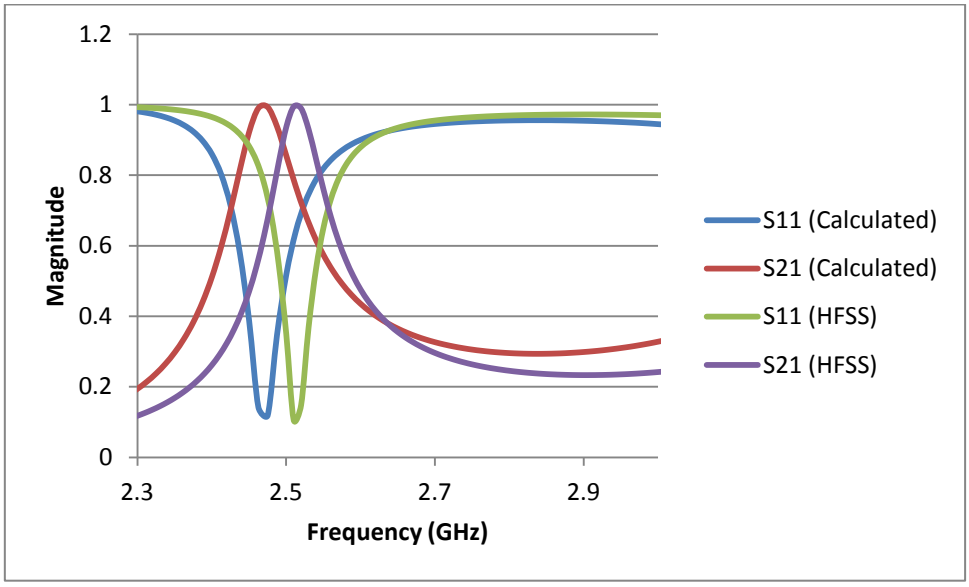

Figure 5.3: S-parameters for E-plane case with L=48.5mm, X= -5mm and N=50

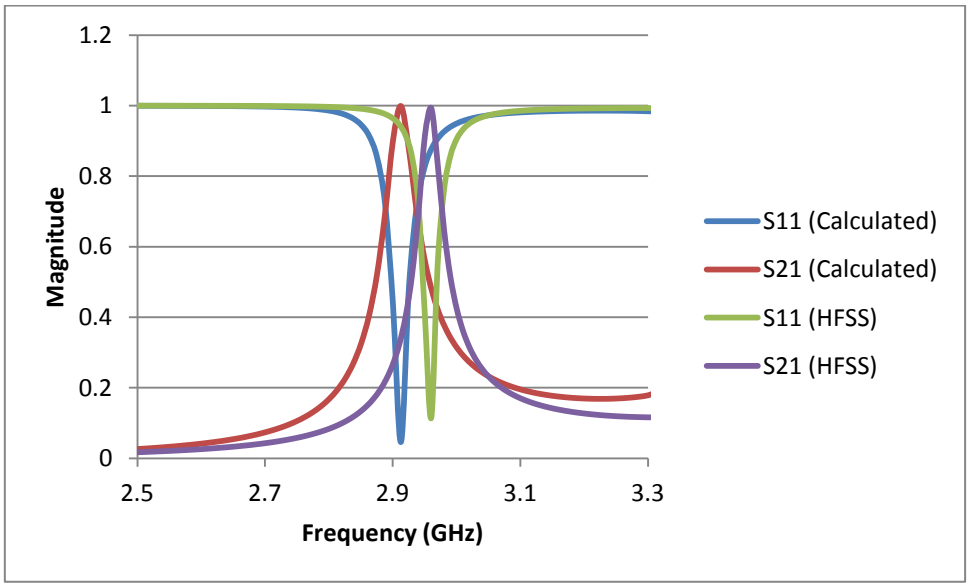

Figure 5.4: S-parameters for E-plane case with L=48.5mm, X= -10mm and N=50

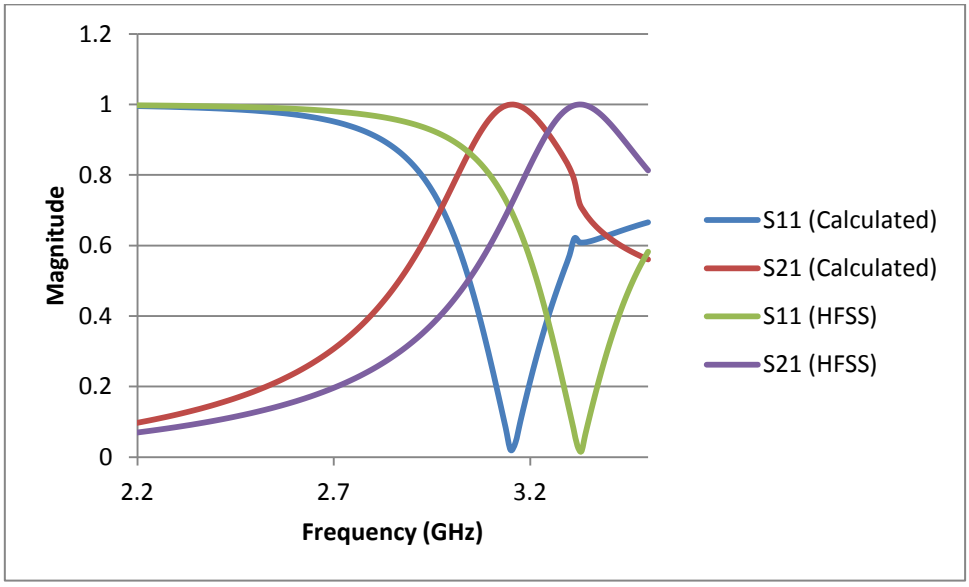

Figure 5.5: S-parameters for E-plane case with L=20mm, X= -5mm and N=50

The next three figures illustrate results for the H-plane case with $N = 50$, and they suggest that the agreement with HFSS is even stronger than for the E-plane case, irrespective of the length of the middle section, over the operational frequency range (i.e. above cutoff) for propagation of the first order mode which is 2.5-3GHz. This modal analysis technique can therefore be used to clearly identify the fundamental (first order) mode which is of importance when considering the practical design of this composite structure. Of course, this modal analysis method can easily provide estimates for the S-parameter curves for higher order modes up to and including N, but this would purely be of theoretical interest.

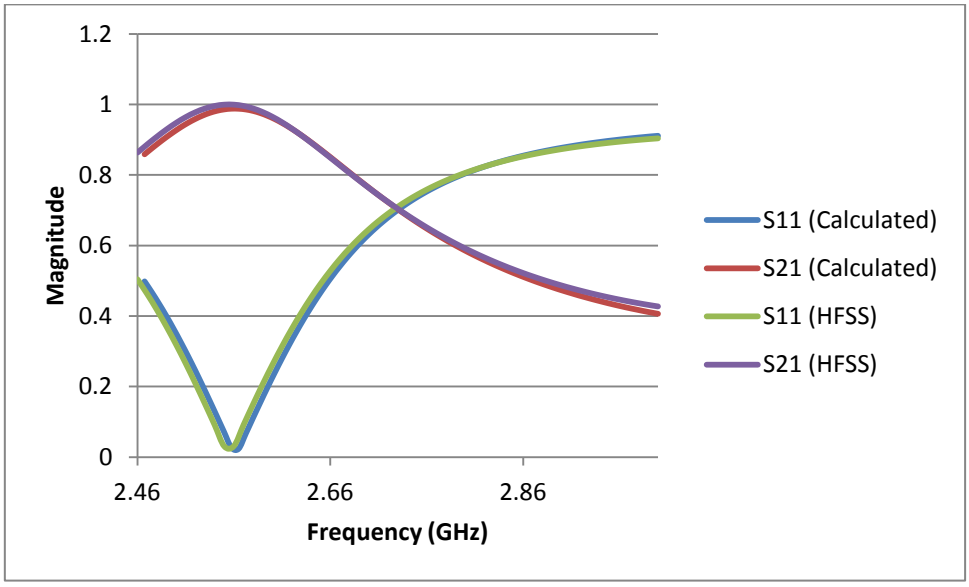

Figure 5.6: S-parameters for H-plane case with L=48.5mm, X= -5mm and N=50

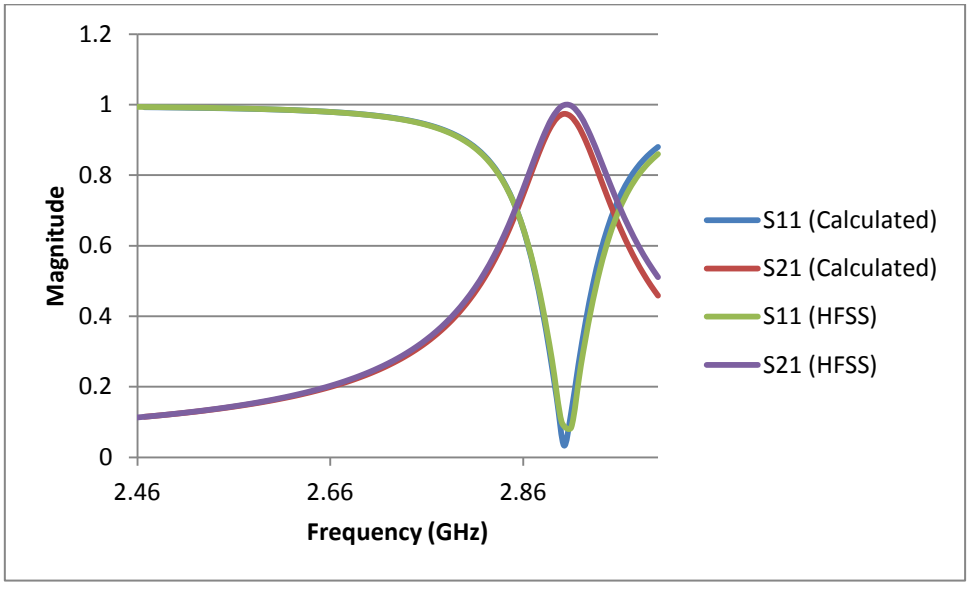

Figure 5.7: S-parameters for H-plane case with L=48.5mm, X= -10mm and N=50

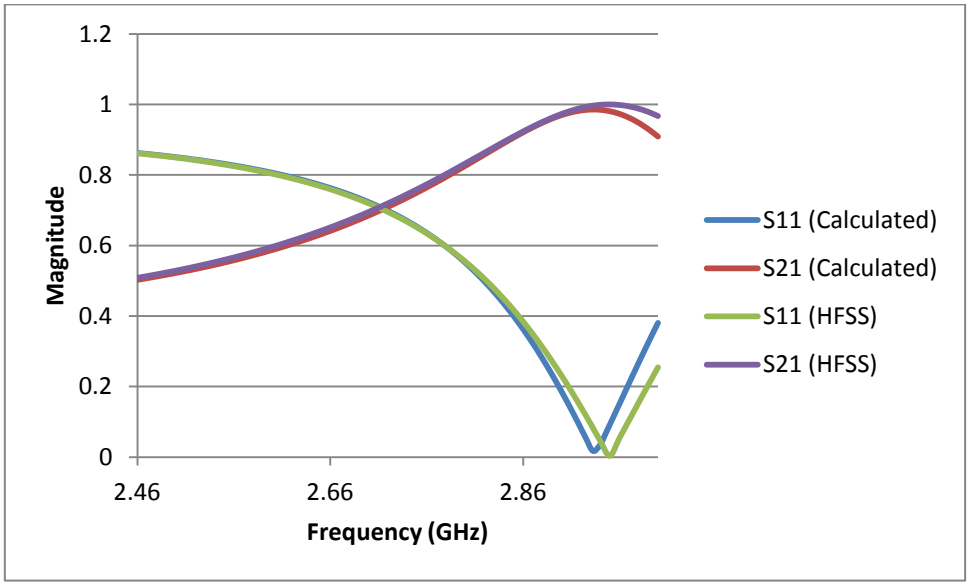

Figure 5.8: S-parameters for H-plane case with L=30mm, X= -5mm and N=50

The following three figures show that if we consider only 4 modes instead of 50 for each of the three previous instances of the H-plane case, then our modal analysis is still significantly accurate, but not quite as close to the CST results as before.

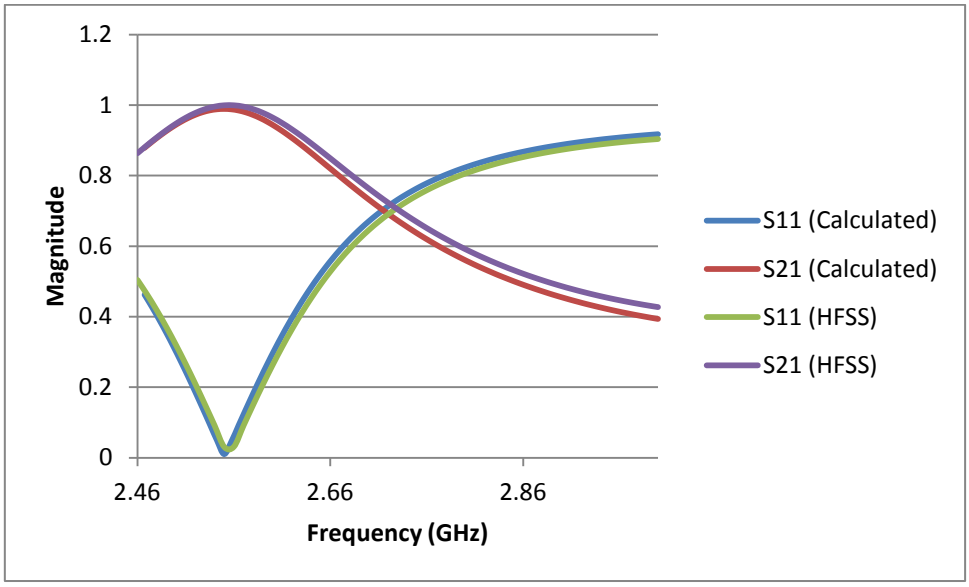

Figure 5.9: S-parameters for H-plane case with L=48.5mm, X= -5mm and N=4

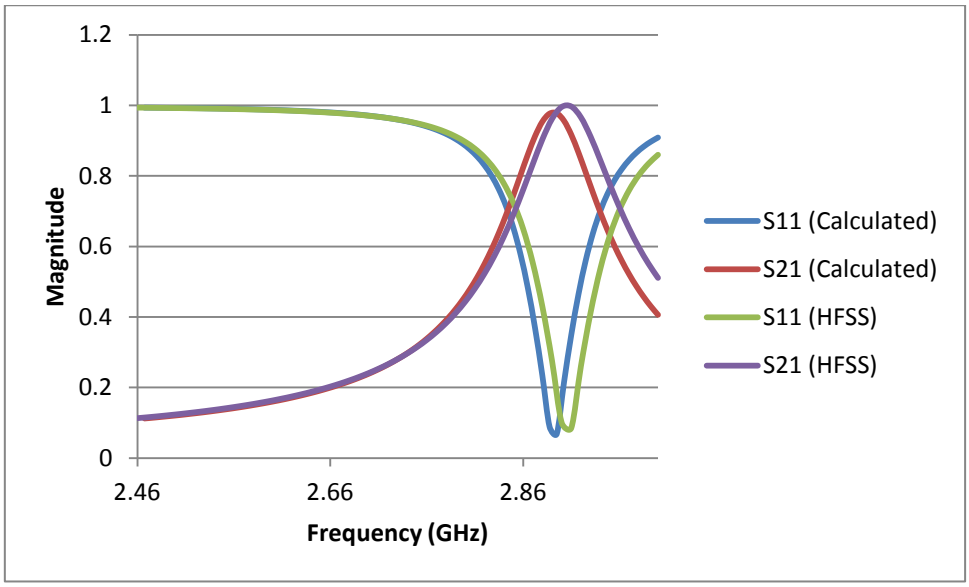

Figure 5.10: S-parameters for H-plane case with L=48.5mm, X= -10mm and N=4

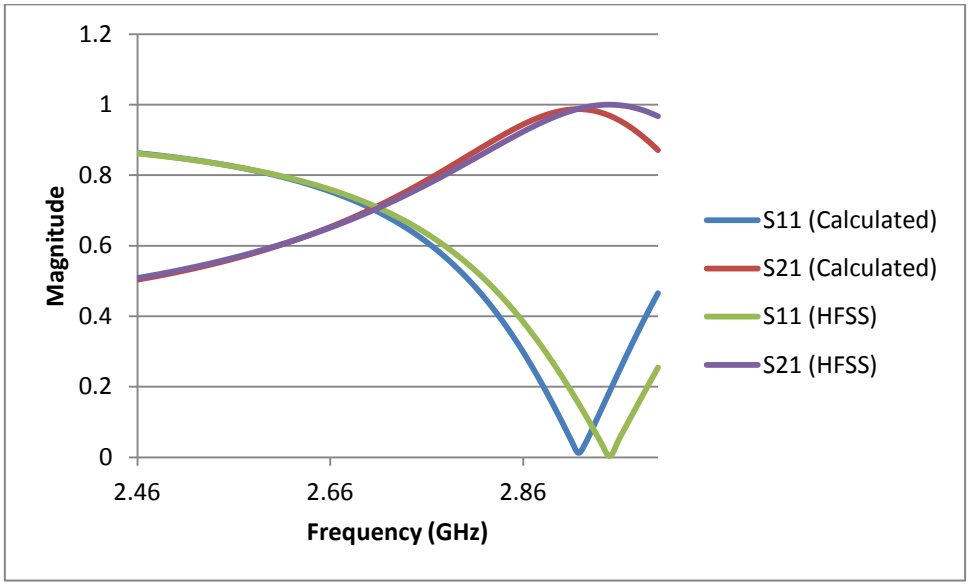

Figure 5.11: S-parameters for H-plane case with L=30mm, X= -5mm and N=4

For the E-plane case, because the E-field must drop to zero on the O_1O_2 plane, it may be that many more points are required in the expansion to model it more accurately, in order for the agreement with HFSS to be as close as it is for the H-plane case with $N = 50$. However, the

results were effectively identical for $N = 40, 50, 60$, and if N is even larger, then the matrices become close to being singular and cannot be evaluated in Matlab. This would suggest it could be possible to make significant improvements by using more advanced methods from numerical analysis in order to find the inverse of large matrices for the Matlab programming.

Note that an unloaded slotted substrate integrated waveguide (SSIW) is effectively a capacitively loaded SSIW. By using the cross-sectional electric field plots of a single SSIW loaded with a capacitance or inductance (shown in Fig. 2.33 and Fig. 2.58 respectively), it is evident that the electric field in the SSIW is predominantly in the longer horizontal section described by L_1 (see Fig. 2.3) and is effectively non-existent in the remaining section annotated by L_2. The SSIW is therefore similar to the HMSIW. We see that like an HMSIW the fundamental mode is of the $TE_{1/2,0}$ type, with the electric field predominantly in the vertical direction, varying almost sinusoidally from zero on the left wall to a maximum at the slot. Indeed the propagation constant of the SSIW is very similar to that of an equivalently sized HMSIW, as mentioned in [19]. In our examples for the modal analysis technique, the transition from a full mode SIW to a SSIW can therefore be used to model an HMSIW fed by a full mode SIW. This is of practical importance, because SSIWs can be used to construct many different types of microwave devices. The SSIW has a small horizontal field in the slot region that can be used to connect discrete devices to the waveguide. This has been used to good effect in [19] to form a microwave switch in a new way. SSIWs are used to make attenuators in [20].

5.6. Estimation of cutoff frequencies of SIW slot antenna

The H-plane modal analysis example that was considered in the previous section can also be used to determine an estimate for the fundamental resonant frequency of a SIW slot antenna, in which the middle section of Figure 5.2 is replaced with a slotted waveguide. This is shown in the following diagram. Note that the horizontal H-plane in Figure 5.2 can be used to model a slot in exactly the same position between O_1 and O_3 at the same offset displacement X from the centre of the guide. In other words, the modal analysis (H-plane) example from Figure 5.2 can be used to model the cutoff frequency characteristics of the SIW slot antenna in Figure 5.12, which is also compared with results from CST Microwave Studio. It should

be noted that the content of this section is in no way meant to design a properly working slot antenna.

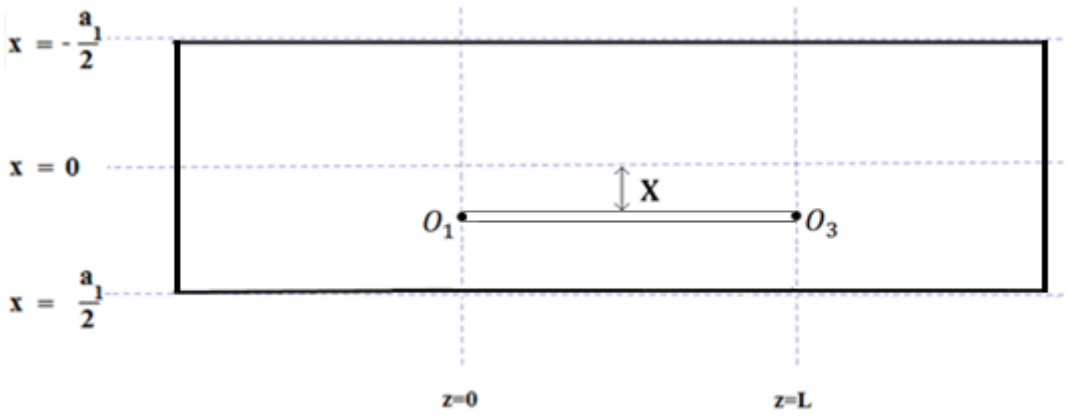

Figure 5.12: Schematic of SIW slot antenna

The values of $a_1 = 61$mm and the slot length $L = 48.5$mm of are the same as before from the previous section. The height of the SIW slot antenna is taken to be 1mm, and its total length is four times the distance L.

The modal analysis technique does not take loss in radiation into consideration, and this is clearly illustrated by the plots in the previous section because the magnitudes of the S-parameters can reach zero and 1. In practice, when the slot antenna radiates at the cutoff frequency, there is some loss (as illustrated in the subsequent plots from CST Microwave Studio). The reason why there is some loss is because there is a resistance which effectively loads the slot. At resonance, the reactive element of the impedance of the slot vanishes. It follows that the impedance of the slot is purely real at the cutoff frequency. The analytic modal technique does not consider the resistive loading of the slot, and is therefore not designed to predict exactly the same magnitudes of the S-parameters as those obtained for the slot antenna. As it will be seen, the behaviour of the S-parameters from the modal analysis is different from that of the slot antenna, in any case. The important point to note is that both models share the same cutoff frequency in theory.

At resonance, the field in the SIW antenna is concentrated around the slot. This is illustrated in the following plot from CST Microwave Studio, for which the offset displacement of the slot is -2.5 mm and the length of the slot is 48.5mm and the cutoff frequency is 2.39 GHz.

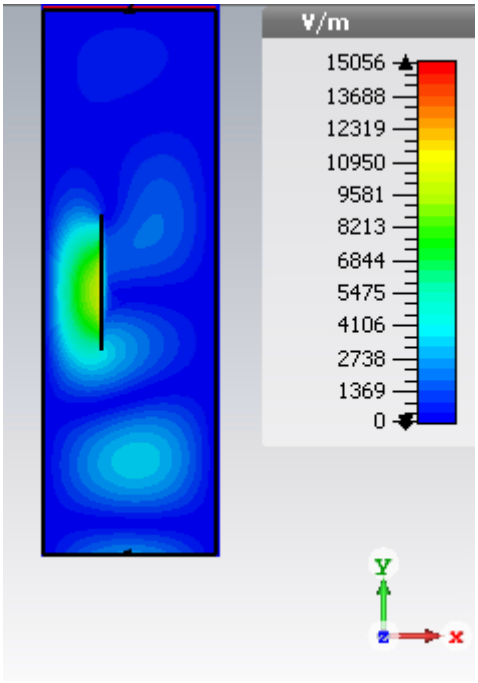

Figure 5.13: SIW slot antenna plot of the magnitude of the E-field at a position of 0.5mm from the base with L=48.5mm, X= -10mm at the resonant frequency.

This field plot shows that electromagnetic waves do not pass through the entire structure when it resonates. By considering the following S-parameter plot as well, it is clear that electromagnetic waves will pass through the entire structure except when it resonates. Note that S_{11} and S_{21} do not quite reach 1 and 0 at resonance respectively, because there is some radiative loss.

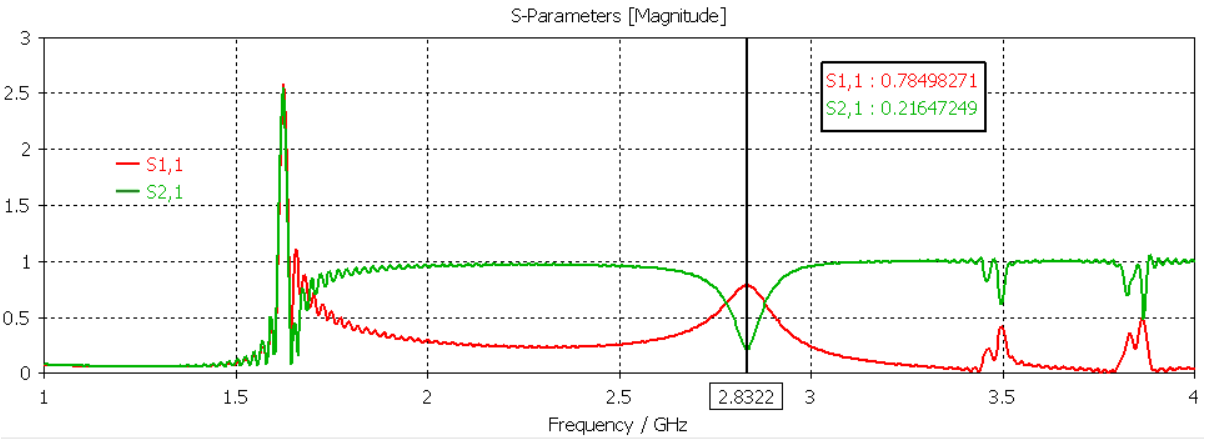

Figure 5.14: S-parameter (CST) plot of SIW slot antenna with L=48.5mm, X= -10mm.

In the case of the corresponding modal analysis model from Figure 5.2, electromagnetic waves only pass through region B from, say, region A to region C, only when the structure (in Figure 5.2) is resonating because of the positioning of the H-planes. This explains why the S-parameter characteristics of this modal analysis appear to be opposite to those for the slot antenna. The actual corresponding calculated modal analysis S-parameter plot (with $\mathrm{L} = 48.5\mathrm{mm}$ and $X = -10\mathrm{mm}$) is given in Figure 5.7, and it predicts (with confirmation from HFSS) the cutoff frequency to be 2.88 GHz which is in reasonably close agreement (within 2% error) with the resonant frequency of 2.83 GHz (as shown in the S-parameter CST plot above) for the slot antenna.

By considering the following S-parameter plot from CST Microwave Studio, it is evident that a SIW slot antenna with $\mathrm{L} = 48.5\mathrm{mm}$ and $X = -5\mathrm{mm}$ has a fundamental resonant frequency of 2.48 GHz. The corresponding prediction from the modal analysis / HFSS H-plane model (from Figure 5.6) is 2.54 GHz.

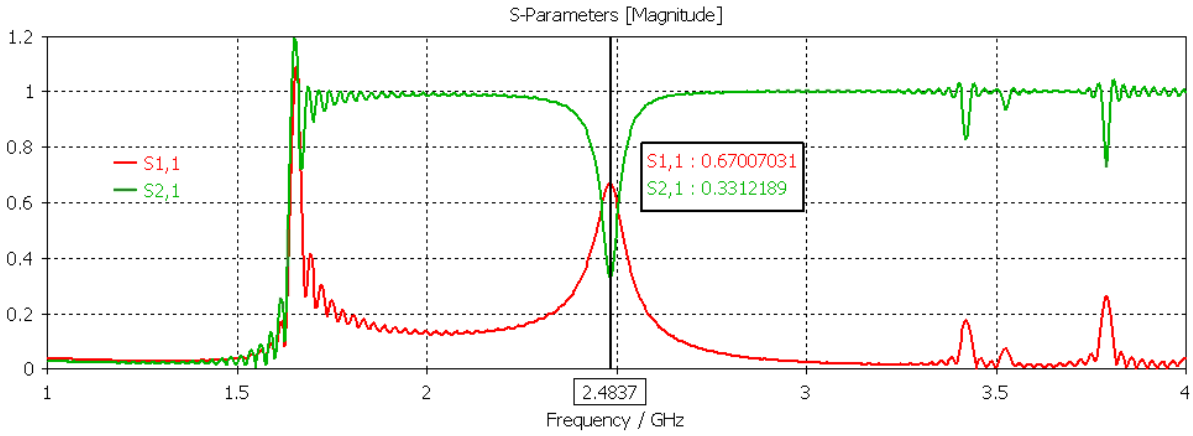

Figure 5.15: S-parameter CST plot of SIW slot antenna with L=48.5mm, X= -5mm.

Similarly, it follows that a SIW slot antenna the offset displacement with L = 48.5mm and $X = -2.5$mm has a fundamental resonant frequency of 2.39 GHz, as shown in the subsequent S-parameter plot.

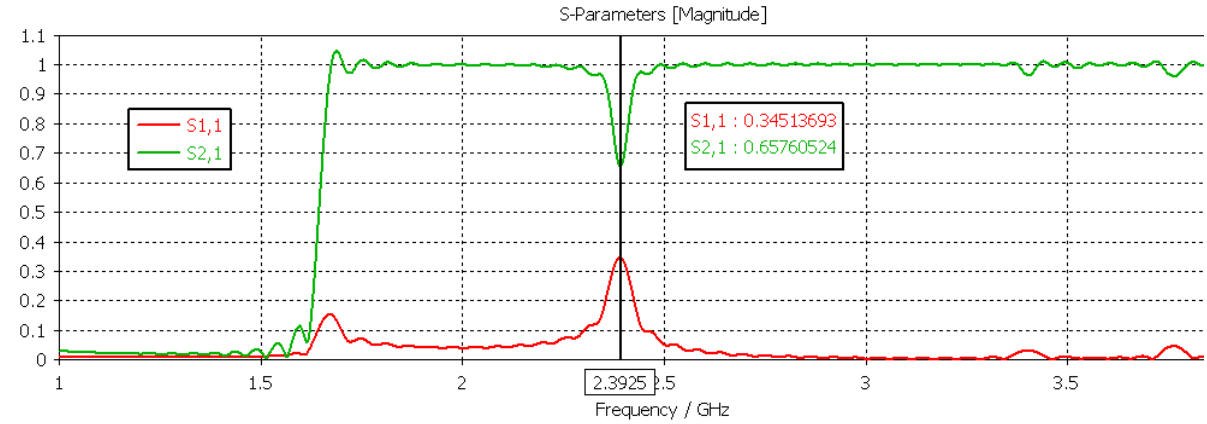

Figure 5.16: S-parameter CST plot of SIW slot antenna with L=48.5mm, X= -2.5mm.

The corresponding prediction from the modal analysis H-plane model (for which L = 48.5mm and $X = -2.5$mm) for the cutoff frequency is is 2.44 GHz. This estimate is within a 2.1% error from the value given by CST Microwave Studio, and it would suggest that the modal analysis technique is very slightly less accurate if the slot is closer to the centre of the waveguide.

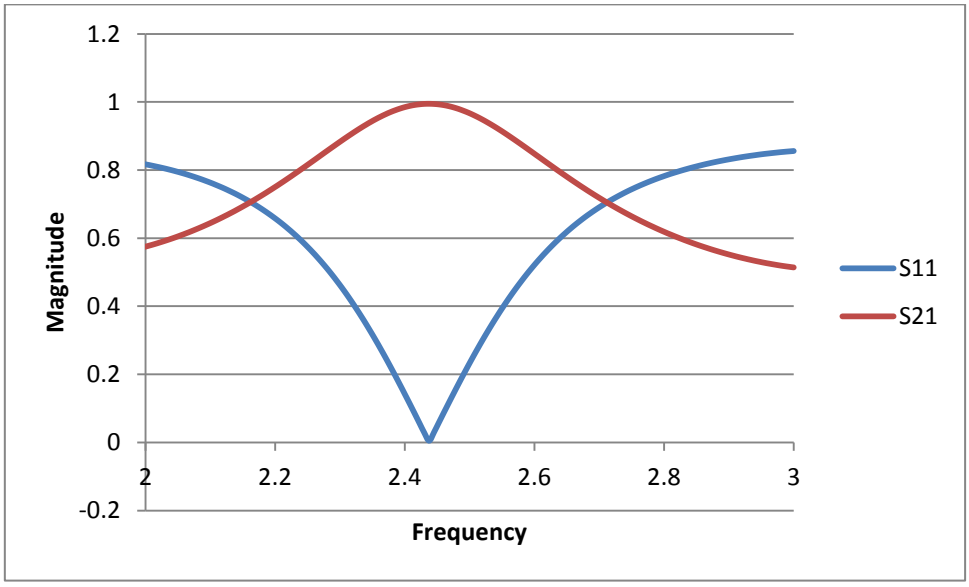

Figure 5.17: Calculated S-parameter plot of H-plane modal analysis model with L=48.5mm, X= -2.5mm.

The following diagram is a farfield plot of the slot antenna with L = 48.5mm and $X = -2.5$mm at the resonant frequency. Though its total efficiency of -4.2 dB (which corresponds to approximately 40%) does not go down to the threshold of -6dB (which could correspond to an efficiency 25%), it is still not quite as small as the radiation efficiency. This suggests that the slot antenna could be slightly better matched. However, it does also indicate that the slot antenna is more efficient if the slot is sufficiently close to the centre of the waveguide.

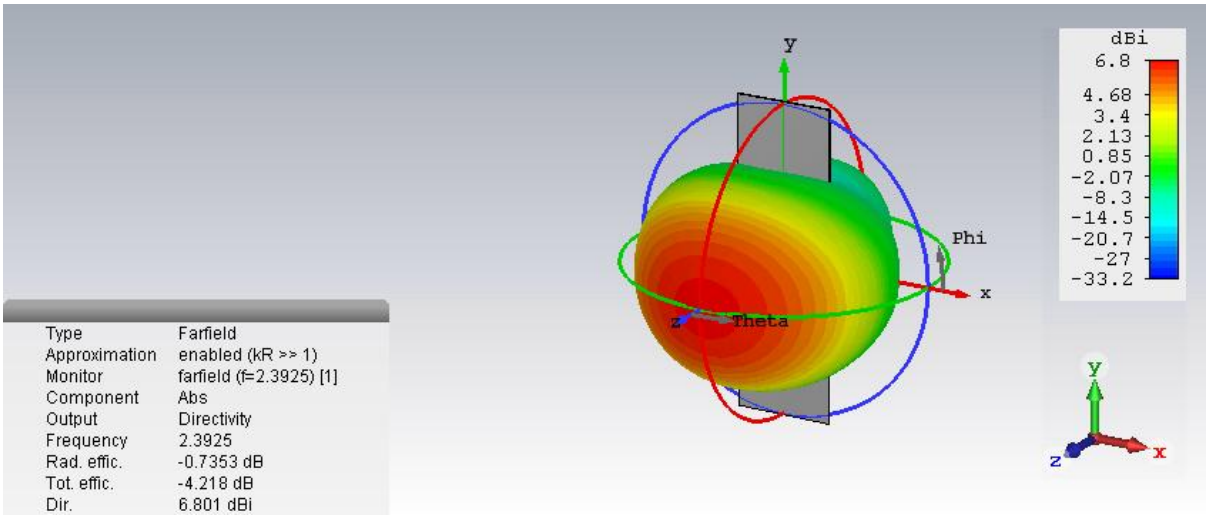

Figure 5.18: Farfield plot of SIW slot antenna with L=48.5mm, X= -2.5mm.

The following results show that the mode matching technique is in reasonably close agreement with CST Microwave Studio in the estimation of cutoff frequencies for slots of different lengths.

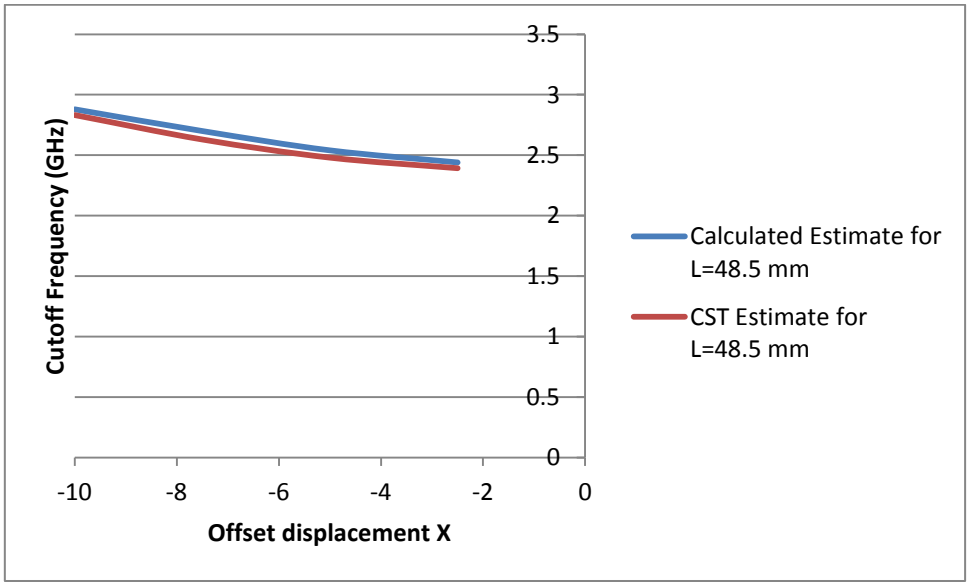

Figure 5.19: Cutoff frequencies of SIW slot antenna with L=48.5 mm

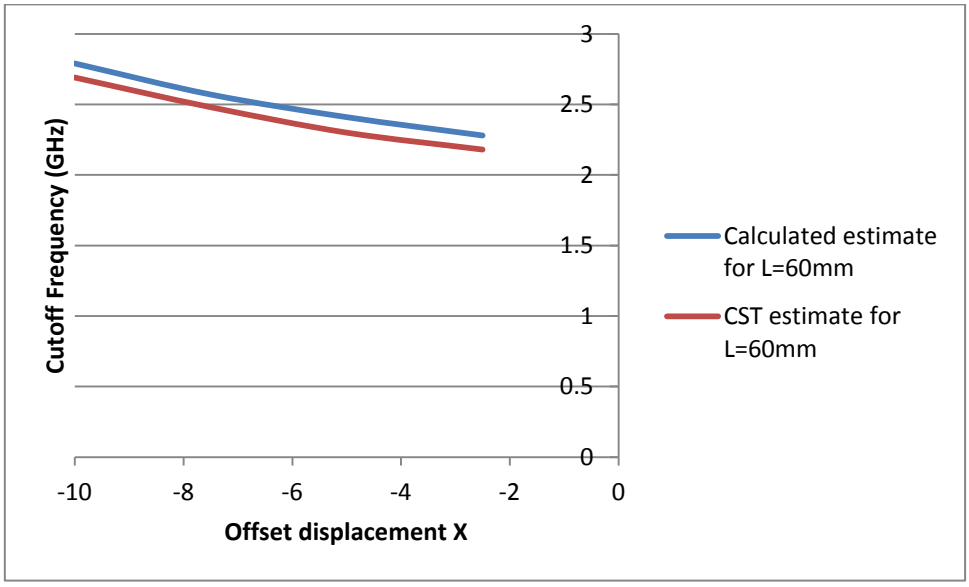

Figure 5.20: Cutoff frequencies of SIW slot antenna with L=60 mm

5.7. Summary

A modal analysis technique is used to derive S-parameters analytically for a general hybrid structure consisting of three waveguide sections such that the middle section is smaller than the other two.

This modal analytic technique is implemented in Matlab to obtain S-parameters plots for a hybrid structure of rectangular waveguides (RWG) with the middle section consisting of either an E-plane step or an H-plane step over suitable range of frequency above cutoff. Numerical examples for both cases are in close agreement with simulations from HFSS, particularly for those with H-plane steps. It has been found that if the total number of modes considered is given by $N = 50$, then the most accurate results are obtained from this modal analysis technique.

The H-plane step model is then used to predict resonant frequencies for slot antenna designs. The H-plane step model based on the mode matching technique is in reasonably close agreement (to within approximately 2%) with CST Microwave Studio in the estimation of cutoff frequencies for slots of different lengths.

5.8. References

1. D.M. Pozar, "Microwave Engineering," 2nd edition, Wiley, New York, 1998.
2. R.E. Collin, "Field Theory of Guided Waves," McGraw-Hill, 1960.
3. N. Marcuvitz, "Waveguide Handbook," McGraw-Hill, 1951.
4. L. Lewin, "Advanced Theory of Waveguides," Iliffe, 1951.
5. R. Mittra and W.M. Lee, "Analytic Techniques in the Theory of Guided Waves," Macmillan, New York, 1971.
6. P.J.B. Clarricoats, "Numerical solution of waveguide-discontinuity problems," Proc. IEE, vol. 118, no. 7, 1967.
7. P.J.B. Clarricoats, "Computer field-matching solution of waveguide transverse discontinuities," Proc. IEE, vol. 118, no. 1, 1971.
8. A. Wexler, "Solution of waveguide discontinuities by modal analysis," IEEE Trans. Microwave Theory Tech., vol. MTT-15, pp. 508-517, Sept 1967.
9. R. H. Macphie and R. Safavi-Naini, "On solving waveguide junction scattering problems by conservation of complex power technique," IEEE Trans. Microwave Theory Tech., vol.MTT-29, pp. 337-343, Apr. 1981.
10. A.S. Omar and K. Schunemann, "Transmission matrix representation of finline discontinuity," IEEE Trans. Microwave Theory Tech., vol. MTT-33, pp. 1333-1339, Dec. 1985.
11. G. Kompa, R. Mehran and I. Wolff, "Calculation method for microstrip discontinuities and T-junctions" Electron. Lett., vol 8, pp. 177-179, Apr. 1972.
12. W. Menzel and I. Wolff, "A method for calculating the frequency-dependent properties of microstrip discontinuities," IEEE Trans. Microwave Theory Tech., vol. MTT-25, pp.107-112, Feb. 1977.
13. T. S. Chu, T. Itoh and Y.C. Shih, "Comparative study of mode-matching formulations for microstrip discontinuity problems," IEEE Trans. Microwave Theory Tech., vol. MTT-33, pp. 1018-1023, Oct. 1985.
14. Y.C. Shih, "Design of waveguide E-plane filters with all metal insert" IEEE Trans. Microwave Theory Tech., MTT-32, pp. 695-704, Jul. 1984.
15. F. Arndt et al., "E-plane integrated filters with improved stopband attenuation," IEEE Trans. Microwave Theory Tech., vol. MTT-32, pp. 1391-1394, Oct. 1984.
16. F. Arndt et al., "Optimized E-plane T-junction series power divider," IEEE Trans. Microwave Theory Tech., vol. MTT-35, pp. 1052-1059, Nov. 1987
17. R.H. Macphie and R.R. Mansour, "An improved transmission matrix formulation of cascaded discontinuities and its application to E-plane circuits," IEEE Trans. Microwave Theory Tech, vol. MTT-34, pp. 1490-1498, Dec. 1986.
18. K. Gray and Y.C. Shih, "Convergence of numerical solutions of step-type waveguide discontinuity problems by modal analysis," 1983 IEEE MTT-S Int Microwave Symp. Dig., pp.233-235, 1983.
19. R.F. Xu, B. Sanz Izquierdo and P.R. Young 2011, "Switchable Substrate Integrated Waveguide," IEEE Microwave Wireless Compon. Lett., vol. 21, no.4, pp. 194-196, 2011.
20. R.F. Xu, A.J. Farrall and P.R. Young 2014, "Analysis of loaded substrate integrated waveguides and attenuators," IEEE Microwave Wireless Compon. Lett., vol. 24, no. 1, pp. 62-65, 2014.

6. Conclusions

6.1. Summary

In the second chapter, the frequency characteristics of the full-mode SIW loaded with respective capacitive and inductive slots are obtained by means of a transverse resonance technique. It is confirmed that an SIW loaded with a very small capacitance was equivalent to a standard half mode rectangular waveguide. The n^{th} order mode of the SIW slotted with a sufficiently large capacitance is shown to be the same as for the $(n-1)^{th}$ order mode of the rectangular waveguide, where $n = 2,3, \ldots$. The $(n-1)^{th}$ order mode in the SIW slotted with a very large inductance is shown to have the cut-off frequency of an n^{th} order mode in a half mode waveguide, where $= 2,3, \ldots$. The standard rectangular waveguide is shown to have several modes which also appear as modes of the SIW loaded with a very small inductance. However, it is found that the standard rectangular waveguide has certain modes which do not appear in the SIW loaded with a very small inductance.

In the third chapter, the frequency characteristics of the HMSIW loaded with respective capacitive and inductive slots are obtained. It is confirmed that the HMSIW slotted with either a sufficiently large capacitance or very small inductance is equivalent to the conventional half mode waveguide. It is demonstrated that for $n = 2,3, \ldots$, the n^{th} order mode of the HMSIW loaded with a large inductance has the cut-off frequency of the $(n-1)^{th}$ mode in a conventional half mode waveguide.

In the second and third chapters, the cut-off frequencies of the slotted SIWs and HMSIWs loaded with specific capacitances and inductances are determined from a transverse analysis technique for the purposes of practical application. These numerical predictions both compare well with, and also in some cases used to clarify, the corresponding values of cut-off frequencies estimated by CST Microwave Studio and HFSS by using S-parameters and dispersion characteristics respectively.

The transverse resonance technique is of considerable importance because it can be used to calculate a whole range of cutoff frequencies as a continuous function, unlike the simulation

packages which can only evaluate discrete cutoff frequencies one at a time. Field plots for some of these practical examples are used to show that the loaded slot plays a major role regarding the design and operation of these structures.

Dispersion curves for SSIW (i.e. slot SIW) structures obtained from HFSS demonstrate that the frequencies for sufficiently large phase values are changed much more by load capacitances than by load inductances, especially when the slot is closer to the centre of the waveguide. It is also apparent from these dispersion characteristics that the cutoff frequencies (which correspond to a phase value of zero) are closer to one another for SIWs loaded with inductances rather than with capacitances, particularly when the slot is closer to the centre of the waveguide. Dispersion curves obtained from HFSS for the third chapter illustrate that the frequencies for sufficiently large phase values for HMSIWs vary significantly less with loaded capacitances and inductances than for SIWs of similar dimensions. The dispersion characteristics from HFSS also illustrate that the cutoff frequencies (which correspond to a phase value of zero) are very much closer to one another if the HMSIWs are loaded with capacitances instead of inductances, especially when the slot is further way from the centre of the guide.

In the latter parts of the second chapter, the earlier efforts to predict cut-off frequencies for specific loaded slots culminate with some novel practical applications. The first such example is an attempt to design a slotted SIW structure (with a load capacitance and load inductance in series) which exhibits hallmarks of a bandpass waveguide filter, which is subsequently matched more efficiently by increasing the thickness of the SIW to 3mm. It is evident from all the S-parameter plots of these loaded waveguide structures that they are much better suited to the design of narrow band devices. This leads to the novel design of two devices, namely a two-port tuneable waveguide resonator which can be adjusted over a frequency interval of 300 GHz and a single port tuneable narrow band antenna which functions over an exceedingly large operational bandwidth of almost 1 GHz. Both these narrow band devices are finely tuned by using loaded capacitances.

In the fourth chapter, the frequency characteristics of the parallel plate SIW loaded with respective capacitive and inductive slots are obtained. It is affirmed that the parallel plate SIW slotted with a sufficiently small capacitance is equivalent to a standard parallel plate

waveguide. The standard parallel plate waveguide is shown to have several modes which also appear as modes of the parallel plate SIW loaded with either a very large capacitance or very small inductance. However, it is proved that the standard parallel plate waveguide has certain modes, depending on the choice for Γ, which do not appear in the parallel plate SIW loaded with either a very large capacitance or very small inductance. It is demonstrated that the cut-off frequency of the n^{th} order mode in the parallel plate SIW slotted with a sufficiently large inductance is equivalent to the cut-off frequency of the $(n-1)^{\text{th}}$ order mode in a standard parallel plate waveguide, where $n = 2,3, \ldots$.

In the final chapter, a modal analysis technique is used to obtain S-parameters of a hybrid waveguide structure composed of three sections, in which the middle section has a smaller width than the other two identical regions, over a suitable range of frequencies. A special instance of this structure is considered, in which the middle section is a slotted SIW (with either an E-plane or H-plane step respectively) and the outer sections are rectangular shaped. The calculated predictions of the S-parameters over the frequency range 2-3 GHz are shown to be in very close agreement with HFSS, particularly for the H-plane case. Finally, the mode matching method is used to predict a rough estimate for the fundamental cutoff frequencies of slotted SIW antenna structures.

6.2. Future work

The HMSIW has several antenna applications, such as the leaky wave antenna [1], the slot antenna [2], the frequency scanning antenna [3] and the slot ray antenna [4]. The half-mode technique is convenient for antenna applications because it allows for fabrication, integration with planar circuits, large bandwidth, with low cost and reduced loss and size. The determination of cut-off frequencies for loaded SIWs and HMSIWs is useful in determining at what frequencies the slot in a given structure can radiate. The work on filters can be readily expanded in a more practical context. For instance, folded SIW structures can be used to make efficient bandpass filters [5]. SIWs can also be used in novel ways to make phase shifters [6] rather than by using traditional means [7]. The phase plots of S-parameters demonstrate that it is possible to construct rudimentary phase shifters from loaded SIWs.

The modal analysis technique that was discussed is not entirely original, and there are several treatments of waveguide discontinuity problems in the existing literature (see [8]-[11]). However, its application to a general case of hybrid waveguide structures allows operational characteristics of many different kinds of slotted SIW structures with discontinuities to be modelled in a novel way. This potentially has a wide range of applications in the form of slot antennas, filters and many other different devices. It was established earlier for the examples of the modal analysis technique that the transition from a full mode SIW to a SSIW can be used to model an HMSIW fed by a full mode SIW. This is of practical importance, because modal analysis can be used to readily determine operational characteristics for SSIWs for the construction of many different types of microwave devices, such as a switches [12] and an attenuators [13].

6.3. References

1. J. Xu, W. Hong, H. Tang, Z. Kuai and K. Wu, "Half mode substrate integrated waveguide (HMSIW) Leaky-Wave Antenna for Millimetre-Wave Applications," *IEEE Antennas and Wireless Propag. Lett.*, vol. 7, 2008.
2. A.J. Farrall and P.R. Young, "Integrated waveguide slot antennas," Electron.Lett., vol.40, No.16, August 2004, pp.974-975.
3. Y. J. Cheng, W. Hong, K. Wu, "Millimetre-Wave Substrate Integrated Waveguide Frequency Scanning Antenna with Quadri-Polarization," IEEE Trans. Antennas Propag., Vol.59, no.6, pp.1848-1855-139, 2010.
4. Q.H. Lai, W. Hong, Z.Q. Kuai, Y.S. Zhang and K. Wu, "Half-Mode Substrate Integrated Waveguide Transverse Slot Array Antennas," IEEE Transactions on Antennas and Propagation, Vol. 57, No. 4, 2009.
5. R. Wang, L.S. Wu and X.-L. Zhou, "Compact folded substrate integrated waveguide cavities and bandpass filters" Progress in Electromagnetics Research, PIER 84, 135-147, 2008.
6. Sellal K., Talbi L., Denidni, T.A. and Lebel J., "Design and implementation of a substrate integrated waveguide phase shifter," IET Microw. Antennas Propag., vol. 2, no. 2, pp. 194-199, 2008.
7. D.M. Pozar, "Microwave Engineering," 2nd edition, Wiley, New York, 1998.
8. R.E. Collin, "Field Theory of Guided Waves," McGraw-Hill, 1960.
9. N. Marcuvitz, "Waveguide Handbook," McGraw-Hill, 1951.
10. L. Lewin, "Advanced Theory of Waveguides" Iliffe, 1951
11. P.J.B. Clarricoats, "Numerical solution of waveguide-discontinuity problems " Proc. IEE, vol. 114, no. 7, 1967.
12. R.F. Xu, B. Sanz Izquierdo and P.R. Young 2011, "Switchable Substrate Integrated Waveguide" IEEE Microwave wireless compon. Lett **21**(4) 194.
13. R.F. Xu, A.J. Farrall and P.R. Young 2014, "Analysis of loaded substrate integrated waveguides and attenuators" IEEE Microwave wireless compon. Lett **24**(1) 62.

7. Appendix: Transverse resonance analysis of loaded SIW

7.1. Background theory

We consider a SIW with a slot that is loaded with an impedance *Z*, which can either be formed by a distributed structure or by periodically loaded discrete impedances. The unit of *Z* will therefore be Ω m or, if we express *Z* as an admittance *Y*, S m^{-1}.

In the transverse direction the equivalent circuit of the waveguide is shown in the figure below.

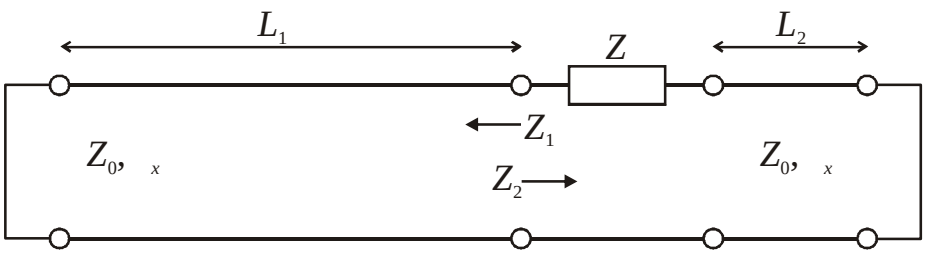

Fig 7.1: Equivalent transverse resonance circuit.

Let Z_1 and Z_2 be the impedances seen looking to the left and right respectively. Then, at resonance, the condition $Z_1 = Z_2$ must be satisfied. By using the propagation constant in the x-direction given by $\gamma_x = \alpha_x + jk_x$, it follows that the resonance condition is

$$Z_0 \, tanh(\gamma_x L_1) = -Z - \, Z_0 \, tanh(\gamma_x L_2) \quad . \qquad (7.1)$$

Since we are considering a TE problem with the transverse resonance technique, the characteristic impedance is given by $Z_0 = \frac{E_y}{H_z} = \frac{j\omega\mu}{\gamma_x}$ [6] and the equivalent voltage and current are set equal to the electric and magnetic fields respectively. However, because we embed discrete components into the waveguide we need to ensure that the equivalent waveguide voltage and current value (and therefore Z_0) are compatible with the voltage and current presented to the impedance *Z*. If the electric field is independent of *y* then the voltage at the impedance will be $E_y b$, where b is the height of the waveguide. The current (per unit length) at the embedded impedance is $J_X = H_z$. Hence we choose

$$Z_0 = j\frac{\omega\mu b}{\gamma_x} \ , \qquad (7.2)$$

which has units of Ω m. Let $\Theta = \gamma_x L_1$, $\Gamma = \frac{L_2}{L_1}$ and

$$Z' = R' + jX' = \frac{Z}{\omega\mu b L_1} \ . \quad (7.3)$$

Then, by substituting equations (7.2) and (7.3) into equation (7.1), we obtain

$$\frac{j\omega\mu b}{\gamma_x} tanh(\gamma_x L_1) = -Z - \frac{j\omega\mu b}{\gamma_x} tanh(\gamma_x L_2)$$

$$\Leftrightarrow tanh(\gamma_x L_1) + tanh(\gamma_x L_2) - jZ'(\gamma_x L_1) = 0$$

$$\Leftrightarrow tanh(\Theta) + tanh(\Gamma\Theta) - jZ'\Theta = 0 \ . \qquad (7.4)$$

There are two types of solution to equation (4). They can be categorized as fast and slow modes, where fast and slow are defined with respect to the velocity of propagation in the substrate material. We analyze lossless propagation when the impedance *Z* is purely capacitive, i.e. when $Z = jX = \frac{1}{j\omega C}$.

Fast mode propagation

For fast mode propagation $\gamma_x = jk_x$, and therefore the field varies sinusoidally across the waveguide cross section, as is the case in conventional waveguide. Under this condition equation (7.4) becomes

$$\begin{aligned} & tanh(jk_xL_1) + tanh(jk_x\Gamma L_1) - jZ'(jk_xL_1) = 0 \\ \Leftrightarrow\ & j\ tan(k_xL_1) + j\ tan(k_x\Gamma L_1) - j(jX')(jk_xL_1) = 0 \\ \Leftrightarrow\ & tan(k_xL_1) + tan(k_x\Gamma L_1) + X'(k_xL_1) = 0 \\ \Leftrightarrow\ & tan(\theta') + tan(\Gamma\theta') - X'\theta' = 0\ , \end{aligned} \qquad (7.5)$$

where we set $\theta' = k_xL_1$ and $Z' = \mathrm{j}X'$. We make use of the standard definition of the propagation constant given by

$$\beta = \varepsilon_r {k_0}^2 - {k_x}^2\ , \qquad (7.6)$$

where $k_0 = \omega\sqrt{\mu_0\varepsilon_0}$.

so that at cutoff, we have

$$\begin{aligned} & {k_x}^2 = \varepsilon_r {k_0}^2 \\ \Leftrightarrow\ & k_x = \sqrt{\varepsilon_r}\ \omega_c\sqrt{\mu_0\varepsilon_0}\ , \end{aligned} \qquad (7.7)$$

where the cutoff angular frequency ω_c is given by

$$\omega_c = \frac{k_x}{\sqrt{\mu_0\varepsilon_0\varepsilon_r}}\quad . \qquad (7.8)$$

By substituting $Z = jX = -j/\omega C$ into (7.3), we have

$$Z' = j\ X' = -\frac{-j}{\omega^2 C\mu b L_1}\ ,$$

so that we have

$$X' = -\frac{1}{\omega^2 C\mu b L_1}\quad . \qquad (7.9)$$

The structure has height $b = 1.5\text{mm}$, slot width $w = 0.5\text{mm}$, relative permittivity $\varepsilon_r = 2.3$, $L_1 = 15\text{mm}$, $L_2 = 5\text{mm}$ and $C = 1\text{pF}$. The solutions of (7.5) can be determined easily using standard numerical techniques, by substituting (7.7), (7.8) and (7.9) into (7.5). Using the above formulae, we can use the transverse resonance technique to predict the following dispersion curves showing how β varies with ω for the slotted waveguide with $\Gamma = 3$ and $\Gamma = 4$.

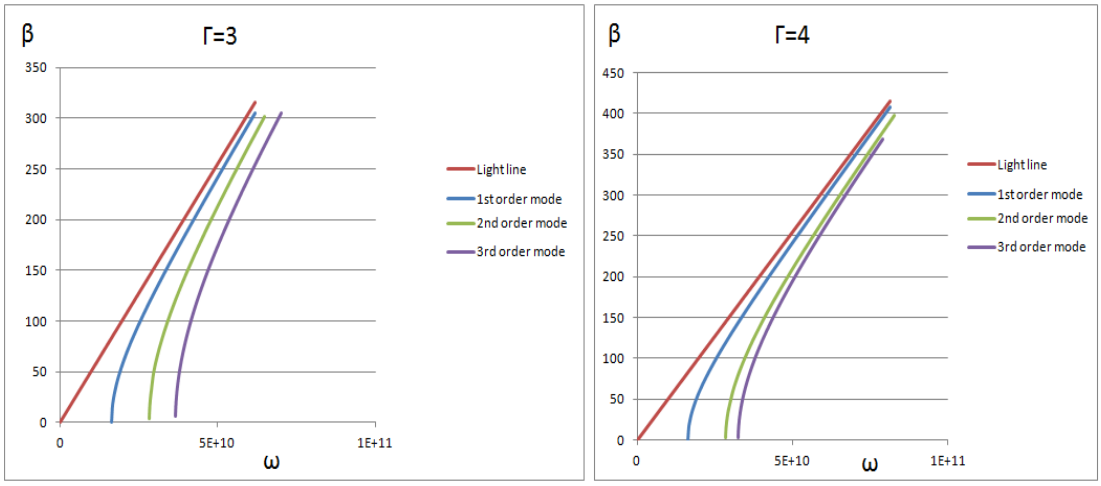

It is however useful to consider the ranges were the solutions lie. Figure x shows a typical plot of the left and right hand side of equation (5) for some X'. The effective reactance X' will of course vary with frequency and therefore the slope of the line $X'\theta'$ will also change. Therefore, unlike conventional waveguide the value of k_x is frequency dependent.